Université d'Ottawa · University of Ottawa

SEISMIC RESISTANCE OF CONCRETE-FILLED SQUARE STEEL HOLLOW STRUCTURAL SECTION BEAM-COLUMNS

by

© **Made S. Hardika**

Under the supervision of

Dr. N. J. Gardner

Thesis submitted to the Faculty of Graduate and Postdoctoral Studies
in partial fulfillment of the requirements for the
Doctor of Philosophy in Civil Engineering
under the auspices of the Ottawa-Carleton Institute for Civil Engineering

Department of Civil Engineering, University of Ottawa
Ottawa, Ontario, Canada
February 2002

ABSTRACT

This thesis describes a research program designed to investigate the seismic performance of square concrete-filled tubular (CFT) columns subjected to a combination of axial load and biaxial bending moment. The square CFT columns included normal-strength and high-strength concrete-filled square steel hollow structural section columns with two ratios of tube wall thickness to tube dimension.

An extensive experimental program included testing twenty-four, concrete filled, square steel hollow structural section column specimens under constant axial compressive load and cyclic horizontal load with horizontal displacement control. This experimental investigation included strength capacity, ductility and flexural stiffness of CFT beam-columns for 203x203x9.5 HSS (Class 1, compact sections) and 203x203x4.8 (Class 4, slender sections) hollow structural section (HSS) filled with either normal strength or high strength concrete.

Class 1 (compact) and Class 4 (slender) HSS CFT columns subjected to constant axial load and cyclic shear displacements exhibited excellent hysteresis behavior using either normal strength concrete or high strength concrete. No premature failure, local buckling before yielding, was observed for either Class 1 or Class 4 HSS CFT columns. The drift ratios exceeded 7%. The moment capacities of HSS CFT columns loaded with the plane of bending across the diagonal were only slightly less than those loaded with the plane of bending parallel to the square side. This reduces the need for elaborate procedures to calculate the biaxial moment capacities at orientations between 0 and 45^0.

The strength capacity of square HSS CFT columns subjected to constant axial compressive load and biaxial cyclic bending moment can be conservatively calculated by column section analysis using fully plastic behavior for both concrete and steel. Strength modification factors α_1 and α_2 accommodate confinement and seismic loading, fast concrete strain rates, effects on the CFT column sections and softening of the columns caused by large axial load.

Flexural stiffness of square HSS CFT columns can be calculated using the ACI 318-99 flexural stiffness formula with modification to the coefficient of the flexural stiffness contributed by the concrete.

ACKNOWLEDMENTS

I would like to express my gratitude to Dr. N. J. Gardner, thesis supervisor, for his guidance and encouragement throughout the course of this study. A sincere gratitude is expressed to my fellow graduate students who assisted me in the fabrication and testing of the column specimens, in particular Mr. Elnabelsy and the structures lab. technician, Mr. Derek Mes.

This undertaking could never been possible without the patience, continuous encouragement, relentless support, and sacrifices of my wife Narti. I am also very grateful to my sons Niko, Michell, and Marthy for their patience and understanding even at their young ages.

I would like to express my sincere appreciation to my parents for their moral supports. Many special thanks are extended to Indonesian Government for financial support of this program.

M S Hardika

TABLE OF CONTENTS

ABSTRACT i
ACKNOWLEDGEMENTS ii
TABLE OF CONTENTS iii
LIST OF TABLES vii
LIST OF FIGURES viii
NOTATION xii

Chapter 1 1
INTRODUCTION 1
1.1 General 1
1.2 Brief History of Concrete Filled Tubular (CFT) Columns 3
1.3 Behaviour of Concrete Filled Steel Tubular Columns 5
1.4 Previous Research 6
1.5 Research Needs 7
1.6 Research Program 8
1.6.1 Research Significance 9
1.6.2 Research Objectives 10
1.7 Scope of the Thesis 10
1.8 Thesis Outline 10
Chapter 2 12
LITERATURE REVIEW 12
2.1 General 12
2.2 Mechanical Properties of Concrete 12
2.2.1 Normal Strength Concrete 13
2.2.2 High Strength Concrete 14
2.2.3 Modulus of Elasticity and Poisson's Ratio of Concrete 15
2.2.4 Triaxial Behaviour of Concrete 17

2.2.5 Confined Concrete 17
2.2.6 Concrete Subjected to Cyclic Loading 19
2.2.7 Equivalent Rectangular Stress Distribution of Concrete 19
2.3 High Strength CFT Columns 20
2.4 Column Stability 22
2.5 Columns under Biaxial Bending 23
2.6 Square CFT Column Tests 27
2.7 Behaviour of Composite Sections 29
2.8 Seismic Behaviour of Composite Columns 34
2.9 Codes Review 35
2.10 Summary 42
Chapter 3 46
SIMPLIFIED COLUMN ANALYSIS 46
3.1 General 46
3.2 Strength Capacity 46
3.2.1 Eurocode 4 47
3.2.2 AISC-LRFD 50
3.2.3 CAN/CSA-S16.1-94 51
3.2.4 CSA A23.3-94 53
3.2.5 ACI 318-99 53
3.2.6 Proposed Method of Analysis 53
3.2.7 Slenderness 56
3.2.8 Combined Axial Load and Biaxial Bending Moment 57
3.3 Development of Parameters for Section Analysis 58
3.4 Ductility 60
3.5 Flexural stiffness 61
Chapter 4 69
EXPERIMENTAL PROGRAM 69
4.1 General 69
4.2 Test Program 70
4.3 Concrete 71

4.3.1 Description 71
4.3.2 Equipment and Method of Testing 71
4.4 Steel Tube (Square HSS) 72
4.4.1 Description 72
4.4.2 Equipment and Method of Testing 72
4.5 Steel Foundation 73
4.6 HSS CFT column specimens 74
4.6.1 Description and Construction Procedure 74
4.6.2 Instrumentation and Testing Procedures 75
4.7 Experimental Data and Data Analyses 78
4.7.1 Bending Moment 79
4.7.2 Axial Load – Bending Moment Interaction Curve 80
4.7.3 Curvature and Moment – Curvature Relationship 80
4.7.4 Flexural Stiffness 81
Chapter 5 95
NORMAL STRENGTH CFT COLUMNS 95
5.1 General 95
5.2 Ancillary Test Results 96
5.3 Observed Behaviour and Test Data 97
5.3.1 SNL Columns 99
5.3.2 SCL Columns 101
5.3.3 DNL Columns 102
5.3.4 DCL Columns 104
5.4 Strength Capacity 105
5.5 Ductility 106
5.6 Flexural Stiffness 108
5.7 Column Classification 109
5.8 Discussion 109
Chapter 6 141
HIGH STRENGTH CFT COLUMNS 142
6.1 General 142

6.2 Ancillary Test Results 143
6.3 Observed Behaviour and Test Data 144
6.3.1 SNH Columns 146
6.3.2 DNH Columns 147
6.3.3 SCH Columns 149
6.3.4 DCH Columns 149
6.4 Strength Capacity 150
6.5 Ductility 151
6.6 Flexural Stiffness 153
6.7 Column Classification 154
Chapter 7 184
SUMMARY AND CONCLUSIONS 184
7.1 Summary 184
7.2 Conclusion 186
7.3 Recommendation for Future Work 187
REFERENCES 189
APPENDIX 198

LIST OF TABLES

Table 3.1 Classifications of rectangular HSS sections 64

Table 3.2 Test results of increase in compressive strength ofconcrete at high strain rates (Bischoff and Perry, 1991) 64

Table 4.1 Test program 82

Table 5.1 Compressive strength of standard cylinder tests of the concrete 113

Table 5.2 Test and analytical results of modulus of elasticity of NSC 113

Table 5.3 The HSS steel properties 114

Table 5.4 Specimens constituent strength at the test 114

Table 5.5 The strength capacity of normal strength CFT columns 115

Table 5.6 Yield moment ratio and ductility of normal strength CFT columns 116

Table 5.7 Flexural stiffness of normal strength CFT columns 117

Table 5.8 Comparison of squash load (P_o) to Euler load P_E) 118

Table 6.1 Compressive strength of standard cylinder tests of the concrete 155

Table 6.2 Test and analytical results of modulus of elasticity of HSC 155

Table 6.3 The HSS steel properties 156

Table 6.4 Specimens constituent strength at the test 156

Table 6.5 The strength capacity of high strength CFT columns 157

Table 6.6 Yield moment ratio and ductility of high strength CFT columns 158

Table 6.7 Flexural stiffness of high strength CFT columns 159

Table 6.8 Comparison of squash load (P_o) to Euler load P_E) 160

LIST OF FIGURES

Figure 2.1 Concrete stress-strain curve (schematic) 44
Figure 2.2 Hognestad's model of stress strain diagram in flexture (Sargin, 1971) ... 44
Figure 2.3 Sturman's stress-strain curves (Sargin, 1971) 45
Figure 2.4 Cyclic envelope and monotonic stress-strain curve 45
Figure 3.1 Eurocode 4 full and approximate interaction diagram 65
Figure 3.2 Coefficient α_1 65
Figure 3.3 Coefficient β_1 66
Figure 3.4 Full plastic rectangular stress distribution 66
Figure 3.5 Coefficient α_2 for Class 4 HSS CFT columns 67
Figure 3.6 Curvature and displacement ductility 68
Figure 4.1 Typical tension test coupons 83
Figure 4.2 Tension test coupons 83
Figure 4.3 Assembled steel foundation 84
Figure 4.4 Photographs of assembled steel foundation 85
Figure 4.5 Photograph of front view of test setup 86
Figure 4.6 Photographs of steel tubes and column specimens 87
Figure 4.7 Typical HSS CFT column specimens 88
Figure 4.8 Front view of test setup 89
Figure 4.9 Side view of test setup 90
Figure 4.10 The schematic acquisition of test system 91
Figure 4.11 LVDTs and strain gauges positions 92
Figure 4.12 Transverse loading history 93
Figure 4.13 System of forces acting on a column specimen 93
Figure 4.14 Uninstalling column DCH - 2 94
Figure 5.1 Compressive strength of normal strength concrete 119
Figure 5.2 The stress strain curve of concrete tested at 28 days 120

Figure 5.3 Horizontal force-displacement of horizontal actuator for SNL specimens 121
Figure 5.4 Horizontal force-displacement of horizontal actuator for SCL specimens 122
Figure 5.5 Horizontal force-displacement of horizontal actuator for DNL specimens 123
Figure 5.6 Horizontal force-displacement of horizontal actuator for DCL specimens 124
Figure 5.7 Shear force & moment vs displacement of SNL specimens 125
Figure 5.8 Shear force & moment vs displacement of SCL specimens 126
Figure 5.9 Shear force & moment vs displacement of DNL specimens 127
Figure 5.10 Shear force & moment vs displacement of DCL specimens 128
Figure 5.11 Moment-curvature relationship of SNL specimens 129
Figure 5.12 Moment-curvature relationship of SCL specimens 130
Figure 5.13 Moment-curvature relationship of DNL specimens 131
Figure 5.14 Moment-curvature relationship of DCL specimens 132
Figure 5.15 Columns DNL-1 and SNL-1 at 8 % drift 133
Figure 5.16 Columns DCL-2 and SCL-2 at 8 % drift 134
Figure 5.17 Column SNL-3, during test and after test 135
Figure 5.18 Columns DCL and SCL after tests 136
Figure 5.19 Strength capacity of SNL columns (without considering M_y effects) ... 137
Figure 5.20 Strength capacity of SCL columns (without considering M_y effects) ... 138
Figure 5.21 Strength capacity of DNL columns 139
Figure 5.22 Strength capacity of DCL columns 140
Figure 5.23 Normalized interaction diagram for normal strength CFT columns ... 141
Figure 6.1 Compressive strength of high strength concrete 161
Figure 6.2 The stress strain curve of high strength concrete tested at 44 days 162
Figure 6.3 Horizontal force-displacement of horizontal actuator for SNH specimens 163
Figure 6.4 Horizontal force-displacement of horizontal actuator for DNH specimens 164

Figure 6.5 Horizontal force-displacement of horizontal actuator for SCH specimens 165

Figure 6.6 Horizontal force-displacement of horizontal actuator for DCH specimens 166

Figure 6.7 Shear force & moment vs displacement of SNH specimens 167

Figure 6.8 Shear force & moment vs displacement of DNH specimens 168

Figure 6.9 Shear force & moment vs displacement of SCH specimens 169

Figure 6.10 Shear force & moment vs displacement of DCH specimens 170

Figure 6.11 Moment-curvature relationship of SNH specimens 171

Figure 6.12 Moment-curvature relationship of DNH specimens 172

Figure 6.13 Moment-curvature relationship of SCH specimens 173

Figure 6.14 Moment-curvature relationship of DCH specimens 174

Figure 6.15 Columns DNH and SNH after tests 175

Figure 6.16 Columns DCH-2 and SCH-2 at 8 % drift 176

Figure 6.17 Columns DCH-3 and SCH-3 at 8 % drift 177

Figure 6.18 Columns DNH-3 and SNH-3 at 7 % drift 178

Figure 6.19 Strength capacity of SNH columns (without considering M_y effects) ... 179

Figure 6.20 Strength capacity of DNH columns 180

Figure 6.21 Strength capacity of SCH columns (without considering M_y effects) ... 181

Figure 6.22 Strength capacity of DCH columns 182

Figure 6.23 Normalized interaction diagram for high strength CFT columns 183

Figure A.1 Transverse strain vs Longitudinal strain of DNL column specimens ... 199

Figure A.2 Transverse strain vs Longitudinal strain of SNL column specimens 200

Figure A.3 Transverse strain vs Longitudinal strain of DCL column specimens ... 201

Figure A.4 Transverse strain vs Longitudinal strain of SCL column specimens 202

Figure A.5 Transverse strain vs Longitudinal strain of DNH column specimens ... 203

Figure A.6 Transverse strain vs Longitudinal strain of SNH column specimens 204

Figure A.7 Transverse strain vs Longitudinal strain of DCH column specimens ... 205

Figure A.8 Transverse strain vs Longitudinal strain of SCH column specimens 206

Figure A.9 Deflected shape of column DNL-1 207

Figure A.10 Deflected shape of column SNL-1 207
Figure A.11 Deflected shape of column DCL-2 208
Figure A.12 Deflected shape of column SCL-2 208
Figure A.13 Deflected shape of column DNH-2 209
Figure A.14 Deflected shape of column SNH-2 209
Figure A.15 Deflected shape of column DCH-2 210
Figure A.16 Deflected shape of column SCH-2 210

NOTATION

A_c = area of concrete, in mm

A_r = area of longitudinal reinforcing bars, in mm

A_s = area of steel tube, in mm

C = a coefficient in Pillai's expression for a biaxial bending beam-column

C_m = a factor relating actual moment diagram to an equivalent uniform moment diagram

C_{mx} = a coefficient to determine equivalent uniform moment in a beam-column about x-axis

C_{my} = a coefficient to determine equivalent uniform moment in a beam-column about y-axis

D = outside diameter of steel tube, in mm

E_c = modulus of elasticity (initial tangent modulus) of concrete, in Mpa

F_{cr} = critical thrust load applied at ends of a member, in kN

E_{c28} = modulus of elasticity of concrete at 28 days, in Mpa

E_{cm28} = average modulus of elasticity of concrete at 28 days, in Mpa

E_{cmt} = average modulus of elasticity of concrete at t days, in Mpa

E_m = modified modulus of elasticity of steel tube, in MPa

E_r = modulus of elasticity of reinforcing steel, in MPa

E_s = modulus of elasticity of steel, in MPa

I = moment of inertia of a section, in mm^4

I_c = moment of inertia of concrete (assumed to be uncracked), in mm^4

I_g = moment of inertia of gross concrete section about centroidal axis, in mm^4

I_s = moment of inertia of steel tube, in mm^4

L = length of a column, in mm

M = applied bending moment, in kN.m

M_c = factored moment to be used for design of compression member, in kN.m

M_1 = smaller factored end moment on compression member, positive if member is bent in single curvature, negative if bent in double curvature, in kN.m

M_2 = larger factored end moment on compression member, always positive, in kN.m

M_{max} = maximum bending moment, in kN.m

M_n = nominal bending moment, in kN.m

M_{nx} = nominal bending moment about x-axis, in kN.m

M_{ny} = nominal bending moment about y-axis, in kN.m

M_{nbx} = nominal bending moment about x-axis at balanced strain condition, in kN.m

M_{nby} = nominal bending moment about y-axis at balanced strain condition, in kN.m

M_o = applied-end moment, in kN.m

M_p = plastic bending moment, in kN.m

M_{px} = plastic-resisting moment about x-axis, in kN.m

M_{py} = plastic-resisting moment about y-axis, in kN.m

M_u = ultimate bending moment, in kN.m

M_{ux} = ultimate bending moment about x-axis, in kN.m

M_{uy} = ultimate bending moment about y-axis, in kN.m

M_{ucx} = maximum moment about x-axis resisted by a biaxially loaded beam-column in the presence of axial load, in kN.m

M_{ucy} = maximum moment about y-axis resisted by a biaxially loaded beam-column in the presence of axial load, in kN.m

M_x = bending moment about x-axis, in kN.m

M_y = bending moment about y-axis, in kN.m

N = applied axial load, in kN

N_o = ultimate strength of a short column under axial load, in kN

$N_{pl,rd}$ = squash load, in kN

N_u = ultimate strength of a slender column under axial load

P = axial compressive load, in kN

P_c = critical load, in kN

P_{cr} = critical centric axial load, in kN

P_{ax} = failure load under axial loading, in kN

P_E = buckling load or critical load in Euler column theory, in Newton

P_n = nominal axial compression, in kN

P_{nb} = nominal axial compression at balanced strain condition, in kN

P_o = maximum nominal axial compression, in kN

P_s = axial compressive load resisted by steel tube, in kN

P_u = ultimate axial compressive load, in kN

P_x = failure load in uniaxial bending about x-axis, in kN

P_{xy} = biaxial failure load, in kN

P_y = failure load in uniaxial bending about y-axis, or column axial load at full-yield condition in kN

Z_c = plastic modulus of concrete cross section, in mm^3

Z_r = plastic modulus of reinforcement, in mm^3

Z_s = plastic modulus of steel cross section, in mm^3

b = width of rectangular or square cross section, in mm

d = outside diameter of steel tube, in mm

e = eccentricity, in mm

e_o = assumed equivalent eccentricity, in mm

f'_c = specified compressive strength of concrete, in Mpa

f'_{cc} = confined concrete strength, in Mpa

f'_{co} = unconfined concrete strength, in Mpa

f_{cm28} = average compressive strength of standard cylinder tests at 28 days, in Mpa

f_{cmt} = average compressive strength of standard cylinder tests at t days, in Mpa

f_l = lateral confinement pressure, in MPa

f_r = stress in longitudinal steel reinforcement, in MPa

f_y = specified yield stress of the steel tube, in MPa

f_{ym} = modified yield strength of the steel tube, in MPa

f_{yr} = specified yield stress of the longitudinal reinforcing bars, in MPa

h = depth of a rectangular cross section, in mm

kL = effective length of the column, in mm

k_1 = a coefficient which reflects the relationship between uniform lateral confinement pressure and strength enhancement in confined concrete.

r = radius of gyration of a column; corner radius of steel tube, in mm

r_m = modified radius of gyration of steel tube, in mm

r_o = polar radius of gyration of the cross section about its shear center, in mm

t = wall thickness of steel tube, in mm

α = an exponent in interaction formula for column subjected to combined axial load and biaxial bending moment; a coefficient in Cai's expression

α_1 = ratio of average stress in rectangular compression block to the specified concrete strength

α_2 = conservatism coefficient

β_1 = ratio of depth of rectangular compression block to depth to the neutral axis

β_d = ratio of the maximum factored axial sustained load to the maximum factored axial load

γ_c = density of concrete, in kg/m^3.

γ_c = partial safety factor for the concrete = 1.5

γ_r = partial safety factor for the reinforcing steel = 1.15

γ_s = partial safety factor for the structural steel = 1.1

Δ = displacement, in mm

Δ_u = ultimate displacement, in mm

Δ_y = yield displacement, in mm

δ_{ns} = moment magnification factor for frames braced against sidesway

η = an exponent used in Tebedge and Chen's expression for biaxial bending column

λ = slenderness parameter of a column

λ_c = slenderness parameter of a composite column

λ_m = modified slenderness parameter of steel tube

μ_Δ = displacement ductility

μ_Φ = curvature ductility

Φ = ratio of steel to concrete strength

Φ_u = ultimate curvature, in radian

Φ_y = yield curvature, in radian

τ = a factor defined in Eq. 3.31

τ' = a factor defined in Eq. 3.32

ω_1 = coefficient used to determine equivalent uniform bending effect in beam-column

Chapter 1

INTRODUCTION

1.1 General

Traditionally stone and masonry columns were used to transmit loads by axial compression, the magnitude of any bending moment was limited because stone and masonry could not take any tension stresses. Over the last 150 years, the advent of steel and reinforced concrete structures required that columns carry bending moments in addition to axial compressive loads, these are sometimes called beam columns. Concrete, an artificial rock-like material, is ideal to carry compressive loads. Reinforced concrete columns, with steel reinforcement to carry tensile force resultants, can be used for beam columns.

The strength capacity of short columns is limited by the stress capacity of the column material(s). However, long or slender compression members, under axial compression (struts), can also fail by buckling, elastic instability, at stresses well below the limiting stresses of the material(s). Determining the buckling loads of slender columns requires knowledge of the flexural stiffness of the section and analysis is complicated by initial lack of member straightness, eccentricity of loads and residual stresses due to the manufacturing processes. Intermediate columns can fail by plastic instability when the stresses are large, above the linear part of the stress strain characteristic of the material(s).

Buckling, elastic or plastic instability, can affect any member or part of a member that is subjected to compressive stresses. Buckling can be general or local. Loads in steel members are often limited by general or local buckling.

During the past decades, the rate of high-rise building construction in major cities has increased rapidly and tall reinforced concrete buildings have become commonplace. The loadings in these buildings necessitate the use of reinforced concrete columns having

large dimensions. To decrease the column dimensions, composite concrete-steel structural sections, as an alternative material, have been used. In some medium-rise buildings, to achieve large spacing of columns, use has been made of steel floor beams to minimize both overall floor depths and deflections. In these cases, the use of steel sections in both columns and beams greatly facilitates the erection of the building's structural frame. Again, to enhance performance of the steel columns, the use of composite concrete-steel structural section columns has been widely accepted. Composite concrete-steel columns can be structural steel sections encased by reinforced concrete or concrete sections encased by steel tubes.

Over the past 40 years, numerous innovative structural systems have evolved in tall building design where structural steel and reinforced concrete have been combined to produce a building having the advantages of each material. The use of these so-called composite-frame structures has as its underlying principle the combination of these two distinctive and different building materials to benefit from the advantages of both: the inherent stiffness and economy of reinforced concrete and the speed of construction, strength and light weight of structural steel.

It has been reported by Griffis (1986) that under axial loads, reinforced concrete columns are approximately 11 times more cost-effective than structural steel columns in terms of strength and stiffness, giving an indication of the potential economy of composite columns that make use of steel and concrete.

The reason why widespread use of concrete filled steel tubular columns did not occur prior to the 1990's was the perception that their fire resistance would be less than a reinforced concrete column and difficulties in fabricating connections.

Studies on the fire resistance of hollow structural section (HSS) columns filled with concrete by Chabot and Lie (1992) showed that the concrete core provided resistance that enable some limited amount of force distribution to take place from the steel tube to the concrete, providing in the process some resistance to fire. Alternatively, these columns can be protected using the same techniques as steel structures, which have improved over recent years.

Comprehensive investigations on the subject of behaviour of concrete-filled tubular (CFT) column-WF beam moment connections under both monotonic and seismic

loading have been reported (Kato, 1982; Kanatani et al., 1987; Deierlein et al., 1989; Sheikh et al., 1989; Vermaas et al., 1996; Graham, 1996; Ricles et al., 1998; Beutel et al., 2000).

Nowadays concrete structures are developed towards high-rise and large span building structures. In these cases, columns are subjected to large compressive loads and, if in a seismic region, they also support large shear forces and bending moments, which need large column dimensions. The use of high strength concrete would be useful and advantageous to reduce the volume of the columns and to increase the useful space of those structures. It is known that high strength concretes behave in a very brittle manner. To take advantage of the strength capacity of high strength concretes and to increase their ductility, concrete-steel composite members seem to be appropriate. The use of crowded lateral reinforcement in reinforced concrete structures can improve the ductility of high strength concretes, but this may cause problems in placing concrete because fresh, high strength concretes are normally very sticky. The use of steel tubes to confine high strength concrete is much better because they do not have this problem.

Research as early as 1903 showed that lateral confinement of concrete could increase the axial strength by multiples of the confining stress. The confining stress can be provided by hoop steel, spirals or continuous steel tube.

The benefit of using steel tubes for confining normal strength concrete has been investigated for years. Many studies on the performance of CFT columns have confirmed that the ductility and the strength of normal concretes increase dramatically. However, most of the research does not include combined axial load and cyclic moment behaviour. The behaviour of high strength concrete filled tubes is under investigation at many research institutions and universities.

1.2 Brief History of Concrete Filled Tubular (CFT) Columns

Concrete-filled tubular columns have become popular in design and construction in recent years. Their use as columns in multi-storey buildings has increased due to their large load-carrying capacity for a reduced cross-section. The most recent application of concrete filled steel tubular columns in structural building is in Tokyo, Japan. The Pacific

Century Place Marunouchi building, 150 m high with 32 stories above ground and 4 below ground scheduled to be completed in November 2001, has four CFT columns with 3.4 m diameter and 55 m high (Anonymous, 2000). Concrete filled steel hollow structural section (CFSHSS) columns have also been used in earthquake resistant structures, particularly in Japan, because of their inherent ductility. Investigations on applications of CFT columns in Europe in 1970's noted that normal strength CFTs had been used extensively for bridge piers.

The use of CFT columns dates back to the early 1900's when a number of bridges and buildings were built using these composite columns. The first reported use of CFT columns was for a road bridge in Great Britain in the late 1870's (Yamanouchi et al., 1998). Since then CFTs have been used in bridges and buildings primarily to resist large axial loads.

Research into the behaviour of composite columns has been in progress since the first tests on encased steel sections conducted by Burr in 1906 (Bradford, 1996). Extensive experimental testing on CFT columns was carried out at several research institutions throughout the world. Emperger (1907), Talbot and Lord (1912), and Mensch (1917) reported tests on composite columns (Munoz and Hsu, 1997).

The use of composite columns is well documented in Japan. Observations made after the Great Kanto earthquake of 1923 (Elnashai, 1998) noted that structures utilizing composite members sustained significantly less damage than reinforced concrete or steel structures. This gave an impetus to researchers to investigate the seismic design of composite structures.

In the early days of column research, test columns were subjected to concentric load and slenderness effects were extensively investigated. In the 1950's column research moved toward the behaviour of columns subjected to combinations of axial load and moment. Slenderness was included in the analyses by magnifying the end moments. More recently interest has moved to investigating the behaviour of columns under axial load but subjected to cyclic moments to represent the forces in columns under earthquake type loads.

Research into the behaviour of CFT columns intensified in the 1950's when researchers in Germany investigated the strength of CFT columns (Nethercot, 1995),

which were used in a variety of applications. Since then comprehensive investigations on the behaviour and performance of CFT columns under monotonic loadings have been conducted by a number of researchers, including Gardner and Jacobsen (1967), Gardner (1968, 1970), Furlong (1967, 1968), Knowles and Park (1969, 1970), Neogi et al. (1969), and the recently reported tests on high-strength CFT columns by Kilpatrick and Rangan (1999).

1.3 Behaviour of Concrete Filled Steel Tubular Columns

Concrete filled steel tubular (CFST), or CFT, columns are one of a number of composite structural members. Composite concrete-steel structural members are members in which steel and concrete act together through adhesion, mechanical interlock and friction, taking advantage of the strength characteristics of both materials. Composite members are designed to maximize the efficiency of the two materials by using, whenever possible, the concrete in compression and the steel in tension.

The initial idea of filling a pipe or tube with concrete is to make it stiffer. Later, investigations were conducted to determine the behaviour and performance of CFT members. Previous comprehensive studies on behaviour of CFT columns noted that CFT columns offer a number of advantages in both design and construction. From a fabrication point of view, the increased strength is obtained at no extra cost, since the steel tube provides permanent formwork for the concrete core, resulting in savings of time and the on-site cost of construction. In addition, it is generally accepted that the steel provides confinement to the concrete inside the tube, which will substantially increase the strength of the concrete core due to its triaxial state of stress. The steel tube also provides well-distributed reinforcement over the cross section, and provides protection of the surface of the concrete from physical damage. Finally, the column load capacity is increased by virtue of the fact that the concrete core in addition to its own strength contribution also helps to prevent inside local buckling of the steel tube resulting in an increase in the critical buckling load. Overall, CFT columns provide many advantages: the load carrying capacity and ductility of the columns are improved, and the speed of construction is increased.

In the early stages of loading, when levels of the longitudinal stress and strain are low, the steel tube has no restraining effect on the concrete core because the Poisson's ratio for concrete is lower than that of steel and the steel 'expands' away from the concrete core. However, as the longitudinal strain increases, the lateral expansion, Poisson's ratio, of the unconfined concrete gradually becomes greater than that of the steel and the concrete contacts the steel. Subsequently a radial pressure develops at the steel-concrete interface, restraining the concrete core and setting up hoop tension in the tube. At this stage, the concrete core is stressed triaxially and the steel tube biaxially, and as a result there is a transfer of load from the tube to the core. This results in a synergistic effect where the load carrying capacity of the composite column is appreciably greater than the sum of the individual compressive strengths of the steel tube and the concrete core (Neogi et al. 1969). Strictly speaking, this is applicable only to circular cross section columns, which develop significant confinement. For rectangular or square composite columns, it has been suggested that this is not always true (Shams and Saadeghvaziri, 1997).

1.4 Previous Research

Previous researches on CFT column systems include the experimental test programs by Furlong (1967, 1968) which involved assessing the strength of circular and square CFT columns and beam columns. The results of these tests demonstrated the benefits of filling a steel tube with concrete. The infilled concrete helped prevent local buckling of the tube's wall from occuring, causing an increase in strength relative to that of the empty steel tube to develop.

Recognizing the importance of developing design guidelines of reinforced concrete, steel and composite structures, U.S. and Japanese researchers formed a joint program of research in these areas, namely the U.S.-Japan Cooperative Earthquake Research Program, which began in 1979 (Goel, 1998). One of the topics in the fifth phase of this joint program was CFT column systems with prioritized research topics on determination of the effect of confinement versus composite action, determination of methods for evaluating axial, shear and flexural stiffness and resistance and ductility

under monotonic and cyclic loading, and determination of bond stress and shear transfer mechanisms between the steel tube and the concrete. In this research, connections and frame systems are also investigated.

A number of studies on the field of CFT columns, mainly with circular cross sections, have been done and reported elsewhere. Summarized investigations of the research on the CFT columns were reported by Aho (1996), Shams and Saadeghvaziri (1997), and Yamanouchi et al. (1998).

1.5 Research Needs

Most research on CFT columns has been done using circular section steel tubes. Short circular CFT columns demonstrate significant increases in load carrying capacity and deformability due to the triaxial state of stress in the concrete. However, triaxial effects do not seem to be significant for slender CFT columns with length to diameter ratios of 8 or greater. While it is unlikely that slender square section CFT's column would be able to develop significant strength enhancement, research on reinforced concrete columns has shown that closely spaced ties and longitudinal reinforcement can increase the ductility of such members.

An additional complication with square or rectangular section columns is that the applied moments may not coincide with the square axis of the cross section. The moment capacity of square section reinforced concrete columns about the diagonal axis can be 20 % less, depending upon the axial load, than the square axis moment capacity (Furlong, 1961; Row and Paulay, 1973).

Extensive research has been carried out in the past years on the behaviour of biaxially loaded reinforced concrete structural members and ultimate strength of composite columns, and the importance of the concrete stress distribution for an accurate analysis of reinforced concrete members has long been recognized. However, the available information on the stress distribution in biaxially loaded composite sections made of concrete-filled steel tubular columns is still limited.

Although several comprehensive studies have been made on the fundamental types of stress-strain relationships for normal and high-strength concretes, research is still needed on the behaviour of confined normal and high strength concrete.

The newly published NEHRP Provisions (1997) have guidelines for the design of seismic resistant connections involving steel reinforced concrete construction, based mostly on the research by Deierlein et al. (1989). However, no guidance was given to the seismic resistant design of square CFT columns.

The gradual development of concrete technology has promoted the use of high-strength concrete in the construction industry. Concrete technology has developed to an extent where concrete compressive strengths up to 100 MPa and higher can be produced without difficulties. There are, however, only a limited number of studies relating to the behaviour of high-strength concrete filled steel tubular columns under cyclic loading.

Columns in structural members subjected to axial compressive load or combined axial compressive load and bending moment are mostly under combinations of compressive load and biaxial bending moments. While the behaviour of reinforced concrete columns under biaxially eccentric axial loads, or axial loads and biaxial moments has been extensively investigated, investigations on the behaviour of square CFT columns under biaxial moments are limited.

Existing design criteria for composite steel-concrete structures, presented in design standards, codes and provision specifications, are fragmented among several different sources and are incomplete for some types of composite structures. This fact encourages researchers to intensively investigate topics related to performance of these types of structures.

1.6 Research Program

A research program was therefore planned and conducted at the University of Ottawa associated with the seismic performance of square CFT columns subjected to a combination of axial load and biaxial bending moment. The square CFT columns included normal-strength and high-strength concrete-filled square steel hollow structural section columns with two ratios of tube wall thickness to tube dimension.

1.6.1 Research Significance

The behaviour of normal-strength and high-strength concrete-filled circular section steel tubular columns under static or monotonic loading has been well investigated (Furlong, 1967, 1968; Gardner and Jacobson, 1967; Knowles and Park, 1969, 1970; Neogi et al., 1969; Tomii et al,1977; Lu and Kennedy, 1994; Zhang and Shahrooz, 1999; Kilpatrick and Rangan, 1999). However, there is relatively little research reported on the strength and behaviour of normal strength or high strength concrete filled steel tubular columns with rectangular or square cross-sections.

A review of the literature indicates that, although research on CFT columns has increased in recent years, information related to the seismic performance of CFT columns is still limited.

While an assortment of research has been conducted on circular CFT columns, there is a lack of research and knowledge on the subject of the seismic behaviour of square CFT beam columns subjected to combined axial load and biaxial bending moments.

Prior to the Northridge earthquake of January 17, 1994, and the Kobe earthquake of January 17, 1995, engineers believed that steel moment-frames would behave in a ductile manner. But investigations at both earthquakes showed a number of steel moment-frame buildings sustained significant damage (Hamburger, 2000). Referring to the damage caused by both 17th January earthquakes, it is necessary, and urgent, to pay more attention to the investigation of such column behaviour and their performance against seismic loading.

With the various possible orientations to place columns in the structural system in the building, square section columns can be subjected to diagonal, or biaxial, bending in seismic regions. At the present time there are no standards which cover the design of concrete-filled square steel tubular columns subjected to diagonal bending moment under seismic loading or biaxial bending moments, either for normal strength or high strength concrete

1.6.2 Research Objectives

The objectives of this study are to examine experimentally the seismic resistance of concrete-filled square steel hollow structural section columns under axial compressive load and biaxial bending moment for normal strength and high strength concrete, to develop analytical models to predict the seismic resistance of these columns, and to propose code design equations.

1.7 Scope of the Thesis

It was decided to limit the scope of the thesis to a study of the seismic resistance of concrete filled square steel HSS (HSS CFT) columns, for both normal strength and high strength concrete core. In this study, shear and torsion effects are not considered.

The studies included an extensive experimental program, which was done by testing twenty-four HSS CFT column specimens under constant axial compressive load and cyclic bending moment with horizontal displacement control. This experimental investigation included strength capacity, flexural stiffness and ductility of CFT beam-columns for 203x203x9.5 HSS and 203x203x4.8 HSS filled with either normal strength or high strength concrete.

The associated method of analysis should be required to be able to predict the seismic strength capacity of HSS CFT columns subjected to combined axial compressive load and biaxial bending moment. Based on this method of analysis, a simplified design code formula is proposed. The proposed method for determination of column strength capacity is a simplified column analysis based on section analysis and is easily adaptable to a code type format.

1.8 Thesis Outline

This thesis consists of seven chapters and an appendix, which follow conventional thesis format. The composition of this thesis corresponds approximately with the chronological sequence of events.

Work in the investigation began by reviewing the available published literature related to the work done to gain familiarity with the scope and methodologies of analysis and experimental programme. Existing papers on concrete mechanical properties, behaviour of high strength CFT columns, theory of column stability and biaxial bending of reinforced concrete and composite columns, square CFT columns, behaviour of composite sections and seismic behaviour of CFT columns are reviewed in Chapter 2. To determine the basic philosophy behind the design of composite columns, a number of codes were reviewed in this chapter.

The proposed methods of analyses on the seismic resistance of square CFT columns are presented in Chapter 3. The analyses of the strength capacity of the column sections were evaluated using simplified column analysis based on uniaxial approach.

The next significant step involved the design of the test program and design and construction of a testing frame. Two series of twelve beam-columns were constructed and tested for verification of the proposed method of analyses on the seismic resistance of square CFT columns subjected to a combination of constant axial compressive load and biaxial bending moment. One series used normal strength concrete and the other high strength concrete. The complete test program is presented in Chapter 4.

Chapter 5 presents the test results, evaluation of the test results and comparison of the test results to analytical results using proposed methods of analysis for normal strength CFT columns. In addition, an in-depth discussion of the seismic resistance of square normal strength CFT columns is presented at the end of this chapter.

For high strength CFT columns, test results, evaluation of the test results. discussion are given in Chapter 6. The evaluation includes strength capacity, ductility, flexural stiffnesses of the column specimens, and classification of column specimens. All evaluations are referred to the proposed methods of analysis discussed in Chapter 3.

A summary of the findings of this investigation is presented in Chapter 7 from which conclusions are drawn and recommendations for further work made. Recorded data from the tests are given in Appendix.

Chapter 2

LITERATURE REVIEW

2.1 General

This Chapter gives an overview of some selected literature available on topics relevant to the work covered in this investigation. Most of the studies consisted of an experimental investigation complemented with an analytical assessment of results. Reviews on experimentally based research are presented mostly in chronological order.

Reviews start with reported investigations on the mechanical behaviour of concrete, which includes the stress-strain behaviours of normal strength and high strength concretes in compression in both the unconfined and confined states, and the modulus of elasticity of plain concrete, with particular emphasis on passive confinement by a steel tube for the stress-strain behaviour of concrete. This is followed by a brief review of the behaviour of high strength concrete-filled steel tubular columns. The theory of column stability and biaxial bending of reinforced concrete and composite columns are also reviewed. Previous work on CFT columns reported in the literature is summarized with emphasis on the test results of square section columns. Moreover, selected published papers covering the strength of composite sections are reviewed. In addition, the review considers the seismic behaviour of composite columns. Finally, a number of codes, standards and specifications are reviewed to illustrate the basic philosophies behind the design of composite columns.

2.2 Mechanical Properties of Concrete

A brief review of published reports on the stress-strain behaviour of concrete in compression is presented. The review includes the stress-strain relationships of normal and high strength concretes, with and without confinement effects, under monotonic and cyclic loading.

The stress-strain relationship of normal strength concrete review is abstracted from Sargin's (1971) research. High strength concrete behaviour is illustrated by Nilson's (1994) investigation. In addition, ACI Committee 363 (1984) reported the state-of-the-art of high-strength concrete, where Saatcioglu and Razvi (1992, 1998) contributed their investigations on confinement effects of circular, rectangular and square reinforced concrete columns for both normal strength and high strength concrete. Finally, Bahn and Hsu's (1998) studies on the stress-strain behaviour of normal strength concrete under cyclic load is reviewed to demonstrate how cyclic load affects the behaviour of normal strength concrete columns.

To complete the review on the stress-strain behaviour of concrete in compression, studies on equivalent rectangular stress block are also reviewed. The review is based upon Ibrahim and MacGregor's (1997) research. The equivalent rectangular stress block model is often used to simplify the concrete section strength analysis.

2.2.1 Normal Strength Concrete

Sargin (1971) developed the general form of the concrete stress-strain relationship in compression from an extensive review of earlier work on the stress-strain relationship of concrete in compression. The stress-strain relationship of concrete in compression follows a definite pattern and consists of an ascending and a descending branches separated by a peak point. The stress-strain diagram passes through the original where it has a slope equal to the initial tangent modulus, E_c. Figures 2.1[1] shows schematically the stress-strain relationship of normal strength concrete. For a given aggregate, E_c is affected mainly by the concrete strength and the rate of loading. Sargin proposed a mathematical model for the stress-strain relationship of concrete in compression, which is a generalized version of the concrete stress-strain relationship proposed by Hognestad (1951), Desayi and Khrisnan (1964), and Saenz (1964). Hognestad's model of stress-strain curve of normal strength concrete in flexure is presented on Figure 2.2.

---

[1] Figures are given at the end of the Chapter

Figure 2.3 shows a comparison between concentric and eccentric stress-strain curve adopting from Sturman et al.'s investigation into the effect of flexural strain gradient on microcracking and stress-strain behaviour of concrete (Sargin, 1971). Sturman et al. concluded that the maximum stress and the corresponding strain of eccentric loading were 20% to 50% higher than that of concentric loading.

Sargin concluded that the shape of the concrete stress-strain curves was related to micro cracking. The proposed equation of compressive stress-strain relationship showed good agreement with the experimental results and with other available test data.

2.2.2 High Strength Concrete

ACI Committee 363 (1984) found that high-strength concretes have some characteristics and engineering properties that may be different from those of normal-strength concretes. The shape of the stress-strain curve for high-strength concrete is slightly different from that of normal strength concrete. The ascending part of the stress-strain curve is more linear and steeper for high-strength concrete, and the strain at the maximum stress is slightly higher for high-strength concrete. The slope of the descending part becomes steeper for high-strength concrete. High-strength concrete exhibits less internal micro cracking than normal strength concrete for a given imposed axial strain. The lower relative lateral expansion during the inelastic range may mean that the effects of triaxial stresses will be proportionally different for high-strength concrete.

Nilson (1994) reported studies on the compressive stress distribution of high strength concrete, where the shape of stress-strain curve in uniaxial compression of the high strength concrete was slightly different from that of normal strength concrete. The stress distribution in bending members of reinforced concrete structures could be modeled as trapezoidal distribution, which was close to the actual compressive stress distribution in the members. However, using a rectangular stress block approach in section analysis of reinforced concrete structures showed that the predicted strengths agreed with the analysis based on the actual stress block or trapezoidal distribution model. Comparative studies on this issue indicated that the rectangular stress block model

was perfectly satisfactory even though the results of calculation based on the rectangular stress distribution gave an upper bound.

Ahmad and Shah (1994) reported that confinement by spiral reinforcement is less effective for high strength concrete columns than for normal strength concrete columns.

Studies on the behaviour of high strength concrete by ACI committee 363 (1984) found that compressive stress distribution for high-strength concrete may be different from that of normal strength concrete. Experimental research has confirmed that differences do exist, and alternatives to the rectangular stress block have been proposed. However ACI 318R-77 suggests that rectangular stress block can be used to analyze cross-sectional strength of reinforced concrete members.

While high-strength concrete reaches its peak stress at a compressive strain slightly higher than that for normal strength concrete, the ultimate strain is lower for high-strength concrete. The constant value of strain at extreme concrete compression fiber at 0.003 prescribed by ACI 318-77 is seen to represent satisfactorily the experimental results for high-strength concrete, although it is not as conservative for high-strength concrete.

While the shape of the compressive stress block used may influence the calculation of column strength, ACI committee 363 found that trial calculations comparing rectangular stress block with trapezoidal stress block indicated only small differences.

2.2.3 Modulus of Elasticity and Poisson's Ratio of Concrete

Thoman and Raeder (1934) suggested that the modulus of elasticity could be determined by the slope of the tangent to the stress-strain curve in uniaxial compression at 25 percent of maximum stress. It was reported that the modulus of elasticity of concretes having compressive strengths ranging from 69 MPa to 76 MPa was from 29 GPa to 36 GPa. ACI committee 363 (1984) concluded that the ACI 318-77 expression overestimates the modulus of elasticity for concrete with compressive strengths over 41 MPa. An empirical equation for predicting elastic modulus for concretes having the

compressive strengths between 21 MPa and 83 MPa was proposed by Martinez et al (1982), as

$$E_c = 3320\sqrt{f_c'} + 6900 \text{ MPa} \qquad (2.1)$$

Many other investigators have reported values for the modulus of elasticity of high-strength concretes varying from 31 to 45 GPa depending on the method of determining the modulus.

Experimental data on values of Poisson's ratio for high-strength concrete are limited. Perenchio and Klieger (1978) reported the Poisson's ratio between 0.20 and 0.28 for normal weight high-strength concretes having compressive strengths ranging from 55 MPa to 80 MPa.

The modulus of elasticity of concrete equations recommended by Eurocode 2, ACI 318-99 and CSA A23.3-94, and Gardner's proposed equation for modulus of elasticity are presented as equations (2.2) to (2.5).

Eurocode 2: $E_{c28} = 9500\,(f_{cm28})^{1/3}$ (2.2)

ACI 318-99: $E_c = \gamma_c^{1.5}\, 0.043\sqrt{f_c'}$ (2.3a)

$$E_c = 4700\sqrt{f_c'} \qquad (2.3.b)$$

CSA A23.3-94: $E_c = (3300\sqrt{f_c'} + 6900)\sqrt{\left(\frac{\gamma_c}{2300}\right)^3}$ (2.4)

Gardner's: $E_c = 4300\sqrt{f_c'} + 3500$ (2.5)

2.2.4 Triaxial Behaviour of Concrete

The behaviour of concrete varies from brittle to very ductile according to the lateral confinement which can be provided either by outside constraints or by transverse reinforcement, which is the common case. All types of transversal reinforcement such as different ties, stirrups or steel sections can be used to provide this lateral confinement. The change of concrete behaviour according to lateral confinement yields the need for triaxial modeling of concrete.

Triaxial containment in CFT columns (Johnson and Buckby, 1979) was found only on circular CFT columns. The triaxial containment effects were indicated by the increase of CFT strength, where the additional strength occurs because the increase in compressive strength of the concrete core, which is restrained laterally by the surrounding steel tube, outweighs the reduction in the yield strength of the steel in vertical compression due to the circumferential tension needed to contain concrete. The containment effects were not present on rectangular CFT columns, except in the corner regions, because the hoop tension could not be developed.

The effects of containment in circular CFT columns reduce as bending moments are applied because the mean compressive strain in the concrete is reduced. The effects also diminishes with increasing slenderness of the columns, because bowing prior to failure increase bending moment and reduces the mean compressive strain in the concrete.

2.2.5 Confined Concrete

Saatcioglu and Razvi (1992) investigated confined reinforced concrete column behaviour. They reported that confined concrete has a similar stress-strain curve pattern, but with different stress-strain characteristics. Circular, square and rectangular columns with spiral, rectilinear reinforcements and welded wire fabric were evaluated to construct the stress-strain relationship for confined concrete. Saatcioglu and Razvi proposed that the confined concrete strength is a superposition of unconfined concrete strength and factored lateral pressure caused by confinement. The unconfined concrete strength is the plain concrete strength in a member under concentric loading, which may be different

from the strength measured using a standard cylinder test. It is believed that the unconfined concrete strength varies between 0.85 f_c' and f_c', where f_c' is the plain concrete strength of the standard cylinder test. The triaxial concrete strength expression in terms of uniaxial strength and lateral confinement pressure can be calculated as

$$f_{cc}' = f_{co}' + k_1 f_l \tag{2.6}$$

$$k_1 = 6.7 (f_l)^{-0.17} \tag{2.7}$$

in which f_{co}' and f_l are unconfined concrete strength and lateral confinement pressure respectively.

The proposed model consists of a parabolic ascending branch, linear descending segment, and a constant residual strength at 20 % of the maximum strength level. The descending segment is constructed by determining the strain corresponding to 85 % of the peak stress. Circular sections with close spaced circular spirals and vertical column reinforcement ensure uniform lateral pressure. Square columns and rectangular sections, on the other hand, experience non-uniform lateral pressure; therefore, they need special treatment to determine the confinement effect. An equivalent uniform pressure is employed to accommodate the non-uniform lateral pressure.

Saatcioglu and Razvi (1998) investigated experimentally the behaviour of confined high strength concrete columns. The experimental program was conducted by testing 26 high-strength concrete columns under concentric compression. The columns were designed to investigate the confinement parameters, distribution of longitudinal reinforcement and concrete strength. From the results, it was found that columns with higher-strength concretes showed steeper ascending branches and failed in a brittle manner at about 0.3 % strain.

Unconfined high-strength concrete columns under monotonically concentric compression are extremely brittle. Confinement by transverse reinforcement enhances the strength of the columns and the lateral pressure required to confine high-strength concrete columns can be provided either by increasing the volumetric ratio or the grade or yield strength of the lateral reinforcement.

2.2.6 Concrete Subjected to Cyclic Loading

Bahn and Hsu (1998) reported that load history has great influence on the stress-strain behaviour of concrete. The non-linear nature of the concrete stress-strain relationship subjected to cyclic loading cannot be easily described by mathematical formulas. Bahn and Hsu's experimental program investigated the behaviour of concrete under cyclic compressive uniaxial loading. The program covered four different loading regimes: monotonic loading, cycles to envelope curve, cycles to common point and cycles with random loading.

A generally accepted behaviour for concrete subjected to cyclic loading is the envelope curve which provides a bound between the upper limit and lower limit for the stress-strain curve. The unloading and reloading curves obtained in tests do not coincide and are not parallel to the initial loading curve. This implies that there is definite stiffness degradation for the entire strain range of stress-strain curve. The dominant characteristics of concrete behaviour are the behaviour of plastic strains, reloading strains, unloading curves, reloading curves for the entire range of strains. Figure 2.4 shows the cyclic envelope and monotonic stress-strain curve of the concrete.

2.2.7 Equivalent Rectangular Stress Distribution of Concrete

Ibrahim and MacGregor (1997) studied the use of the ACI rectangular stress block for high-strength concrete (HSC) and ultra high-strength concrete (UHSC) sections (HSC up to 100 MPa, and UHSC over 100 MPa). A series of data test results on 90 tests of concentrically and 94 tests of eccentrically loaded columns made from NSC, HSC and UHSC were used in the investigation.

The rectangular stress block was defined by the average stress block parameter, α_1 and parameter of the depth of equivalent rectangular stress block, β_1. In ACI 318-95, the parameter α_1 is assumed to have a constant value of 0.85, and the parameter β_1 is defined as

$$\beta_1 = 0.85; \text{ for } f_c' \leq 30\,\text{MPa} \tag{2.8}$$

$$\beta_1 = 0.85 - 0.008(f_c' - 30) \geq 0.65; \text{ for } f_c' > 30\ \text{MPa} \tag{2.9}$$

The maximum compressive strain is assumed to have constant value of 0.003.

Ibrahim and MacGregor proposed a modified rectangular stress block using the ACI procedure. To accommodate the advance in concrete technology, which covers HSC and UHSC, the expression of α_1 and β_1 should be adjusted. The following equations were chosen to represent the parameters α_1 and β_1

$$\alpha_1 = 0.85 - \frac{f_c'}{800} \geq 0.725 \tag{2.10}$$

$$\beta_1 = 0.95 - \frac{f_c'}{400} \geq 0.70 \tag{2.11}$$

For concrete strengths greater than 100 MPa, α_1 and β_1 are both taken constant and are equal to 0.725 and 0.70, respectively.

2.3 High Strength CFT Columns

From the previous section, it is obvious that high-strength concretes behave differently from normal strength concretes. The following section reviews the behaviour of high-strength concrete-filled circular steel tubular columns under monotonic or cyclic load, which include high-strength concrete-filled thin walled circular steel tubes, CFT columns under single and double curvature bending caused by eccentric compressive load at both ends, and short and long CFT column tests.

Boehme (1989) investigated the strength of thin walled circular steel tubes filled with high-strength concrete. Rangan and Joyce (1992) investigated the strength of eccentrically loaded slender steel tubular columns filled with high-strength concrete. Prion and Boehme (1994), and Kilpatrick (1996) investigated the behaviour of circular high strength concrete filled steel tubular columns. Prion and Boehme studied the beam-column behaviour of steel tubes filled with high-strength concrete under monotonic and cyclic loads. Kilpatrick's research was focused on the effects of the slenderness and

eccentricity of circular steel tubular columns filled with high-strength concrete in single and double curvature column tests.

Boehme (1989) conducted an investigation on the axial load and bending moment capacity of thin walled circular steel tubes filled with high strength concrete using a series of eighteen specimens, having 6-in outside diameter, 0.065 in wall thickness and D/t ratio of 92.3. Test results were compared to the calculations using the compatible strain model (used in Europe and the ACI code) and a superposition model used by the Japanese.

Boehme concluded that the compatible strain model adequately describes the behaviour of these specimens. Triaxial effects on the concrete core were found to be negligible in axially loaded short columns, although confinement of crushed concrete did improve the post ultimate bending capacity of the specimens.

Rangan and Joyce (1992) tested nine slender circular steel tubular columns filled with high-strength concrete. The columns, as pin-ended columns, were subjected to equal eccentric compressive load at both ends, which formed single curvature bending. The test parameters were slenderness ratio and eccentricity of the applied load.

Rangan and Joyce proposed a simple method for calculation of the strength of columns. In the calculation, it was assumed that a slender eccentrically loaded circular steel tubular column filled with concrete reached the axial load capacity when the maximum moment is equal to the ultimate bending moment at the midheight of the column calculated by performing an analysis for the cross-sectional strength at midheight. It was assumed that failure occurred when the extreme fiber compressive strain in the concrete reached a limiting value of 0.003, as in the ACI Building Code, and the stress-strain relationship of concrete followed Hognestad's model.

Rangan and Joyce concluded that the calculated column strengths were slightly conservative and became very conservative for columns with small eccentricities, perhaps due to the assumption of ultimate concrete strain.

Prion and Boehme (1994) conducted an experimental program consisting of four types of tests: short column, beam, beam-column and eccentrically loaded column tests. For beam-column tests, six circular cross-section specimens were tested monotonically to failure and two were subjected to cyclic loads. The latter specimens failed after 4 ½

cycles when loading was cycled at a level of two or three times the yield deformation. All the test specimens behaved in a relatively ductile manner.

Prion and Boehme concluded that the behaviour of high-strength concrete-filled thin steel tubes can be modeled using strain compatibility for the ultimate strength using a rational model that treats the steel and concrete components as separate elements for post-ultimate strength. The superposition model is appropriate to the fact that thin steel tubes do not provide sufficient confinement to develop the full capacity of the concrete. Because of local buckling of the tube wall, the plastic moment capacity of the steel section could not be developed. The concrete core was found to contribute significantly to the moment capacity of the members. Cyclic loading of the beam-column specimens demonstrated favourable hysteretic behaviour.

Kilpatrick (1996) tested a series of forty-one slender and stocky circular steel tubular columns filled with high-strength concrete under short term monotonically increasing applied longitudinal deformation. Slenderness and load eccentricity were studied for single and double curvature column tests. Three different levels of strain transfer were examined which corresponded to the conditions of full bond, partial bond, and no bond.

The test results on the slender columns showed reductions in strength as column slenderness or load eccentricity increased. Bond between concrete and steel was not important provided the concrete was confined longitudinally and laterally. The beneficial effect of confinement of the concrete appeared to be minimal with high-strength concrete and may diminish as flexure became increasingly dominant. The strength and flexural stiffness of columns increased for double curvature columns.

2.4 Column Stability

This section reviews the general theory of column stability, based upon steel column analysis, and columns under biaxial bending. The guide to stability design criteria for metal structures under the topics of column stability developed by Galambos (1998) is adopted in this review.

Galambos reported on the column stability of steel structures and composite structures. The theory of column stability for concentrically loaded, slender columns is clearly understood by using Euler column theory. The buckling load or critical load in Euler column theory is defined as

$$P_E = \frac{\pi^2 EI}{(kL)^2} \tag{2.12}$$

where EI is the elastic stiffness and kL is the effective length of the column. k can take values ranging from 0.5 to 2, depending on the end restraint. If the material is still elastic when buckling occurs, the strength of a perfectly straight prismatic column with perfect central loading and well-defined end restraints is the Euler load, P_E. Indeed, when the columns are no longer elastic, the Euler column theory is violated. Yielding reduces the stiffness of the steel columns. The inelastic behaviour of a column is radically different from the elastic column. The Euler buckling load is then modified depending upon the changes in stiffness due to yielding

Determining the maximum strength of steel columns is a complicated process because initial imperfections, material nonlinearities and / or residual stresses must be considered. Elastic columns can be designed based on the Euler column theory, but inelastic columns are usually designed with empirical column formulas. There are four column design formulas: empirical formulas based on the results of column tests, formulas based on the yield limit state, formulas based on the tangent-modulus theory, and the formulas based on the maximum strength. The maximum strength of steel columns depends on material properties, the residual stress magnitude and distribution, cross-sectional dimensions, the shape and the magnitude of the initial out-of-straightness, and the moment-rotation relationships of the end restraints.

2.5 Columns under Biaxial Bending

Virdi and Dowling (1973) evaluated an analytical method for obtaining the failure load of biaxially loaded composite columns using a series of nine tests on concrete

encased steel H section columns of varying lengths and varying biaxial eccentricities. Allowance was made in the theory for residual stresses and initial lack of straightness of the column was included by assuming an initial bow at midlength of $6x10^{-5}$ (L^2/D) about both axes, where D is the overall depth of the steel section in the plane considered. There was broad agreement between theory and test. This was probably because of the test columns being less imperfect than was assumed.

The biaxial failure load formula originally proposed by Bresler (1960) for reinforced concrete columns was recommended.

$$\frac{1}{P_{xy}} = \frac{1}{P_x} + \frac{1}{P_y} - \frac{1}{P_{ax}} \tag{2.13}$$

in which P_{xy} is the biaxial failure load, P_x and P_y are the failure loads in uniaxial bending, and P_{ax} is the failure load under axial loading when bending is constrained to occur about the x-axis. This formula was found to be uniformly conservative, in one case by as much as 48.5 %. The error arises partly in the proposed formula, which is a rough approximation to the true interaction surface, and partly in the right hand side terms, which are themselves conservative due to the accumulative effects of assumptions made in deriving the design method. For short columns, the errors are small enough to be acceptable, but a more economical method for long columns is needed.

Hsu (1988) proposed an equation of the failure surface to provide an alternative analysis of reinforced concrete columns subjected to combined axial load and biaxial bending moment. The proposed equation of the failure surface, as a general equation representing both the strength interaction diagrams and failure surface of reinforced concrete columns under combined axial load and biaxial bending moment, was expressed as

$$\left(\frac{P_n - P_{nb}}{P_o - P_{nb}}\right) + \left(\frac{M_{nx}}{M_{nbx}}\right)^{1.5} + \left(\frac{M_{ny}}{M_{nby}}\right)^{1.5} = 1.0 \tag{2.14}$$

in which P_n = nominal axial compression, P_o = maximum nominal axial compression, M_{nx}, M_{ny} = nominal bending moments about x- and y-axis, respectively, P_{nb} = nominal axial compression at balanced strain condition, and M_{nbx}, M_{nby} = nominal bending moments about x- and y-axis, respectively, at balanced strain condition.

A total of 21 square and rectangular sections of short and tied reinforced concrete columns were analyzed by the proposed equation of failure surface. The results of the study showed that the proposed failure surface equation gives a simpler analytical tool to determine the ultimate strength of the columns than other methods.

Galambos (1998) summarized investigations of beam-columns subjected to combined axial load and biaxial bending moment. The general form of interaction formulas for beam-columns subjected to a combination of axial load and biaxial bending moment can be approximated as

$$f\left(\frac{P}{P_u}, \frac{M_x}{M_{ux}}, \frac{M_y}{M_{uy}}\right) \le 1.0 \tag{2.15}$$

For design purposes it is convenient to separate the problem into two phases: short columns, and intermediate and slender columns. Strength of short columns can be expressed as

$$\frac{P}{P_y} + 0.85\left(\frac{M_x}{M_{px}}\right) + 0.6\left(\frac{M_y}{M_{py}}\right) \le 1 \tag{2.16}$$

in which the different coefficients for the two moment terms are a reflection of the different shapes of the uniaxial interactions.

Predictions that are more accurate may be obtained using

$$\left(\frac{M_x}{M_{px}}\right)^{\alpha} + \left(\frac{M_y}{M_{py}}\right)^{\alpha} \le 1 \tag{2.17}$$

$$\alpha = 1.6 - \frac{P/P_y}{2\ln(P/P_y)} \tag{2.18}$$

in which M_{px} and M_{py} are the moment capacities about the respective axes, reduced for the presence of axial load, and P_y is column axial load at full-yield condition. The moment capacities may be obtained from

$$\frac{P}{P_y} + 0.85\left(\frac{M_0}{M_p}\right) \le 1 \quad ; \quad M_0 \le M_p \tag{2.19}$$

in which M_o and M_p are applied-end moment and plastic-bending moment respectively.

The strength of intermediate and slender columns for hollow square and rectangular box sections may be obtained by employing Pillai's (1974) expression

$$\frac{P}{P_u} + C\left[\frac{C_{mx}M_x}{M_{ux}(1-P/P_{ex})} + \frac{C_{my}M_y}{M_{uy}(1-P/P_{ey})}\right] \le 1 \tag{2.20}$$

in which

$$C = \frac{(e_x^2 + e_y^2)^{1/2}}{e_x + e_y} \tag{2.21}$$

where e_x and e_y are eccentricities about the respective axes.

Tebedge and Chen (1974) proposed a nonlinear expression of strength of intermediate and slender columns as

$$\left(\frac{C_{mx}M_x}{M_{ucx}}\right)^{\eta} + \left(\frac{C_{my}M_y}{M_{ucy}}\right)^{\eta} \le 1 \tag{2.22}$$

for square box sections, η should be taken as

$$\eta = 1.3 + \frac{1000}{(L/r)^2}\frac{P}{P_u} \geq 1.4 \qquad (2.23)$$

Theoretical procedures for assessing beam-column strength under biaxial loading are rather complex, so that even in the elastic range numerical solutions are required.

2.6 Square CFT Column Tests

A number of published papers are reviewed, starting with Furlong (1967), followed by Tomii and Sakino's (1979), and Matsui and Tsuda's (1987) studies on the strength and behaviour of concrete-filled steel square tubular beam-columns with large width-thickness ratios, and ending with Lu and Kennedy's (1992) investigation on the flexural behaviour of concrete-filled square hollow structural section columns.

Furlong (1967) conducted 22 square composite column tests, 17 columns were tested under combinations of axial load and bending moment and 5 columns subjected to axial load only. He proposed methods of strength analysis for axially loaded columns and columns subjected to combined axial compressive load and bending moment. For the axially loaded columns, the squash load was determined by calculating superposition of concrete strength and steel strength of the column section. Concrete strength was calculated based on f_c' rather than $0.85 f_c'$ as used for ordinary reinforced concrete. For the columns under axial load and bending moment, the lower limit of bending moment was taken as the plastic moment capacity of steel tube alone. Test results showed good agreement to the proposed method of analysis for axially loaded columns. For columns under combined axial load and bending moment, however, the estimate strength capacity was undesirably low.

Tomii and Sakino (1979) tested a series of 36 square section specimens to examine the moment-thrust-curvature characteristics of square sections under fixed axial loads and increasing uniform bending moments.

Tomii and Sakino proposed a method for determining the ultimate moment that used the value of concrete stress, f_c' recommended by Furlong. The procedure is the same as used by the ACI for reinforced concrete design. It was found that their proposed

method is less conservative for the columns subjected to axial loads greater than 0.58 times the squash load. The squash load was defined as superposition of the strength of concrete and steel for short column under concentric axial load.

Tomii and Sakino concluded that the magnitude of constant axial load and wall width-thickness ratio of steel tube had a significant effect on an inelastic behaviour of concrete-filled square steel tubular columns subjected to combinations of axial loads and bending moments.

Matsui and Tsuda (1987) tested a total of 26 specimens to study the strength and behaviour of concrete-filled steel square tubular beam-columns with large width-thickness ratios under constant vertical and varying horizontal loads. It was observed that the restoring strength of empty tubular columns decreases rather rapidly at the occurrence of web local buckling after local buckling of the tube flanges.

Ultimate strength of composite sections was calculated by assuming fully plastic stress distribution on both materials. The test results showed that concrete-filled steel square tubular columns subjected to monotonic transverse and axial compressive load can attain the strength calculated from the fully plastic stress distribution. The width-thickness ratio of these tubes ranged between 47 and 94. The u timate strength of concrete-filled steel tubular columns can be fairly well predicted by fully plastic section analysis. The deformation capacity of concrete-filled tubular columns is much larger than that of empty steel tubular specimens. It was recommended that the limit of width-thickness ratio of a concrete-filled steel tube could be increased to twice that for empty tubes.

Lu and Kennedy (1992) investigated the flexural behaviour of concrete-filled hollow structural sections. The investigation covered four different cold-formed square and rectangular steel hollow structural sections with two-point loading providing a constant moment region to investigate the flexural characteristics of the steel sections alone and of concrete filled sections. For steel alone, the flexural resistance depends on the maximum strains that can be developed before local buckling occurs. All specimens were loaded monotonically to failure.

The behaviour of composite beam sections showed an initial elastic response followed by inelastic behaviour with gradually decreasing stiffness until the maximum

moment was reached. Failure occurred when an outward buckle of the top flange of the steel section developed in the constant moment region. The moment-curvature diagrams showed that concrete-filled steel hollow structural sections increased significantly the capacity over an empty hollow structural section. A proposed model of composite section analysis based on rectangular stress block on steel stress taken as the average corresponding to steel strain at 0.014 in compression and at 0.023 in tension.

2.7 Behaviour of Composite Sections

To date, many studies on the strength of composite sections have been published. The published papers cover the strength of concrete-encased steel structural section columns and concrete-filled steel tubular columns. In this review, both composite column types are presented. Because of the limited space available, only the papers by Basu (1967), Basu and Sommerville (1969), Johnson (1975), Lachance and Hays (1980), Lachance (1982), Dunberry et al. (1987), Cai (1987), Zhang and Shahrooz (1999) are taken as representative among a numbers of papers collected in this study. It does not mean that other investigations are less important to the subject being studied.

Basu (1967) did research on composite columns at Imperial College. The research covered theoretical analysis for the ultimate strength of pinned-ended concrete encased steel sections and concrete-filled rectangular hollow sections, subjected to any combination of end load and end moments about one or both of the two principal axes. A wide range of columns having different cross-sections and slendernesses were considered, and Basu found that the behaviour of such columns could be predicted by four parameters.

Basu and Sommerville (1969) proposed ultimate strength design method for composite columns which covered concrete encased steel sections and concrete-filled rectangular hollow sections. The method was applicable to pinned-ended uniform composite members, having a cross-section symmetrical about two perpendicular axes, and subjected to axial load and combination of end moments.

Johnson (1975) discussed composite columns which covered concrete-encased steel columns and concrete-filled steel tubular columns for composite column design.

Composite column design is based on the ultimate-strength design method of Basu and Sommerville.

The method of computing the load-deflection curve and the maximum load for an eccentrically-loaded concrete-filled steel tubes had been developed at Imperial College and compared with the results of tests on columns of circular cross-section. It was assumed that plane sections remained plane and that the uniaxial stress-strain curves for steel and concrete are applicable. There is a tendency for separation to occur between concrete and steel tube at low stress because concrete has a lower Poisson's ratio than steel at this stage. At high compressive stresses, internal micro cracking in the concrete causes it to "swell" and its "apparent" Poison's ratio increases. Its outwards movement is restrained by the steel, which confines the concrete. The increase in strength of the concrete due to the confinement is more than the loss of longitudinal compressive strength of steel due to circumferential tension. Furlong (1968) and Sen (1969) studied the increase in the strength of the column due to this effect. The confinement of the composite columns decreases with increasing slenderness and increasing eccentricity of loading, but it is not significant in square and rectangular composite column sections.

A computer program developed by Neogi, Sen, and Chapman (1969) was used to calculate ultimate loads for pin-ended filled tubes of circular, square and rectangular hollow sections, and the results have been published as design tables.

Lachance and Hays (1980) developed a general nonlinear theory for determining the static ultimate strength of reinforced concrete composite sections under combined axial load and uniaxial bending moment. The analysis is based upon a general nonlinear theory derived for one, two or three different materials having arbitrary stress-strain curves. The study is limited to a sectional theory, in that buckling of the member is not considered. It is well known that the stress-strain diagrams obtained experimentally from plain concrete cylinders do not necessarily represent accurately the real behaviour of reinforced concrete.

The results of the nonlinear computer analysis of steel wide-flange sections encased in reinforced concrete indicated that neglecting the concrete tensile strength gives an error of 0.01 %. The maximum difference between the results obtained by concrete stress-strain curves corresponding to ultimate compressive strains of 0.003 and

0.004 was 9 %. Residual stresses had no influence on ultimate strength capacity of composite sections.

Lachance (1982) developed a mathematical model for arbitrary composite sections subjected to combined axial load and biaxial bending. Twelve different types of concrete stress distribution were used to analyze different composite sections. Three basic shapes of concrete stress-strain diagrams were used for allowable compressive strain and ultimate strength.

As the previous research by Lachance and Hays (1980) had found that residual stresses have no influence on the ultimate strength capacity of composite sections, residual stresses were not considered in the analysis.

From the investigation, Lachance found that the shape of concrete stress-strain diagram has little effect on either ultimate curvature or ultimate biaxial bending capacity of composite sections. The maximum permissible strain in the concrete influences both strength and deformation.

Dunberry et al. (1987) reported a test program that included rectangular steel columns filled with concrete under axial load. Four series of specimens were loaded to failure, which consisted of steel columns, composite columns loaded on both materials, and composite columns loaded part on top of the column and part at the connection. The strength capacity of the specimens was best described as the squash load capacity of the composite short columns. The squash load was shown to accurately predict the ultimate strength of square concrete-filled hollow structural sections, but underestimated the capacity of concrete-filled circular steel tubes. Test results showed that the failure loads lie close to or above the predicted squash load.

The experimental results demonstrated the predominant failure mechanism to be local buckling. A significant difference in local buckling modes between steel and composite specimens could be anticipated. Local buckling usually occurred after yielding of the steel, and any improved buckling behaviour due to presence of the concrete would not result in a significantly higher steel load capacity.

The axial compressive strength capacity of a short composite column loaded at the beam connection is lower than when it is loaded in direct bearing. The maximum strength reduction is about 8 % of the strength of composite column loaded in direct

bearing. Local buckling of the steel tube below the connection was the primary cause of failure. The load transfer mechanism is dependent on the length of the connection, its ability to rotate and the eccentricity of load on the connection.

Cai (1987) conducted research in seven phases of tests on concrete-filled circular steel tube columns, which covered concentrically loaded short and long columns, pure bending members, eccentrically loaded columns bent in single curvature with equal eccentricities at both ends and with eccentricity at only one end, columns bent in double curvature, and restrained cantilever columns.

The tests showed that the concrete-filled steel tube columns behaved in a ductile manner and the influences of loading conditions and slenderness ratio ($L/D \leq 4$) on the ultimate strength of short columns are not pronounced. The ultimate strength of short columns under axial load was calculated using the limit equilibrium method of Gvozdev (1934), who was the pioneer of determining the collapse load of concrete-filled steel tube columns by this method, which employed the basic assumptions: at limit stage, the concrete core is stressed triaxially and the steel tube biaxially; yielding of the steel tube is governed by the Von Mises yield criterion.

Cai proposed equations for obtaining the ultimate strength of concrete-filled steel tubular columns. The ultimate strength of short columns under axial load was proposed as

$$N_o = A_c f_c' (1 + \alpha\Phi) \tag{2.24}$$

$$\alpha = 1.1 + 1/\sqrt{\Phi} \tag{2.25}$$

$$\Phi = A_s f_s / A_c f_c' \tag{2.26}$$

For long columns under axial load

$$N_u = \varphi_l \varphi_e N_o \tag{2.27}$$

$$\varphi_l = 1 - 0.115 \sqrt{L_o/D - 4} \tag{2.28}$$

$$\varphi_e = \frac{1}{1+1.85\frac{e_o}{r_o}} \tag{2.29}$$

in which L_o, D, e_o and r_o are length, diameter, assumed equivalent eccentricity, and polar radius of gyration of the cross section about its shear center of the column, respectively. For standard columns subjected to combined axial and uniaxial bending moment

$$\frac{N_u}{\varphi_1 N_o} + 0.74\frac{M_u}{\varphi_1 M_o} = 1 \tag{2.30}$$

$$\frac{M_u}{\varphi_1 M_o} = 1 \tag{2.31}$$

The strength of cantilever columns can be converted to that of an equivalent end supported standard column whose length and end loading combination are identical to those of the cantilever column considered.

Zhang and Shahrooz (1999) evaluated the applicability of the ACI standard procedure for the analysis of concrete-filled steel tubular columns. Preliminary studies showed that the ACI standard procedure could reliably be used for computing capacity of concrete-filled tubes provided normal strength steel tubes were used.

Zhang and Shahrooz's proposed procedure was based on the ACI standard procedure assuming that the steel tube has fully yielded when the cross-sectional capacity is developed and the maximum concrete strain will be greater than 0.003. In this model, a concrete-filled tube is divided into a sufficiently large number of steel and concrete layers. Idealization of steel and concrete constitutive relationships is a very important step in fiber analysis. Local buckling of steel tubes in concrete-filled tubes is not as critical as that for hollow steel tubes. Well-established confined concrete models for reinforced concrete members (e.g. Mander's model, Sheikh and Uzumeri's model, and

Saatcioglu and Razvi's model) were considered not applicable to concrete-filled steel tubular columns.

The ACI standard procedure for section analysis of reinforced concrete columns predicts the capacity of short concrete-filled steel tubular columns made with normal strength tubes filled either with normal or high-strength concrete. Capacity of slender concrete-filled steel tubular columns computed by the ACI moment magnifier method, is reasonably close to that computed based on second-order analysis in which the material and geometric nonlinearities are taken account.

2.8 Seismic Behaviour of Composite Columns

Aboutaha and Machado (1999) experimentally investigated cyclic response of steel-tube high-strength reinforced concrete (STHSRC) columns by testing three STHSRC and three ordinary reinforced concrete (ORC) columns subjected to constant axial loads and cyclic lateral load/displacement.

Test results showed that STHSRC exhibit better seismic resistance than ORC columns, particularly when subjected to high axial compressive loads. Aboutaha and Machado concluded that the steel tube improved column strength, stiffness and ductility. Although the strength is increased insignificantly, steel tube can maintain very large displacement. A rectangular steel tube with maximum width to wall thickness ratio (b/t) of 38 may be used successfully to confine high-strength columns to enhance column ductility.

Ricles and Paboojian (1994) studied experimentally the seismic behaviour of steel-encased composite columns subjected to combined axial, flexural, and shear loading. The experimental program involved eight specimens.

The analysis involved modeling the cross-section as a media of discrete fibers, each fiber possessing its own material characteristics corresponding to either steel or concrete. Full strain compatibility between steel and concrete was assumed, with plane sections remaining plane. The concrete constitutive law was based upon that proposed by Mander et al., where the effect of confinement of the concrete on its stress-strain relationship is considered. The displacement ductility is the ratio of displacement, Δ, to

the displacement at yield, Δ_y. The displacement Δ_y refers to the displacement at the nominal ACI flexural capacity, M_{ACI} (with all strength reduction factors having a value of ϕ = 1.0) under combined loading, and corresponding to full composite action. The displacement Δ_y was experimentally determined by dividing the measured lateral displacement corresponding to the column base moment of 0.75 M_{ACI} by a factor of 0.75.

Test results showed that the steel-encased composite columns have exceptional cyclic strength and ductility if adequate confinement of the concrete core surrounding the structural shape is provided in the flexural plastic hinge zone. The flexural capacity of composite columns under combined axial and lateral loading was found to be accurately predicted by analytical models based upon full composite action. The ACI and AISC-LRFD provisions for composite column strength are conservative in prediction of flexural capacity under combined axial and flexural loading. The flexural stiffness of steel-encased composite columns is well approximated by $0.5E_cI_g$. For seismic resistance design, the test results indicate that it would be reasonable to rely on only the shear capacity of the encased W-shape.

2.9 Codes Review

This section summarizes the basic philosophy behind some design codes in the design of composite columns, especially for concrete filled steel tubular columns. There are great differences between the concrete codes and the steel codes in design provisions for composite columns. The codes reviewed in this section include the Architectural Institute of Japan (AIJ) Standard, Eurocode 4 (1984 and 1994), AISC-LRFD (1986 and 1994) provisions, CAN/CSA-S16.1 (1984 and 1994), CSA Standard A23.3-94, ACI 318-95 and ACI 318-99.

Wakabayashi (1987) reviewed the AIJ Standard. In Japan, concrete-filled steel tubes were first applied to columns of subway stations, and then as columns in buildings. The first and second editions of the standard for structural calculation of mixed tubular steel-concrete composite structures of the AIJ were published in 1967 and 1980. The design method employed in the fourth edition of the AIJ Standard (1987) is basically allowable stress design supported by elastic analysis of the structure. The calculation of

the allowable strength of members is based on the superposed strength method. The standard also contains methods for calculating the ultimate strength of members based on the superposed strength method.

Stark (1987) reviewed Eurocode 4. The first draft of Eurocode 4 was completed in English in October 1984. It had to be consistent with the August 1983 draft of Eurocode 2 (concrete structures) and the July 1983 draft of Eurocode 3 (steel structures). These codes were written in a limit state design format. For steel sections, Eurocode 4 uses the same classifications of cross-sections as Eurocode 3; plastic, compact, semi-compact and slender.

Two simplified design methods are given for composite column design. The first method was developed at the University of Bochum and makes use of the European column curves, given in Eurocode 3. This is a simple method of calculating the interaction curve between axial load and bending moment for a specific cross-section. The basic parameters are the squash load, the ultimate moment capacity of the cross-section and the Euler critical load of the column. An extra factor 0.9 is applied to account for the use of the rectangular stress block as well as other approximations. The second method for composite columns was developed at Warwick University. It is quicker to use but limited in scope.

Johnson and Anderson (1993) published the explanation of the Eurocode 4 in "Designers' Handbook to Eurocode 4 Part 1.1". The first draft of Eurocode 4 was prepared in 1983-84. The current (1994) text of Part 1.1 was developed from the 1985 draft. It was affected by substantial changes in Eurocode 2 and Eurocode 3 between 1984 and 1992, by new research, by developments in practice, and by comments from the member states of the EEC.

The design of composite columns by the Eurocode 4 is a strength design method. Resistance of cross-sections to axial loads is defined by the plastic resistance, the ultimate axial load that a short column can sustain assuming that the structural steel and reinforcement are yielding and the concrete is crushing. For concrete-filled sections, a coefficient of 1.0 is applied on the concrete strength instead of 0.85 in encased sections. This is because the concrete component develops a higher resistance because of confinement by the steel section. In all tubes filled with concrete, the effect of

confinement reduces as bending moments are applied; this is because the mean compressive strain in the concrete and the associated lateral expansion are reduced.

The section analysis begins with a squash load calculated by combining the resistance of the steel, concrete, and reinforcement which is modified for the slenderness of the column. The squash load for concrete-filled rectangular tubes is defined as

$$N_{pl,rd} = A_s \frac{f_y}{\gamma_s} + A_c \frac{f_c'}{\gamma_c} + A_r \frac{f_{yr}}{\gamma_r} \tag{2.32}$$

in which subscripts s, c and r indicate steel, concrete, and longitudinal steel reinforcement respectively, and γ indicates partial safety factor of related material.

For concrete filled circular tubes, confinement of the concrete can be taken into account when the slenderness ratio of the column λ is less than or equal to 0.5 and the load eccentricity e is less than or equal to d/10, where d is the outside diameter of the steel tube. Length effects are handled with a different approach than in U.S. codes. The slenderness parameter of the column is defined by

$$\lambda = \sqrt{\frac{A_s f_y + 0.85 A_c f_c' + A_r f_{yr}}{P_e}} \leq 2.0 \tag{2.33}$$

$$P_e = N_{cr} = \frac{\pi^2 (EI)_e}{(kL)^2} \tag{2.34}$$

$$(EI)_e = E_s I_s + E_c I_c + E_r I_r \tag{2.35}$$

When composite columns experience moments about two principal axes simultaneously, failure will occur in a biaxial mode, represented by an interaction surface. No convenient method of defining the biaxial interaction surface has been found. Simplified interaction formulae are therefore used in design, based on separate calculations for uniaxial design moments about each principal axis.

Pinkham (1987) reviewed the 1986 AISC-LRFD specifications. The 1986 AISC-LRFD specifications were the result of a research project whose aim was to develop design criteria for steel buildings based on the use of first-order probabilistic principles. During this development, the name of Load and Resistance Factor Design was applied to the design method in order to emphasize the use of factors on both the load and the resistance sides of the design equation.

In the LRFD Specifications, design provisions are also provided for steel tubular shapes filled with concrete. The design of composite columns is based on the design equations for steel columns with the slenderness and area parameters modified for the presence of the concrete. The interaction of axial compression and flexure on composite column sections uses the general method provided in the AISC-LRFD specifications for steel section alone with some slight modifications. A number of limitations are provided in order to qualify a column as composite. Steel shape shall be at least 4% of the gross composite column area. Concrete strength, f_c', shall be at least 20 MPa and not more than 55 MPa. The maximum specified yield stress of the steel shape should not exceed 380 MPa. The minimum wall thickness shall be $b\sqrt{f_y/3E_s}$, where b is the width of each face of filled rectangular tubing.

The American Institute of Steel Construction (1994) uses similar philosophy and procedures of column design to both in LRFD and in ASD (Allowable Stress Design). There are two equations governing column strength that based on the limit state of flexural buckling: an equation for inelastic buckling and one for elastic buckling. Both equations include the effects of residual stresses and initial out-of-straightness. The boundary between inelastic and elastic buckling is $\lambda_c = 1.5$, where

$$\lambda_c = \frac{kL}{r\pi}\sqrt{\frac{f_y}{E_s}} \tag{2.36}$$

For $\lambda c \leq 1.5$, the inelastic buckling equation is

$$F_{cr} = \left(0.658^{\lambda_c^2}\right) f_y \tag{2.37}$$

For $\lambda_c > 1.5$, the elastic buckling equation is

$$F_{cr} = \left(\frac{0.877}{\lambda_c^2}\right) f_y \tag{2.38}$$

Chapter I of the AISC-LRFD Specification covers composite members, which include concrete-encased and concrete-filled steel columns and beam columns. Composite design assumes that the steel and concrete work together in resisting loads. The design philosophy of the AISC-LRFD method is to create modified cross-sectional properties, strength, modulus of elasticity, and radius of gyration for the composite columns and then employ the steel column formulae to design composite columns with substitution of the related parameters of both column materials. As a simplification for concrete-filled steel tubular columns, the nominal flexural strength of the composite section can be taken equal to plastic moment capacity for composite section, which comes from the steel tubes only. In order to use the AISC-LRFD procedures, the limitations given in the 1986 AISC-LRFD should be satisfied.

The Canadian Steel Codes, CAN3-S16.1-M84 (CISC, 1985) also recommend design procedures for composite columns. CAN3-S16.1-M84 classifies sections of compression elements, based on width-thickness ratios, into 4 classes: class 1 sections (plastic design sections), class 2 sections (compact sections), class 3 sections (non-compact sections) and class 4 sections. Concrete-filled hollow structural sections of class 1, 2, or 3 sections may be assumed to carry compressive load as composite columns. Concrete-filled hollow structural sections of class 4 sections may also be designed as composite columns if the width-thickness ratios of the walls do not exceed $1350 / \sqrt{f_y}$ or $28000 / f_y$ for rectangular sections or circular sections, respectively.

CAN/CSA-S16.1-94 (CISC, 2000) extended the recommendations of CAN3-S16.1-M84. Clause 18 of CAN/CSA-S16.1-94 discusses composite members consisting of steel hollow structural sections (HSS) filled with concrete. The strength of CFT columns subjected to axial compression and bending may be calculated using either Method 1 (Bending resisted by composite section) or Method 2 (Bending assumed to be

resisted by the steel section alone). In Method 1, both steel and concrete resist axial compressive load and bending moment proportionally. On the other hand, in Method 2, only axial compressive load is resisted by both materials, the bending moment is resisted by steel only. Method 1 is more rational because it considers composite interaction between the two materials, and the strength is developed by the composite section.

CSA Standard A23.3-94 Design of Concrete Structures (1994) recommended the design of composite columns with a concrete core encased by structural steel should be in accordance with CAN/CSA-S16.1. In general, the structural steel elements shall be designed in accordance with CSA Standard S16.1 for any construction or other load applied prior to the attainment of composite action.

ACI 318-95 requires a sectional analysis similar to that for normal reinforced concrete columns in order to calculate the cross-sectional strength. Slenderness effects are treated similarly to those for reinforced concrete columns. Using a magnified moments to account for slenderness effects, the composite column strength may be expressed as

$$M_c = \delta_{ns} M_2 \tag{2.39}$$

where

$$\delta_{ns} = \frac{C_m}{1 - \frac{P_u}{0.75 P_c}} \geq 1.0 \tag{2.40}$$

in which P_u and P_c are ultimate applied axial compressive load and critical load respectively. For members with transverse loads between supports, $C_m = 1.0$, and without transverse loads

$$C_m = 0.6 + 0.4 \frac{M_1}{M_2} \geq 0.4 \tag{2.41}$$

M_1/M_2 is positive if the column is bent in single curvature.

$$P_c = \frac{\pi^2 EI}{(kL)^2} \tag{2.42}$$

in which

$$EI = \frac{(E_c I_g / 5)}{1 + \beta_d} + E_s I_t \tag{2.43}$$

As for reinforced concrete cross sections, the strengths of composite columns are limited to 0.8 P_u for encased shapes and 0.85 P_u for CFT columns. The limitations of wall thickness in ACI are the same as those in AISC-LRFD. While the allowable reinforcement ratios for non-composite compression members are between 1 and 8 %, no statement is made for composite compression members.

The capacity of a composite column subjected to combined axial and flexural loading is based on satisfying strain compatibility and equilibrium to develop a moment-axial load interaction relationship for member capacity. A maximum concrete compressive strain of 0.003 and the Whitney stress block, having a magnitude of 0.85 f'_c, is used for the concrete, where f'_c is the concrete compressive strength.

ACI Committee 318 (1999) recommended the same rules be used for computing the load-moment interaction strength of reinforced concrete sections and concrete-filled tubing sections. The procedures for determining the capacity of composite columns subjected to combined axial and flexural bending moment are the same as those in the previous codes (ACI 318-95). There is a revision in the provisions for slenderness effects in compression members in the ACI 318-95 to better recognize the use of second-order analyses.

For composite columns in which the steel tube makes up a large percentage of the cross-section, the load transfer due to creep is not significant; therefore, in determining

the flexural stiffness of compressive members, only the flexural stiffness of the concrete is reduced for sustained load effects.

2.10 Summary

Stress-strain relationship of concrete in compression can be modelled using one among available proposed models. Hognestad's stress-strain relationship model of concrete in compression is widely used as a basic model of both unconfined and confined concrete.

Strength section analysis of reinforced concrete members uses an equivalent rectangular compressive concrete stress distribution, concrete stress-strain model is less important. Investigations confirmed that using equivalent stress distribution in section analysis is reasonably acceptable. Each reinforced concrete design code uses unique equivalent stress distribution model. Ibrahim and MacGregor investigated the equivalent stress distribution of normal strength, high strength and ultra high strength concrete. This investigation was designed to cover wide variety of concrete.

Strain rate affects concrete strength. Concrete strength increases when strain rate is increased. Investigations showed that the compressive strength of concrete increased about 5 to 20 % for concrete subjected to earthquake loading.

It was recognized that high strength concrete is more brittle than normal strength concrete. Confinement by spiral reinforcement is less effective for high strength concrete.

Recommended codes formulas of modulus of elasticity of concretes are between 80 % and 120 % of the measured values.

Studies on confined concrete columns showed that circular reinforced concrete columns or circular CFT columns experienced more effective confinement than those of rectangular or square columns. Rectangular or square tubes confined concrete core effectively at the corners but less effective at sides of section columns. Investigations showed that no confinement effect was found on slender rectangular and square CFT columns. Investigations on short columns showed some results with confinement effect and some others without confinement effect. Aboutaha and Machado concluded that a

rectangular steel tube with maximum width to thickness ratio of 38 might be used successfully to confine high strength reinforced concrete columns.

The ACI standard procedure for section analysis of reinforced concrete columns well predicted the capacity of short CFT columns under monotonic loading. Investigations showed that the predicted strengths of CFT columns under monotonic loading reasonably agreed to the test results.

Research confirmed that thin steel tubes did not provide sufficient confinement to develop the full capacity of the concrete. Matsui and Tsuda recommended that the limit of width-thickness ratio of CFT columns could be increased to twice of that for empty tubes.

Tomii and Sakino's proposed method of analysis for strength of square CFT column under monotonic loading, using modified ACI procedure for section analysis of reinforced concrete columns, showed good agreement to the test results for columns under axial load less than 58 % of squash load but less conservative for axial load greater than 0.58 times the squash load.

It can be concluded that reinforced concrete column section analysis with some manipulation would reasonably well predict strength capacity of square HSS CFT columns subjected to axial compressive load and cyclic bending moment.

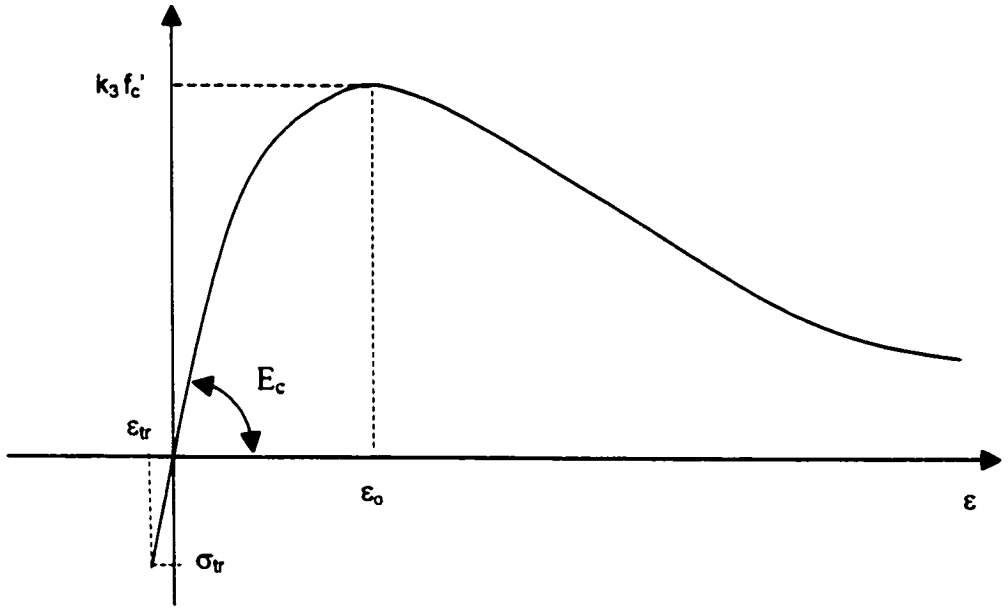

Figure 2.1 Concrete stress-strain curve (schematic)

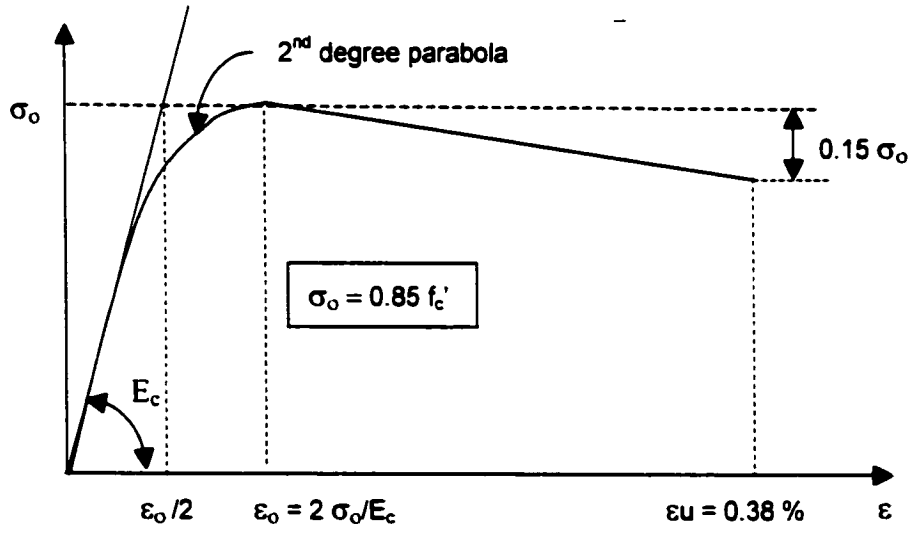

Figure 2.2 Hognestad's model of stress-strain diagram in flexure (Sargin, 1971)

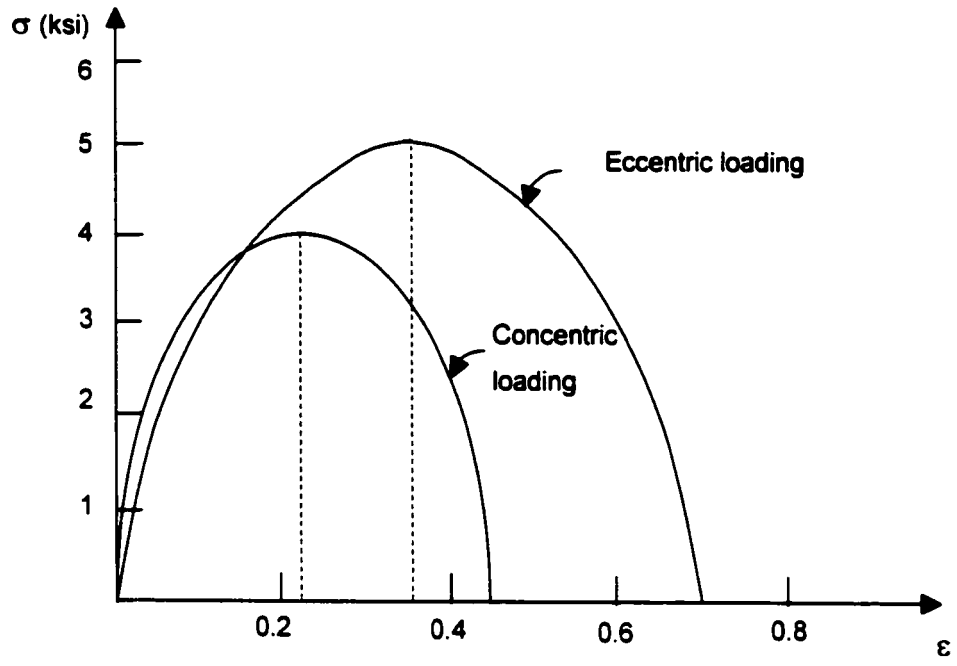

Figure 2.3 Sturman's stress-strain curves (Sargin, 1971)

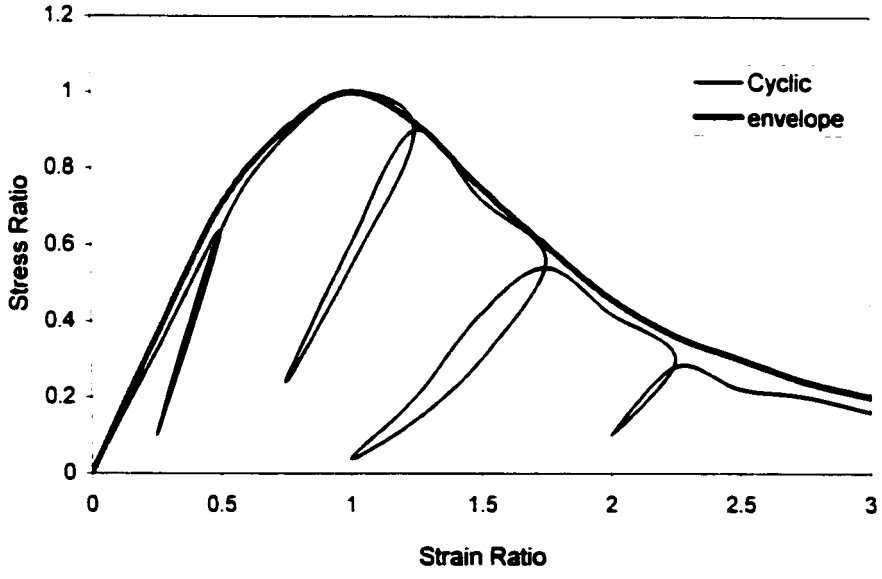

Figure 2.4 Cyclic envelope and monotonic stress-strain curve

Chapter 3

SIMPLIFIED COLUMN ANALYSIS

3.1 General

This chapter discusses column theory directed to formulate simplified column analyses. This is followed by the more detailed review of the design parameters used to support the proposed simplified column formulas. The evaluations of related parameters are based on the literature review on reinforced concrete columns and concrete filled tubular columns under monotonic loading. Simplified column analysis covers strength capacity, ductility, and flexural stiffness of CFT columns.

This chapter uses the concepts expressed in the various codes to develop ACI 318/CSA code type provisions.

3.2 Strength Capacity

The ultimate strength capacity of columns is determined not only by the strength of the materials but also by structural stability. In this case, buckling mostly affects the stability of slender columns. Consequently, column analyses depend on two main things: strengths of the materials and structural stability for slender columns. For stocky columns, stability is not an issue in column analysis because material failure occurs before buckling affects the stability of the columns.

Based on the position of the loads applied on the column sections, column analysis can be classified into two methods of analyses: columns subjected to uniaxial bending and columns subjected to bending in two orthogonal planes or biaxial bending. To simplify the analysis of biaxial columns, analyses are based on the uniaxial column approach with some limitations on the applications of this approach.

All the major codes reviewed, Eurocode 4, AISC-LRFD specifications, CAN/CSA-S16.1-94, CSA Standard A23.3-94 and ACI 318-99, permit section analysis

to be used to determine the load-bending moment interaction of CFT columns. The assumptions permitted vary giving different amounts of conservatism. Various approaches are recommended to take account of slenderness effects, local buckling and combined axial load and biaxial moments.

Reiterative calculations are required to determine the axial load-bending moment interaction in planes other than an axis of symmetry.

Local buckling is accommodated by limiting the dimension or thickness ratios to those used for steel sections. Table 3.1[2] shows the CAN/CSA-S16.1-94 classifications and limitations of width to thickness ratios of rectangular HSS sections.

Slenderness effects are taken into account by either modifying the interaction curves, Eurocode 4, CAN/CSA-S16.1-94 and AISC-LRFD specifications, or moment magnifiers, ACI 318-99 and CSA A23.3-94, with the short column axial load-moment interaction curve.

3.2.1 Eurocode 4

Eurocode 4, the most recent of the major codes received, is discussed in detail as it includes the concepts used in other, previous, codes.

Eurocode 4 recommends using the full plastic rectangular stress blocks for both steel tube and concrete in determination of strength capacity of short CFT columns under combined axial load and bending moment. The rectangular stress block for concrete in compression extends to the neutral axis and the equivalent stress taken equal to the standard cylinder concrete strength, f_c'. Composite columns under combined axial load and bending moment behave similarly to reinforced concrete columns in that the maximum flexural capacity is attained when there is some axial load present to restrain flexural cracking in concrete.

Following the Eurocode 4 procedures for creating the full interaction diagram is difficult and time consuming for design purposes. It requires an interactive procedure that is difficult to perform without the use of a computer. The interaction diagram can be

---

[2] Tables are given at the end of the Chapter

approximated by using a polygonal path through key points. The approximate interaction curve can be constructed using four points A (0, N_{pl}), B (M_{pl}, 0), C (M_{pl}, N_{pm}) and D (M_{max}, $N_{pm}/2$), shown in Figure 3.1. The maximum internal moment M_{max} at point D on the curve may be written as

$$M_{max} = Z_s f_y + \tfrac{1}{2} Z_c f_c' + Z_r f_r \tag{3.1}$$

where

Z_s = plastic modulus of steel cross-section

Z_c = plastic modulus of overall concrete cross-section

Z_r = plastic modulus of reinforcement

f_r = stress in longitudinal steel reinforcement.

For CFT columns without longitudinal bars as steel reinforcement. Equation (3.1) can be rewritten as

$$M_{max} = Z_s f_y + \tfrac{1}{2} Z_c f_c' \tag{3.2}$$

in which. for rectangular CFT columns

$$Z_s = \frac{bh^2}{4} - \tfrac{2}{3}(r+t)^3 - (r+t)^2(4-\pi)\left(\frac{h}{2} - t - r\right) - Z_c \tag{3.3}$$

$$Z_c = \frac{(b-2t)(h-2t)^2}{4} - \tfrac{2}{3} r^3 - r^2(4-\pi)\left(\frac{h}{2} - t - r\right) \tag{3.4}$$

Other points can be calculated using the following expressions

The axial load, point A. can be calculated

$$N_{pl} = \eta_2 f_y A_s + f_c' A_c \left(1 + \eta_1 \frac{t f_y}{h f_c'}\right) \tag{3.5}$$

Neutral axis at mid section, point C

$$N_{pm} = A_c f_c' \tag{3.6}$$

$$M_{pl} = M_{max} - \left[2\,t h_n^2 f_y + \tfrac{1}{2}(b-2t)h_n^2 f_c'\right] \tag{3.7}$$

where

$$h_n = \frac{A_c f_c'}{2bf_c' + 4t(2f_y - f_c')} \tag{3.8}$$

Confinement and slenderness effects are combined the factors η_1 and η_2

$$\eta_1 = \eta_{10}\,(\,1 - 10\,e / D\,) \geq 0.0 \tag{3.9}$$

$$\eta_2 = \eta_{20} + (\,1 - \eta_{20}\,)\,(\,10\,e / D\,) \leq 1.0 \tag{3.10}$$

$$e = M / N \tag{3.11}$$

$$\eta_{10} = 4.9 - 18.5\,\lambda + 17\,\lambda^2 \geq 0.0 \tag{3.12}$$

but for $\lambda \geq 0.5$

$$\eta_{10} = 0.0 \tag{3.13}$$

$$\eta_{20} = 0.25\,(\,3 + 2\,\lambda\,) \leq 1.0 \tag{3.14}$$

$$\lambda = \frac{KL}{\pi}\left(\frac{A_s f_y + A_c f_c'}{E_s I_s + 0.8\,E_c I_c}\right)^{1/2} \tag{3.15}$$

The expressions above have been rewritten using common notation, in place of the original code notation.

3.2.2 AISC-LRFD

AISC-LRFD recommends using the same design procedure for CFT column design as steel columns, except that modified parameters, calculated from the composite cross-section, are used in place of the steel properties. These modified parameters for CFT columns are as follows

$$f_{my} = f_y + 0.85 f_c' \frac{A_c}{A_s} \tag{3.16}$$

$$E_m = E_s + 0.4 E_c \frac{A_c}{A_s} \tag{3.17}$$

$$r_m = \max (r_{steel}, 0.3\ h) \tag{3.18}$$

$$\lambda_m = \frac{kL}{r_m \pi} \sqrt{\frac{f_{my}}{E_m}} \tag{3.19}$$

The strength of the column is determined by following the procedure for steel column design using the modified parameters. Critical stress is calculated using Equation (3.20) or (3.21). Finally, the nominal strength of the column is calculated using Equations (3.22) and (3.23).

For $\lambda_m \leq 1.5$

$$f_{cr} = \left(0.658^{\lambda_m^2}\right) f_{my} \tag{3.20}$$

For $\lambda_m > 1.5$

$$f_{cr} = \frac{0.877}{\lambda_m^2} f_{my} \tag{3.21}$$

$$P_n = A_s f_{cr} \tag{3.22}$$

$$M_n = Z f_y \tag{3.23}$$

3.2.3 CAN/CSA-S16.1-94

CAN/CSA-S16.1-94 has two methods of analysis of rectangular CFT columns under axial compressive load and bending moment. Method 1 is based on bending moment resisted by the composite section, and Method 2 is based on the bending moment resisted by the steel section alone. AISC-LRFD has similar method of analysis to Method 2 of CAN/CSA-S16.1-94. Method 1 may be expressed as

$$\frac{P}{P_u} + \frac{\varpi_1 M}{M_u\left(1 - \frac{P}{P_E}\right)} \le 1.0 \tag{3.24}$$

Method 2 can be written

$$\frac{P - \tau' P_c}{\tau P_s} + \frac{\varpi_1 M}{\tau M_o\left(1 - \frac{P - \tau' P_c}{P_E}\right)} \le 1.0 \tag{3.25}$$

in which, ω_1 = 1.0 or 0.85 for members subjected to distributed loads or a series of point loads or subjected to a concentrated load or moment between supports respectively.

$$P_u = \tau' P_c + \tau P_s \tag{3.26}$$

$$M_u = \frac{A_s f_y e}{2} + \left[0.85 c(b - 2t) f_c'\right]\left(e' - \frac{e}{2}\right) \tag{3.27}$$

where e and e' are lever arms between the compressive resistance and the tensile resistance of steel and between the compressive resistance of concrete and the tensile resistance of steel respectively. Confinement effects are accommodated by τ and τ' and slenderness by λ_c and λ_s.

$$M_o = Z_s f_y \tag{3.28}$$

$$P_c = 0.85 f_c' A_c \lambda_c^{-2} \left(\sqrt{1 + 0.25 \lambda_c^{-4}} - 0.5 \lambda_c^{-2} \right) \tag{3.29}$$

$$P_s = A_s f_y \left(1 + \lambda_s^{4.48} \right)^{-0.446} \tag{3.30}$$

$$\tau = \frac{1}{\sqrt{1 + \rho + \rho^2}} \tag{3.31}$$

$$\tau' = 1 + \left(\frac{25 \rho^2 \tau}{D/t} \right) \left(\frac{f_y}{0.85 f_c'} \right) \tag{3.32}$$

$$\rho = 0.02 \, (25 - L/D) \tag{3.33}$$

$$\lambda_c = \frac{KL}{r_c} \sqrt{\frac{f_c'}{\pi^2 E_c}} \tag{3.34}$$

$$\lambda_s = \frac{KL}{r_s} \sqrt{\frac{f_y}{\pi^2 E_s}} \tag{3.35}$$

For rectangular CFT columns with $L/D \geq 25$, $\tau = \tau' = 1.0$. In which L and D are length of the column and width of the column section respectively. The concrete in compression is taken to have a rectangular stress block of intensity f_c' over a depth of 0.85 c, where c is the depth of the concrete in compression.

3.2.4 CSA A23.3-94

CSA Standard A23.3-94 recommends using CAN/CSA-S16.1 for the design of CFT columns

3.2.5 ACI 318-99

ACI 318-99 recommends using conventional reinforced concrete design procedures for determining the strength of CFT columns. In reinforced concrete design, ACI 318-99 allows the use of an equivalent rectangular compressive stress distribution to replace the more exact concrete stress distribution. In the equivalent rectangular stress distribution, an average stress of 0.85 f_c' ($\alpha_1 = 0.85$) is used with a rectangle of depth a = 0.85 c ($\beta_1 = 0.85$) for concrete with $f_c' \leq 30$ MPa. For concrete strengths above 30 MPa, β_1 should be reduced continuously at a rate of 0.008 for each MPa in excess of 30 MPa, but β_1 should not be taken less than 0.65. These can be rewritten as

$$\alpha_1 = 0.85 \tag{3.36}$$

$$\beta_1 = 0.85; \text{ for } f_c' \leq 30 \text{ MPa} \tag{3.37}$$

$$\beta_1 = 0.85 - 0.008\,(f_c'-30) \geq 0.65; \text{ for } f_c' > 30 \text{ MPa} \tag{3.38}$$

3.2.6 Proposed Method of Analysis

All codes reviewed have similar procedures for strength design for rectangular CFT columns. The only differences between the codes are the compressive concrete stress block, the value of the multiplier on concrete cylinder strength, the limiting ultimate strain of the concrete and how to deal with slenderness effects. Accepting the appropriateness of a rectangular stress distribution, Figures 3.2 and 3.3 show coefficients α_1 and β_1 respectively.

Studies on comparisons of CFT column strength capacity calculated using Eurocode 4-85, ACI 318-83 and AISC-LRFD-86 (Beedle, 1991) showed that ACI 318-83

and AISC-LRFD-86 were 20% and 32% more conservative than the Eurocode 4 for stocky columns under intermediate axial forces and bending moments. At slenderness ratios of 12 and 20, ACI 318-83 and AISC-LRFD-86 gave about 25% and 36 % less than Eurocode 4-85, except at extreme values of axial force. At a slenderness ratio of 30, the resistance given by Eurocode 4-85 was about 33% higher than those given by ACI 318-83 or AISC-LRFD-86.

A design procedure to calculate the strength capacity of square CFT columns under combined axial compressive load and uniaxial bending moment is proposed based upon the design procedure of reinforced concrete column section analysis (ACI 318-99) in determining the strength capacity of CFT columns, which is similar to the design procedure of Eurocode 4. This simplified column analysis is based on section analysis.

Uniaxial columns consist of columns under pure axial load and columns subjected to combined axial compressive load and bending moment in the plane of one of the principal axes of section. In practice, it is impossible to construct structural columns under pure axial load, but in structural analysis, columns under pure axial load are theoretically evaluated. The ultimate strengths of short columns under pure axial load are defined as the squash load. Studies on the strength of columns subjected to pure axial compressive load have been well investigated. The squash load formulas for CFT columns proposed by Furlong and by Kobayashi, no confinement of concrete or biaxial effects on the steel tube, have been accepted and adopted by some design codes. The squash load formula is the sum of the individual strengths of each material; in this case the strengths of the steel tube and the core concrete.

The strength of short columns basically depends on the strength of the section which represent the strength of materials. In case of CFT columns, the strength is developed by interaction of both materials, and it is superposition of the individual strength capacities of each material.

The strength of stocky CFT columns subjected to concentric axial compressive load, defined as the squash load, may be determined using the proposed formula by Furlong (1967)

$$P_o = f_y A_s + f_c' A_c \tag{3.39}$$

Unlike reinforced concrete columns, the full concrete strength from standard cylinder test (f_c') is used in determining the capacity of CFT columns.

Equation (3.39) may not be suitable for high strength CFT columns and CFT columns under seismic loading. Studies show that concrete under seismic loading is stronger than that under monotonic loading. Moreover, the strength of the concrete core in CFT columns is increased by the confinement effect of steel tube. If the steel tube provides perfect confinement on the concrete, the concrete strength may be determined as full confined concrete strength and may be approximated based on the confined concrete strength formula proposed by Gardner or Saatcioglu et al or that proposed by Park et al (1982), or other confined concrete strength formula. Conversely, when the steel tube does not provide good confinement on the concrete, the confinement effects are reduced and the concrete strength is less than that with full confinement. To anticipate these cases, Equation (3.39) is modified and may be rewritten as

$$P_o = f_y A_s + \alpha_1 \alpha_2 f_c' A_c \tag{3.40}$$

where

$$\alpha_1 \alpha_2 \geq 0.85 \tag{3.41}$$

Development of parameters α_1 and α_2 is discussed in Section 3.3.

Studies on the strength capacity of CFT members under monotonic bending moment by Lu and Kennedy showed that using ACI procedures for reinforced concrete section analysis gave good agreement with the experimental results. This method of analysis is based on the equilibrium condition of internal forces in the member section, with the strength of the steel tube specified by its yield strength and the concrete strength by the rectangular stress distribution of the factored average strength of the concrete. At the ultimate strength, strain compatibility of the section is less important; therefore, it can be disregarded.

Referring to Lu's method of analysis, it is reasonable to adopt ACI procedures for traditional reinforced concrete section analysis to determine the strength capacity of CFT

columns subjected to seismic loading. The proposed section analysis is based on assumption of fully plastic section with slight modification when the section reaches its ultimate strength and the equivalent rectangular stress distribution of concrete. Figure 3.4 shows diagrams of full plastic rectangular stress distributions of concrete and steel tube for normal square and diagonal orientations.

A model of the seismic resistance of CFT columns appropriate for design would be based on the specific minimum yield strength of the steel tube and the factored cylinder compressive strength of the concrete with the neutral axis established to satisfy the equilibrium conditions. Hence, two conditions must be satisfied: the sum of the forces equals zero and the sum of the bending moment equals zero. The ACI 318-99 procedure for reinforced concrete section analysis and full plastic rectangular stress blocks for both steel tube and concrete are applied to the CFT short column section analysis.

3.2.7 Slenderness

The strength of short columns may be approached by calculating the capacity of the column section without taking into account the effect of geometry, in this case, buckling effects are not considered. In contrast, buckling is very important in the analysis of slender columns. The famous theory for elastic slender column analysis is the Euler column theory. Column capacity in Euler column theory is calculated by the following formula

$$P_{cr} = \frac{\pi^2 EI}{(k L)^2} \tag{3.42}$$

where P_{cr} is the critical or buckling load, EI is the flexural stiffness, kL is the effective length of the column. The strength of the material does not affect the capacity of the column especially for steel columns where the modulus of elasticity of steel is independent of the strength. Therefore, it is not beneficial to use high strength steel for column to improve the load capacity of a slender column.

Adopting Euler column theory to the CFT slender column analysis, the flexural stiffness of composite materials has to be known. ACI 318-99 recommends that the flexural stiffness of reinforced concrete elements is the superposition of the flexural stiffness of the steel and 20 % of the flexural stiffness of concrete. The Australian and Swiss Codes base their flexural stiffnesses on the moment and curvature at balanced failure.

Equation (3.42) is suitable only for column analysis under concentric compressive load. For a slender column subjected to combined axial compressive load and bending moment, equation (3.43) is more appropriate.

$$M_u = \left(1 - \frac{P}{P_{cr}}\right) M \tag{3.43}$$

where M_u is moment capacity at load P, P is axial applied load, P_{cr} is critical centric axial load and M is moment capacity of short column. P_{cr} is determined from equation (3.42).

3.2.8 Combined Axial Load and Biaxial Bending Moment

Columns subjected to combined axial compressive load and biaxial bending moment can be analyzed using biaxial column analyses. Two groups of analyses have been widely used for analyzing reinforced concrete biaxial columns: Bresler's reciprocal formula and the failure surface or contour formula. The later is more accurate and more studied in recent years. Steel design codes also recommend using the failure surface formula for biaxial column analyses.

For CFT columns subjected to combined axial load and biaxial bending moment, the failure surface equation can be used. The proposed equation is

$$\frac{P}{P_o} + \left(\frac{M_x}{M_{ux}}\right)^{\bar{\gamma}} + \left(\frac{M_y}{M_{uy}}\right)^{\bar{\gamma}} \leq 1.0 \tag{3.44}$$

A special case of square columns subjected to axial load and biaxial bending moment is when the columns are loaded in diagonal direction. The minimum moment capacity of a square reinforced concrete column is when the plane of action of the moment is along a diagonal. As the diagonal is an axis of symmetry, section analysis can be done in the same manner as when the plane of action of the moment is parallel to the sides of the section. Consequently, square CFT columns subjected to axial compressive load and equal biaxial bending moment (for the special case, loaded in diagonal direction) can be analyzed based on the uniaxial approach.

3.3 Development of Parameters for Section Analysis

Previous investigations have showed that concrete has slightly different behaviour when subjected to high rates of loading typical of seismic loading. Paulay et al (1992) reported that the effect of strain rate on concrete was significant for both strength and stiffness. Response of concrete to seismic loading for concrete strength of $f_c' = 30$ MPa is about 27 % above the strength of concrete under monotonic loading. Table 3.2 shows test results of investigation on the behaviour of concrete at high strain rates, especially at the ranges of strain rate for earthquake loading. It is necessary to recognize the strength of concrete under eccentric seismic loading to be higher than that of under concentric monotonic load in determining the capacity of CFT short column. It is obvious from Table 3.2 that the compressive strength of concrete increases about 5 to 20 % for concrete under earthquake loading. Bischoff and Perry (1991) estimated the strain rate during an earthquake to be 0.001 to 0.01 per second. An enhancement value of 10 % of cylinder strength, as a conservative estimate, may be adopted to the strength formula of CFT columns subjected to seismic loading of combined axial compressive load and bending moment.

The strength may be calculated based on section analysis, as used in analyzing reinforced concrete columns. The Eurocode 4 rectangular stress block is adopted instead of applying actual stress-strain relationship in analysis. In this case, the ultimate stress is $\alpha_1 f_c'$, where α_1 depends on the concrete strength, and the height of stress block is the full distance from the surface in compression to the neutral axis. The neutral axis is

determined from compatibility and the equilibrium of internal and external forces. Based on Ibrahim and MacGregors' proposed parameters for the rectangular stress block with some modification for CFT in seismic region, it is proposed to use Equation (3.45) to determine parameter α_1. The parameter α_1 maybe summarized mathematically in the following expression

$$\alpha_1 = 1.2 - 0.0025\, f_c';\ \ 0.9 \le \alpha_1 \le 1.1 \tag{3.45}$$

Section analysis of traditional reinforced concrete columns uses $\alpha_1 f_c'$ as concrete strength in equivalent rectangular stress distribution. If the ACI procedures are applied to CFT columns subjected to combination of axial compressive load and cyclic bending moment, the $\alpha_1 f_c'$ should be modified to $\alpha_1\alpha_2 f_c'$. The parameter $\alpha_1\alpha_2$ should accommodate effectiveness of the confinement effect of concrete by steel tube. In this study, effectiveness of the confinement effect of concrete by steel tube is expressed by parameter α_2. Because the steel tube confines the concrete, the confinement effect is dominantly affected by the strength and stiffness of the steel tube to resist the outward force of the concrete. For HSS steel tubes, the resistance against the expansion force of the concrete are mainly determined by the wall thickness of the tube and the axial load applied. For Class 1 HSS CFT columns, the wall thickness is appropriate to confine the concrete and the axial load capacity is affected by the confinement. Conversely, for Class 4 HSS CFT columns, the wall thickness is not sufficient to significantly confine the concrete. Further, it is apparent that high strength concretes are more brittle than normal strength concrete and this can be taken into account in the α_2 term. As a result, parameter α_2 should be equal to 1.0 for Class 1 HSS CFT columns and less than 1 for Class 4 HSS CFT columns. These may be written, for Class 1 HSS CFT columns

$$\alpha_2 = 1.0 \tag{3.46}$$

and for Class 4 HSS CFT columns

$$\alpha_2 = 1 - \left(\frac{2.46}{\ln f_c'}\right)\left(\frac{P}{P_o}\right) \tag{3.47}$$

Figures 3.2, 3.3 and 3.5 show the proposed values of parameters α_1, β_1 and α_2 respectively.

3.4 Ductility

Ductility is the extent to which a material can sustain plastic deformation without rupture, or the ability of a structure and selected structural components to deform beyond elastic limits without excessive strength or stiffness degradation. It is accepted that a ductile member of a structure is more desirable than a brittle one. However, how to measure, or describe, ductility is subject to discussion.

Two kinds of ductility are considered in this section: displacement ductility and curvature ductility. Displacement ductility may be expressed as

$$\mu_\Delta = \frac{\Delta_u}{\Delta_y} \tag{3.48}$$

and curvature ductility as

$$\mu_\Phi = \frac{\Phi_u}{\Phi_y} \tag{3.49}$$

Figure 3.6 is used to define ultimate and yield displacement and curvature.

The New Zealand Standard NZS 4203-1984 defines the ultimate displacement, Δ_u, as the displacement corresponding to reduction in strength of the structure, with respect to horizontal forces, shall not exceed 20 % of its maximum strength. This criterion is adopted in the analysis in this section.

Reinforced concrete structures adopt the criterion of yield curvature based on the curvature prior to the peak point at a moment of 75% of maximum moment, not based on

the first yield curvature. In this case, the equivalent yield curvature is approximately one-third times higher than first yield curvature (Paulay et al, 1992). The yield curvature, Φ_y, and yield displacement, Δ_y, are defined based on the first-yield curvature and first yield displacement respectively. The ratios of yield moments to maximum moments should be calculated to check the inconsistency of equivalent yield curvature on reinforced concrete structure criterion if it is applied to the CFT columns.

3.5 Flexural stiffness

Flexural stiffness of a member is the product of modulus of elasticity of the material, or materials, and the second moment of area of the cross section of the member.

It is easy to define the modulus of elasticity of a linear elastic material. However, to define the modulus of elasticity of nonlinear elastic or inelastic materials is more complicated. This can be seen in the codes, standards or provisions, where each has its own unique method of calculating the modulus of elasticity. There is no consensus among the codes or standards in determining the modulus of elasticity of inelastic materials or non-linear elastic materials. For example, the modulus of elasticity of concrete is different if calculated from different codes or standards.

Three code expressions, Eurocode 2, ACI 318-99, CSA A23.3-94, and one formula proposed by Gardner to calculate the modulus of elasticity of concrete are reviewed here and compared to the test data. Based on this review, two formulas for calculating the modulus of elasticity of normal strength concrete and high strength concrete are proposed. For normal strength concrete, the equation refers to the Eurocode 2 formula with the coefficient adjusted, and for high strength concrete, it refers to ACI 318-99. The modulus of elasticity of normal strength concrete maybe written as

$$E_{cmt} = E_{cm28} (f_{cmt} / f_{cm28})^{1/2} \tag{3.50}$$

In which

$$E_{cm28} = K_1 (f_{cm28})^{1/3} \tag{3.51}$$

From the experimental information $K_1 = 10222$ was determined.
The modulus of elasticity of high strength concrete can be written as

$$E_c = K_2\sqrt{f_c'} \tag{3.52}$$

where K_2 was found by experiment to be 4650.

Using the appropriate formula for calculating modulus of elasticity of concrete, the flexural stiffness of CFT column can be determined. ACI 319-99 and CSA A23.3-94, recommend using Equation (3.53) for determining the flexural stiffness of reinforced concrete and composite columns.

$$EI_{ACI} = 0.2\,E_cI_c + E_sI_s \tag{3.53}$$

Previous investigations recognized that Equation (3.53) was very conservative when applied to CFT columns. This might be caused by different behaviour of reinforced concrete and CFT columns. In reinforced concrete and structural steel encased by concrete, steel dominantly contributes stiffness to the flexural stiffness of columns. In contrast, concrete contributes more flexural stiffness in CFT columns than that in reinforced concrete columns. As a result, in formulating the equation of flexural stiffness of CFT columns, using ordinary flexural stiffness of reinforced concrete columns, the coefficient of the flexural stiffness of the concrete should be examined.

The modulus of elasticity of concrete is calculated based on the concrete strength, and the concrete strength in CFT columns affected by the confinement of the steel tube as discussed in the previous section. In addition, the ratio of concrete to steel areas affects the stiffness of CFT columns. It is known that flexural stiffness of a member is the product of modulus of elasticity and second moment of area of the member section. In determining the flexural stiffness of reinforced concrete or CFT columns, the second moment of area of the section is approximated from the gross second moment of area of the section. ACI 318-99 uses a coefficient 0.2 for this approximation. In section analysis, the area of the compressive concrete block determines the exact second moment of area

of CFT column section. Sections with thick tubular wall thickness have less compressive concrete area than those with thin wall thickness. Consequently, CFT columns made with thick tube walls have smaller coefficients of flexural stiffness of concrete than those made with thin walls. This expression maybe formulated mathematically for two types of CFT columns.

For Class 1 HSS CFT columns;

$$EI = 0.3\ E_c I_c + E_s I_s \tag{3.54}$$

For Class 4 HSS CFT columns;

$$EI = 0.6\ E_c I_c + E_s I_s \tag{3.55}$$

Table 3.1 Classifications of Rectangular HSS Sections

Codes	Class 1 (Plastic Design)	Class 2 (Compact)	Class 3 (Noncompact)	Class 4 (Slender)
CAN/CSA-S16.1-94	$\frac{b}{t} \le \frac{420}{\sqrt{f_y}}$	$\frac{b}{t} \le \frac{525}{\sqrt{f_y}}$	$\frac{b}{t} \le \frac{670}{\sqrt{f_y}}$	$\frac{b}{t} > \frac{670}{\sqrt{f_y}}$
AISC-LRFD 1994	$\frac{b}{t} \le \frac{499}{\sqrt{f_y}}$	$\frac{b}{t} \le \frac{499}{\sqrt{f_y}}$	$\frac{b}{t} \le \frac{625}{\sqrt{f_y}}$	$\frac{b}{t} > \frac{625}{\sqrt{f_y}}$

Note:

AISC-LRFD classifies HSS into compact, noncompact or slender element sections. In Table 3, this classification was modified as Class 1 or 2 for compact, Class 3 for noncompact and Class 4 for slender sections.

Table 3.2 Test results of increase in compressive strengths of concrete at high strain rates (Bischoff and Perry, 1991)

Reference, Year	Static loading		Dynamic loading	
	f_c' (MPa)	$\dot{\varepsilon}_s$ (s^{-1})	$\dot{\varepsilon}_d$ (s^{-1})	Increase in f_c' (%)
Jones and Richart, 1936	35	10^{-5}	2×10^{-3}	15
Ban and Muguruma, 1960	32	6×10^{-5}	2×10^{-3}	8
Wesche and Krause, 1972	26 - 76	10^{-5}	10^{-3}	5 - 20
Sparks and Menzies, 1973	30	10^{-5}	10^{-3}	5
Krawinkler and Moncarz, 1982	38	6×10^{-5}	2×10^{-2}	20
Ahmad and Shah, 1985	37 - 48	3×10^{-5}	3×10^{-2}	16

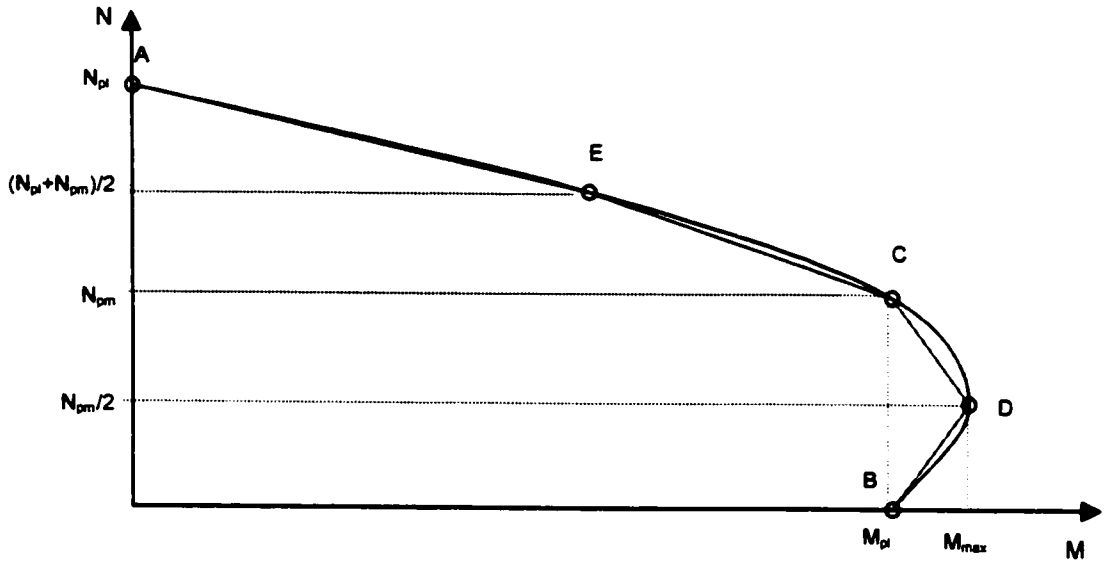

Figure 3.1 Eurocode 4 Full and Approximate Interaction Diagram

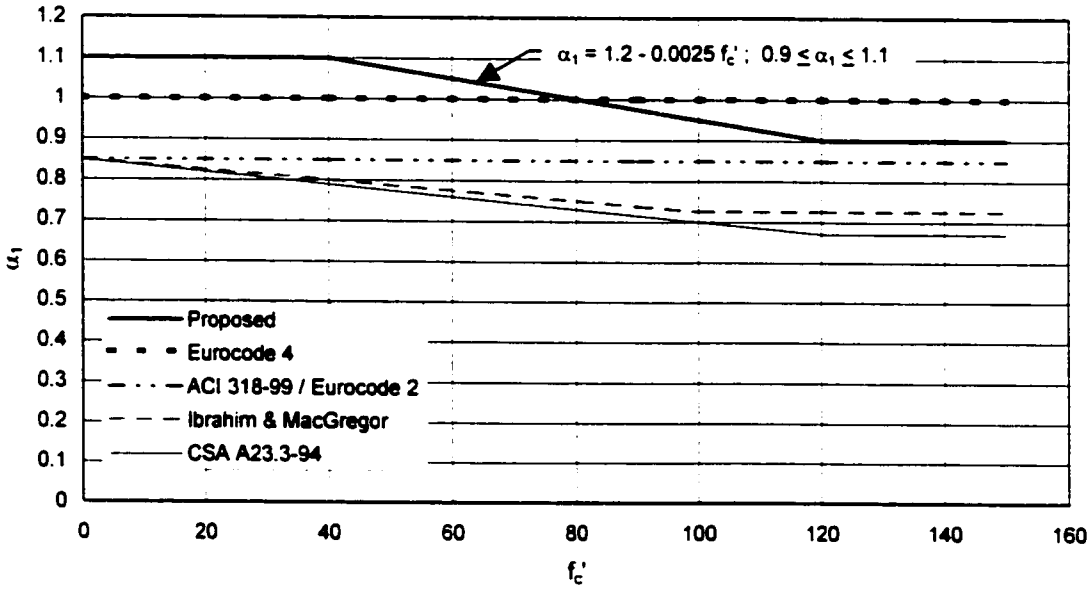

Figure 3.2 Coefficient α_1

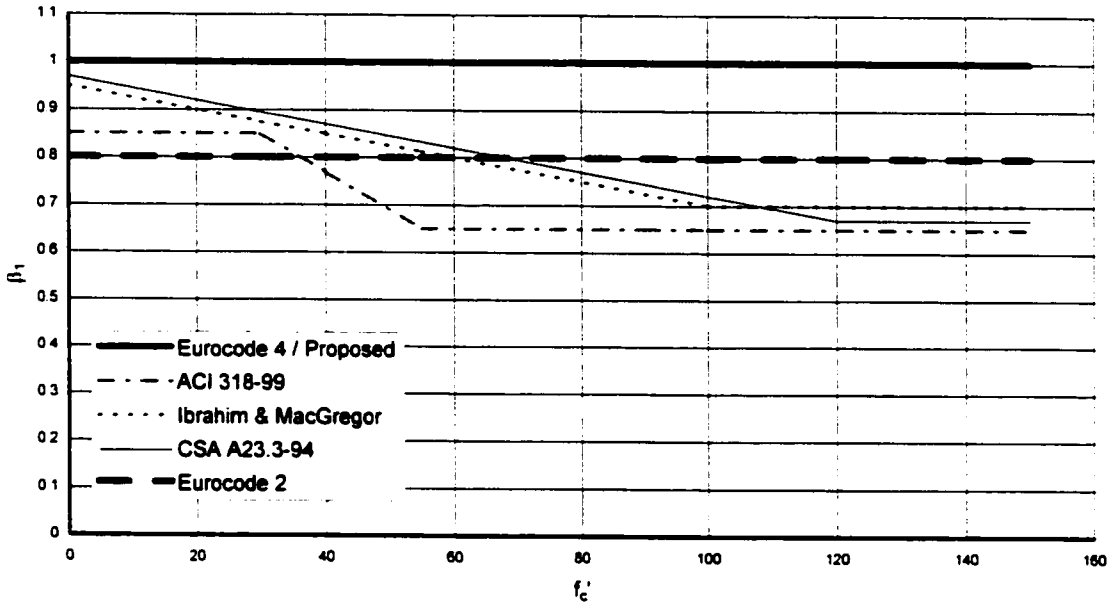

Figure 3.3 Coefficient β_1

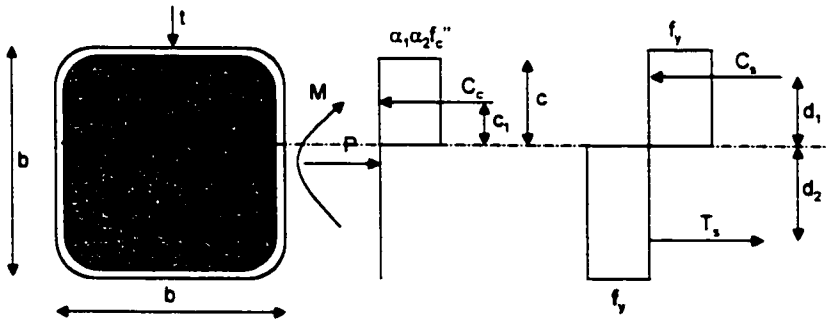

a. Normal square orientation

Figure 3.4 Full Plastic Rectangular Stress Distribution

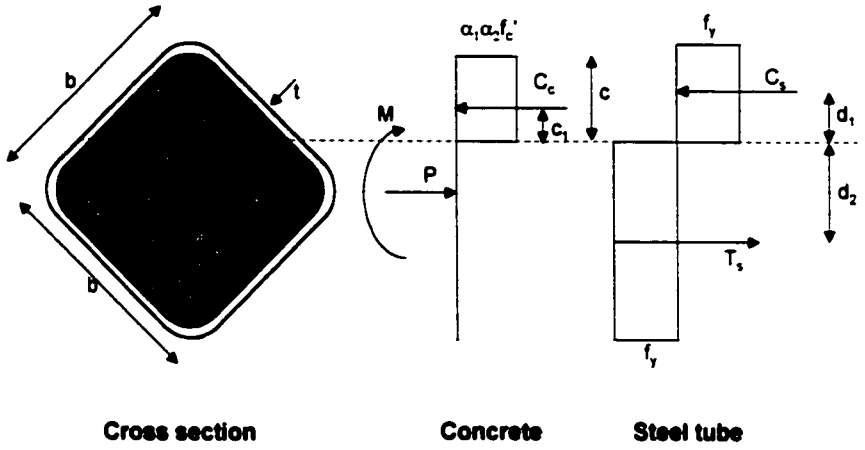

b. Diagonal orientation

Figure 3.4 Full Plastic Rectangular Stress Distribution (continued)

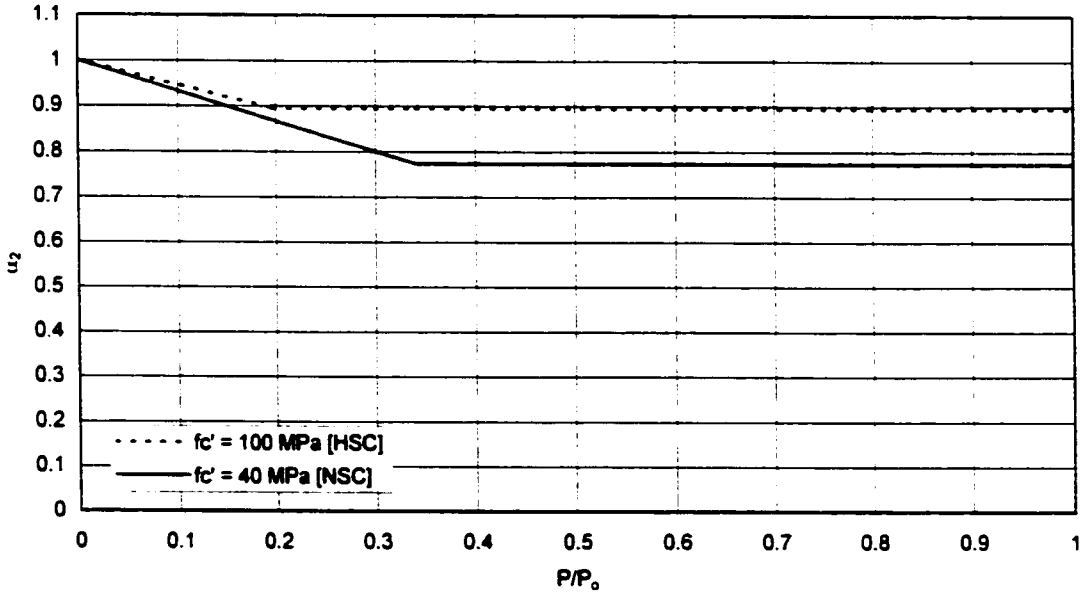

Figure 3.5 Coefficient α_2 for Class 4 HSS CFT columns

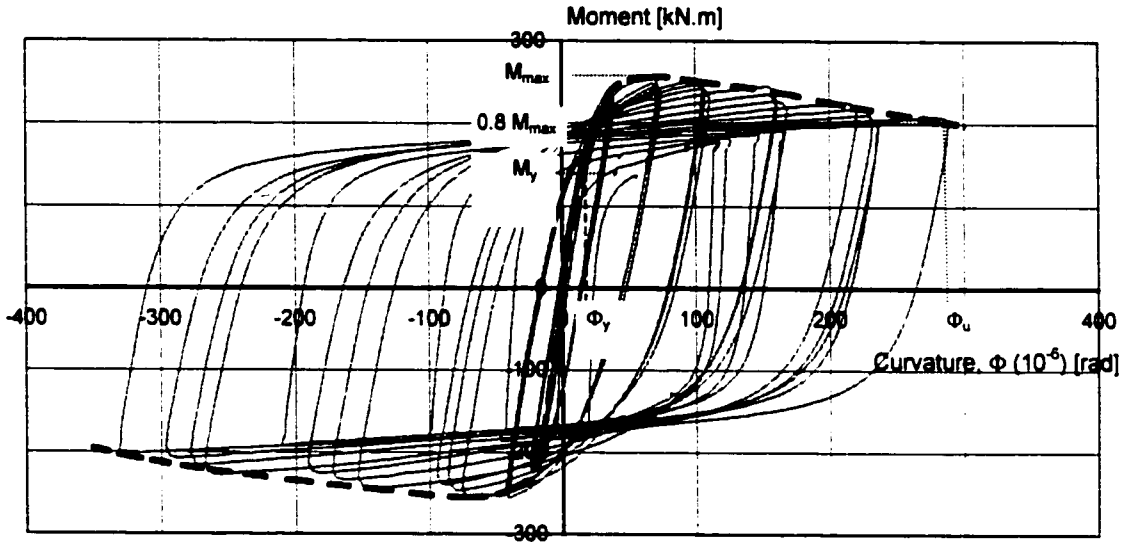

a. Curvature ductility

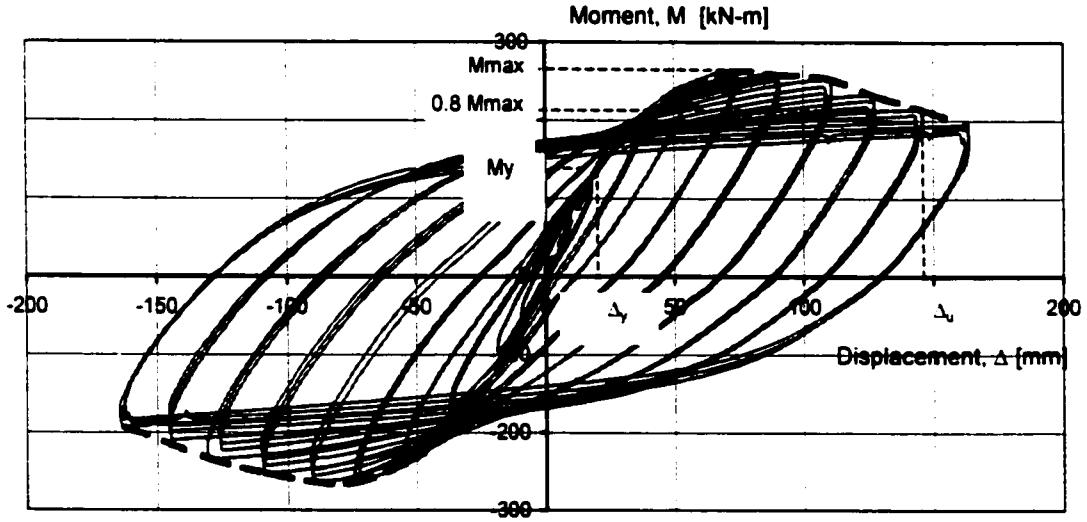

b. Displacement ductility

Figure 3.6 Curvature and Displacement Ductility

Chapter 4

EXPERIMENTAL PROGRAM

4.1 General

The experimental program was developed to examine the seismic resistance, strength capacity and ductility, of square HSS CFT beam-columns filled with normal strength concrete (NSC) or high strength concrete (HSC). The program included preparation, design, and construction of column specimens and ancillary tests.

The investigation consisted of loading cantilever columns under a combination of constant compressive axial load and an incremental cyclic shear displacement applied at the column free end. Sets of three nominally identical columns were tested at different levels of compressive axial load to develop the experimental load-moment interaction surfaces. The variables investigated were concrete strength, steel section wall thickness and orientation of the section relative to the plane of action of the shear displacement, either conventionally parallel to the section sides or across its diagonal.

The lower columns in framed building structures during an earthquake are subjected to an axial load due to the weight of the building and lateral forces forcing the columns into shear bending.

The existence of the point of zero moment allows a cantilever column with the load applied at free end to represent a lower floor column. This experimental program was modeled for this situation. The fixed base of the cantilever column was provided by shimming the column into a custom fabricated base. The axial load was provided through a transfer-loading beam bolted to the top of the column which was pulled down by two servo-controlled MTS actuators. The lateral or shear force was provided by a third MTS actuator acting horizontally on the transfer loading beam.

This chapter begins with an outline of the test program undertaken. Ancillary tests consisted of standard compressive cylinder tests for concrete and coupon tension tests for

the HSS steel. Descriptions of the specimens and the methods used to determine the properties of the concrete are given. Details of the HSS steel tube and the standard test procedures used to determine the mechanical properties of the steel are provided. A description of the fabrication of the steel foundation is also given. In addition, construction procedures and testing methods used for the stub column specimens are described. Finally, methods of collecting the experimental data and data analyses are discussed briefly.

4.2 Test Program

The test program was designed conforming to the discussion in Chapter 3. Twenty-four square HSS CFT columns were constructed using two types of HSS (203x203x9.5 HSS and 203x203x4.8 HSS), two types of concretes (normal strength concrete and high strength concrete) and two kinds of loading test orientations (normal square orientation and diagonal orientation). Six columns were constructed using 203x203x9.5 HSS (Class 1 HSS sections) and the remaining six using 203x203x4.8 HSS (Class 4 HSS sections) for each concrete strength. Three columns of each combination of concrete strength and tube wall thickness were tested under a combination of axial compressive load and bending moment in a diagonal orientation and the remaining in a normal square orientation. The axial compressive loads on each column were unique.

The investigation covered the seismic resistance of square HSS CFT made of Class 1 and Class 4 sections filled with concrete. According to CAN/CSA-S16.1-94, Class 1 and Class 4 sections have maximum width-thickness ratios of $420/\sqrt{f_y}$ and minimum width-thickness ratios of $670/\sqrt{f_y}$ respectively. Using the minimum specified yield strength of HSS in accordance with ASTM A500 Grade C, $f_{y,min}$ = 345 MPa, the width-thickness ratio limits of Class 1 and Class 4 sections are 22.6 and 36.1 respectively. The HSS section sizes were selected with due regard to what was readily available and within the capacity of the testing equipment available. A 203x203x9.5 HSS, with width-thickness ratio of 21.3, represents Class 1 sections (plastic design

sections), and the 203x203x4.8 HSS, with a width-thickness ratio of 42.7, represents Class 4 sections (slender sections).

Column specimen length was determined by summation of the embedded length of the column in the steel foundation and with consideration of the physical limitations of the MTS hydraulic actuators to be used to test all column specimens. While the total column specimen lengths were 1905 mm, the effective freestanding column height used in the analyses was 1800 mm because the loads were applied 276 mm above the top of column, through a loading beam. A summary of the test program is given in Table 4.1.

4.3 Concrete

4.3.1 Description

The design strengths of the concrete used to construct the column specimens were 40 MPa for the NSC and 90 MPa for the HSC. Both the NSC and HSC were ordered from a local ready mix supplier with significant experience in the manufacture and delivery of commercial concrete.

4.3.2 Equipment and Method of Testing

Tests to determine the unconfined compressive strength of the concrete were conducted on a Fourney testing machine with 2225 kN capacity. The flow rate of the hydraulic fluid is controlled by varying the current supplied to the d.c. motor which drives the pump. This can be manually adjusted so that load is applied to the specimen at a rate which could be visually coordinated with a load pacer. For all specimens, load was applied at an approximate incremental rate of 5 kN/sec (0.28 MPa/sec).

Tests to determine the stress-strain relationship of the concrete were conducted using the same testing machine and procedures used to determine the unconfined compressive strength of the concrete. Each specimen was instrumented using a compressometer with LVDs or a dial gage to measure displacement.

For normal strength concrete columns, three cylinders were tested on the same day as the column specimens were tested and additional tests were conducted at ages

from 21 to 178 days. For the high strength concrete columns, the cylinder tests were done at ages 14, 21, 28, 44, 63 and 80 days. Complete test data are tabulated in Tables 5.1 and 6.1 for normal strength and high strength concrete columns respectively.

4.4 Steel Tube (Square HSS)

4.4.1 Description

All HSS CFT columns were constructed using standard, commercially available, square HSS distributed by local steel supplier. The tube was supplied in stock lengths of either 14.63 m or 7.32 m. Two sizes of square welded HSS were used in this investigation, namely 203x203x9.5 and 203x203x4.8. The product conformed to the requirements of ASTM A500 Grade C, which requires minimum yield strength of 50 ksi or 345 MPa and a minimum ultimate tensile strength of 62 ksi or 427 MPa.

Based on the assumption that the length supplied would be 7.32 m, each supplied tube was cut for 3 column specimens, each 1905 mm-length, and a length of 430 mm for tension test coupons. Tension test coupons were machined from each side of each tube; therefore, the length of 430 mm produced four coupons. Figure 4.1 shows the dimensions of a typical tension test coupon.

The HSS Class 1 and HSS Class 4 sections were delivered in six batches. The properties of each batch of HSS were investigated. Six sets of tension test coupons machined from each batch, HSS tubes of SNL/DNL, SCL, DCL, SNH, DNH and SCH/DCH, were tested. Each set consisted of four tension test coupons.

4.4.2 Equipment and Method of Testing

Four tension test coupons were milled from the designated portion of each of the stock lengths of steel tube. Dimensions of the coupons were selected with due regard to American Society for Testing and Materials ASTM A 370-1995 and the requirements of the testing machine. After the milling process was completed, residual stresses produced during the manufacture of the tube were released causing the coupon to bend in the longitudinal direction. Figure 4.2 shows a photograph of the coupons before testing. It

was subsequently straightened as a result of being placed in the jaws of the testing machine. To measure strains, electrical resistance strain gauges were glued to both sides of the reduced section of the coupons.

Tension tests were conducted to establish the stress-strain relationship of steel tube used in column specimens. The tensile coupon tests were performed using a Tinius Olsen testing machine. A strain rate of 0.0005/min was used during the test. Test procedures followed the procedures in the ASTM Standard A 370-1995.

4.5 Steel Foundation

All column specimens were tested using a single, reusable steel foundation. The multiuse steel foundation was made of steel HSS and steel plate. It has a square hole, or socket, at the center into which the column specimens are inserted. The hole was sized to enable specimens to be mounted either normally or diagonally. Figures 4.3 and 4.4 show the steel foundation.

The bottom part of the steel foundation was fabricated using six pieces of 203x203x9.5 HSS of various lengths; i.e. 1,524 mm, 1,575 mm and 1,676 mm from side to the center respectively. All six pieces were welded both sides longitudinally to each other to form a plane surface approximately 1,218 x 1,524 mm^2. This base, shown in Figures 4.3 and 4.4, functioned to mount the foundation to the strong floor, using four 63.5 mm diameter bolts, and to locate and attach the two vertical actuators on both sides of the column specimen. The four middle sections of the six pieces of HSS were filled with plain concrete with a compressive strength of 60 MPa. The concrete reduced, or restrained, the HSS from deformation and stiffened the system. In addition, to ensure all six pieces work as a plate unit system, two steel plates were welded transversally on top each side of this plane system.

The socket, in which the column specimens were clamped, was assembled on top of this plane surface using two 203x203x9.5 HSS of each side on four sides to form a hole with square horizontal cross section at the top center of the plane surface. The hole dimensions are 280 mm square and 406.4 mm deep. A piece of steel plate 280x280x25.4 mm was placed at the bottom of the hole, on top of the plane surface. As a result, the

effective depth of the hole was 381 mm. This hole was used to hold the column specimens during the test.

For normal orientation (square) column specimens, steel plates were placed around the specimen as shims to fit and wedge the column specimen into the steel foundation. The normally oriented specimens were mounted with a deliberate offset of 12.7 mm between the plane of action of the horizontal load and the centroid of the section causing some torsion and a minor biaxial moment. This was to ensure that the experimental results would be less than those of perfectly oriented specimens.

For the diagonal orientation column specimens, triangular composite wedges, made of Sikadur 42 regular with a specified strength of 90 MPa at 7 days and the corner parts of 203x203x4.8 HSS, and steel plates were used. The diagonally oriented specimens were mounted so the plane of action of horizontal load was across a diagonal of the steel section.

4.6 HSS CFT column specimens

4.6.1 Description and Construction Procedure

All pieces of steel tube used to make the beam-column specimens were cut from the stock length. Each column specimen had a total length of 1905 mm, and the free length of the cantilever column is 1524 mm. A stock length of steel tube of 7320 mm can be cut into 3 column specimens and the remaining length used for tension test coupons. All specimens were accurately cut so that the ends of the specimen were perpendicular to the longitudinal axis of the specimen.

Before the tubes were filled with concrete, all tubes were thoroughly cleaned inside and outside. One end of each tube was sealed using polyethylene sheet to prevent leakage of fresh concrete when the tubes were filled with fresh concrete. The tubes were filled with concrete vertically; therefore, all tubes were placed vertically and the tube ends with polyethylene were at the bottom. All empty tubes were secured in a vertical position to a HSS frames system before placement of the concrete. Figure 4.5 shows a photograph of a set of empty steel tubes before being filled with concrete. All twelve

specimens filled with NSC were cast on December 21, 1999, and the second set with HSC was cast on March 28, 2000.

Bolts were used to fix the specimens to the loading beam which transferred the axial and transverse loads from the actuators to the specimens. Four normal strength (grade 5) steel bolts 19 mm diameter and 305 mm length were provided for each specimen filled with NSC. For specimens filled with HSC, high strength (grade 8) bolts were used. All bolts were placed at the top end of the column specimens as the concrete was poured.

Fresh concrete was placed in each tube in three approximately equal layers, each of which was subjected to about fifteen seconds of intense vibration from a 38 mm diameter poker vibrator. After the specimen had been topped up with concrete, the vibrator was held against the outside of the tube near the top for several seconds so that the concrete at the top would be adequately compacted. The concrete was then struck off flush with the top of the tube and covered with a plywood cap plate that held the four bolts in position. Four bolts were embedded in the concrete, in each column specimen, to transfer the loads from the assembled beam loading to the specimen. Figure 4.6 shows a set of column specimens after casting. A typical diagonal bending moment specimen and a typical biaxial bending moment specimen are illustrated in Figure 4.7.

The following day each specimen was cleaned and inspected. Any concrete standing proud of the top of the tubes was chipped away and free water was periodically added to the top of the specimens. All specimens were cured in a wet condition and covered with polyethylene at room temperature. The intensive curing period was 7 days. After 7 days, the plywood cap plates were removed and the top of each specimen surfaced to the same level as the steel tube to get a smooth flat surface.

4.6.2 Instrumentation and Testing Procedures

The test setup consisted of the column specimen, steel foundation, three servo-computer controlled MTS hydraulic actuators system, loading beam, actuator restraining steel frame system (A-frame). Two steel frames were provided to restrain out-of-plane displacements. Figures 4.8 and 4.9 show the front view and the side view of test setup

respectively. Although the figures show the diagonal orientation specimens (DBM), the same test setup was used for normal orientation (square) specimens (BBM). A schematic of the test system is illustrated in Figure 4.10.

The HSS CFT column specimens were tested using three MTS servo-computer controlled hydraulic actuators. Two actuators were used to apply a constant vertical compressive load. These actuators sat on, and were attached to, the steel foundation using four 38 mm bolts for each actuator. The third actuator was used to produce horizontal, or transverse, load. Each actuator has a load capacity of 1000 kN in both compression and tension, a maximum stroke of 508 mm, and was connected using four 38 mm diameter, 400 mm long bolts at each end.

All specimens were instrumented using LVDTs and electrical-resistance strain gauges (strain gauges). The actuators had calibrated load cells and LVDTs. Four LVDTs, three temposonic LVDTs, and eighteen strain gauges were used for each specimen. There were slightly different instrumentation configurations between the DBM specimens and BBM specimens. The locations of the gauges are shown in Figure 4.11.

Strain gauges were glued on the specimens at two levels; ten strain gauges were glued 60 mm above the foundation top surface (fixed-end surface), and eight strain gauges were glued 140 mm above the first level. Two strain gauges were installed at each level and each side of the specimen, in both the longitudinal and transversal directions. The remaining two strain gauges were installed longitudinally at 60 mm at the opposite, front and back, corners of the specimen.

Four LVDTs were placed on the specimen, three LVDTs on the front and one at the back at 500 mm above the foundation top surface. The front LVDTs were installed at 100 mm, 300 mm and 500 mm above the fixed-end surface. All were installed at the mid-width of the front or back faces of the specimen. Three Temposonic LVDTs were installed; one of them at the level of horizontal actuator to measure the horizontal displacement at the level of horizontal actuator, 1800 mm above top surface of foundation, and two Temposonic LVDTs were at the top surfaces of the foundation at the back and front. These two Temposonic LVDTs were used to measure the vertical displacement of the top surface of foundation, which indicates the restraint of the foundation system. Figure 4.11 illustrates the LVDTs and strain gauges positions.

Test procedures started by placing the specimen into the socket in the steel foundation after the foundation system had been secured to the strong floor and the two vertical actuators had been aligned in their positions. The specimen was secured into the socket using steel shims or composite steel-concrete shims. The loading beam was placed on top of the column specimen and clamped to the specimen using the four 19 mm bolts provided. The actuators were secured to the loading beam.

Installing the LVDTs and strain gauges at the selected locations completed the preparation of the specimen test setup. The LVDTs were installed at the points selected, and the strain gauges glued to the surfaces of specimen at the selected points and all cables were connected to the computer system to record the displacements and the strains.

Two types of control were used for a test: load control and displacement control. Load control was used to maintain the axial compressive load on the vertical actuators to the desired load. After application, the axial load was kept constant during the test. The axial compressive load applied to the specimens was specific to each specimen. The maximum applied axial load was selected with due regard to the limited capacity of the actuators. The axial compressive loads applied on the specimens are tabulated in Table 4.1.

Displacement control was used to adjust the displacement at the point of applied horizontal load produced by the horizontal actuator. The displacement control followed the lateral displacement reversals program in Figure 4.12 with three cycles at each specified drift.

The horizontal actuator was located to produce a shear displacement 1800 mm above the restraint point with increments of 1mm per second for 0.5%, 1% and 2% drifts, of 2 mm per second for 3%, 4% and 5 % drifts, and of 3 mm per second for 6%, 7 % and 8% drifts. Drift is the ratio of horizontal displacement at the point of inflection to the height of the column.

For documentation, photographs were taken during the test and the measurements automatically recorded on the computer every second. Figure 4.14 shows a photograph taken during uninstall of the diagonal column specimen (DCH-2). Visual observation was

also provided to record the physical changes on the specimen that were not recorded by the system.

4.7 Experimental Data and Data Analyses

Experimental data were collected during the tests of specimens. As mentioned previously, the objectives of the experimental program were to examine the seismic resistance of column specimens, which included load carrying capacity and ductility of columns under cyclic loading.

The axial compression and transverse loads, displacements and strains at certain points were recorded during the test. The tabulated data consisted of transverse load, displacements and strains scanned every second.

The shear-displacement, moment-displacement, moment-curvature relationships and axial compressive load–bending moment interaction curves are plotted from the data. Because of the experimental set up, the axial load was not vertical but acted on a line through the swivel points of the vertical actuators – the upper one of which moved during testing applying a horizontal component of load. Consequently, the raw data has to be converted before plotting. Figure 4.13 shows the system of forces acting on a column specimen.

Shear force V is calculated as

$$V = H - P\frac{\Delta}{L} \tag{4.1}$$

Moment at the restraint point (B in Fig. 4.13) is calculated using the following formula

$$M_B = \left[\sqrt{L^2 - \Delta^2} - d\right]H + \frac{d}{L}P\Delta \tag{4.2}$$

For d = 140 mm and L = 1940 mm, Equation 4.2 can be rewritten as

$$M_B = \left[\sqrt{3.7636 - \Delta^2} - 0.14\right] H + 0.072165\, P\, \Delta \qquad (4.3)$$

where P and H in kN, and M_B in kN.m.

The curvature at a section was calculated by subtracting the strain at the back of displacement direction from the strain in the front of displacement direction and dividing it by the distance between the two points considered.

The flexural stiffness (EI) of the column specimens can be determined from the moment-curvature relationship. The ductility of the column is estimated by dividing the maximum displacement (displacement at ultimate capacity) by the yield displacement. By definition, yield displacement is the displacement when the steel starts yielding. The yield displacement was determined by evaluating the measured data. When the strain of the steel was about 0.002 (assuming the steel starts yielding at strain of 0.002), the displacement is the yield displacement.

4.7.1 Bending Moment

The maximum bending moment is calculated using Equation 4.3 for both BBM and DBM column specimens. The vertical actuators also produce a bending moment (in the transverse direction) on the BBM column specimens; as a result, BBM column specimens experience biaxial bending moment. The moment calculated using Equation 4.3 is the major moment and specified as M_x, and perpendicular to M_x is a minor moment M_y due to the eccentricity of the axial compressive load. M_y may be calculated using Equation 4.5.

$$M_y = P\, e \qquad (4.4)$$

In this experimental program e = 0.0127 m. Equation 4.5 can be rewritten as

$$M_y = 0.0127\, P \qquad (4.5)$$

4.7.2 Axial Load – Bending Moment Interaction Curve

The strengths of the columns are best summarized by plotting the axial load-bending moment relationship as an interaction curve.

Comparison of the analytical results, using the proposed equation, to the experimental results was done by plotting both results in the same graph for each column specimen type.

4.7.3 Curvature and Moment – Curvature Relationship

The assumption of plane sections before bending remaining plane after bending was adopted in section evaluation. Based on this assumption, the curvature, Φ, may be calculated from the measured data using Equation 4.6 or 4.7 for BDM or BBM specimens respectively.

$$\Phi = \frac{-(\varepsilon_f - \varepsilon_b)}{280000} \tag{4.6}$$

$$\Phi = \frac{-(\varepsilon_f - \varepsilon_b)}{203000} \tag{4.7}$$

where ε_f, ε_b = strain in front and strain at back of the displacement direction respectively. The measured strain data of strain gauges # 17 and # 18 were used to calculate the curvature. Depending on the displacement direction, the strains at strain gauges #17 and #18 could be ε_f or ε_b. Compressive strain is indicated by a negative sign.

As curvature was measured some distance above the base, for moment-curvature relationships, the moment was calculated at the level at which the curvature was measured. Bending moments at the level of strain gauges # 17 and # 18 were calculated using Equation 4.2 and substituting h = 1.74 m and L = 1.94 m into this equation. Both calculated curvature and bending moment were plotted into the moment-curvature (M–Φ) relationship curve.

4.7.4 Flexural Stiffness

From the moment-curvature curve, the flexural stiffness, EI, of the HSS CFT columns were determined as a ratio of yield moment to first yield curvature. Another way to determine the flexural stiffness is by plotting a line from the origin to the point on curve at the yield moment. This EI value can be used for further analyses.

Table 4.1 Test program

Specimen number	Hollow structural section (HSS)					Specified concrete strength, f_c' [MPa]	Column orientation	Axial load [kN]	Age at test [days]
	Designation	b	t	b/t	Section class				
DNL - 1	203x203x4.8	203	4.8	42	4	40	Diagonal	290	44
DNL - 2								725	62
DNL - 3								1200	70
DCL - 1	203x203x9.5	203	9.5	21	1	40	Diagonal	430	80
DCL - 2								800	94
DCL - 3								1740	87
SNL - 1	203x203x4.8	203	4.8	42	4	40	Square	300	101
SNL - 2								700	104
SNL - 3								1200	105
SCL - 1	203x203x9.5	203	9.5	21	1	40	Square	430	106
SCL - 2								860	107
SCL - 3								1740	111
SCH - 1	203x203x9.5	203	9.5	21	1	90	Square	570	6
SCH - 2								1200	20
SCH - 3								1750	23
SNH - 1	203x203x4.8	203	4.8	42	4	90	Square	520	41
SNH - 2								1150	43
SNH - 3								1700	42
DCH - 1	203x203x9.5	203	9.5	21	1	90	Diagonal	630	48
DCH - 2								1550	56
DCH - 3								1900	57
DNH - 1	203x203x4.8	203	4.8	42	4	90	Diagonal	540	59
DNH - 2								1100	62
DNH - 3								1850	64

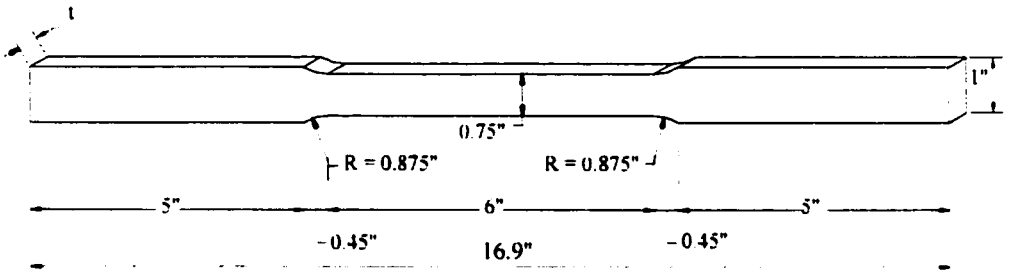

Note :
t = wall thickness of steel tubing

Figure 4.1 Typical tension test coupon

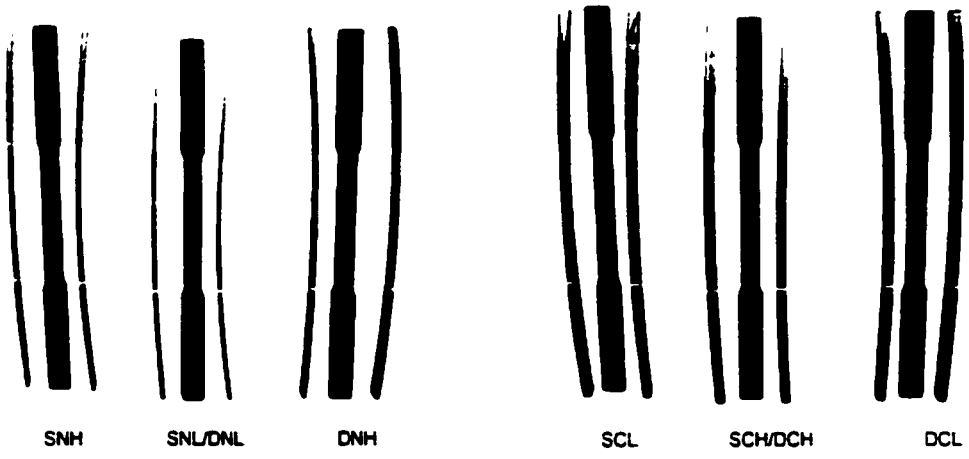

a. Class 4 HSS steel tube coupons

b. Class 1 HSS steel tube coupons

Figure 4.2 Tension test coupons

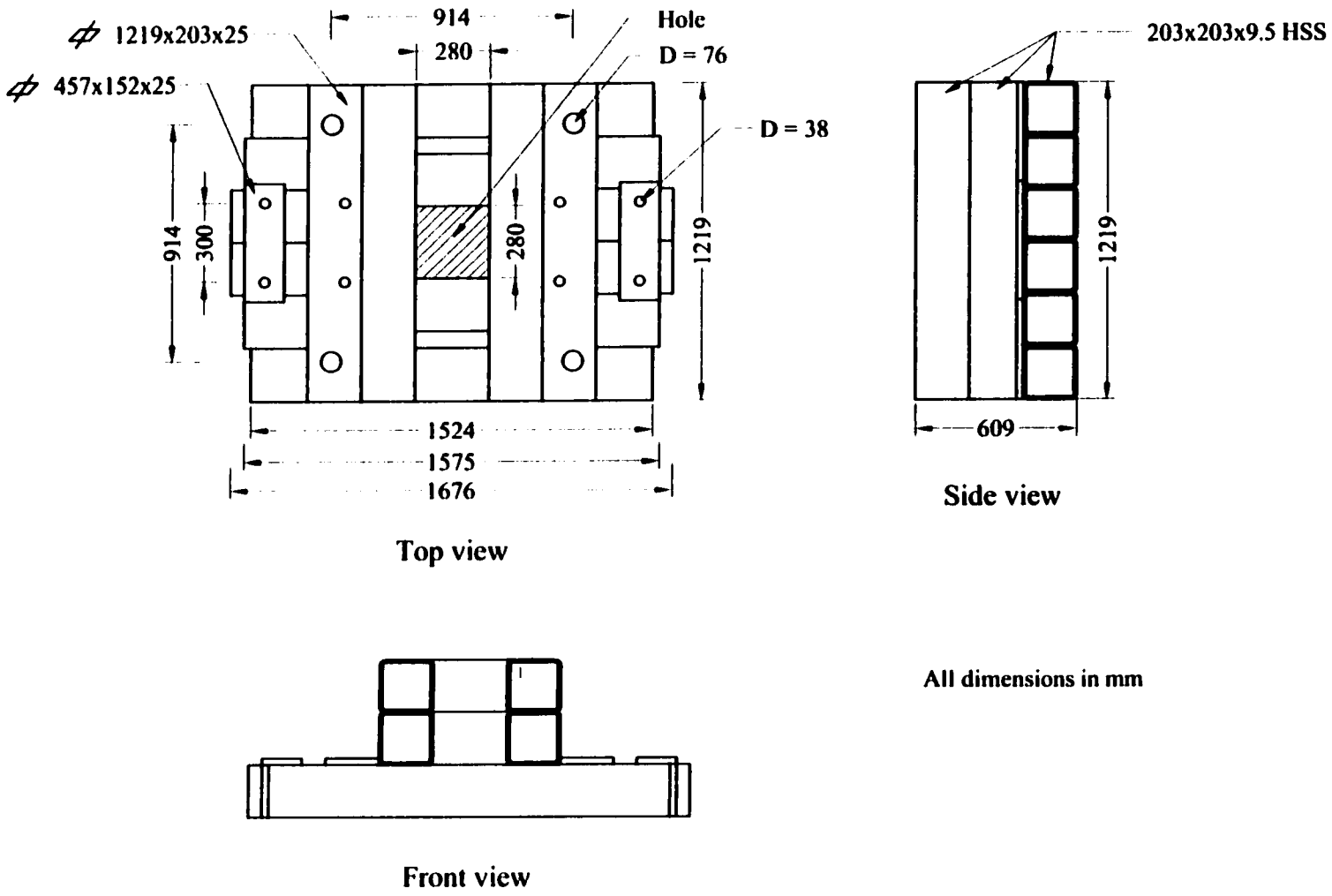

Figure 4.3 Assembled steel foundation

a. Perspective view

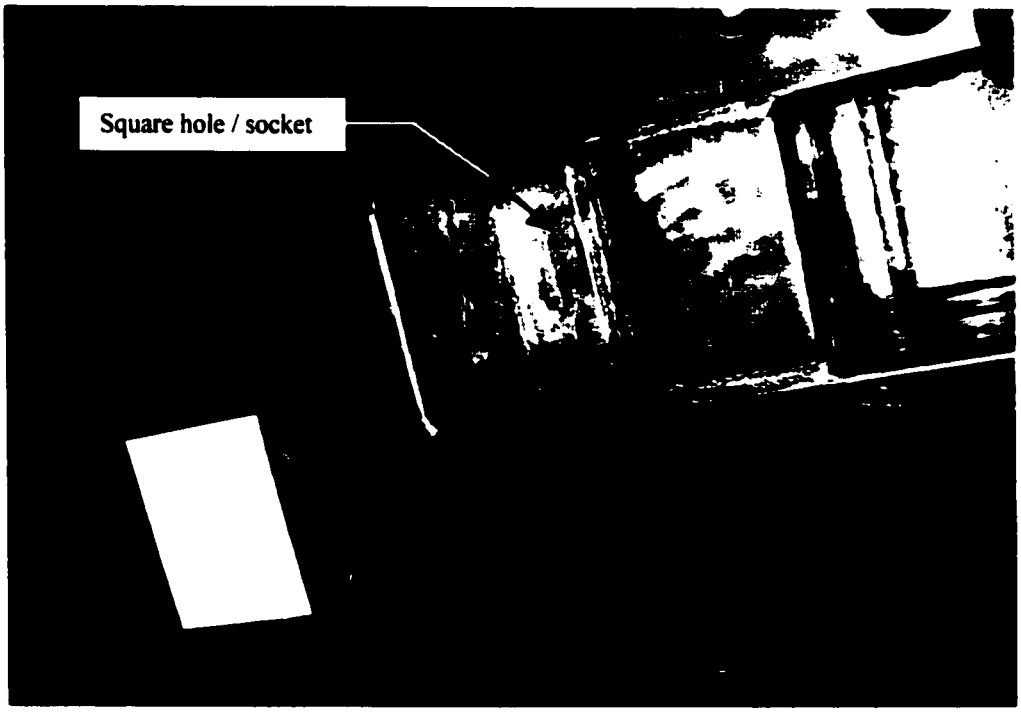

b. Top view

Figure 4.4 Photographs of assembled steel foundation

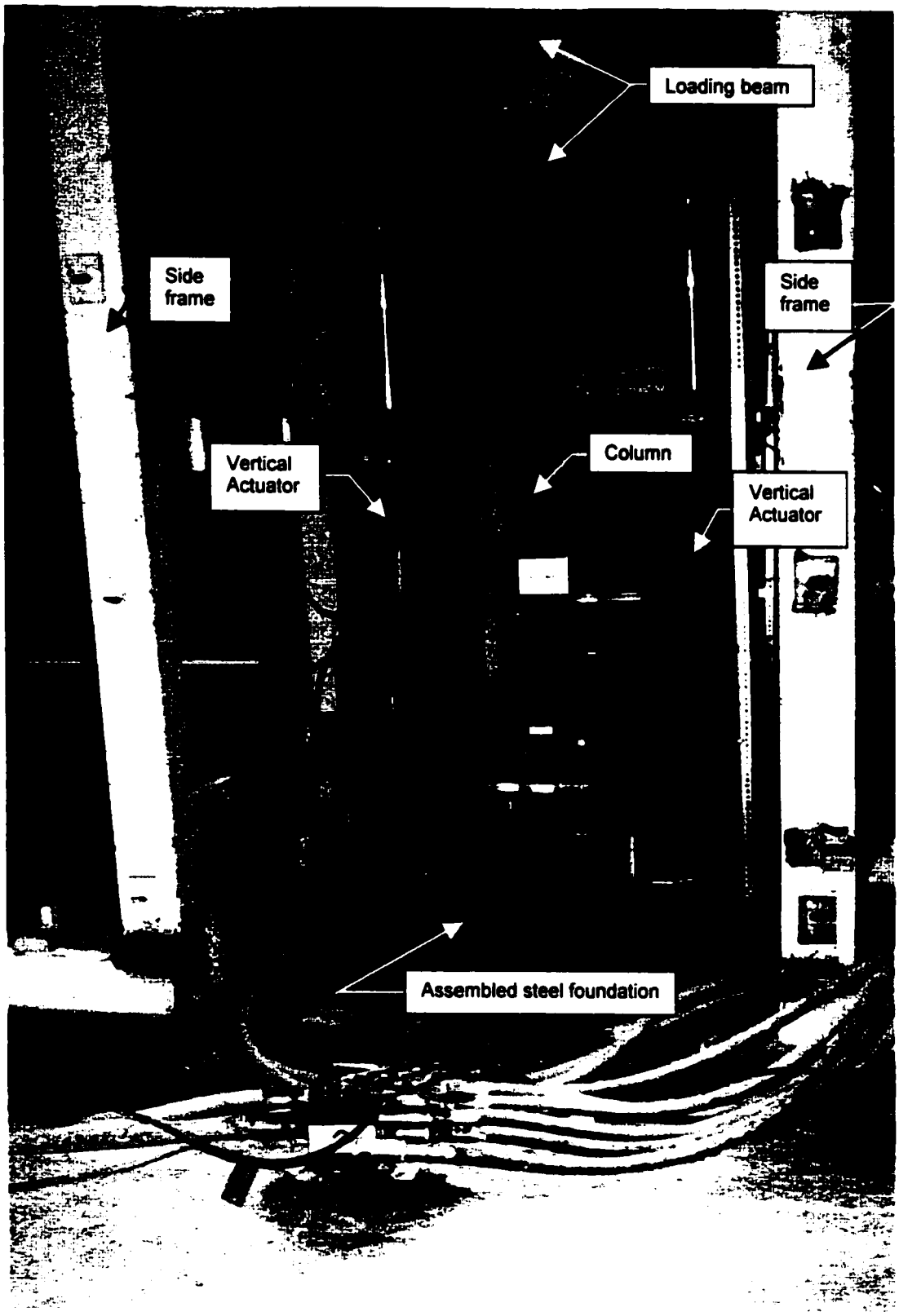

Figure 4.5 Photograph of front view of test setup

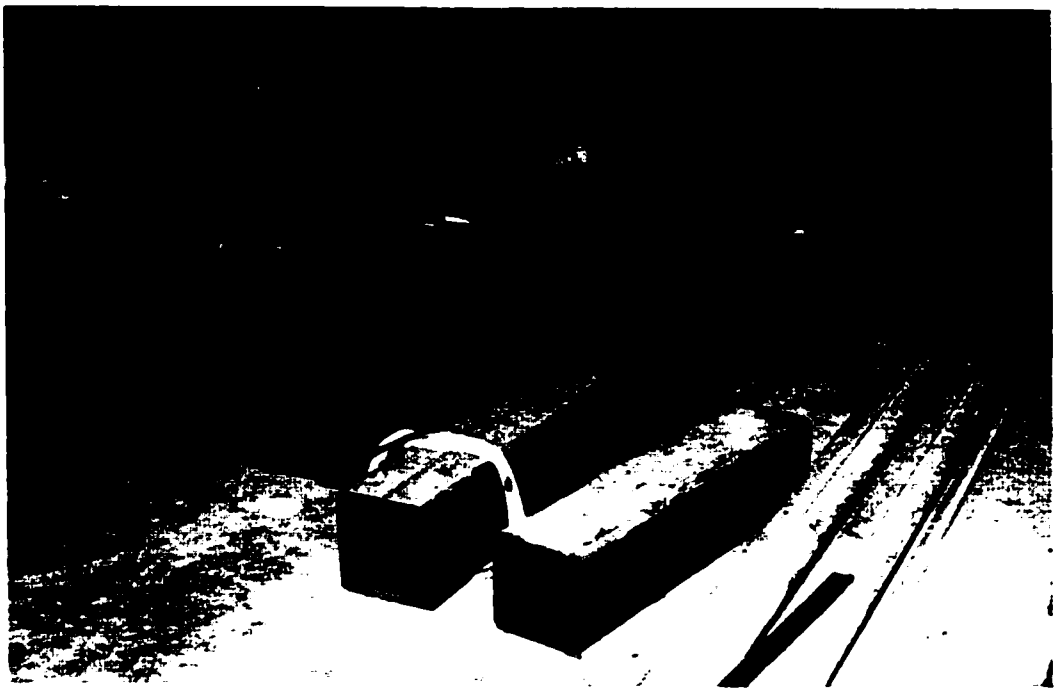

a. Prepared HSS

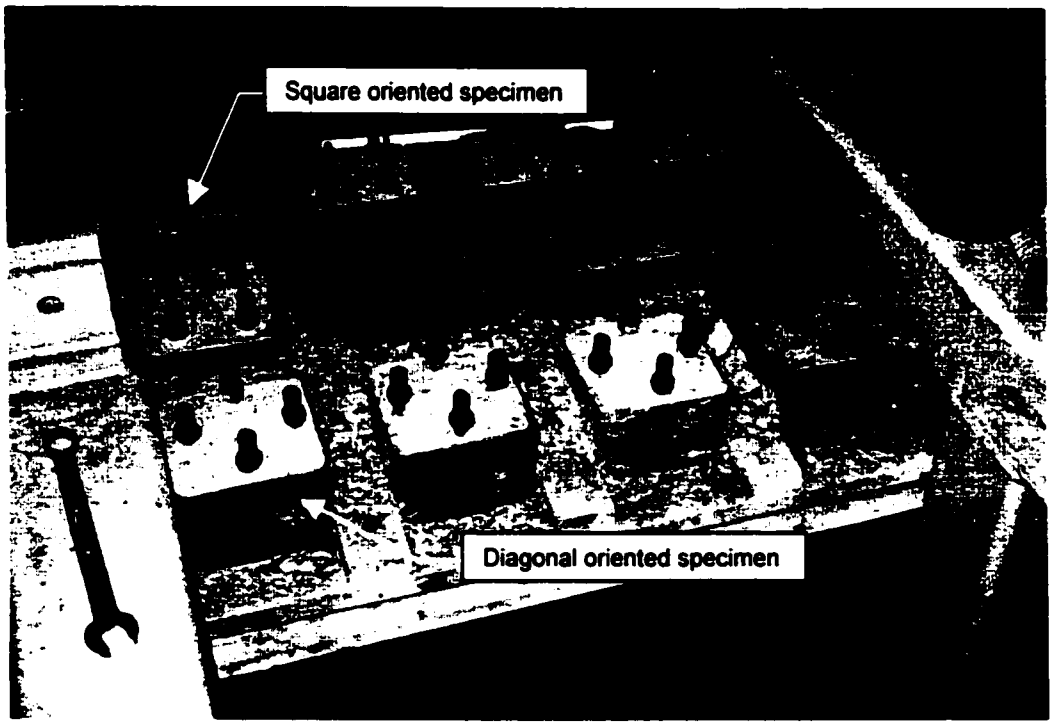

b. HSS CFT column specimens

Figure 4.6 Photographs of Steel tubes and column specimens

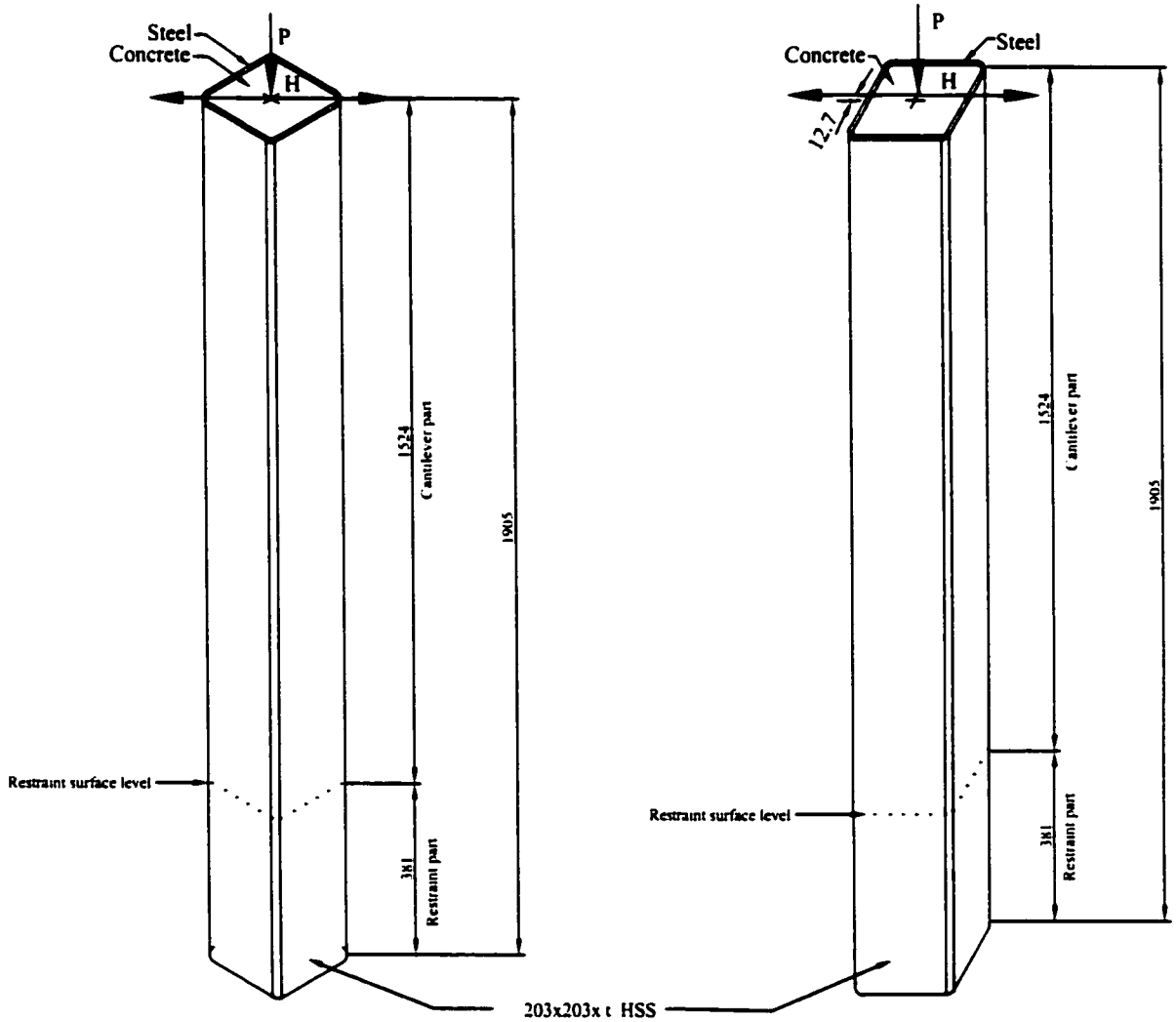

(a)Typical diagonal bending moment specimen (b) Typical biaxial bending moment specimen

Figure 4.7. Typical HSS CFT column specimens

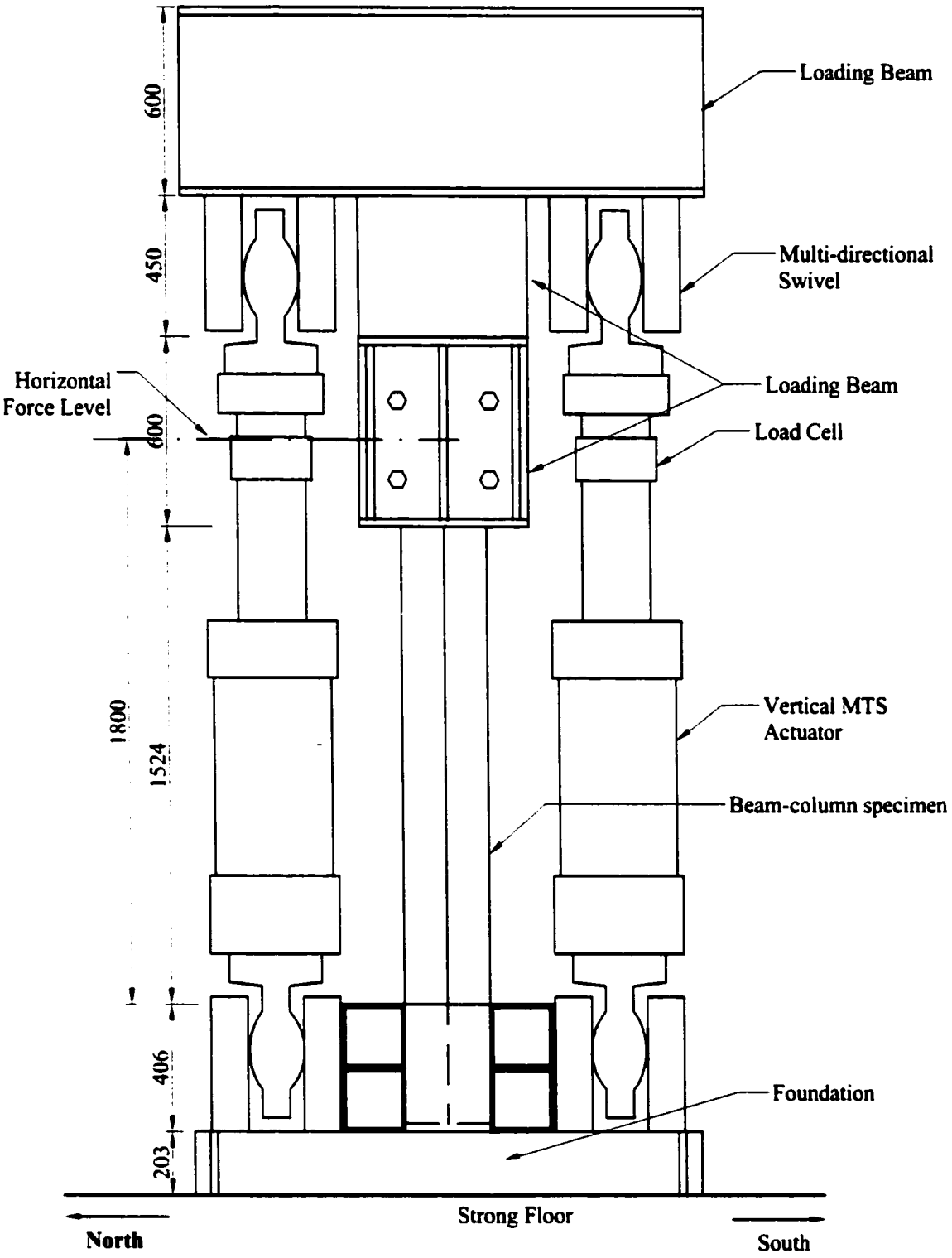

Figure 4.8 Front View of Test Setup

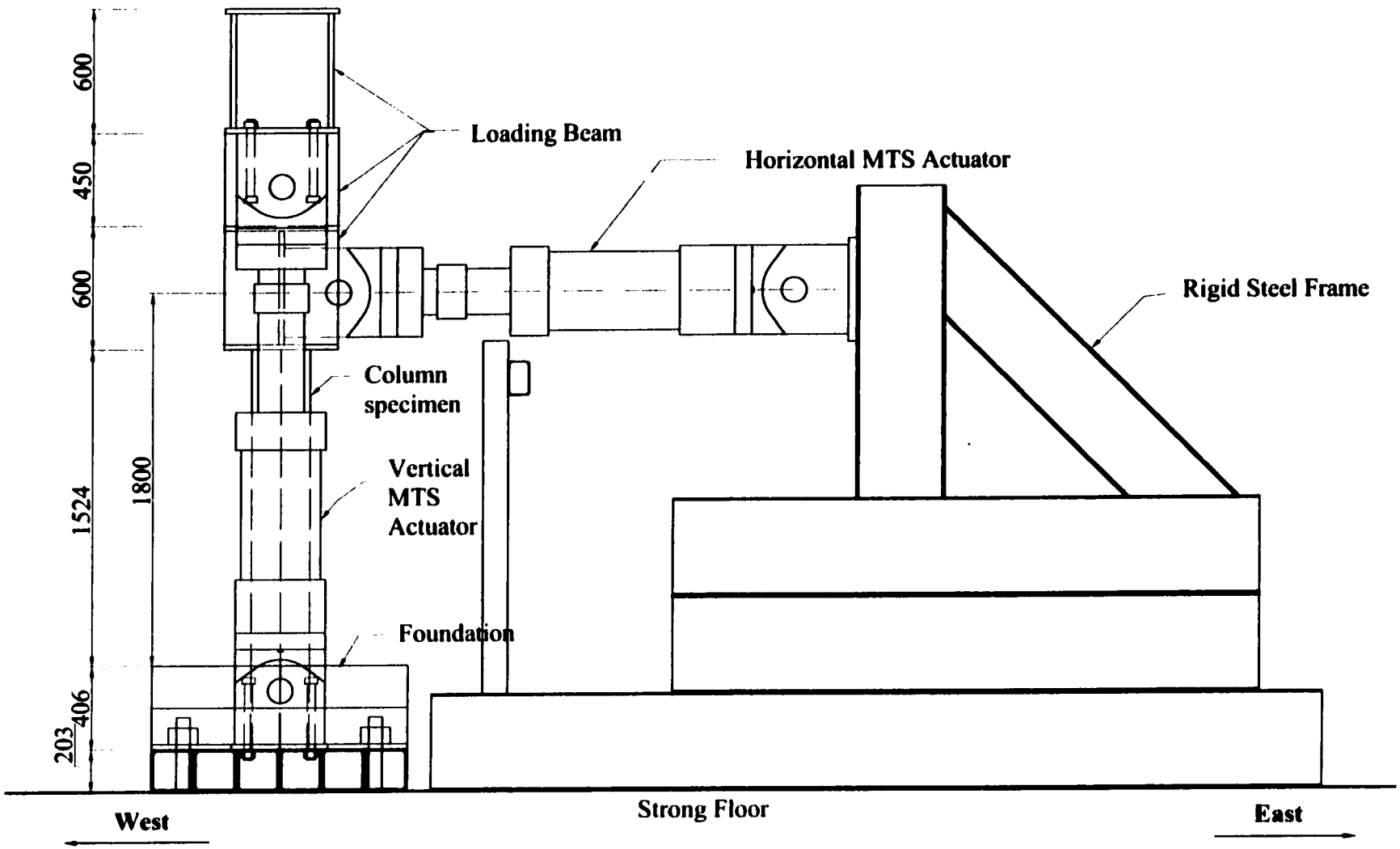

Figure 4.9 Side View of Test Setup

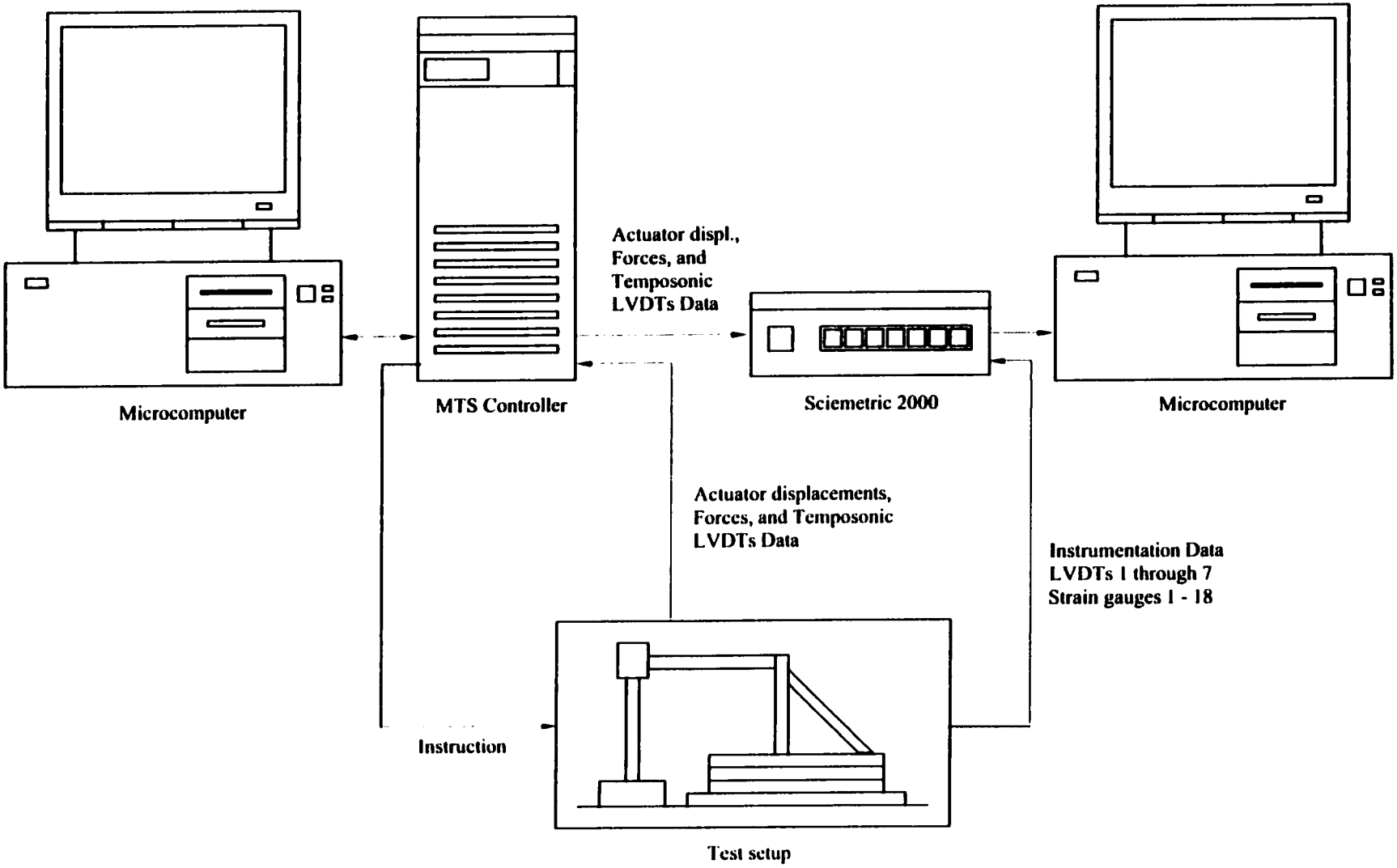

Figure 4.10 The schematic acquisition of test system

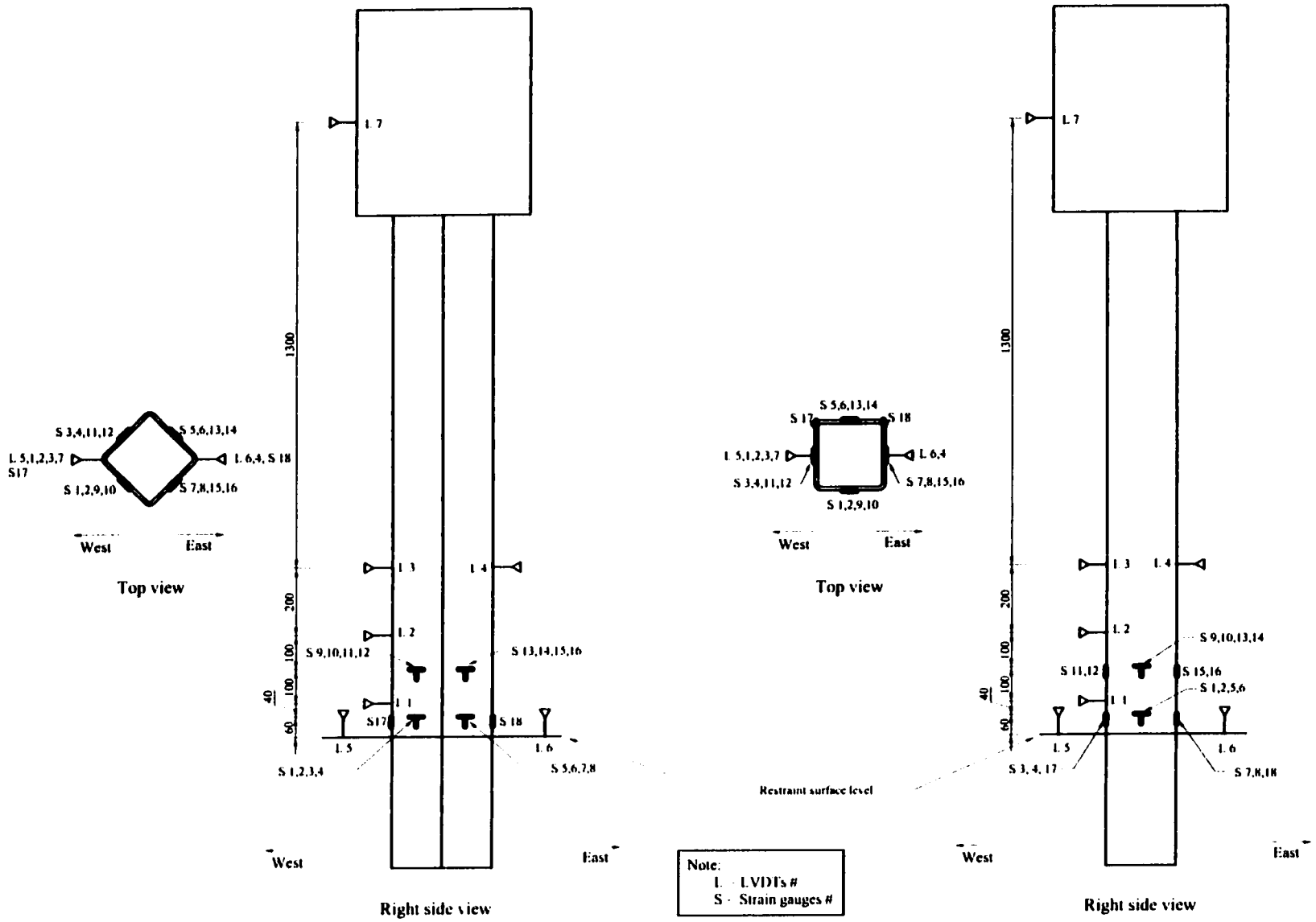

(a) DBM column specimen

(b) BBM column specimen

Figure 4.11 LVDTs and Strain Gauges positions

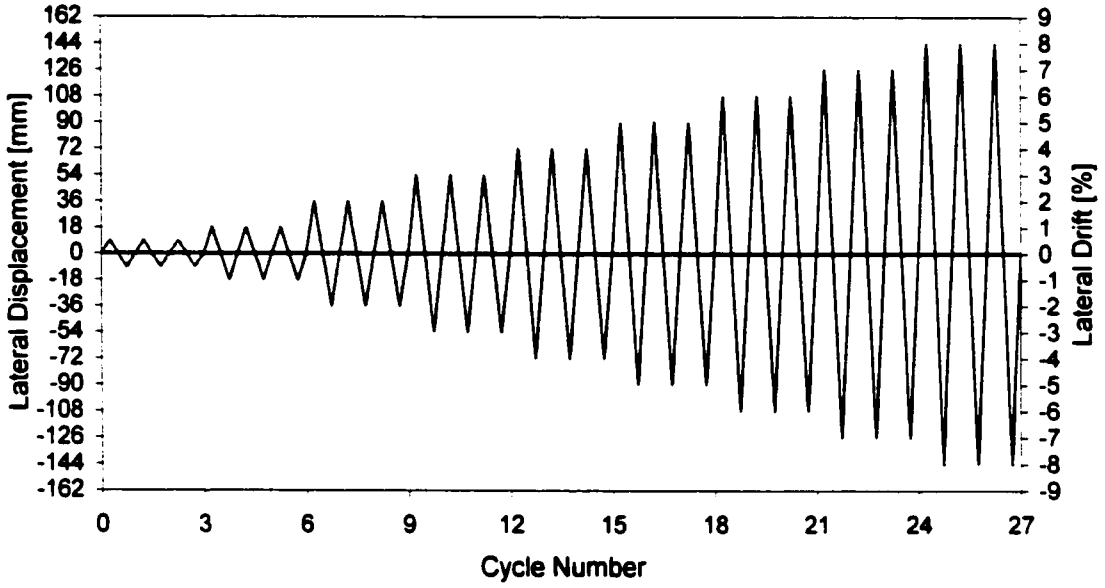

Figure 4.12 Transverse loading history

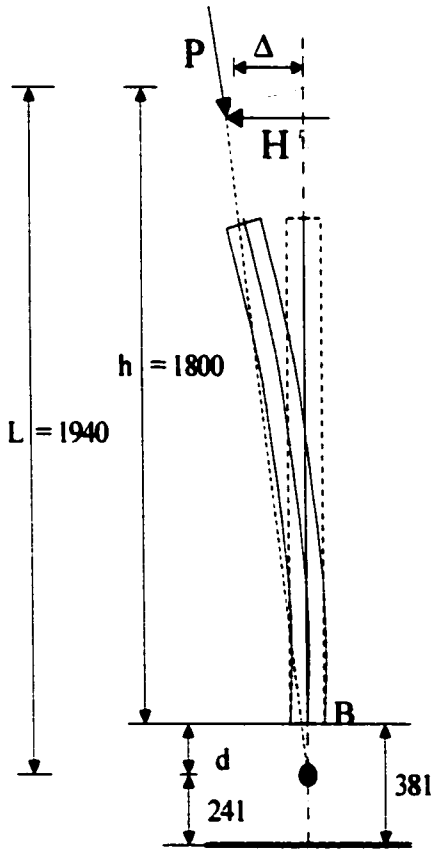

Figure 4.13 System of forces acting on a column specimen

Figure 4.14 Uninstalling column DCH - 2

Chapter 5

NORMAL STRENGTH CFT COLUMNS

5.1 General

A total of twelve square steel HSS columns filled with normal strength (specified strength, f_c' = 40 MPa) concrete were tested under combined constant axial compressive load and cyclic biaxial bending moment. Six of the columns were fabricated with 203x203x9.5 HSS and six with 203x203x4.8 HSS. The 203x203x9.5 HSS are classified as Class 1 sections and the 203x203x4.8 HSS are classified as Class 4 sections according to CAN/CSA-S16.1-94.

The results and evaluations of the test data are presented in the next sections. The evaluations include strength capacity, ductility and stiffness of the CFT columns. All data are presented in tables and graphical formats.

This Chapter starts with test results of individual test materials, which include the stress-strain relationship and the compressive strength of the concrete (standard cylinder test specimens), and the stress-strain relationships and tensile strengths of HSS coupon tests. The tensile strength of the HSS steel is characterized by its yield and ultimate strengths.

These are followed by the observed behaviour and test data of the beam-column tests. The strength capacity of the CFT columns, and comparison of the experimental results to the analytical results using the proposed method of section analysis are discussed in detail. As part of the seismic evaluation of the columns, the ductility of the CFT columns is also discussed. To check column classifications, the flexural stiffnesses of the CFT column specimens were calculated. Finally, the CFT column specimens were evaluated, based upon the flexural stiffness of the column, to determine if the column specimens could be classified into short columns or slender columns.

5.2 Ancillary Test Results

The object of the ancillary tests is to determine the mechanical properties of the materials used in the research program. The ancillary tests consist of standard compressive cylinder tests for the concrete and tension coupon tests for the HSS steel. A total of thirty-nine standard concrete cylinders, 152 mm diameter and 305 mm high, were tested in accordance with CSA A23.2-94 to determine the compressive strength of the core concrete. The tests were done at ages from 21 to 178 days after casting. In addition, three sets of tension coupons were tested in accordance with ASTM A370-95, to determine the strengths of the HSS.

Table 5.1 shows the results of the concrete cylinder tests. Three test results data, cylinders 1 tested at 70 and 94 days and cylinder 2 tested at 111 days, were rejected because these cylinders experienced premature failure. Data for cylinder 2 tested at 80 days was not taken into account in determining the average strength of the concrete because it was too strong compared to the other two. Moreover, the average strengths of the cylinders tested at 94 and 111 days showed significant bias against the expected trend. In general, the measured average values do not illustrate the expected trend; therefore, the test data was analyzed using the least squares method. As a result, data from Table 5.1 were plotted in Figure 5.1, which also shows the curve of the least square, best-fit, third-degree polynomial for the test data. This best-fit curve is expressed by the following equation

$$f_c'(t) = 0.00001\,t^3 - 0.0041\,t^2 + 0.5032\,t + 25.124 \qquad (5.1)$$

where $f_c'(t)$ is the concrete strength in MPa and t is the age of the concrete, in days. Equation (5.1) was used to determine the strength of the concrete in CFT column section analyses.

In addition to the compressive peak strength of standard cylinder tests, the tests included the stress-strain relationship of concrete cylinders. Figure 5.2 shows the stress-strain curve of the three standard concrete cylinders tested at 28 days and the average modulus of elasticity, or secant modulus, of the normal strength concrete. The average modulus of elasticity of three cylinders and analytical results of modulus of elasticity of

normal strength concrete calculated using four equations, Eurocode 2, Gardner's 2001 proposal, ACI 318-99, and CSA A23.3-94, are presented in Table 5.2. Calculation of modulus of elasticity of normal strength concrete using the Eurocode 2 equation gave the best agreement to the average test results. Consequently, this equation was adopted for calculation of modulus of elasticity of normal strength concrete with the Eurocode 2 coefficient increased from 9500 to 10222.

Table 5.3 shows the average tensile strength of the HSS steel, which includes yield strength and ultimate strength. The yield strength and corresponding strain were obtained from the 0.2% offset method. The average coupon yield strengths varied from 390 MPa to 410 MPa.

5.3 Observed Behaviour and Test Data

The behaviour of each CFT column specimen was observed during the tests of all specimens. In general, the behaviour of the test specimens was recorded automatically using a computer data acquisition reading from the instrumentation system on the specimens. However, not all of the significant behaviour of the specimens could be recorded automatically. In cases where the data could not be recorded automatically, visual observation was mandatory. For example, to illustrate positions and patterns of local buckling, it was not possible to record these events automatically.

There are two groups of CFT column specimens according to the geometric orientation of the column sections as they were tested, namely square (SNL and SCL) and diagonal (DNL and DCL) specimens. Letters N (thin) and C (thick) were chosen to identify the two types of HSS employed in the test program; Class 1 sections are indicated by letter C and Class 4 by letter N. Diagonal specimens represent the special case of biaxial bending moment with equal values of major and minor bending moments. The square specimens had a small minor bending moment and torsion produced by virtue of the 12.7 mm offset between the centroid of the section and the centerline of the loading beam.

Column specimens were tested under combination of constant axial compressive load, produced by the vertical actuators, and cyclic bending moment, produced by the

horizontal actuator. The cyclic incremental horizontal forces were under displacement control. Displacement rates were 1 mm/sec, 2 mm/sec and 3 mm/sec for drifts up to 2%, 5% and 8% respectively. The tests took about 4 hours.

The data recorded automatically during tests of the CFT column specimens are presented in this section in graphical format, which consist of load–displacement, moment–displacement and moment–curvature relationships of each CFT column specimen. Load–displacement relationships represent the strength and deformation characteristics of the columns. There are two sets of load data in the load–displacement data. The load data include the raw load data, where the loads are the horizontal loads applied by the horizontal actuator, and the calculated shear forces applied to the critical cross section. Applied shear forces were calculated by including the effect of inclined axial load produced by the two vertical actuators.

Figures 5.3 to 5.6 show the horizontal force–displacement relationships of the horizontal actuator for all normal strength CFT column specimens. These show the applied actuator forces and displacements measured 1800 mm above the fixed base of the columns.

The combination of horizontal force from the horizontal actuator and the component of inclined axial load of the vertical actuators produce an applied shear force on the column specimen. The shear force and bending moment responses are illustrated in the shear force–displacement and moment–displacement relationship graphs of the column specimens in Figures 5.7 to 5.10. It can be seen that the cyclic paths of the shear–displacement and moment-displacement graphs are fat indicating that the columns have good energy dissipation. An interesting behaviour in these graphs is when the applied axial force is greater than 20% of the squash load and at large displacements (more than 3% drift), the displacements disagree with the shear forces or, in other words, the displacements were in the opposite direction to the shear forces. This anomalous behaviour occurred because the horizontal component of the inclined axial load was greater than the horizontal force applied by the horizontal actuator.

Figures 5.11 to 5.14 show the relationships between bending moment and curvature at the recorded strain section, 60 mm above fixed base. These curvatures were calculated from the recorded measured strains.

The sign conventions applied throughout this chapter are; shear forces, horizontal forces and horizontal displacements are positive in the West direction (pushing load on horizontal actuator) and negative in the East direction. Bending moments and curvatures associated with positive shear forces and displacements are positive, and negative for negative displacements.

Selected photographs of specimens during and after the tests are supplied on Figures 5.15 to 5.18.

5.3.1 SNL Columns

The SNL series of columns consisted of three columns: SNL-1, SNL-2 and SNL-3. Each column was tested under a defined, specific constant axial compressive load and a cyclic incremental shear force which produced maximum bending moment at the fixed base. Constant axial compressive loads of 300 kN, 700 kN and 1200 kN were applied at the inflection points of columns SNL-1, SNL-2 and SNL-3 respectively with a 12.7 mm offset from the centroid of the column cross section perpendicular to the shear force direction. This offset axial load produced a minor bending moment of 3.81 kN.m, 8.89 kN.m, and 15.24 kN.m on columns SNL-1, SNL-2 and SNL-3 respectively. In addition, the offset applied shear force produced torsion of 0.71% of the cyclic major bending moment on the columns.

Complete tests data of the SNL columns are supplied in graphical format in Figures 5.3, 5.7 and 5.11. Figures 5.3, 5.7, 5.11 show the horizontal force-displacement, load-displacement and moment-curvature relationships of the SNL column specimens respectively. Figure 5.11 shows the moment-curvature relationship of SNL columns. Strain gages glued on the specimens did not measure the strain as well as expected, because after yielding the strain could not be read proportionally, some were not glued perfectly and others were affected by the local buckling.

Visual observations during the loading test on SNL-1 specimen noted that the steel tube started buckling at the third cycle of 3% drift. The first buckle was at the west side of the tube. Then buckling developed at the east, north and south sides of the tube at the first cycle of 4 % drift, first, and second cycles of 5% drift respectively. The buckle

propagated to all sides and increased in each successive cycle, and the corners of the steel tube buckled. The corner buckle started at 6% drift. The buckle was located 70 mm to 80 mm above the fixed-end surface, or about two-fifth of the width of the steel tube. The northeast and southeast, and the northwest and southwest corners started cracking during the first and the second cycles of 8% drift respectively.

An unexpected accidental error occurred at the last cycle of 6% drift when the test was running without recording test data for the last half cycle. This is shown by the straight line on the graphs (Figures 5.3-a and 5.7-a) from the last third cycle in the east direction of 6% drift to the first cycle of the 7% drift. This is the only loss of test data and it does not affect the results. Accordingly, the analyses were done without considering the missing data.

Column SNL-2 behaved in similar manner to column SNL-1. The buckling started earlier than that on SNL-1. It started at the first cycle of 3 % drift on both (the west and east) sides, followed by buckling on the north and south sides at the third cycle of 3% drift. All buckling took place 75 mm to 85 mm above the fixed-end surface. The corner of the tube started buckling after 5% drift and started cracking at the third cycle of 7% drift. All buckling and cracking increased progressively and by the end of the test the four corners had open cracks averaging about 100 mm in length and 12 mm in width. It could be seen from the open cracks that crushed concrete filled the buckled space and this caused enhancement of the strength capacity of the column after outward buckling of the steel tube.

Column SNL-3 followed the same test procedures as the previous columns and behaved in similar manner. However, buckling occurred on all sides of the steel tube as early as the second cycle of 2% drift was completed. The buckle locations were about 85 mm to 90 mm above the fixed-end surface. No cracks developed in this column, but the second buckle developed at the first cycle of 4% drift on the east side of the tube. Moreover, a second ring of buckles on all sides of the tube occurred by the third cycle of 4% drift located 215 mm to 230 mm above the fixed end surface.

After developing the second outward buckle, the column could resist more shear force or moment because the critical section became larger as crushed concrete filled the buckled areas.

Overall, the SNL columns had good absorbed energy dissipation even though the HSS are classified as Class 4 sections. No premature local buckling occurred and the columns behaved in a ductile manner.

5.3.2 SCL Columns

Three CFT columns made of Class 1 HSS were investigated. These column specimens were identified as SCL-1, SCL-2 and SCL-3 with constant axial compressive loads of 430 kN, 860 kN and 1740 kN, torsion and constant minor bending moments of 5.46 kN.m, 10.92 kN.m and 22.10 kN.m respectively. The test procedures used for the SNL columns were used for the SCL.

Complete tests data of the SCL columns are supplied in graphical format in Figures 5.4, 5.8 and 5.12. Figures 5.4, 5.8, 5.12 show the horizontal force-displacement, load-displacement and moment-curvature relationships of the SCL column specimens respectively.

Column SCL-1 experienced a ring of local buckles after a few cycles of loading. Local buckling appeared visually on the west and east sides of specimens as the first cycle of 4% drift was completed. The other two sides started buckling at the third cycle of 6% drift. The ring local buckle developed 75 mm to 90 mm above the fixed-end surface.

Prior to 3% drift, the bolts connecting the loading beam to the specimen were not secured perfectly which caused rocking of the loading beam against the top surface of specimen. The effect is clearly shown on the graphs, in Figures 5.4 and 5.8, where the cycle pattern is not smooth around zero load.

The maximum degradation of the horizontal force of the horizontal actuator between the first cycle and the last cycle of every drift beyond the maximum horizontal force, at first cycle of 4% drift, was 9 kN

Column SCL-2 experienced local buckling which started on the east and west sides of the column at the third cycle of 3% drift. As the buckles became larger, the north and south sides started buckling at the third cycle of 5% drift, and then a ring local buckle developed 75 mm to 80 mm above the fixed-end surface at the third cycle of 6% drift.

The column resistance suddenly dropped when ring local buckling developed and after that, the resistances remained about constant. The decrease of column resistance was caused by local buckling followed by crushing of the concrete. When a buckle develops, there is a gap between the concrete and the steel tube which causes loss of confinement of the concrete. As a result, the concrete strength decreases and the column capacity should decrease. However, the column strength capacity is about constant, even the concrete strength decreases, because the cross section is larger than the original section after the crushed concrete has filled the gap.

Column SCL-3 started developing local buckles on both the east and west sides at the third cycle of 2% drift, and on the north and south sides at the second cycle of 3% drift. A ring local buckle developed in the third cycle of 4 % drift at 85 mm to 100 mm above the fixed-end surface. As the ring local buckle spread progressively, the northeast corner cracked at the third cycle of 6% drift and followed by the southeast corner. In addition, local buckles developed on the north and east sides at 225 mm and 230 mm above the fixed-end surface respectively.

The behaviour of column SCL-3 was similar to column SCL-2, but the capacity dropped significantly at 4% drift; the strength capacity decreased by about 20% between the first and the third cycles of four percent drift.

Overall, the SCL columns behaved in similar manner to the SNL columns. The strength of the columns dropped after the maximum capacity had been reached. The strength capacity dropped significantly for the column with the higher axial compressive load.

5.3.3 DNL Columns

A series of three CFT column specimens made of Class 4 HSS filled with normal strength concrete were investigated. The square section CFT column was positioned diagonally as it was tested. The specimens were marked as DNL-1, DNL-2 and DNL-3 and had axial compressive loads of 290 kN, 725 kN and 1200 kN respectively.

Complete tests data of the DNL columns are supplied in graphical format in Figures 5.5, 5.9 and 5.13. Figures 5.5, 5.9, 5.13 show the horizontal force-displacement,

load-displacement and moment-curvature relationships of the DNL column specimens respectively.

Column DNL-1 started local buckling on the east (northeast and southeast) sides at the second cycle of 4% drift. This was followed by buckling on the northwest and southwest sides and east corner of the column at the second cycle of 5% drift. A ring local buckle was completed at the third cycle of 5% drift, and it was located 55 mm to 70 mm above the fixed-end surface. Both corner fractures, east and west corners, were developed at the first cycle of 7% drift.

The first local buckle developed on Column DNL-2 on the northeast and southeast sides of the HSS at the third cycle of 3% drift. Buckling increased with every cycle thereafter, and the cyclic loading caused local buckling on the northwest and southeast sides of the HSS as the first cycle of 4% drift was completed. These were followed by a ring local buckle when both east and west corners of the HSS started buckling at the third cycle of 4% drift. After the third cycle of 7% drift was completed, the west corner of the HSS started cracking followed by cracking on the opposite corner at the next cycle. The ring buckle developed at 70 mm to 90 mm above the fixed-end surface.

Column DNL-3 experienced local buckling first on the northwest and southwest sides of the HSS steel at the first cycle of 3% drift. In addition, at the same drift but in the opposite direction of loading (East), the northeast and southeast sides of the HSS buckled. A ring local buckle developed 70 mm to 85 mm above the fixed-end surface after the corners of the HSS buckled at the last cycle of 4% drift. The second ring local buckle was located 190 mm to 200 mm above the base, and started on the northwest and southwest sides of the HSS at the second cycle of 5% drift. This ring was completed during the first cycle of 6% drift. The first crack developed at the west corner at the second cycle of 7% drift followed by a crack at the east corner at the third cycle of 7% drift. Finally, a third local buckle developed on the northwest and southwest sides of the HSS during the first cycle of 8% drift.

5.3.4 DCL Columns

To complete the test program, three CFT column specimens, DCL-1, DCL-2, and DCL-3, made of Class 1 square HSS filled with normal strength concrete oriented diagonally were investigated. Constant axial loads of 430 kN, 800 kN and 1740 kN were applied on top of the DCL-1, DCL-2 and DCL-3 specimens respectively.

Complete tests data of the DCL columns are supplied in graphical format in Figures 5.6, 5.10 and 5.14. Figures 5.6, 5.10, 5.14 show the horizontal force-displacement, load-displacement and moment-curvature relationships of the DCL column specimens respectively.

The first specimen tested in this group was column DCL-1. Nevertheless, unfortunately, at the first test of this specimen could not be completed because after completing the second cycle of 2% drift, the concrete filled foundation broke. As a result, the test was stopped, and the test was rerun four days later with a new concrete filled foundation. The second test followed the standard procedures of the normal test specimen, but started from one percent drift. As evaluation of the horizontal applied loads for 1% and 2% drift of the first and the second tests showed an average difference of 10% higher for the later test, it was decided to use the later complete test data in all analyses.

It was observed that local buckling started first on the northwest and southwest sides of the HSS at the second cycle of 7% drift. At the last cycle of 7% drift, a ring local buckle developed. No cracks were found on this specimen during the test.

Column DCL-2 experienced both a ring local buckle and a crack at the west corner. Local buckling started on the southwest and northeast sides of the HSS as soon as the last cycle of 4% drift was completed followed by the other sides at the second cycle of 5% drift. A ring local buckle was observed 75 mm to 90 mm above the fixed-end surface after the first cycle of 7% drift was completed, and a crack on the west corner was found at the last cycle of 8% drift.

Column DCL-3 had a ring local buckle and cracks on both the west and east corners after the test. The first local buckle started almost at the same time as the second cycle of 3% drift was completed. A ring local buckle started developing 90 mm to 110 mm above fixed-end surface after the second cycle of 4% drift. The first crack was

observed at the east corner of the HSS at the first cycle of 6% drift and the second crack developed at the west corner at the first cycle of 7% drift.

5.4 Strength Capacity

Strength capacity is an important aspect of structural behaviour. To provide a tool for design and analysis of square normal strength CFT columns subjected to constant axial compressive load and cyclic biaxial bending moment, this investigation was conducted with emphasis on the strength capacity of these types of columns. The objective of this study was to formulate a design code equation for seismic resistance of square CFT columns under combined axial compressive load and biaxial bending moment.

The first formulation of the seismic strength of square CFT columns subjected to a constant axial compressive load and a biaxial bending moment is by applying the uniaxial bending moment section analysis approach. The proposed method of analysis, discussed in Chapter 3, is based on the ACI procedures for reinforced concrete section analysis with slight modifications in determining the rectangular concrete stress block. The small minor axis bending moment, less than 10% of major axis bending moment and torsion are neglected.

Using the proposed method of analysis from Section 3.2.6 combined with the measured material constituent strengths at the test age tabulated in Table 5.4, the strength capacity of the normal strength CFT columns was calculated and the results are presented in Table 5.5.

Table 5.5 also illustrates comparisons of experiment to predicted bending moment of all twelve beam-column specimens. Each set of three column specimens, SNLs, SCLs, DNLs, and DCLs, are evaluated. The results are presented in Table 5.5, where the mean values of ratios of experimental to predicted results are 1.041, 1.155, 1.105 and 1.138 for SNL, SCL, DNL and DCL specimens respectively. In addition, the coefficients of variations of these ratios vary from 0.12% to 2.12%, the values of 2.11%, 2.12%, 2.05% and 0.12% for SNL, SCL, DNL, and DCL specimens respectively. Overall, the mean value is 1.110 and the coefficient of variation is 4.39%.

Strength calculations for the SNL and SCL columns are conservative even without considering the softening effects of the minor bending moment. In addition, the DNL and DCL column predictions are also conservative. These results indicate that the strength capacity can be conservatively predicted by uniaxial bending moment section analysis neglecting the effect of minor bending moment

Figures 5.19 to 5.23 illustrate clearly the comparison of predicted strength capacity to experimental results of each type of columns. Predicted strength capacities for these figures were calculated based on the average concrete compressive strength of the three columns in each type of CFT columns.

Overall, the predicted results are conservative, therefore, it can be concluded that the method of analysis is appropriate for these types of columns, especially for CFT columns under diagonal bending moment i.e. for the columns under equal biaxial bending moment where the columns are not affected by torsion.

5.5 *Ductility*

Two kinds of ductility are considered in this section: displacement ductility and curvature ductility. Displacement ductility and curvature ductility were determined using Equations (3.48) and (3.49) respectively.

The New Zealand Standard NZS 4203-1984 defines ultimate displacement, Δ_u, as the displacement corresponding to reduction in strength of the structure with respect to horizontal forces, shall not exceed 20 % of its maximum strength. This criterion is adopted in the analysis in this section.

Reinforced concrete structures use the criterion of yield curvature based on the curvature prior to the peak point at a moment of 75% of maximum moment, not based on the first yield curvature. In this case, an equivalent yield curvature is approximately one-third times higher than first yield curvature (Paulay et al, 1992). This expression is not used here. The yield curvature, Φ_y, and yield displacement, Δ_y, are defined based on the first-yield curvature and measured first yield displacement respectively. To check the inconsistency of equivalent yield curvature on reinforced concrete structure criterion if it

is applied to the CFT columns, the ratios of yield moments to maximum moments have been calculated.

Table 5.6 shows the ductility of test results of normal strength CFT columns. Neither displacement ductility nor curvature ductility of the test results illustrate a specific trend. The displacement ductility μ_Δ of CFT column specimens varies from 2.920 to 9.058. In addition, the curvature ductility μ_Φ varies over a wide range, from 3.356 to 19.814. Because the ductility values vary widely, it is more useful to use ultimate displacement drifts of columns as an indicator in illustrating the ductility of columns. It is important to recognize that the single discrete value of ductility can be misleading since the calculated ductility is very sensitive to the criterion used to establish the ductility.

The displacement ductility of the Class 1 HSS CFT columns is larger than that of the Class 4 HSS CFT columns. This phenomenon can be explained as follows; the steel areas of Class 1 HSS CFT columns are larger than that of Class 4 HSS section. Steel is a ductile material. Conversely, concrete is a brittle material. Combination of concrete – steel materials produce a ductile composite material. Consequently, in general, the more steel in the composite section, the more ductile is the section.

Displacement ductility of normal strength CFT columns shows a trend where the larger the axial compressive load applied on the column, the larger the displacement ductility.

The ratios of yield moments to maximum moments varied from 0.392 to 0.768. For Class 4 HSS CFT columns, the yield moments at the yield curvature and the yield displacement are from 64% to 77% of maximum moments. For Class 1 HSS CFT columns, however, the ratios of yield moments to maximum moments at the yield curvature and the yield displacement are less than that of Class 4 HSS CFT columns. This indicates the criterion of equivalent yield curvature of reinforced concrete structures could not be applied for the CFT columns. A more reasonable criterion is the first yield curvature and the first yield displacement.

5.6 Flexural Stiffness

Flexural stiffness of a member is defined as the product of modulus of elasticity of the material, or materials, and moment of inertia of cross section of the member.

Table 5.7 shows the flexural stiffness of normal strength CFT columns. Evaluation of experimental and analytical, calculated using Eurocode 2, ACI 318-99, CSA A23.3-94 and Gardner's 2001 proposed formulas, results of the modulus of elasticity of normal strength concrete presented in Table 5.2 shows the calculation using Eurocode 2 formula gave the best results. Consequently, the modulus of elasticity of concrete is calculated using the modified Eurocode 2 formula (Equation 3.50 and 3.51). The flexural stiffness is determined using ACI formula (Equation 3.53) and proposed formulas (Equations 3.54 and 3.55).

The ACI formula of flexural stiffness of composite columns is too conservative when it is applied for square CFT columns under combined axial compressive load and cyclic biaxial bending moment.

The proposed formula for Class 1 HSS CFT columns shows a good agreement to the experimental results. Column DCL-1 is over estimated, others are conservative. The mean value of the ratio of experimental to proposed results is 1.0171, and the coefficient of variation is 4.13%. More precisely, if the formula is applied to the SCL columns, the results are under estimated, with a mean ratio of 1.0414 and the coefficient of variation of 2.42%. However, when it is used to calculate the flexural stiffness of DCL columns, the results are over estimated, with the mean ratio of 0.9928 and the coefficient of variation of 4.51%. This result was strongly biased by the result of column DCL-1 test. If column DCL-1 test result is neglected, the proposed formula produces safe predictions of flexural stiffness.

For Class 4 HSS CFT columns, the proposed formula produces safe predictions. All proposed results are on the lower bound side. The mean ratio of experimental results to prediction of all class 4 HSS CFT columns is 1.0380 and the coefficient of variation is 1.91%. Moreover, the mean ratios of experimental results to prediction of DNL and SNL columns are 1.0214 and 1.0545 respectively, and the coefficient of variations are 0.76% and 0.95% for DNL and SNL columns respectively.

Overall, the mean ratio is 1.0275, and the coefficient of variation is 3.23%. It can be concluded that these proposed formulas are appropriate to predict the flexural stiffness of normal strength CFT columns subjected to combined axial compressive load and cyclic biaxial bending moment for seismic events.

5.7 Column Classification

A conventional method of classification of columns is by comparing their load carrying capacity based on the squash load and the Euler load. If the squash load of the column is more critical than Euler load, the column is classified into stocky columns. However, if the Euler load is more critical then the column is classified into slender column.

The conventional method of classification of columns is applied herein to classify the experimental column specimens. Table 5.8 shows comparison of squash load to Euler load of normal strength CFT columns. All squash loads of columns are less than the Euler loads; therefore, they are classified into stocky columns.

5.8 Discussion

All normal strength CFT column specimens behaved in similar manner in resisting combined axial compressive load and cyclic bending moment produced by lateral displacement of the horizontal actuator. It was observed that the maximum moment resistances of the columns occurred as the steel tube started local buckling. When the steel tubes were buckling, CFT columns as a system lost their capacities. Outward buckling of the steel tube caused the concrete to lose its confinement (if any), and often the steel tube started buckle after the concrete crush.

Saatcioglu and Razvi (1992) reported that square and rectangular reinforced concrete columns with rectilinear reinforcements experienced non-uniform lateral pressure. Maximum lateral pressure occurred at the corner because rectilinear reinforcement more effective at the corners than at sides of the cross section columns.

This behaviour showed the effectiveness of confined concrete on the square or rectangular reinforced concrete columns.

Square CFT columns behave very closely similar to square reinforced concrete columns with rectilinear reinforcements. Test results confirmed this behaviour where the confinement effects on square column sections is much more effective at the corners of the sections than that at the sides. It is apparent that sides of HSS steel sections are less stiff than their corners, hence the HSS steel sections confined concrete more effectively at the corners than at the sides. As a result, square CFT columns experience confinement effects, but are not as effective as on the circular CFT columns, when subjected to axial compressive load or combined axial compressive load and bending moment.

Previous studies (Johnson and Buckby, 1979) reported the confinement of the rectangular tubes only at the corners of the column section. It was observed in this investigation that the corners of the steel tubes were stiffer than the sides which was indicated by the sides buckling before the corners. This property enhances the effectiveness of concrete confinement at the corners.

Observation showed that the columns oriented diagonally across the section started local buckling two to three cycles later than the columns oriented normal square. Strengths of diagonal columns are less than that of normal oriented columns. The differences are not significant, less than 3.6 %. Although diagonal oriented columns experienced later local buckling, the strengths are less than that of normal oriented columns. Consequently, the event of starting local buckling cannot be used to indicate the strength of the column sections.

Most proposed strength analyses of CFT columns follow procedure for design of conventional reinforced concrete columns. Section analysis procedures are adopted with variation in the concrete strain limits, concrete stress-strain models, slenderness effects and load or stress distribution in the CFT sections. Previous proposed analyses have been successful for certain condition. For example, Tomii and Sakino's (1979) proposed method for determining the ultimate moment was excellent for CFT columns under monotonic axial loads less than 58% of the squash loads.

Learning from the weakness of the Tomii and Sakino's proposed method, the stress distribution of the concrete can be modified by including the axial compressive

effects on determination of concrete stress distribution. When this factor was included in the equivalent stress distribution and checked with the strength test results, it showed good agreement.

The idea of including the axial load effects was based on assumption that the steel tube confined the concrete in square CFT columns. The strength capacity of the section decreases when the tube is unable to, or ineffective, confined the concrete core because of large axial load. To accommodate this phenomenon, the strength capacity of concrete core should be treated by introducing a factor, namely α_2, (less or equal to 1.0) depending on the axial compressive load applied on the CFT column, type of concrete and steel tube wall thickness (section classification). Class 1 HSS sections are more compact than Class 4 HSS section; therefore, Class 1 HSS sections produce effective confinement when used for CFT columns. Class 4 HSS sections are, however, less effective in confining the concrete core in CFT columns. As a results, using $\alpha_2 = 1.0$ and $\alpha_2 = 1.0 - (2.34 / \ln f_c')$ (P/P_o) are appropriate for CFT columns made of Class 1 and Class 4 HSS sections respectively.

Comparison of predicted to test results of column strength shows good agreement. All predicted strengths are conservative, and the predicted strengths of diagonal columns are more conservative than that of normal square columns. This is reasonable because the strengths of square columns were calculated based on the test data without considering the minor bending moment and torsion. In general, the proposed method of analysis is appropriate for determining the strengths of CFT columns subjected to axial compressive load and cyclic biaxial bending moment.

There is no consensus among engineers or researchers for determining method of analysis for column ductility. Determination of ductility is sensitive to the method of analysis.

Ductility of columns is mostly determined by its material ductility. Ductility of reinforced concrete columns is determined by the amount and configuration of shear reinforcement. Using the reinforced concrete columns as a model of CFT columns, the ductility of CFT columns should be affected by the steel tube used for CFT columns. In this case, wall thickness of HSS steel section is the main factor that affect the ductility of the columns. The thicker the wall thickness of HSS, the more ductile the column will be.

Test results confirmed this phenomenon. Class 4 HSS CFT columns are less ductile than Class 1 HSS CFT columns. Class 1 HSS CFT columns have excellent ductility. Orientation of the columns did not show a uniform trend, but if drifts are used as an indicator for ductility, both diagonal columns and normal square columns roughly have the same ductility.

Flexural stiffness of normal strength CFT columns was determined using proposed method of analysis based on the concrete compressive strength of standard cylinder tests. There was no enhancement of the concrete strength for seismic loading, because the difference of the modulus of elasticity of the concrete based on the strength with and without enhancement is about 3%, which is acceptable for design purposes.

Flexural stiffness of normal strength CFT columns calculated using proposed method shows good agreement to the test results. Column DCL-1 is the only column over estimated. By exempting column DCL-1, it can be concluded that the proposed method is appropriate for calculation of flexural stiffness of normal strength square CFT columns subjected to combined axial compressive load and cyclic biaxial bending columns.

Table 5.1 Compressive strength of standard cylinder tests of the concrete

Age [days]	Concrete strength [MPa]			
	Cylinder 1	Cylinder 2	Cylinder 3	Average
21	35.2	35.5	32.2	34.3
28	36.6	35.3	35.1	35.7
44	38.4	41.6	41.6	40.5
62	41.8	45.3	40.2	42.4
70	26.0*	45.7	43.1	44.4
80	44.3	49.3[$]	44.4	44.4
87	44.0	46.7	45.3	45.3
94	31.0*	39.5	43.7	41.6[#]
101	45.5	45.9	44.5	45.3
111	46.0	33.0*	48.0	47.0[#]
120	44.0	44.9	46.0	45.0
178	46.7	46.2	46.7	46.5

* Data omitted
[$] Not included in average
[#] Significant abnormal trend

Table 5.2 Test and analytical results of modulus of elasticity of NSC

Procedure	E_c [1] [MPa]
Cylinder tests [2]	33,815
Eurocode 2: $E_c = 9500\,(f_{cm})^{1/3}$	31,426
Gardner: $E_c = 4300\sqrt{f_c'} + 3500$	29,372
ACI 318-99: $E_c = 4700\sqrt{f_c'}$	28,278
CSA A23.3-94: $E_c = \left(3300\sqrt{f_c'} + 6900\right)\left(\gamma_c/2300\right)^{1.5}$	26,755

[1] $f_c' = f_{cm28} = 36.20$ MPa
[2] Average value of 3 cylinders

Table 5.3 The HSS steel properties

Designation	Nominal				Measured			
	Dimension [mm]		Tensile strength [MPa]		Dimension [mm]		Tensile strength [MPa]	
	b	t	$f_{y,min}$	$f_{u,min}$	b	t	f_y	f_u
SNL	203.2	4.76	345	425	203.2	4.41	390.4	470.8
SCL	203.2	9.52	345	425	203.2	8.98	393.2	482.4
DNL	203.2	4.76	345	425	203.2	4.41	390.4	470.8
DCL	203.2	9.52	345	425	203.2	8.92	410.8	488.5

Table 5.4 Specimens constituent strength at the test

Specimen	f_c' [MPa]	f_y [MPa]	Specimen's age at test [days]
DNL – 1	40.2	390.4	44
DNL – 2	42.9	390.4	62
DNL – 3	43.7	390.4	70
DCL – 1	44.3	410.8	80
DCL – 2	44.4	410.8	94
DCL – 3	44.4	410.8	87
SNL – 1	44.4	390.4	101
SNL – 2	44.4	390.4	104
SNL – 3	44.4	390.4	105
SCL – 1	44.4	393.2	106
SCL – 2	44.4	393.2	107
SCL – 3	44.4	393.2	111

Table 5.5 The strength capacity of normal strength CFT columns

Designation	Axial load P [kN]	Bending moment [kN.m]		$\frac{M_{exp}}{M_{pre}}$	μ	c.of v. [%]
		Predicted* M_{pre}	Experiment M_{exp}			
SNL – 1	300	131.70	140.12	1.064	1.041	2.11
SNL – 2	700	137.60	142.63	1.037		
SNL – 3	1200	128.30	131.18	1.022		
SCL – 1	430	226.61	257.37	1.136	1.155	2.12
SCL – 2	860	230.02	263.86	1.147		
SCL – 3	1740	212.01	250.77	1.183		
DNL – 1	290	124.80	135.16	1.083	1.105	2.05
DNL – 2	725	128.57	141.75	1.103		
DNL – 3	1200	120.74	136.22	1.128		
DCL – 1	430	223.40	254.44	1.139	1.138	0.12
DCL – 2	800	226.70	257.67	1.137		
DCL – 3	1740	214.48	244.26	1.139		
				Overall :	1.110	4.39

Coefficient of variation; c. of v. = $\frac{\sigma}{\mu}$

* Effects of M_y are neglected for square (SNLs and SCLs) columns

Table 5.6 Yield moment ratio and ductility of normal strength CFT columns

Designation	Δ_y [mm]	Φ_y (10^{-6})	M_y [kN.m]	$\frac{M_y}{M_{max}}$	μ_Δ	μ_Φ	Drift [%]
SNL – 1	35.732	14.265	107.59	0.768	3.527	14.942	7
SNL – 2	25.821	14.658	108.70	0.762	3.513	10.475	5
SNL – 3	11.773	10.717	80.76	0.616	4.697	11.831	3
DNL – 1	36.678	12.141	87.20	0.645	2.935	3.356	6
DNL – 2	31.040	13.466	96.41	0.680	2.920	15.503	5
DNL – 3	15.474	11.971	86.74	0.637	3.399	11.730	3
SCL – 1	33.344	17.936	173.28	0.673	4.886	19.473	9
SCL – 2	18.968	14.865	145.97	0.553	5.694	14.800	6
SCL – 3	9.416	11.493	116.42	0.464	7.727	17.135	4
DCL – 1	22.433	13.502	118.29	0.465	7.200	3.980	9
DCL – 2	15.916	12.526	118.73	0.461	8.013	19.814	7
DCL - 3	7.943	10.093	95.78	0.392	9.058	19.403	4

Table 5.7 Flexural stiffness of normal strength CFT columns

Designation	HSS			Concrete			EI [kN.m^2]			$\frac{EI_{exp}}{EI_{prop}}$	μ	c. of v. [%]
	f_y [MPa]	E_s [MPa] $(10)^5$	I_s [mm^4] $(10)^6$	f_c' [MPa]	E_c[1] [MPa]	I_c [mm^4] $(10)^6$	EI_{ACI}[2]	EI_{Prop}[3]	EI_{Exp}			
DNL – 1	390.4	1.965	22.602	40.2	35634	118.791	5288	6981	7182	1.0288	1.0214	0.76
DNL – 2	390.4	1.965	22.602	42.9	36811	118.791	5316	7065	7159	1.0133		
DNL – 3	390.4	1.965	22.602	43.7	37153	118.791	5324	7089	7246	1.0221		
SNL – 1	390.4	1.965	22.602	44.4	37449	118.791	5331	7110	7542	1.0607	1.0545	0.95
SNL – 2	390.4	1.965	22.602	44.4	37449	118.791	5331	7110	7416	1.0430		
SNL – 3	390.4	1.965	22.602	44.4	37449	118.791	5331	7110	7536	1.0598		
For class 4 HSS CFT columns											1.0380	1.91
DCL – 1	410.8	1.969	41.713	44.3	34765	97.654	8944	9309	8761	0.9411	0.9928	4.51
DCL – 2	410.8	1.969	41.713	44.4	37449	97.654	8945	9310	9479	1.0181		
DCL – 3	410.8	1.969	41.713	44.4	37449	97.654	8945	9310	9490	1.0193		
SCL – 1	393.2	1.999	41.942	44.4	37449	97.390	9114	9478	9661	1.0193	1.0414	2.42
SCL – 2	393.2	1.999	41.942	44.4	37449	97.390	9114	9478	9820	1.0360		
SCL – 3	393.2	1.999	41.942	44.4	37449	97.390	9114	9478	10130	1.0688		
For class 1 HSS CFT columns											1.0171	4.13
Overall											1.0275	3.23

Coefficient of variation; c. of v. = $\frac{\sigma}{\mu}$

(1) $E_{cmt} = E_{cm28} (f_{cmt} / f_{cm28})^{1/2}$; $E_{cm28} = 10222 (f_{cm28})^{1/3}$

(2) $EI_{ACI} = 0.2 E_c I_c + E_s I_s$

(3) $EI_{Prop} = 0.6 E_c I_c + E_s I_s$; for class 4 HSS CFT (DNL, SNL) specimens

(3) $EI_{Prop} = 0.3 E_c I_c + E_s I_s$; for class 1 HSS CFT (DCL, SCL) specimens

Table 5.8 Comparison of squash load (P_o) to Euler load (P_E)

Designation	Theory		Experiment		P_o [kN]
	EI_{ACI} [kN.m^2]	EI_{prop} [kN.m^2]	EI_{Exp} [kN.m^2]	P_E [kN]	
SNL – 1	5331	7110	7542	5743.56	2774.77
SNL – 2	5331	7110	7416	5647.41	2774.77
SNL – 3	5331	7110	7536	5738.99	2774.77
DNL – 1	5288	6981	7182	5469.41	2639.94
DNL – 2	5316	7065	7159	5451.89	2726.62
DNL – 3	5324	7089	7246	5518.14	2752.30
SCL – 1	9114	9478	9661	7357.27	4333.97
SCL – 2	9114	9478	9820	7478.36	4333.97
SCL – 3	9114	9478	10130	7714.44	4333.97
DCL – 1	8944	9309	8761	6671.88	4434.41
DCL – 2	8945	9310	9479	7218.67	4438.18
DCL - 3	8945	9310	9490	7227.05	4438.18

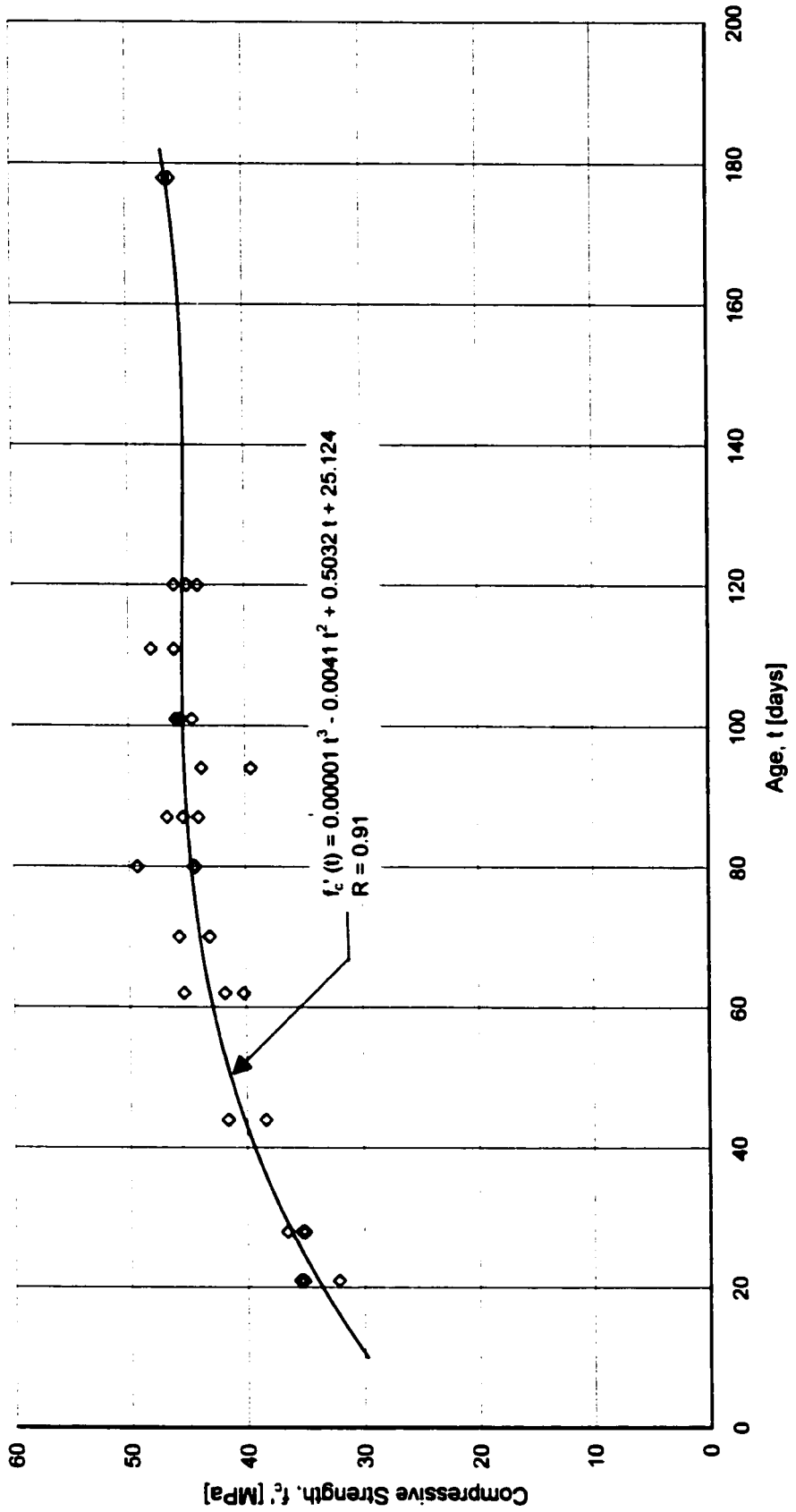

Figure 5.1 Compressive strength of normal strength concrete

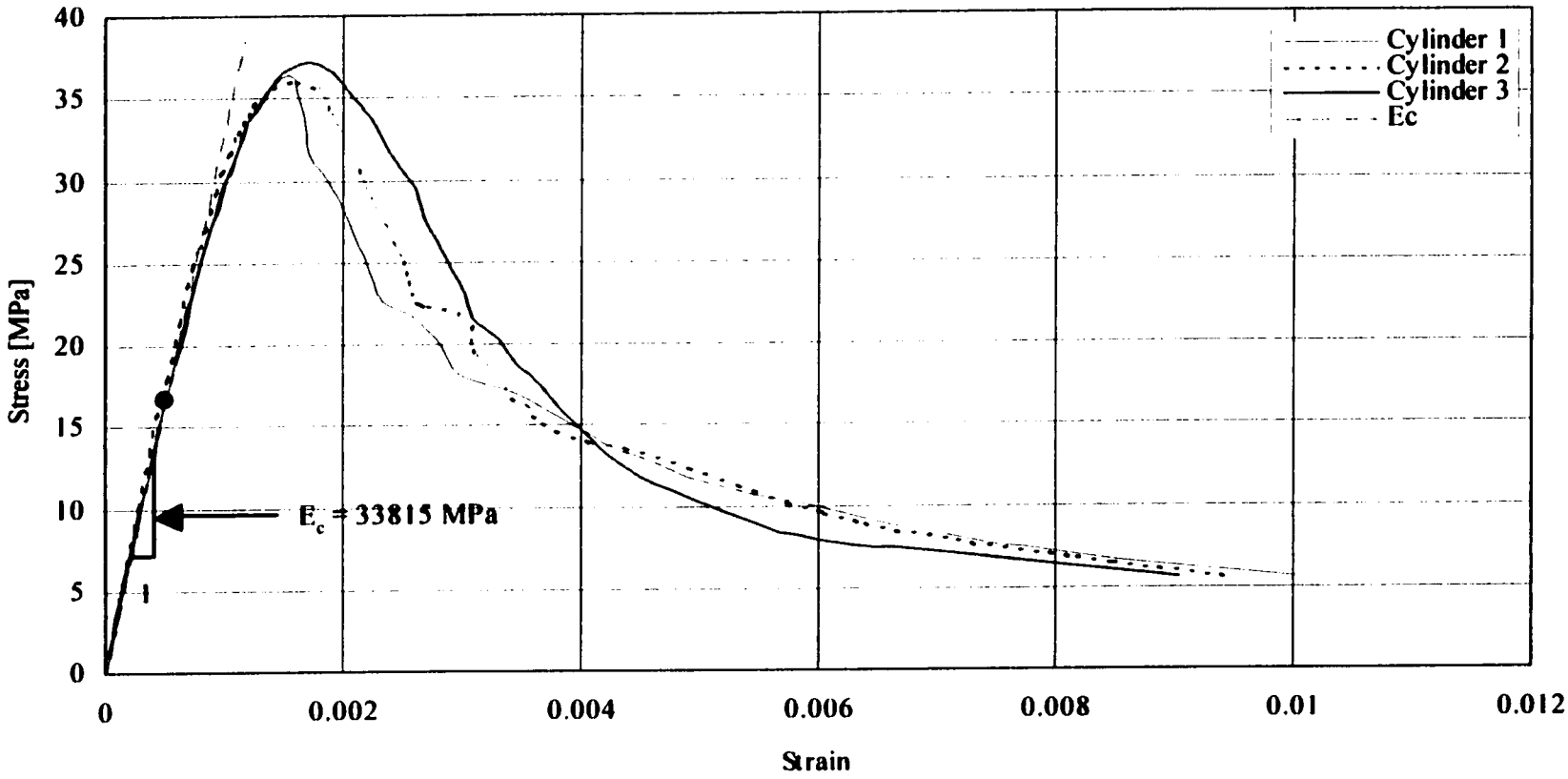

Figure 5.2 The stress-strain curve of concrete tested at 28 days

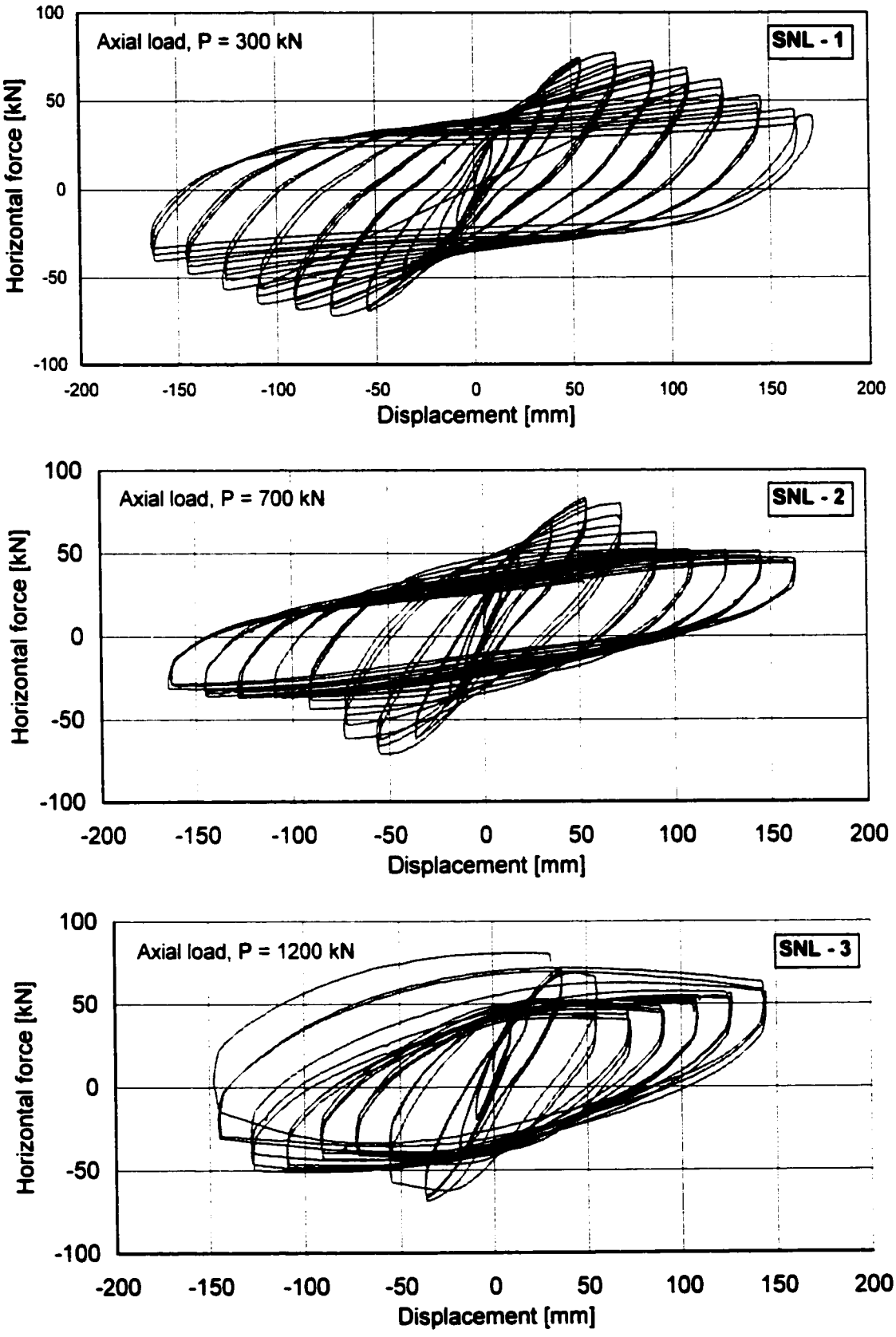

Figure 5.3 Horizontal force-displacement of horizontal actuator for SNL specimens

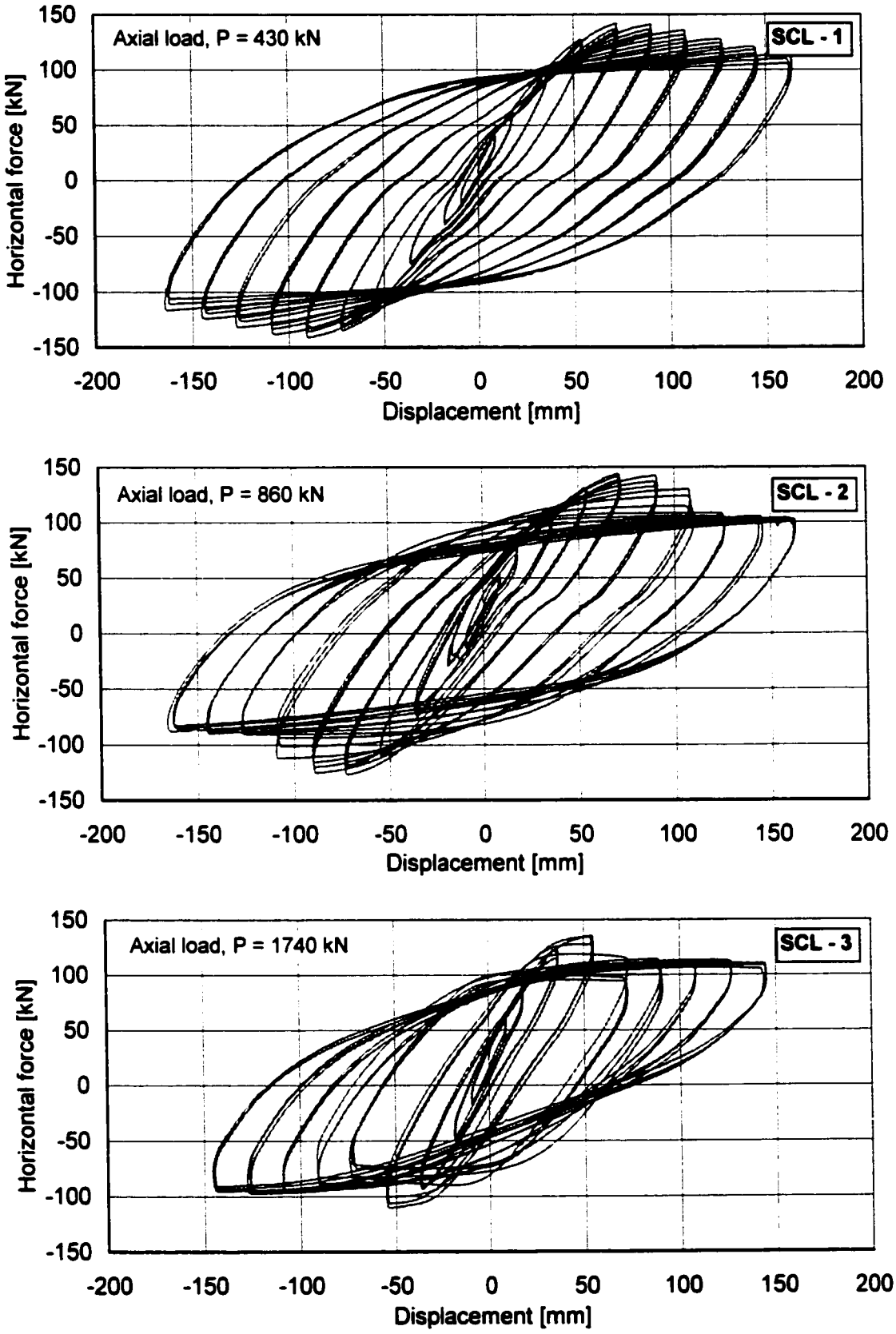

Figure 5.4 Horizontal force-displacement of horizontal actuator for SCL specimens

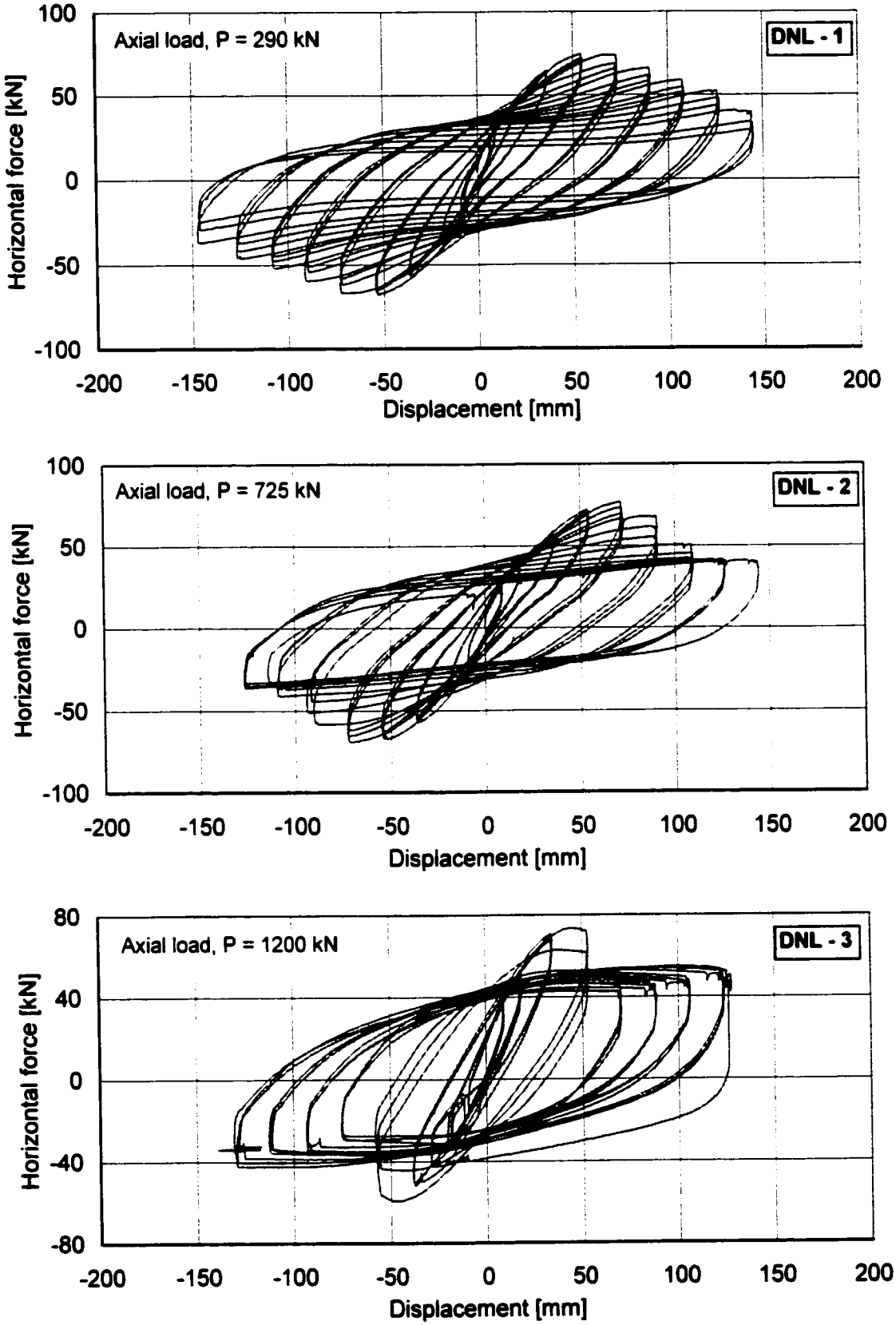

Figure 5.5 Horizontal force-displacement of horizontal actuator for DNL specimens

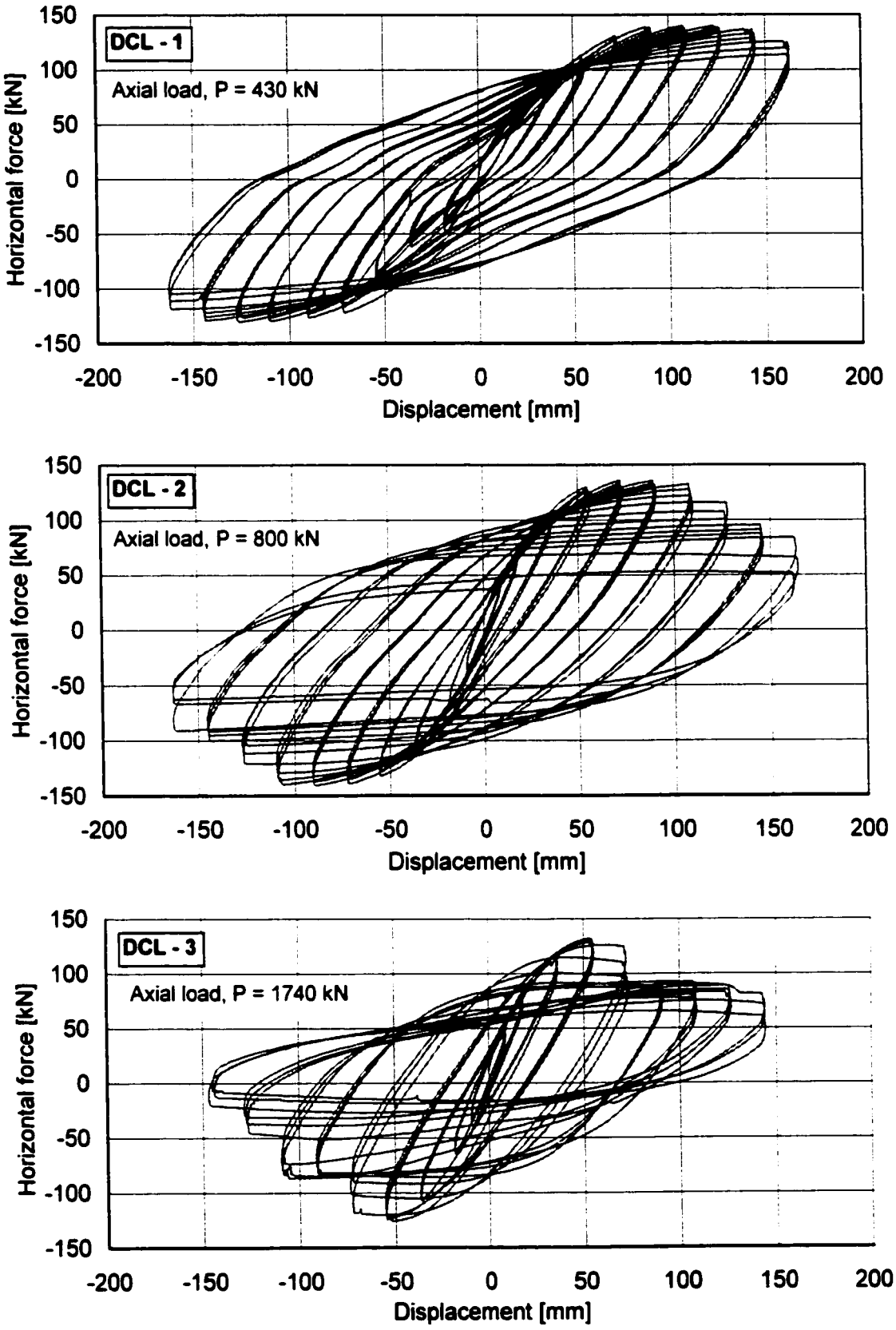

Figure 5.6 Horizontal force-displacement of horizontal actuator for DCL specimens

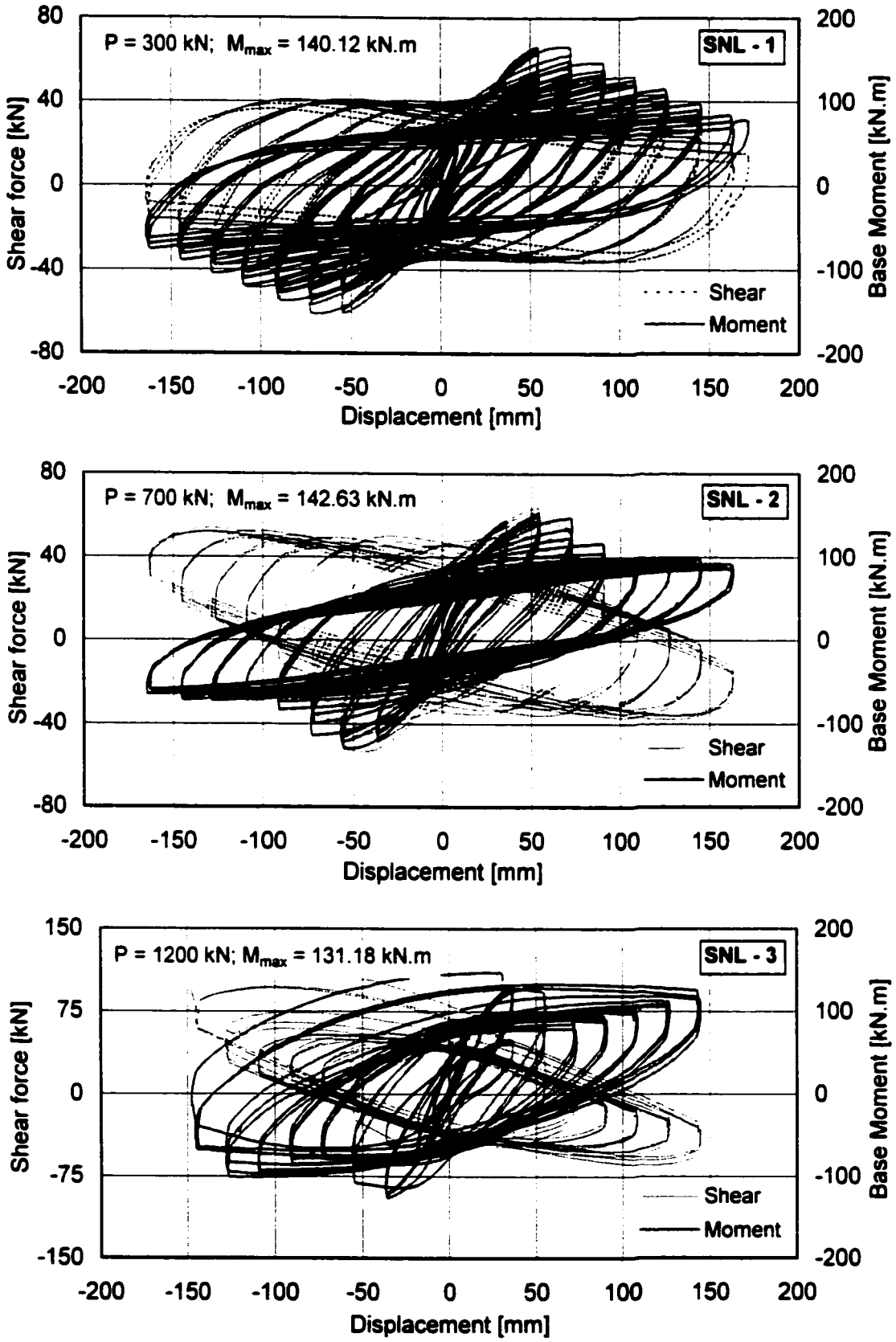

Figure 5.7 Shear Force & Moment vs Displacement of SNL specimens

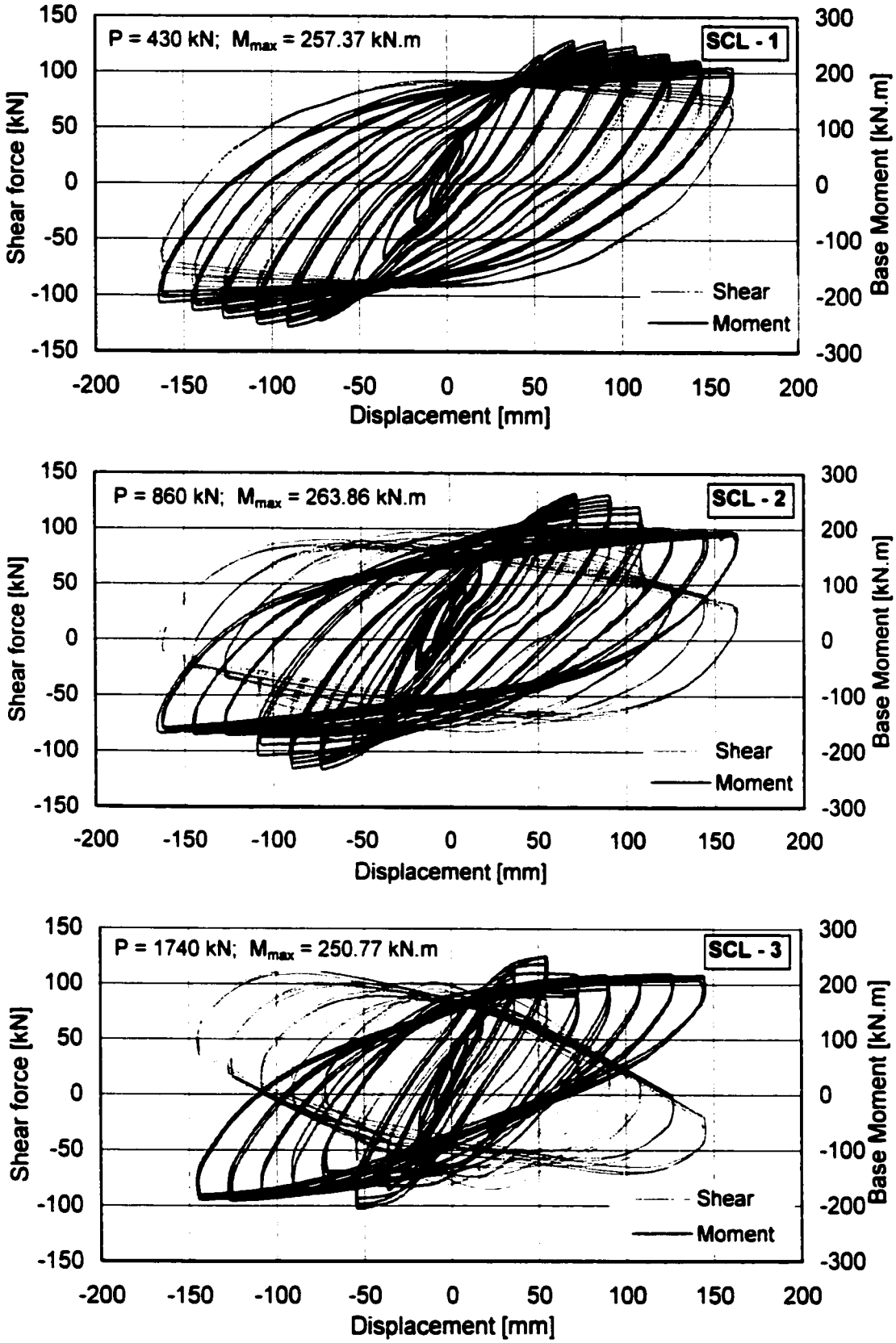

Figure 5.8 Shear Force & Moment vs Displacement of SCL specimens

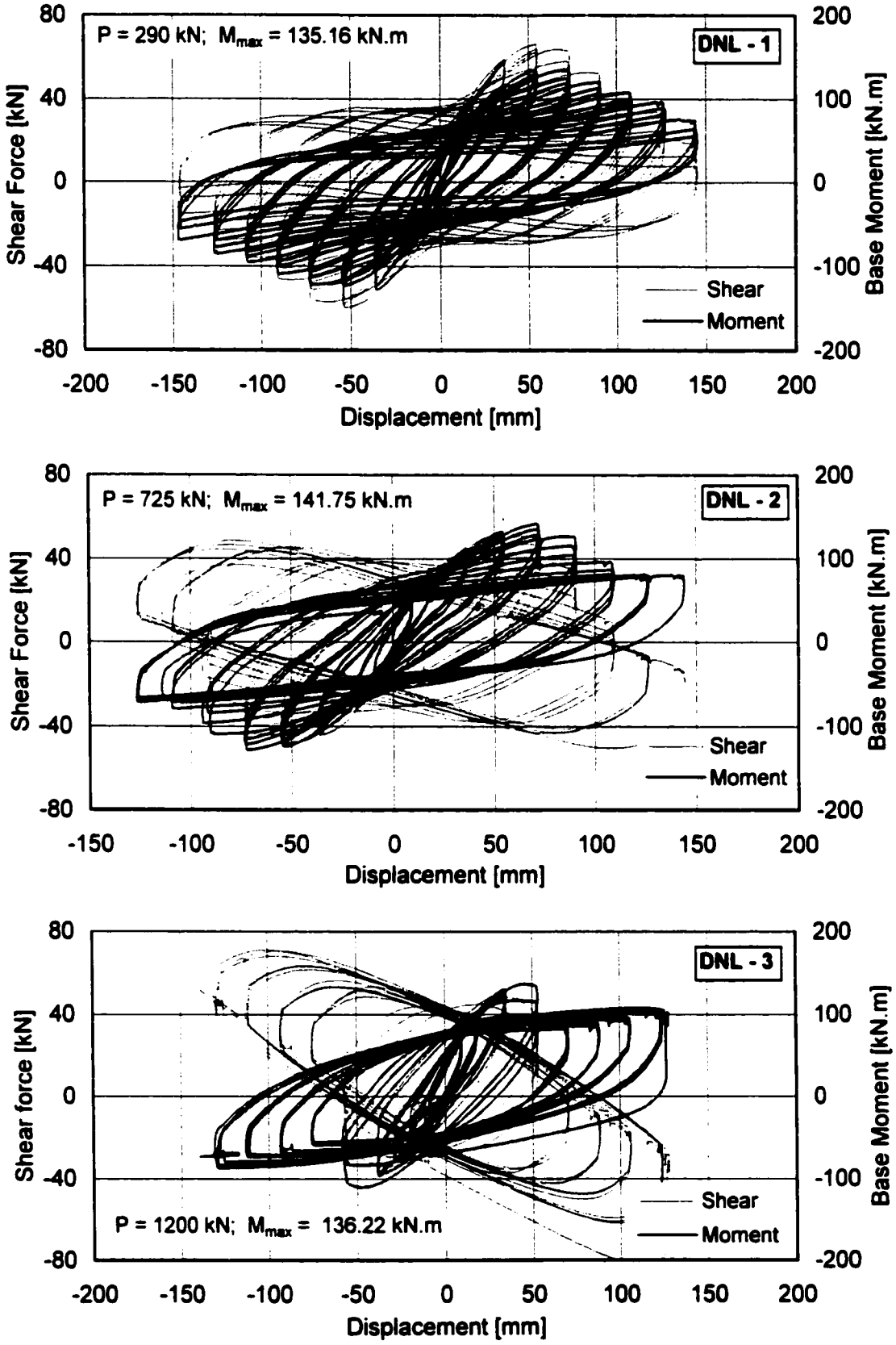

Figure 5.9 Shear Force & Moment vs Displacement of DNL specimens

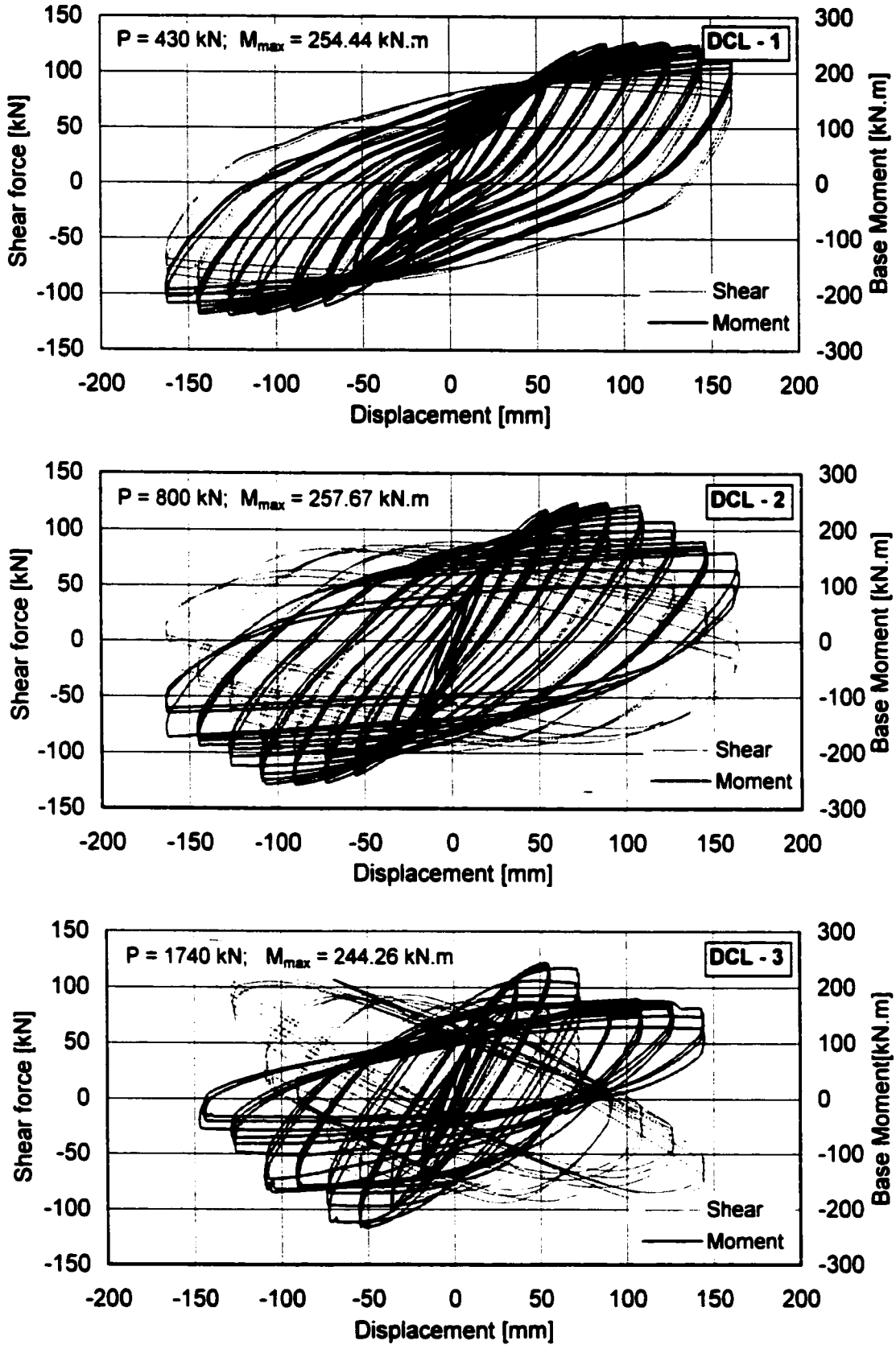

Figure 5.10 Shear Force & Moment vs Displacement of DCL specimens

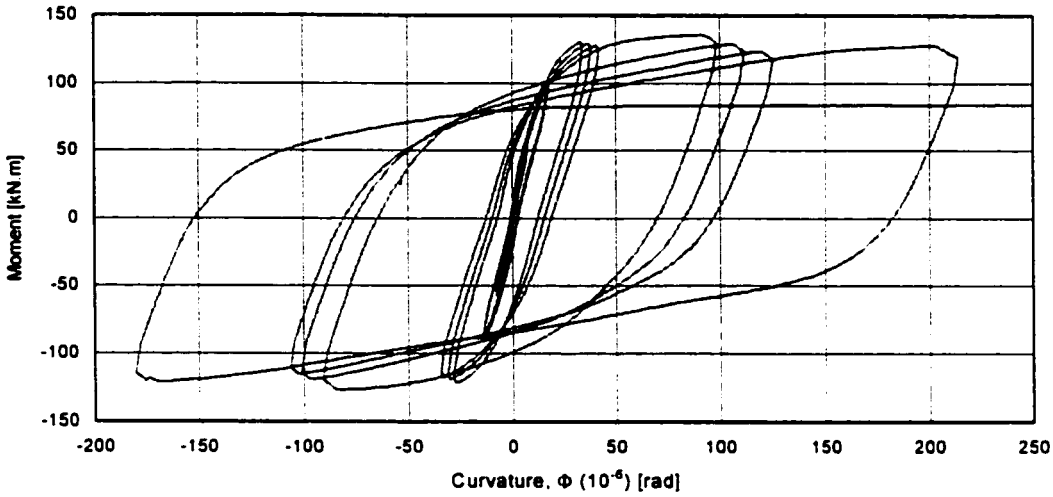

a. SNL - 1

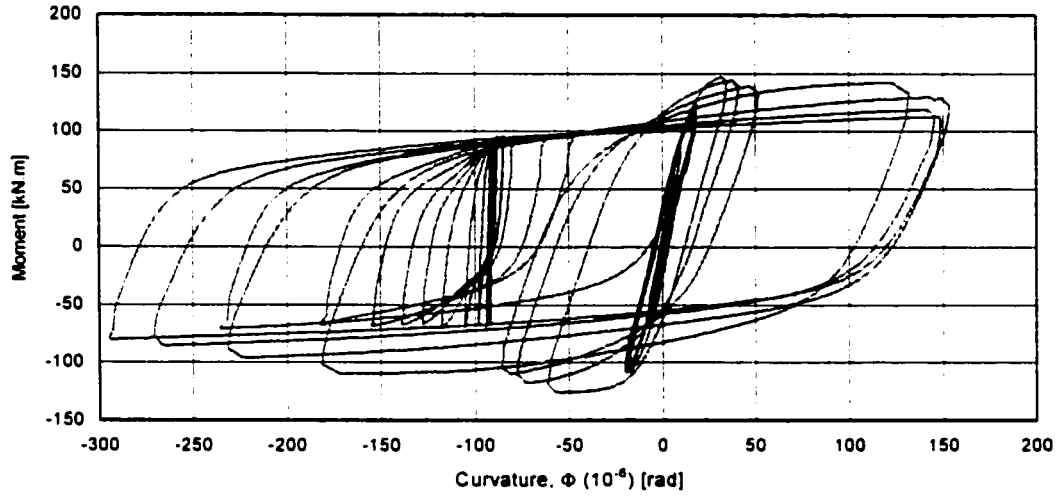

b. SNL - 2

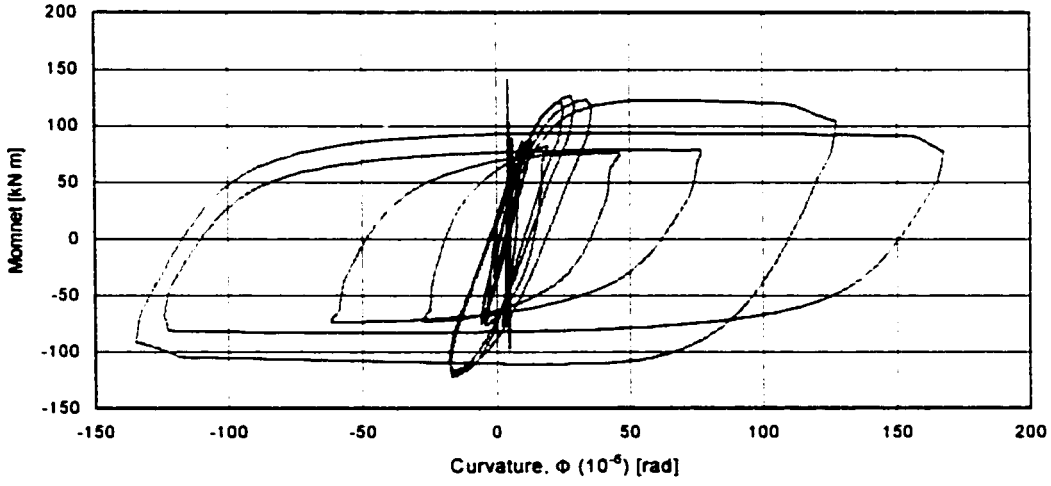

c. SNL - 3

Figure 5.11 Moment – Curvature relationship of SNL specimens

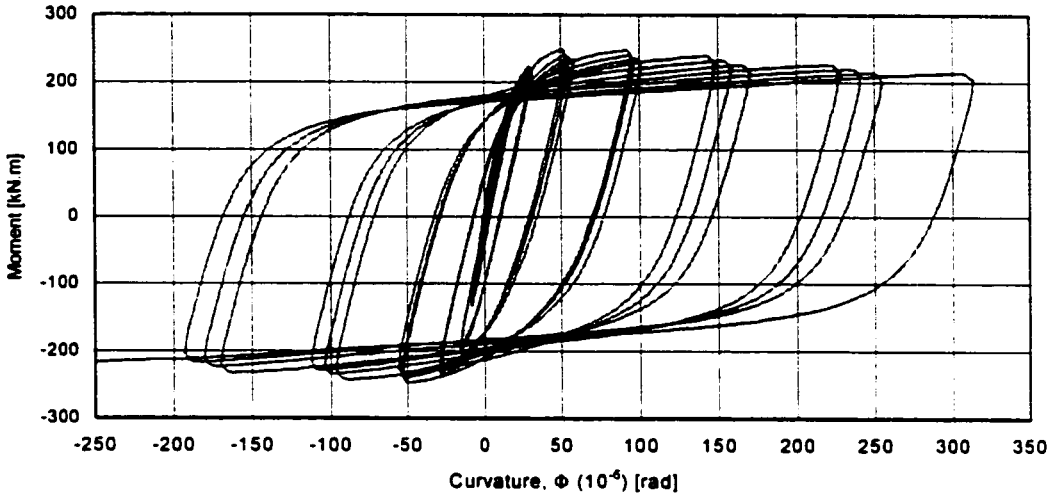

a. SCL - 1

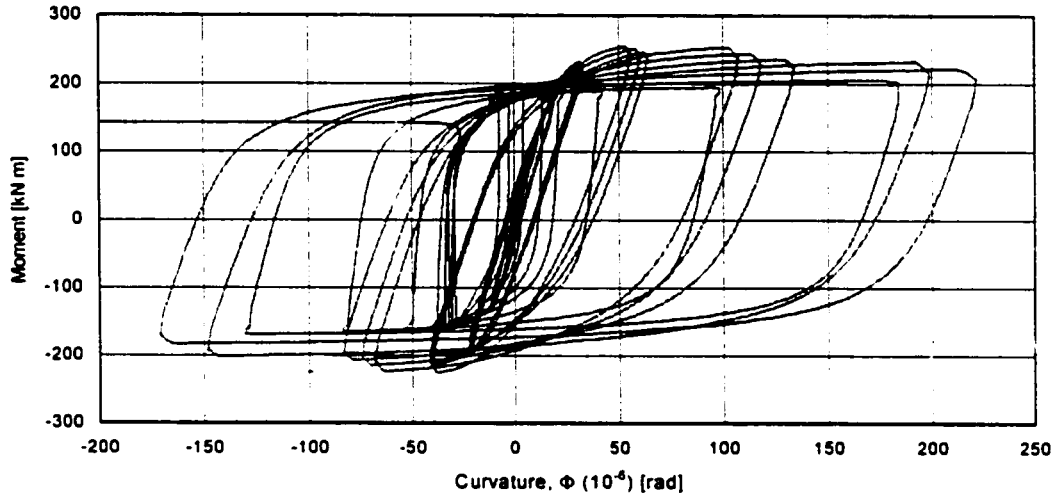

b. SCL - 2

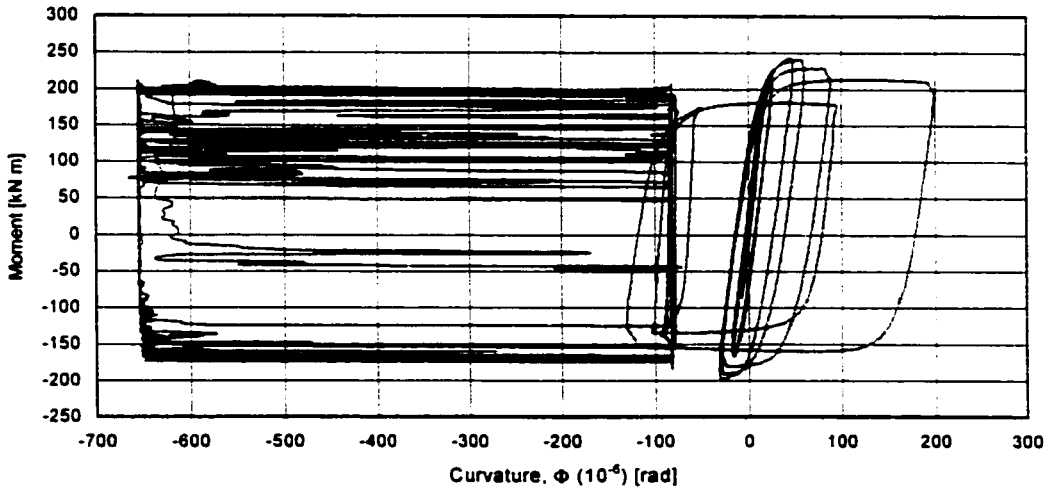

c. SCL - 3

Figure 5.12 Moment – Curvature relationship of SCL specimens

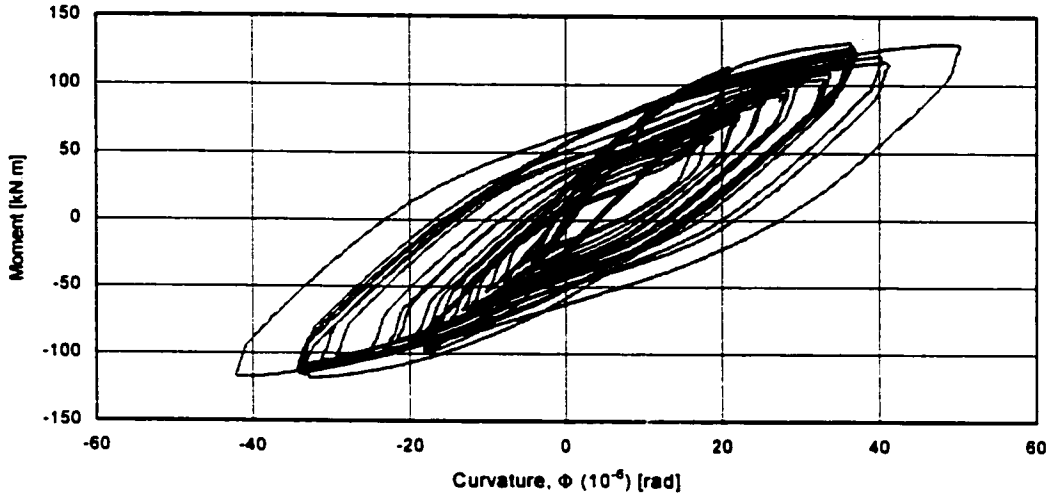

a. DNL - 1

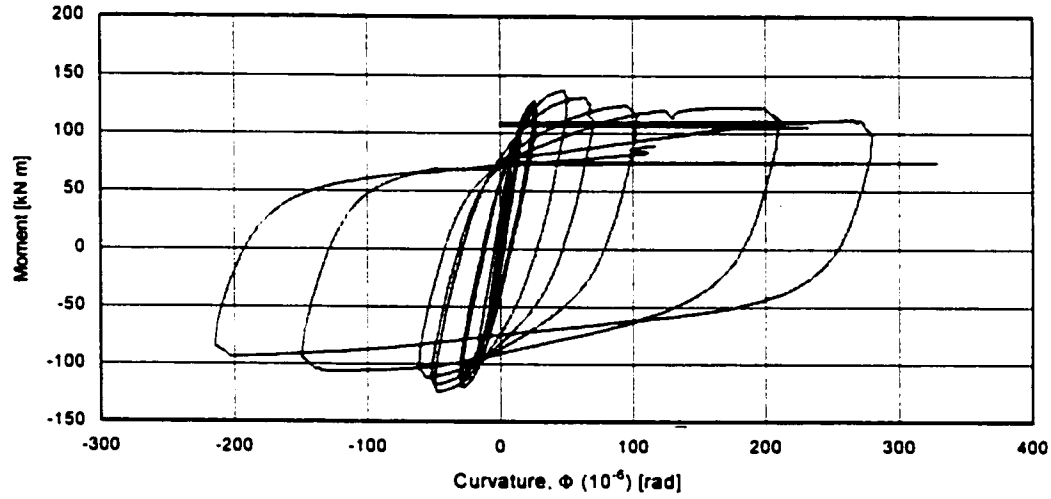

b. DNL - 2

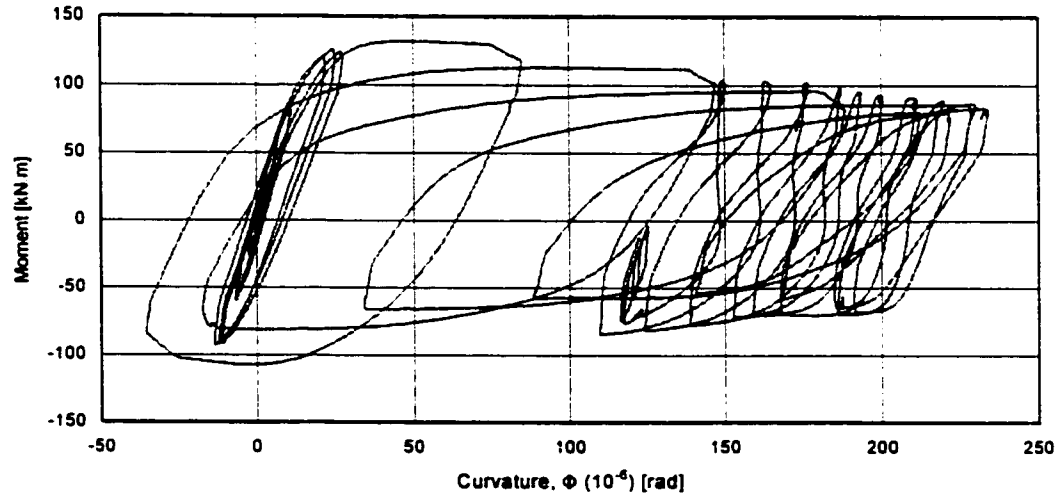

c. DNL - 3

Figure 5.13 Moment – Curvature relationship for DNL specimens

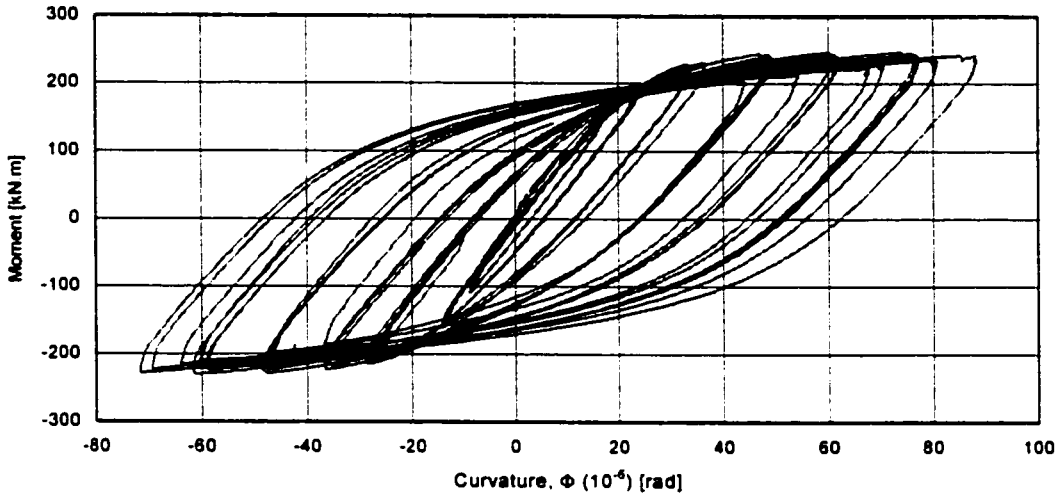

a. DCL - 1

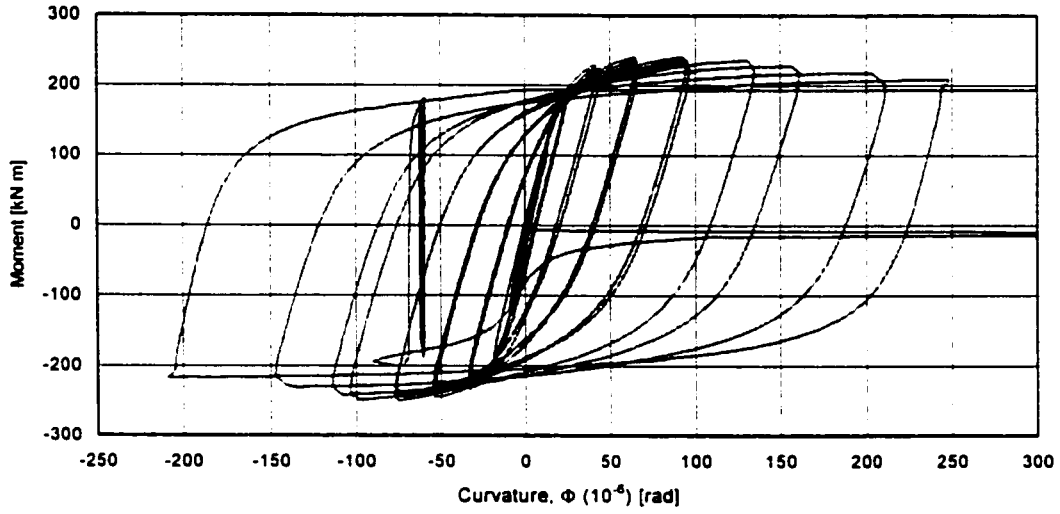

b. DCL - 2

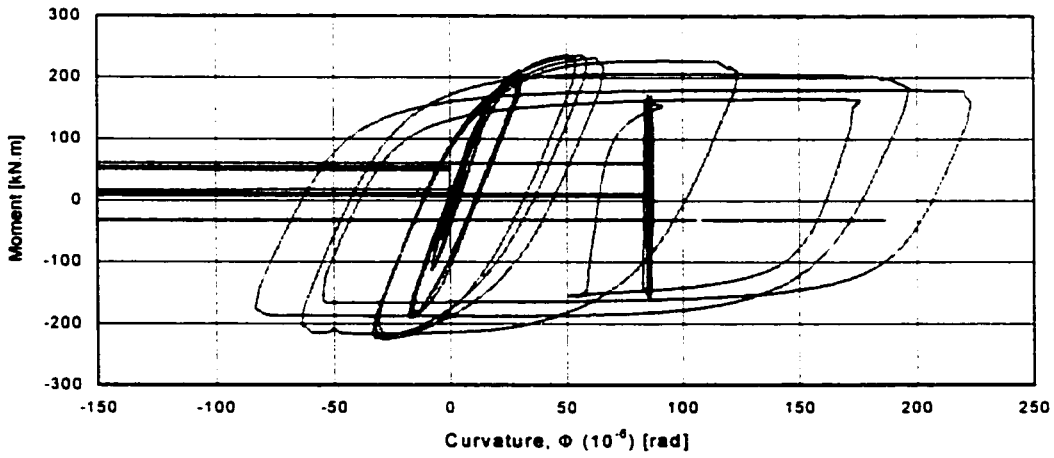

c. DCL – 3

Figure 5.14 Moment – Curvature relationship of DCL specimens

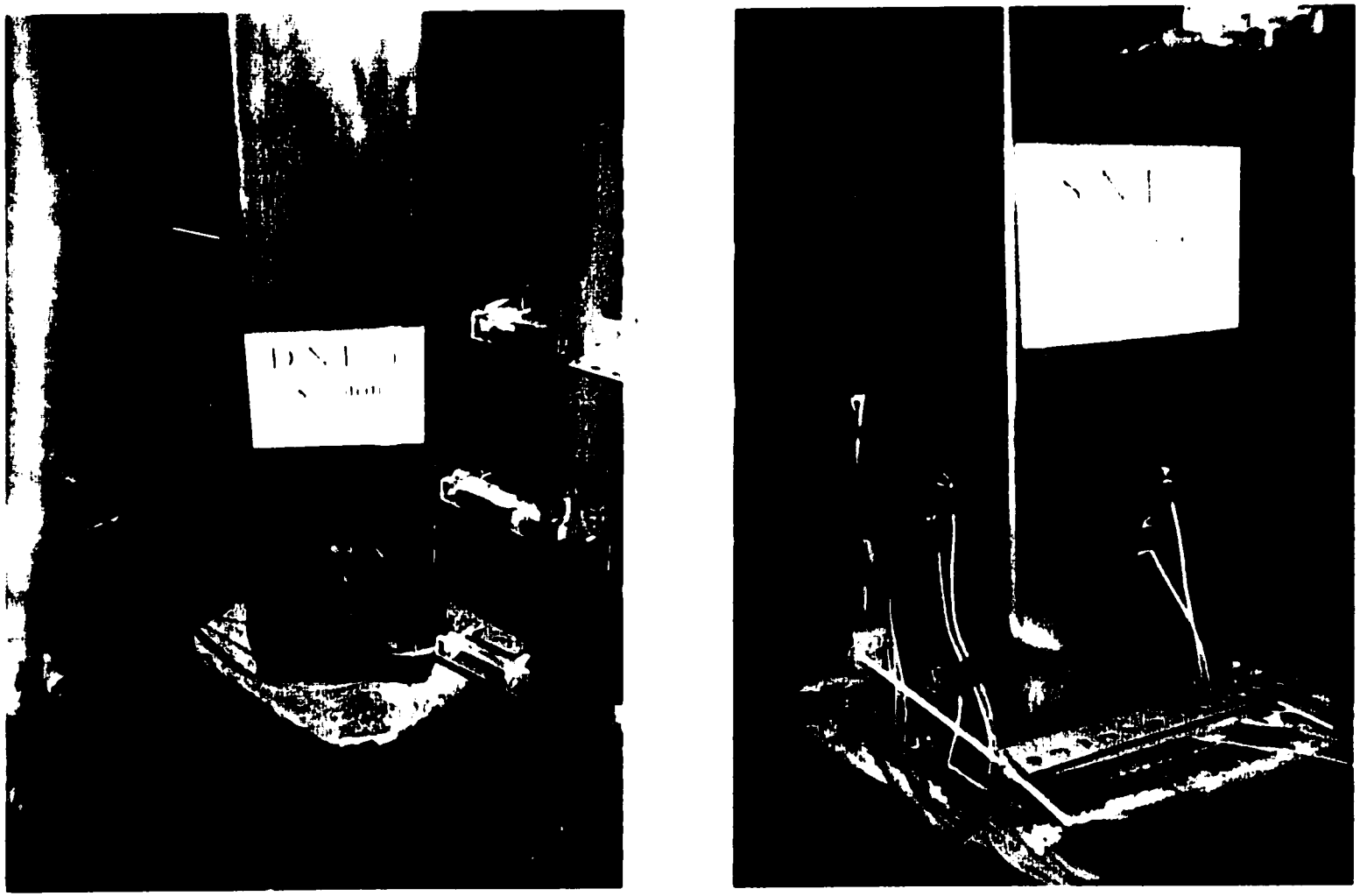

Figure 5.15 Columns DNL-1 and SNL-1 at 8 % drift

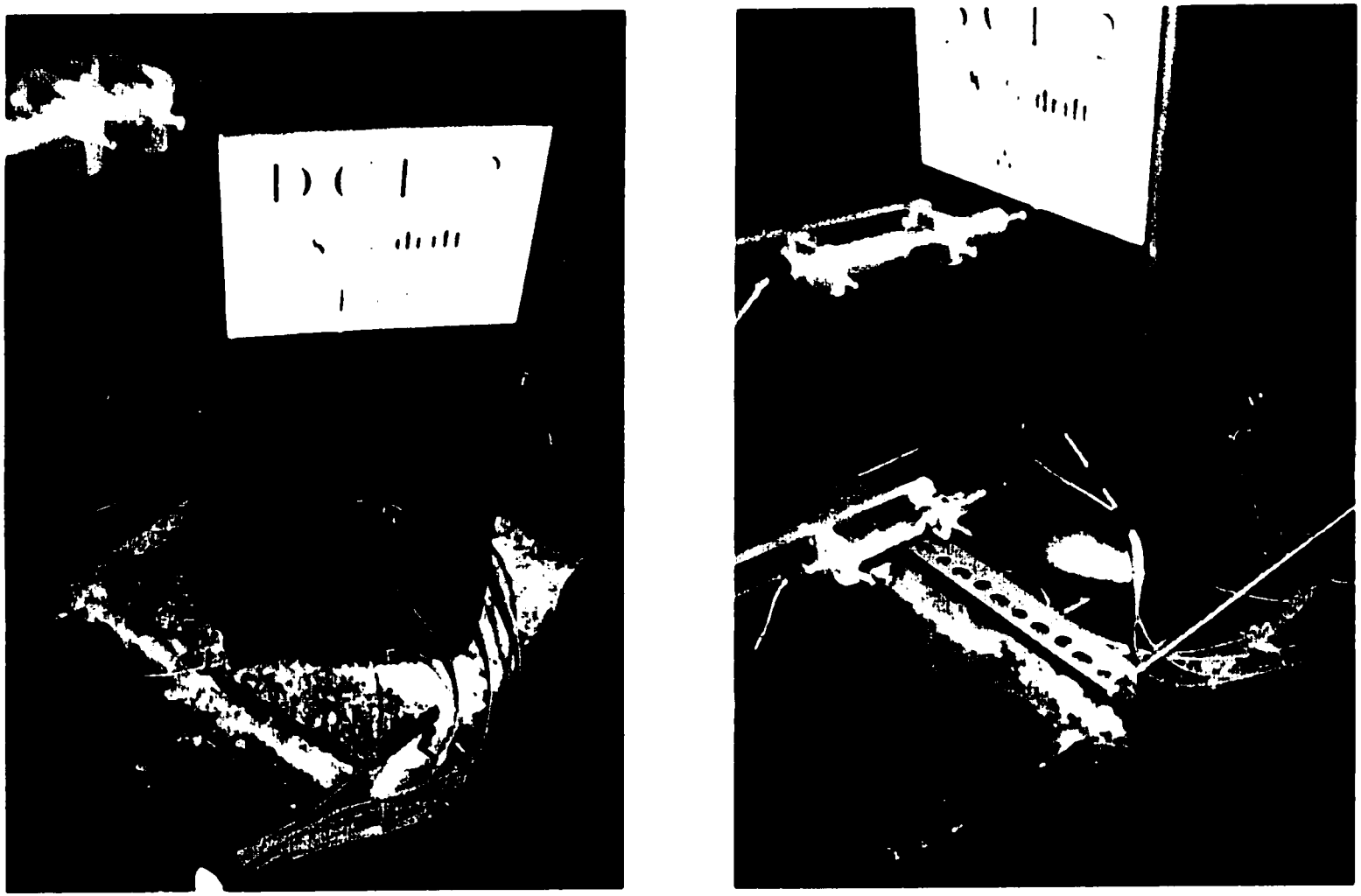

Figure 5.16 Columns DCL-2 and SCL-2 at 8 % drift

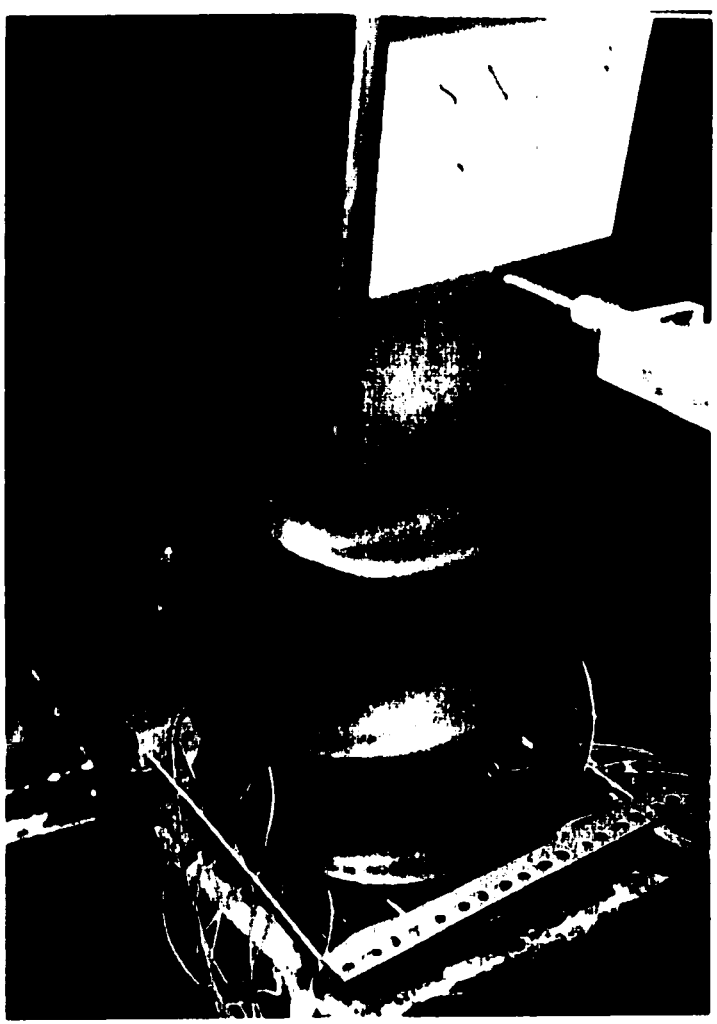

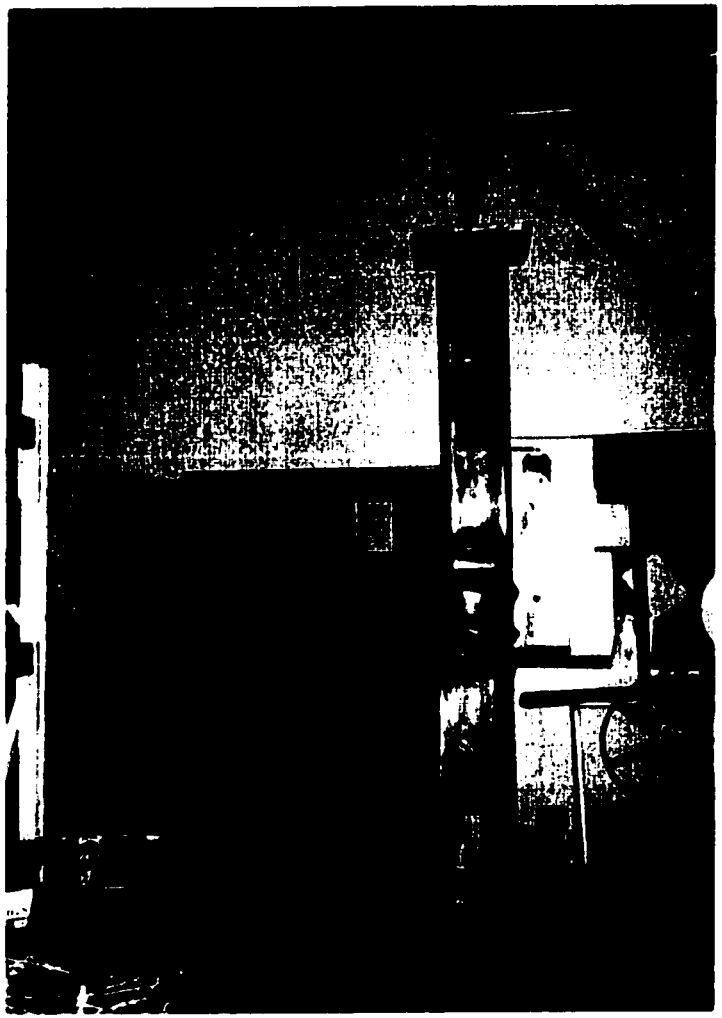

Figure 5.17 Column SNL-3, during test and after test

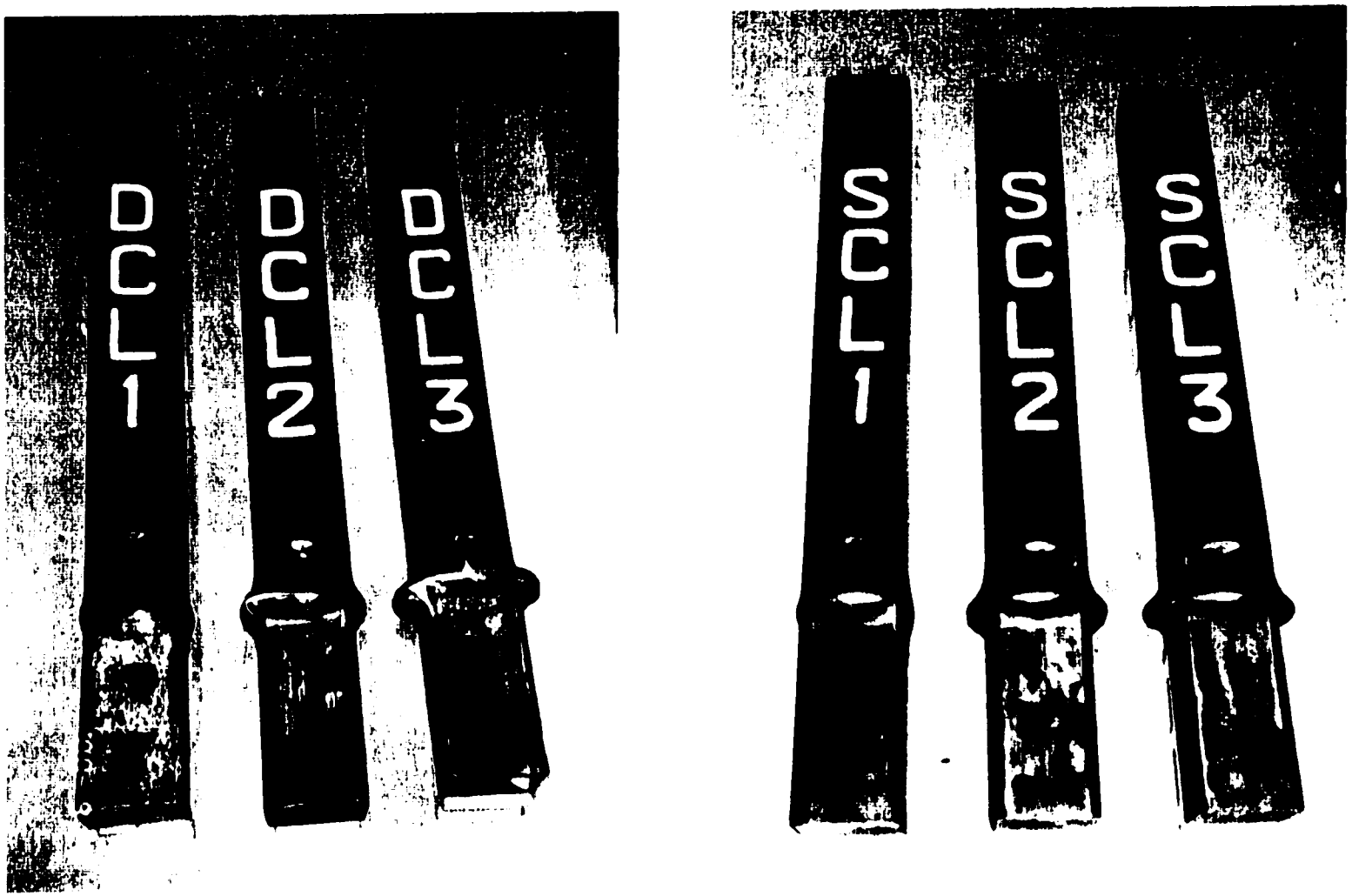

Figure 5.18 Columns DCL and SCL after tests.

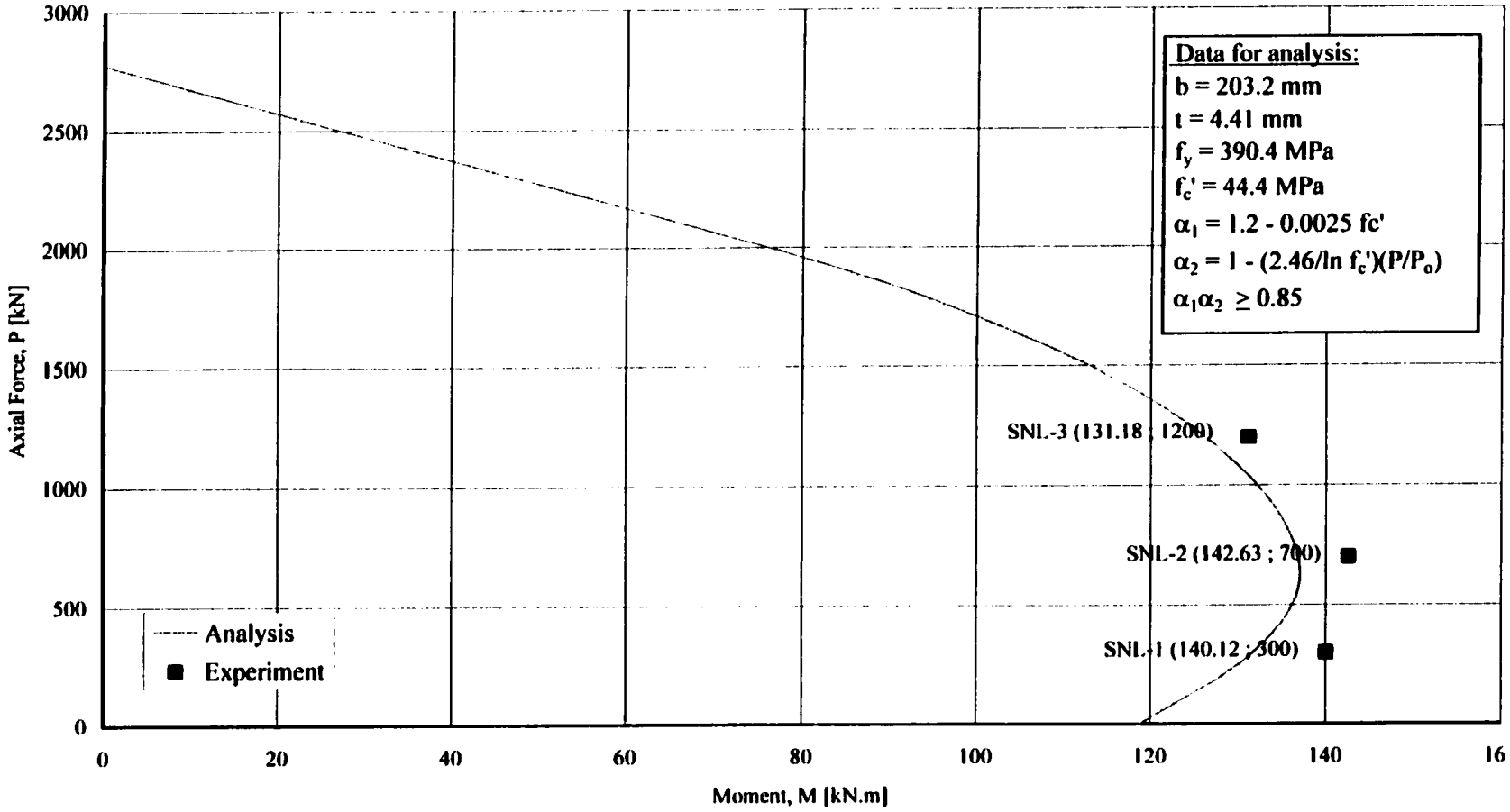

Figure 5.19 Strength Capacity of SNL Columns (without considering M_y effects)

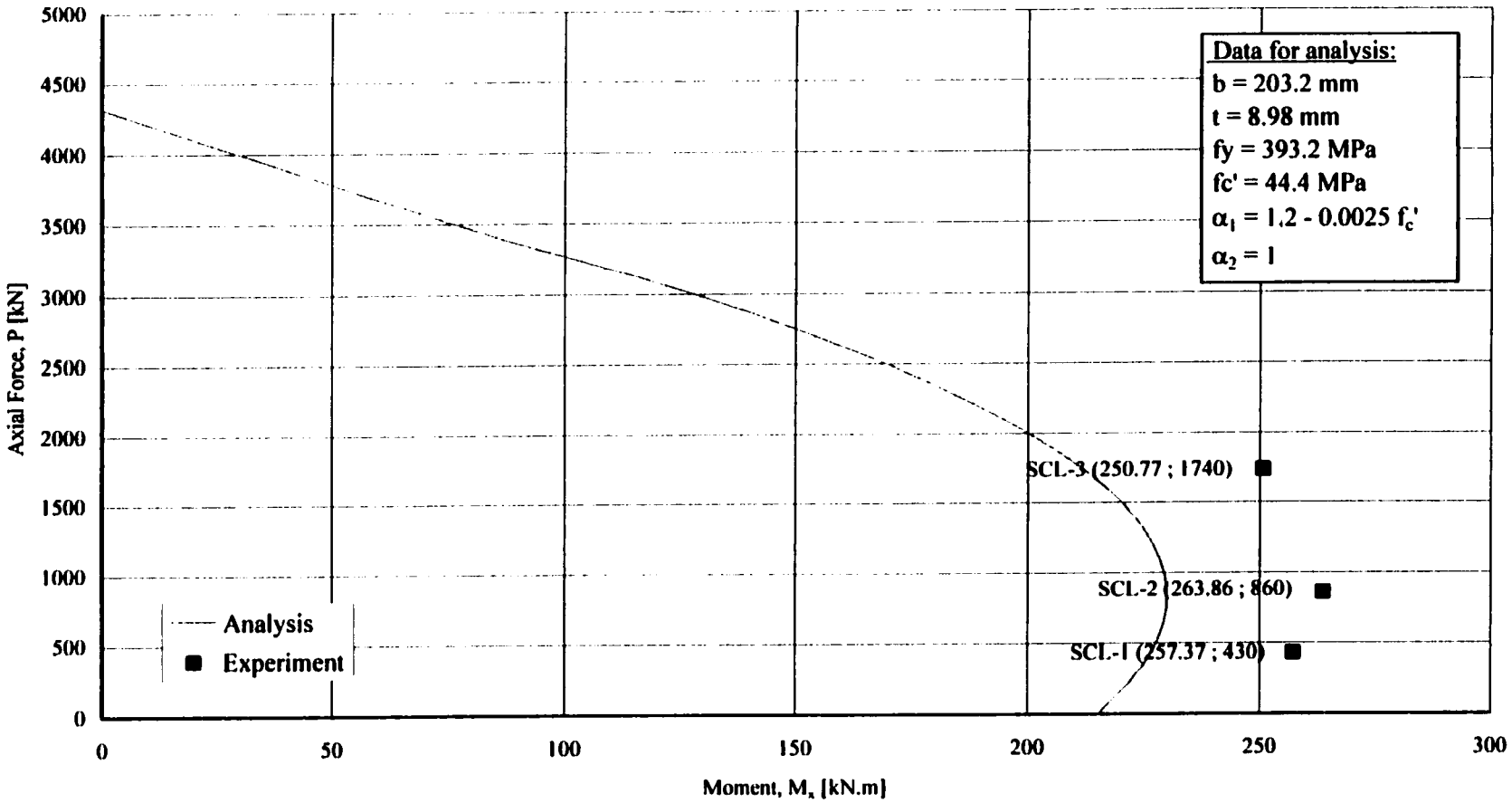

Figure 5.20 Strength Capacity of SCL Columns (without considering M_y effects)

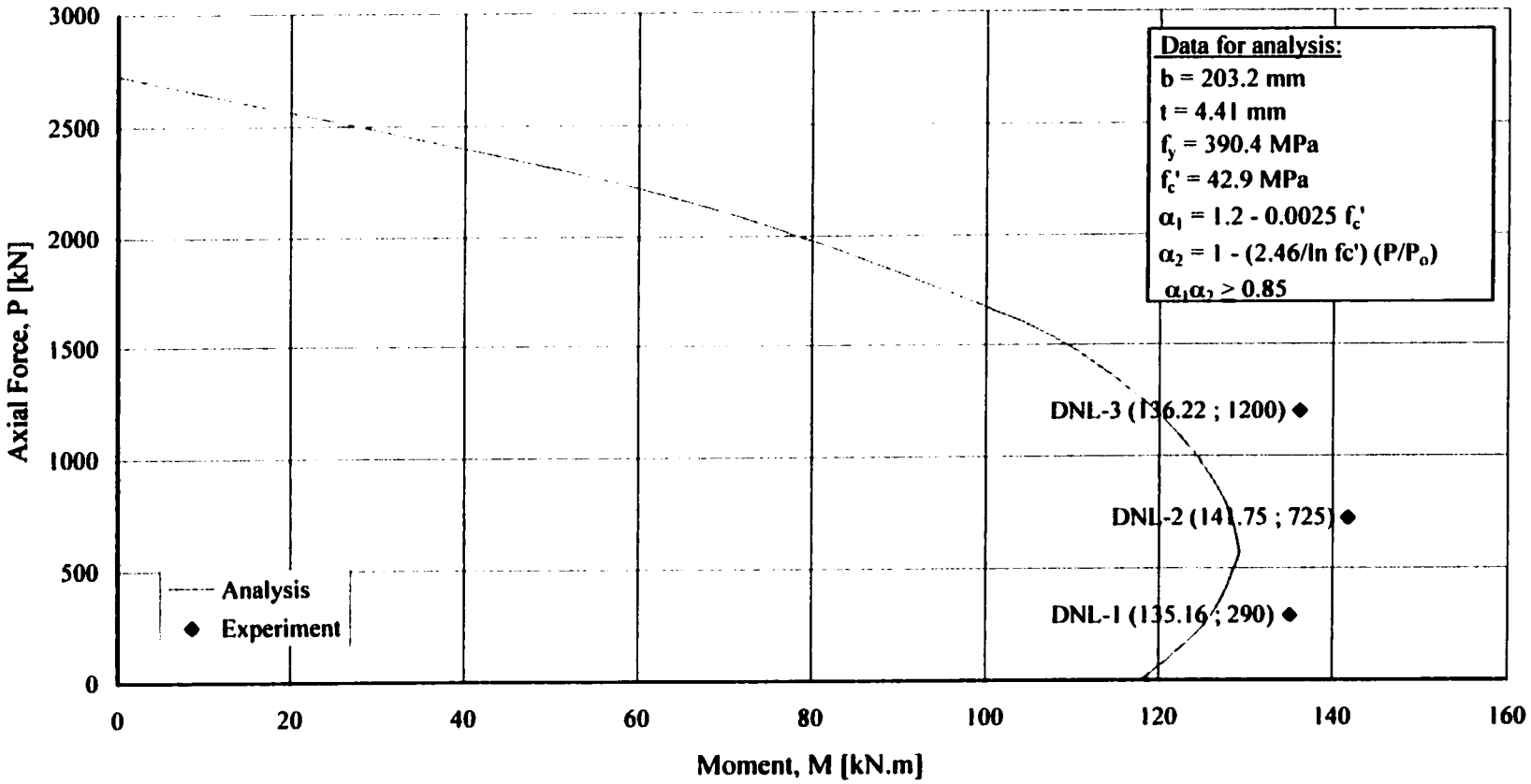

Figure 5.21 Strength Capacity of DNL Columns

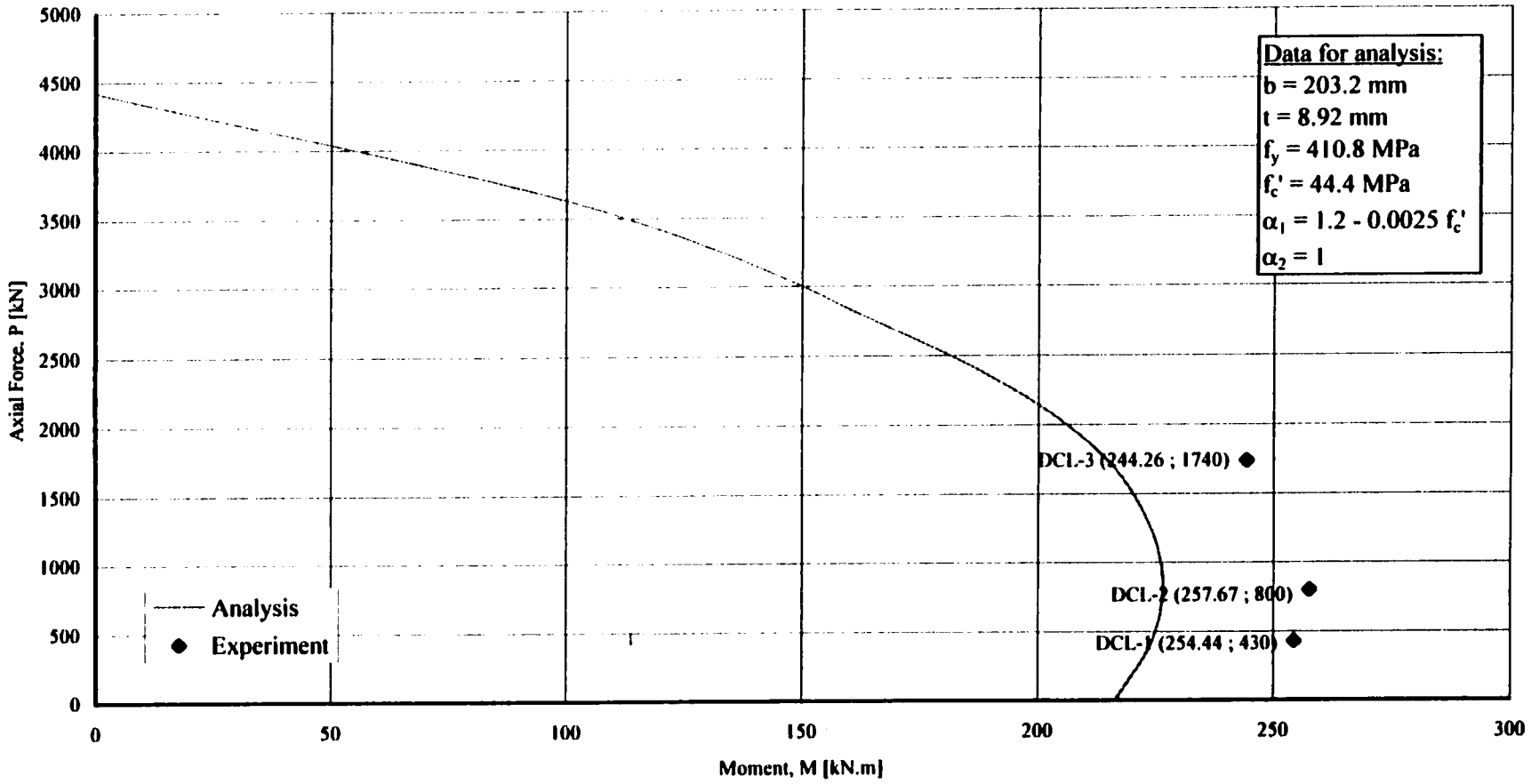

Figure 5.22 Strength Capacity of DCL Columns

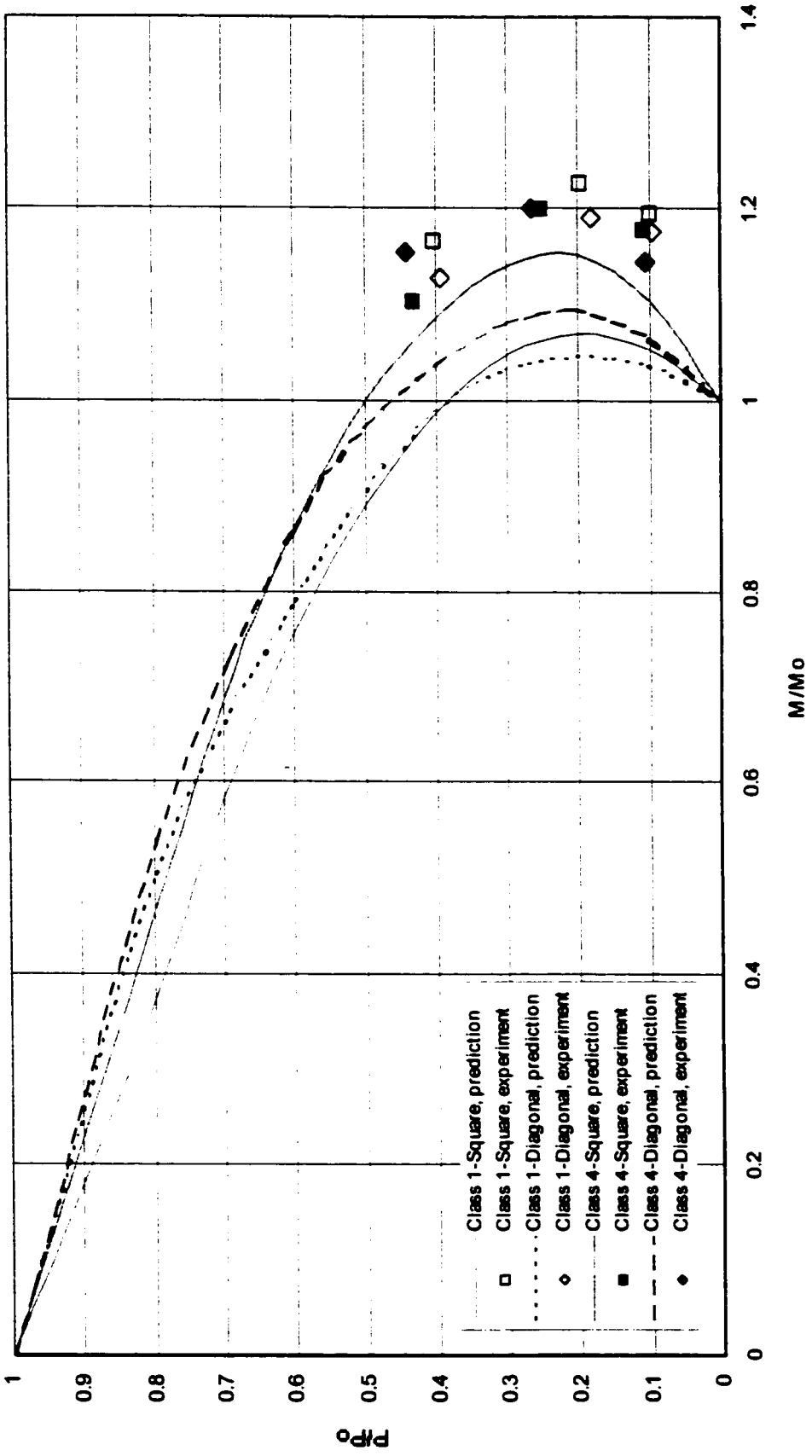

Figure 5.23 Normalized interaction diagram for normal strength CFT columns

Chapter 6

HIGH STRENGTH CFT COLUMNS

6.1 General

Investigations on high strength CFT columns included a series of twelve square steel HSS columns filled with high strength concrete (specified strength, f_c' = 90 MPa). Two types of HSS were used in this investigation, namely Class 1 and Class 4 sections according to CAN/CSA-S16.1-94. Column specimens were grouped into two groups: normal and diagonal orientation specimens according to the geometric orientation of the column sections when they were tested. All column specimens were tested under a constant axial compressive load and a cyclic biaxial bending moment. For the square columns, biaxial bending moment was produced by a horizontal force applied at the inflection point of the columns as the major moment, and an offset axial compressive load as a minor moment. The offset transversal load produced torsion as well. For columns positioned diagonally (diagonal specimens), which is a special case of biaxial bending columns, biaxial bending moment was produced by a horizontal force applied diagonally across the section at the inflection point of the cantilever columns.

Evaluations of the CFT columns, which include strength capacity, ductility and stiffness, are based on the test data that includes results of ancillary tests and column specimen tests. Ancillary tests cover standard concrete cylinder tests for high strength concrete and tension coupon tests for the HSS. Column specimen tests follow the procedure discussed in Chapter 4.

Results and evaluations of the test data are presented in tabular and graphical formats in the next sections. They start with ancillary test results. These are followed by observed behaviour and test data of CFT column specimens, and evaluations of strength capacity, ductility, and stiffness of CFT columns. Finally, column classification completes the evaluation of CFT columns, and concludes this chapter.

6.2 Ancillary Test Results

Ancillary tests provide individual material structural properties data that can be used for predicting the strength capacity and stiffness of the CFT column specimens. These tests consisted of standard compressive cylinder tests for the concrete and coupon tension tests for the HSS steel. Both standard compressive cylinder tests and coupon tension tests provide information of strength capacity and the stress-strain relationship of each material.

Eighteen standard concrete cylinders, 152 mm diameter and 305 mm high, were tested in accordance with CSA A23.2-94 to determine the compressive strength of the concrete, and three cylinders were tested to obtain the stress-strain relationship of the concrete. The tests were done at ages from 14 to 80 days after casting. In addition, three sets of tension coupons were tested in accordance with ASTM A370-95, to determine the material strengths of the HSS.

The results of the compressive strength tests of standard concrete compressive cylinders are presented in Table 6.1 and Figure 6.1. Table 6.1 shows six sets of three concrete cylinder strength data and their average strengths. Some data were rejected in determining the average strength because the cylinder failed prematurely, or the test results were irrational compared to the expected trend of concrete strength with the age of the tests. Figure 6.1 shows individual results, the curve of average strength and the least squares best fit curve of the test data. The expression of the best-fit curve is

$$f_c'(t) = 0.0002\,t^3 - 0.0332\,t^2 + 1.9992\,t + 58.633 \qquad (6.1)$$

where t is the age of the concrete, in days. Equation (6.1) was used to determine the strength of the concrete in CFT column section analyses.

The accuracy of the results of the standard compressive cylinder tests depends mainly on the cylinder preparation. It was observed that premature failure occurred when the top surface of the cylinder was not perpendicular to the axis of the cylinder. Although the surface was capped using sulfur compound capping material, premature failure still occurred.

In addition to the compressive peak strength of standard cylinder tests, the tests included the stress-strain relationship of concrete cylinders. Figure 6.2 shows the stress-strain curve of three standard concrete cylinders tested at 44 days and the average modulus of elasticity of high strength concrete produced by three standard test cylinders. The average test and analytical results, using Eurocode 2-94, Gardner's 2001 proposal, ACI 318-99 and CSA A23.3-94 equations, of modulus of elasticity (secant modulus) of high strength concrete are shown in Table 6.2. Referring to Table 6.2, the best prediction of modulus elasticity of high strength concrete was using Gardner's 2001 proposed equation; however, this equation was not adopted in calculating the modulus of elasticity of high strength concrete as it could not be easily adjusted to the test results. The modulus of elasticity of high strength concrete was calculated using Equation 3.52. Figure 6.2 shows the peak strengths of high strength concrete were at strains about 0.0025.

6.3 *Observed Behaviour and Test Data*

The behaviour of the CFT column specimens was observed during the tests. There are two ways of recording the observation of the behaviour of the column specimens: manually and automatically. The manual and automatic recorded data were collected based on the visual observation and using a computer acquisition system respectively. The recorded observations are presented in subsequent subsections.

The automatic recorded data of the CFT column tests are presented in this section in graphical format, which consist of load–displacement, moment–displacement and moment–curvature relationships of each CFT column specimen. Load–displacement relationships represent the strength and deformation characteristics of the columns. There are two sets of load data in the load–displacement data. The load data include the raw load data, where the loads are the horizontal loads applied by the horizontal actuator, and the shear forces applied to the critical cross section. Applied shear forces were calculated by including the effect of the inclined axial load produced by the two vertical actuators.

Figures 6.3 to 6.6 show the horizontal force–displacement relationships of the horizontal actuator for all high strength CFT column specimens. These show the applied

actuator forces and displacements measured 1800 mm above the fixed base of the columns.

The combination of horizontal actuator force and the horizontal component of the inclined axial compressive load of the vertical actuators produce an applied shear force on the column specimen. The shear force and bending moment responses are illustrated in shear force–displacement and moment–displacement relationship graphs of the column specimens in Figures 6.7 to 6.10. It can be seen that the cyclic paths of the shear–displacement and of moment-displacement graphs are fat indicating that the columns have good energy dissipation. An interesting behaviour in these graphs is the displacements disagree with the shear forces or, in other words, the displacements were in the opposite direction to the shear forces. This occurred when the applied axial force was greater than 10% of the squash load and at large displacements (more than 3% drift) for Class 1 HSS CFT columns, and when the displacements are large for Class 4 HSS CFT columns. This anomalous behaviour occurred because the horizontal component of inclined axial load was greater than applied horizontal force of the horizontal actuator.

Figures 6.11 to 6.14 show the relationships between bending moment and curvature at the recorded strain section, 60 mm above fixed base. These curvatures were calculated from the recorded measured strains.

The sign conventions applied throughout this chapter are; shear forces, horizontal forces and horizontal displacements are positive in the west direction (pushing load on horizontal actuator) and negative in the east direction. Bending moments and curvatures associated with positive shear forces and displacements are positive, and negative for negative displacements.

Selected photographs of specimens during and after the tests are supplied in Figures 6.15 to 6.18.

There are two types of CFT column specimens according to geometric orientation of the column sections as they were tested: square (SNH and SCH) and diagonal (DNH and DCH) specimens. Letters N (thin) and C (thick) were chosen to identify the two types of HSS employed in the test program - Class 1 indicated by letter C and Class 4 by letter N. Diagonal specimens represent the special case of biaxial bending moment with equal values of major and minor bending moments. The square specimens had a small minor

bending moment produced by the axial load position being offset 12.7 mm from the centreline of the section and a torsion of 0.71% of the major bending moment.

The following sections detail the observed behaviour of square thin wall specimens (SNH), diagonal thin walled specimens (DNH), square thick walled specimens (SCH), and diagonal thick walled specimens (DCH).

6.3.1 SNH Columns

A series of three column specimens made of Class 4 HSS filled with high strength concrete were investigated. The specimens were identified as SNH-1, SNH-2 and SNH-3. Each column was tested under a specific constant axial compressive load and cyclic incremental displacement which produced critical bending moment at the fixed base. Constant axial compressive loads of 520 kN, 1150 kN and 1700 kN were applied at the inflection point of columns SNH-1, SNH-2 and SNH-3 respectively with a 12.7 mm offset from the center gravity of the column cross section perpendicular to the shear force direction. This offset axial load produced a minor bending moment of 6.60 kN.m, 14.61 kN.m. and 21.59 kN.m on columns SNH-1, SNH-2 and SNH-3 respectively. The cyclic incremental shear forces were applied at the inflection point of the column specimen under displacement control. Displacement rates were 1 mm/sec, 2 mm/sec and 3 mm/sec for drifts up to 2%, 5% and 8% respectively. The tests took about 4 hours for each column specimen.

Complete results of the SNH columns are supplied in graphical formats. The applied horizontal force-displacement, load-displacement, and moment-curvature relationships are given in Figures 6.3, 6.7 and 6.11 respectively.

Visual investigations during the loading test on SNH-1 specimen noted that the steel tube started buckling at the first cycle of 3% drift. The first buckle was at the west side of the tube. Then buckling developed at the east, north and south sides of the tube at the second cycle of 3% drift, first, and second cycles of 4% drift respectively. As buckling propagated to all sides and increased in each successive cycle, the corners of the steel tube also buckled. This corner buckling started at the first cycle of 6% drift. The buckle was located 95 mm to 105 mm above the fixed-end surface, or about a half of the

width of the steel tube. When the shear forces were at the first cycle of 8% drift, both the north-east and south-east corners cracked, and at the second cycle of 8% drift, the east side, the north-west and south-west corners cracked. All buckling increased progressively and by the end of the test, 8% drift, the four corners had open cracks averaging about 90 mm long and maximum widths about 15 mm. It could be seen from the open cracks that crushed concrete filled the buckled space and this caused enhancement of the strength capacity of the column after outward buckling of the steel tube.

Column SNH-2 behaved in a similar manner to column SNH-1. Buckling started earlier than that on the SNH-1. It started at the third cycle of 2 % drift on both the west and east sides, followed by buckling on the north and south sides at the second cycle of 3% drift. All buckling took place 90 mm to 105 mm above the fixed-end surface. The corner of the tube started buckling after 4% drift. No crack was observed, but a second ring local buckle started developing at the second cycle of 7 % drift.

Column SNH-3 followed the same test procedure as the previous columns and behaved in similar manner. However, a local buckle started on the west side of the steel tube at the second cycle of 2% drift. This was followed by a ring local buckle developing at the first cycle of 3% drift. The buckle positions were about 80 mm to 100 mm above the fixed-end surface. No cracks developed in this column, but a second ring local buckle developed at the second cycle of 4% drift located 210 mm to 230 mm above the fixed-end surface.

After developing the second outward buckle, the column could resist more shear force because the critical section became larger by crushed concrete filling the buckled areas.

Overall, the SNH columns had good absorbed energy dissipation even though the HSS is classified as Class 4 sections. No premature local buckling occurred and the columns behaved in a ductile manner.

6.3.2 DNH Columns

To complete the test program on Class 4 HSS CFT columns, a total of three CFT column specimens, DNH-1, DNH-2, and DNH-3, made of Class 4 square HSS, filled

with high strength concrete, oriented diagonally were investigated. Constant axial loads of 540 kN, 1100 kN and 1850 kN were applied on top of the DNH-1, DNH-2 and DNH-3 specimens respectively.

Complete results of the DNH columns are supplied in graphical format. The applied horizontal force-displacement, load-displacement, and moment-curvature relationships are given in Figures 6.4, 6.8 and 6.12 respectively.

The first specimen tested was column DNH-1. It was observed that the first local buckle started on the southwest side of the HSS at the second cycle of 3% drift. At the third cycle of 5% drift, a ring local buckle developed. A second ring local buckle developed at the second cycle of 7 % drift. The first and second ring local buckles were located 60 mm to 100 mm and 190 mm to 200 mm respectively above the fixed-end surface. Cracks started at the east and west corners of this specimen at the third cycle of 7 % drift. Open cracks, 200 mm long and 20 mm wide, at the west corner and 150 mm long and 15 mm wide at the east corner were observed at the end of the test.

Column DNH-2 experienced both ring local buckles and cracks at the west and east corners. Local buckling started on the southeast and northeast sides of the HSS as soon as the last cycle of 3% drift was completed followed by the other sides during the second cycle of 4% drift. A ring local buckle was observed 60 mm to 80 mm above the fixed-end surface after the third cycle of 5% drift, and cracks on the west and east corners were found at the second cycle of 7% drift. In addition, a second ring local buckle developed at 190 mm to 200 mm above fixed-end surface at the third cycle of 7% drift.

Column DNH-3 had two ring local buckles after the test. The first ring local buckling developed 50 mm to 90 mm above fixed-end surface after the third cycle of 2% drift was completed. The second ring local buckle developed at 170 mm to 240 mm above the fixed-end surface at the first cycle of 5 % drift. No crack was found until the test was terminated at the last cycle of 7% drift because the horizontal actuator worked improperly. This column specimen was the last test of the whole test program.

6.3.3 SCH Columns

A series of three CFT column specimens made of Class 1 HSS filled with high strength concrete were investigated. The specimens were identified as SCH-1, SCH-2 and SCH-3 and had their unique axial compressive loads: 570 kN, 1200 kN and 1750 kN respectively. These loads produced constant minor bending moments of 7.24 kN.m, 15.24 kN.m and 22.22 kN on the SCH-1, SCH-2 and SCH-3 specimens respectively.

Complete results of the SCH columns are supplied in graphical format. The applied horizontal force-displacement, load-displacement, and moment-curvature relationships are given in Figures 6.5, 6.9 and 6.13 respectively.

Column SCH-1 started local buckling on the east and west sides at the first cycle of 4% drift. This was followed by local buckles on the north side of the column at the first cycle of 6% drift and on the south side at the third cycle of 6 % drift. A ring local buckle was completed at the third cycle of 7% drift located 75 mm to 95 mm above the fixed-end surface.

The first local buckle developed on Column SCH-2 was on the east side of the HSS at the first cycle of 3% drift. This was followed by a local buckle on the west side at the second cycle of 3% drift. The buckling increased with every cycle thereafter, and the cyclic loading caused local buckling on the north and south sides of HSS steel after the third cycle of 4% drift was completed. These were followed by a ring local buckle which developed when all corners of the HSS started buckling at the third cycle of 5% drift 88 mm to 102 mm above the fixed-end surface.

Column SCH-3 experienced the first local buckle on the west and east sides of the HSS at the first cycle of 3% drift. The north and south sides local buckles developed at the first cycle of 4% drift. A ring local buckle developed 94 mm to 105 mm above the fixed-end surface after the corners of HSS steel buckled at the third cycle of 4% drift.

6.3.4 DCH Columns

To complete the test program on Class 1 of HSS CFT columns, three CFT columns made of Class 1 HSS oriented diagonally were investigated. These column specimens were identified as DCH-1, DCH-2 and DCH-3 with constant axial

compressive loads of 630 kN, 1550 kN and 1900 kN respectively. The same test procedures used for the SNH series of columns were used.

Complete results of the DCH columns are supplied in graphical format. The applied horizontal force-displacement, load-displacement, and moment-curvature relationships are given in Figures 6.6, 6.10 and 6.14 respectively.

Column DCH-1 experienced a ring of local buckles after a few cycles of loading. Local buckling appeared visually on the northwest side of the specimen after the first cycle of 5% drift was completed. The other three sides started buckling at the second cycle of 5% drift. The ring local buckle developed 80 mm to 90 mm above the fixed-end surface at the last cycle of 7% drift.

Column DCH-2 experienced local buckling which started on the southwest side of the column at the first cycle of 4% drift. At the next cycle, all sides of the column buckled. As the buckling became larger, the corners started buckling at the third cycle of 5% drift, and a ring local buckle developed at 75 mm to 85 mm above the fixed-end surface.

Column DCH-3 started developing local buckles on all sides at the second cycle of 4% drift. A ring local buckle developed at the third cycle of 4 % drift, and it was located 80 mm to 100 mm above the fixed-end surface. As the ring local buckling spread progressively, the east and west corners cracked at the third cycle of 7% drift. Column DCH-3 behaved similarly to column DCH-2

Overall, the DCH columns behaved similar to the SNH columns. The strength of the columns dropped after the maximum capacity had been reached. The strength capacity dropped significantly on the column with the higher axial compressive load.

6.4 Strength Capacity

The first formulation of design equation of seismic strength of square high strength CFT columns subjected to a constant axial compressive load and a biaxial bending moment is by applying the uniaxial bending moment section analysis approach. The proposed method of analysis, as discussed in Chapter 3, is based on the ACI procedures for reinforced concrete section analysis with modifications in determining the

equivalent rectangular concrete stress distribution. In addition, the small minor axis bending moment, less than 10% of the major axis bending moment, and torsion are neglected for the square oriented specimens.

Using the proposed method of analysis and the material strengths at the age of test tabulated in Table 6.4, the strength capacity of high strength CFT columns were calculated and the results are presented in Table 6.5.

Table 6.5 also gives comparisons of experiment to predicted bending moment of all twelve beam-column specimens. Each set of three specimens, SNHs, DNHs SCHs, and DCHs, are evaluated. The results are presented in Table 6.5, where the mean values of the ratios of experimental results to predicted results are 1.044, 1.067, 1.082 and 1.031 for the SNH, DNH, SCH and DCH series respectively. In addition, the coefficients of variation of these ratios vary from 1.62% to 4.63%, the values of 2.67%, 4.63%, 1.62% and 2.38% for SNH, DNH, SCH, and DCH specimens respectively. Overall, the mean value is 1.056 and the sample coefficient of variation is 3.25%.

The results for the SNH and SCH columns are conservative even without considering the softening effects of the minor bending moment and torsion. In addition, the DNH and DCH column predictions are also conservative. It can be concluded that the strength capacity can be conservatively predicted by uniaxial bending moment section analysis neglecting the effect of the minor bending moment and torsion.

Figures 6.19 to 6.23 illustrate clearly the comparison of predicted strength capacity to experimental results of each type of columns. Predicted strength capacities in these figures were calculated using the average concrete compressive strength of the three columns in each group of CFT columns.

Overall, the predicted results are conservative, therefore, it can be concluded that the method of analysis is appropriate for these types of columns, especially for CFT columns subjected to low axial compressive load.

6.5 Ductility

The ductility of high strength CFT columns was evaluated using the same criteria as those used for the normal strength CFT columns discussed in Chapter 5. Displacement

ductility μ_Δ and curvature ductility μ_Φ were calculated using Equations 3.48 and 3.49 respectively. Yield displacement and yield curvature were defined based on the first-yield displacement and first yield curvature respectively. The ultimate displacement and ultimate curvature were determined from the curves, moment-displacement and moment curvature relationship respectively. The ultimate displacement and ultimate curvature were defined based on the displacement and curvature at 80% maximum moment beyond the peak point respectively.

Table 6.6 shows the ductility results of the high strength CFT columns. Neither displacement ductility nor curvature ductility of the test results illustrate specific trends. The displacement ductility μ_Δ of the CFT column specimens varies from 2.42 to 9.95. In addition, the curvature ductility μ_Φ varies over a wide range, from 3.05 to 18.61. Because the ductility values vary widely, it is more useful to use ultimate displacement drifts of the columns as the indicator to illustrate the ductility of columns.

Displacement ductility of Class 1 HSS CFT columns is larger than that of the Class 4 HSS CFT columns. This phenomenon can be explained as follows; the steel areas of Class 1 HSS CFT columns are larger than that of Class 4 HSS section. Steel is a ductile material. Conversely, concrete is a brittle material. Combination of concrete – steel materials produce a ductile composite material. Consequently, in general, the more steel is in the composite section, the more ductile is the section.

The ratios of yield moments to maximum moments vary from 0.43 to 0.76. For Class 4 HSS CFT columns, the yield moments at the yield curvatures and the yield displacements are from 51% to 76% of maximum moments. For Class 1 HSS CFT columns, the yield moments at the yield curvatures and the yield displacements are less than those of Class 4 HSS CFT columns. This indicates the criterion of yield curvature of reinforced concrete structures should not be applied on the CFT columns. The more reasonable criterion is the first yield curvature and the first yield displacement.

6.6 Flexural Stiffness

Determination of the experimental flexural stiffness of high strength CFT columns followed the same procedure as that used for normal strength CFT columns in Chapter 3.

After comparing formulas for the modulus of elasticity of concrete, Eurocode 2, ACI 318-99, CSA A23.3-94 and Gardner's 2001 proposed formulas, to the experimental results in Table 6.2, it was observed that Gardner's 2001 proposed formula was the best fit to the experimental results. However, to calculate the modulus of elasticity at the various test age, the modulus of elasticity of concrete was calculated using the Equation 3.52.

Table 6.7 gives the flexural stiffness of high strength CFT columns. The flexural stiffness was determined using the ACI formula (Equation 3.53) and the proposed formulas (Equations 3.54 and 3.55).

The ACI formula of flexural stiffness of composite columns is too conservative when it is applied for square high strength CFT columns under combined axial compressive load and cyclic biaxial bending moment.

The Equation 3.55 produces safe predictions for Class 4 HSS CFT columns. The mean value of the ratio of experimental to proposed results is 1.088, and the coefficient of variation is 6.87%. The mean ratios of experimental to prediction results of the DNH and SNH columns are 1.025 and 1.152 respectively with coefficients of variation of 1.47% and 3.50% for the DNH and SNH columns respectively.

For Class 1 HSS CFT columns, the Equation 3.54 produces safe predictions. All proposed results are on the lower bound side. The mean ratio of experimental results to prediction of all Class 1 HSS CFT columns is 1.126 and the coefficient of variation is 4.66%. More precisely, the mean ratios of experimental results to prediction of SCH and DCH columns are 1.111 and 1.141 respectively, and the coefficients of variation are 6.19% and 3.38% for the SCH and DCH columns respectively.

Overall, the mean ratio is 1.107, and the coefficient of variation is 5.83%. It can be concluded that the Equations 3.54 and 3.55 are appropriate to predict the flexural stiffness of high strength CFT columns subjected to combined axial compressive load and cyclic biaxial bending moment.

6.7 Column Classification

The conventional method of classification of columns is applied to classify the experimental column specimens. Table 6.8 shows the comparison of squash load to Euler load of high strength CFT columns. The squash loads were calculated based on the HSS steel properties in Table 6.3 and the material strengths in Table 6.4. All squash loads of columns are less than the Euler loads; therefore, they are classified into stocky columns.

Table 6.1 Compressive strength of standard cylinder tests of the concrete

Age [days]	Concrete strength [MPa]			
	Cylinder 1	Cylinder 2	Cylinder 3	Average
14	83.6	74.0	58.0*	78.8
21	87.2	93.0	49.8*	90.1
28	90.6*	92.9	97.9	95.4
44	99.5	86.1*	102.4	100.9
63	105.8	96.7	104.2	102.2
80	98.7	107.5	63.4*	103.1

*Data omitted

Table 6.2 Test and analytical results of modulus of elasticity of HSC

Procedure		E_c [1] [MPa]
Cylinder tests [2]		47,028
Eurocode 2:	$E_c = [9500\ (f_{cm28})^{1/3}](f_{cmt}/f_{cm28})^{1/2}$	45,127
Gardner:	$E_c = 4300\sqrt{f_c'} + 3500$	46,975
ACI 318-99:	$E_c = 4700\sqrt{f_c'}$	47,519
CSA A23.3-94:	$E_c = (3300\sqrt{f_c'} + 6900)(\gamma_c/2300)^{1.5}$	43,590
Proposed:	$E_c = 4650\sqrt{f_c'}$	47,013

[1] $f_{cmt} = f_c' = 102.22$ MPa ; $f_{cm28} = 92.97$ MPa
[2] Average value of 3 cylinders

Table 6.3 The HSS steel properties

Designation	Nominal				Measured			
	Dimension [mm]		Tensile strength [MPa]		Dimension [mm]		Tensile strength [MPa]	
	b	t	$f_{y,min}$	$f_{u,min}$	b	t	f_y	f_u
SNH	203.2	4.76	345	425	203.2	4.37	411.4	491.7
SCH	203.2	9.52	345	425	203.2	9.18	377.7	462.0
DNH	203.2	4.76	345	425	203.2	4.36	404.9	479.0
DCH	203.2	9.52	345	425	203.2	9.18	377.7	462.0

Table 6.4 Specimens constituent strength at the test

Specimen	f_c' [MPa]	f_y [MPa]	Specimen's age at test [days]
SCH – 1	82.9	377.7	16
SCH – 2	86.9	377.7	20
SCH – 3	89.5	377.7	23
SNH – 1	98.6	411.4	41
SNH – 2	99.1	411.4	43
SNH – 3	98.9	411.4	42
DCH – 1	100.2	377.7	48
DCH – 2	101.6	377.7	56
DCH – 3	101.8	377.7	57
DNH – 1	102.1	404.9	59
DNH – 2	102.6	404.9	62
DNH – 3	103.0	404.9	64

Table 6.5 The strength capacity of high strength CFT columns

Designation	Axial load P [kN]	Bending moment [kN.m]		$\frac{M_{exp}}{M_{pre}}$	μ	c.of v. [%]
		Predicted* M_{pre}	Experiment M_{exp}			
SNH – 1	520	158.6	160.77	1.014	1.044	2.67
SNH – 2	1150	177.81	190.04	1.069		
SNH – 3	1700	181.53	190.32	1.048		
DNH – 1	540	155.64	173.75	1.116	1.067	4.63
DNH – 2	1100	170.46	182.10	1.068		
DNH – 3	1850	173.85	176.90	1.018		
SCH – 1	570	240.51	265.07	1.102	1.082	1.62
SCH – 2	1200	253.78	272.91	1.075		
SCH - 3	1750	255.30	272.93	1.069		
DCH – 1	630	240.83	250.82	1.041	1.031	2.38
DCH – 2	1550	253.74	265.86	1.048		
DCH – 3	1900	252.62	253.25	1.003		
				Overall :	1.056	3.25

c. of v. = $\frac{\sigma}{\mu}$ (coefficient of variation)

* Effects of M_y and torsion are neglected for square (SNH and SCH) columns

Table 6.6 Yield moment ratio and ductility of high strength CFT columns

Designation	Δ_y [mm]	Φ_y (10^{-6})	M_y [kN.m]	$\frac{M_y}{M_{max}}$	μ_Δ	μ_Φ	Drift [%]
SNH – 1	26.423	13.249	112.78	0.701	4.020	17.709	6
SNH – 2	18.663	12.852	116.05	0.611	4.025	15.174	4
SNH – 3	22.555	15.918	144.54	0.759	2.422	4.572	3
DNH – 1	18.976	14.730	121.78	0.701	4.748	3.045	5
DNH – 2	26.019	16.066	129.17	0.709	3.547	15.920	5
DNH – 3	10.102	11.032	90.46	0.511	5.339	11.265	3
SCH – 1	28.339	16.480	167.17	0.631	4.513	13.933	6
SCH – 2	21.136	13.496	148.19	0.543	4.339	8.495	5
SCH – 3	18.640	14.578	168.08	0.616	3.915	6.208	4
DCH – 1	20.395	11.321	123.00	0.490	7.043	6.033	8
DCH – 2	10.659	10.632	121.31	0.456	9.951	18.609	6
DCH - 3	12.719	9.333	109.15	0.431	7.237	15.116	5

Table 6.7 Flexural stiffness of high strength CFT columns

Designation	HSS			Concrete			EI [kN.m^2]			$\frac{EI_{exp}}{EI_{prop}}$	μ	c. of v. [%]
	f_y [MPa]	E_s [MPa] $(10)^5$	I_s [mm^4] $(10)^6$	f_c' [MPa]	E_c [1] [MPa]	I_c [mm^4] $(10)^6$	EI_{ACI} [2]	EI_{Prop} [3]	EI_{Exp}			
DNH – 1	404.9	2.059	22.368	102.1	46986	119.040	5724	7961	8267	1.0384	1.0251	1.47
DNH – 2	404.9	2.059	22.368	102.6	47101	119.040	5727	7970	8040	1.0088		
DNH – 3	404.9	2.059	22.368	103.0	47192	119.040	5729	7976	8200	1.0281		
SNH – 1	411.4	1.963	22.415	98.6	46174	118.990	5499	7697	8512	1.1059	1.1523	3.50
SNH – 2	411.4	1.963	22.415	99.1	46290	118.990	5502	7705	9030	1.1720		
SNH – 3	411.4	1.963	22.415	98.9	46244	118.990	5501	7702	9080	1.1790		
For class 4 HSS CFT columns											1.0887	6.87
DCH – 1	377.7	2.001	42.701	100.2	46546	96.513	9443	9892	10860	1.0978	1.1408	3.38
DCH – 2	377.7	2.001	42.701	101.6	46871	96.513	9449	9902	11410	1.1523		
DCH – 3	377.7	2.001	42.701	101.8	46917	96.513	9450	9903	11610	1.1724		
SCH – 1	377.7	2.001	42.701	82.9	42338	96.513	9362	9770	10140	1.0378	1.1109	6.19
SCH – 2	377.7	2.001	42.701	86.9	43347	96.513	9381	9800	10980	1.1205		
SCH – 3	377.7	2.001	42.701	89.5	43991	96.513	9394	9818	11530	1.1744		
For class 1 HSS CFT columns											1.1259	4.66
Overall											1.1073	5.83

Coefficient of variation; c. of v. = $\frac{\sigma}{\mu}$

[1] $E_c = 4650\sqrt{f_c'}$

[2] $EI_{ACI} = 0.2\,E_cI_c + E_sI_s$

[3] $EI_{Prop} = 0.6\,E_cI_c + E_sI_s$; for class 4 HSS CFT (DNH, SNH) specimens

[3] $EI_{Prop} = 0.3\,E_cI_c + E_sI_s$; for class 1 HSS CFT (DCH, SCH) specimens

Table 6.8 Comparison of squash load (P_o) to Euler load (P_E)

Designation	Theory		Experiment		P_o [kN]
	EI_{ACI} [kN.m^2]	EI_{prop} [kN.m^2]	EI_{Exp} [kN.m^2]	P_E [kN]	
SNH – 1	5499	7697	8512	6482.26	5136.52
SNH – 2	5502	7705	9030	6876.74	5155.42
SNH – 3	5501	7702	9080	6914.82	5147.86
DNH – 1	5724	7961	8267	6295.68	5367.36
DNH – 2	5727	7970	8040	6122.81	5386.27
DNH – 3	5729	7976	8200	6244.66	5401.39
SCH – 1	9362	9770	10140	7722.05	5435.27
SCH – 2	9381	9800	10980	8361.75	5571.65
SCH – 3	9394	9818	11530	8780.60	5660.29
DCH – 1	9443	9892	10860	8270.36	6025.09
DCH – 2	9449	9902	11410	8689.21	6072.82
DCH - 3	9450	9903	11610	8841.52	6079.64

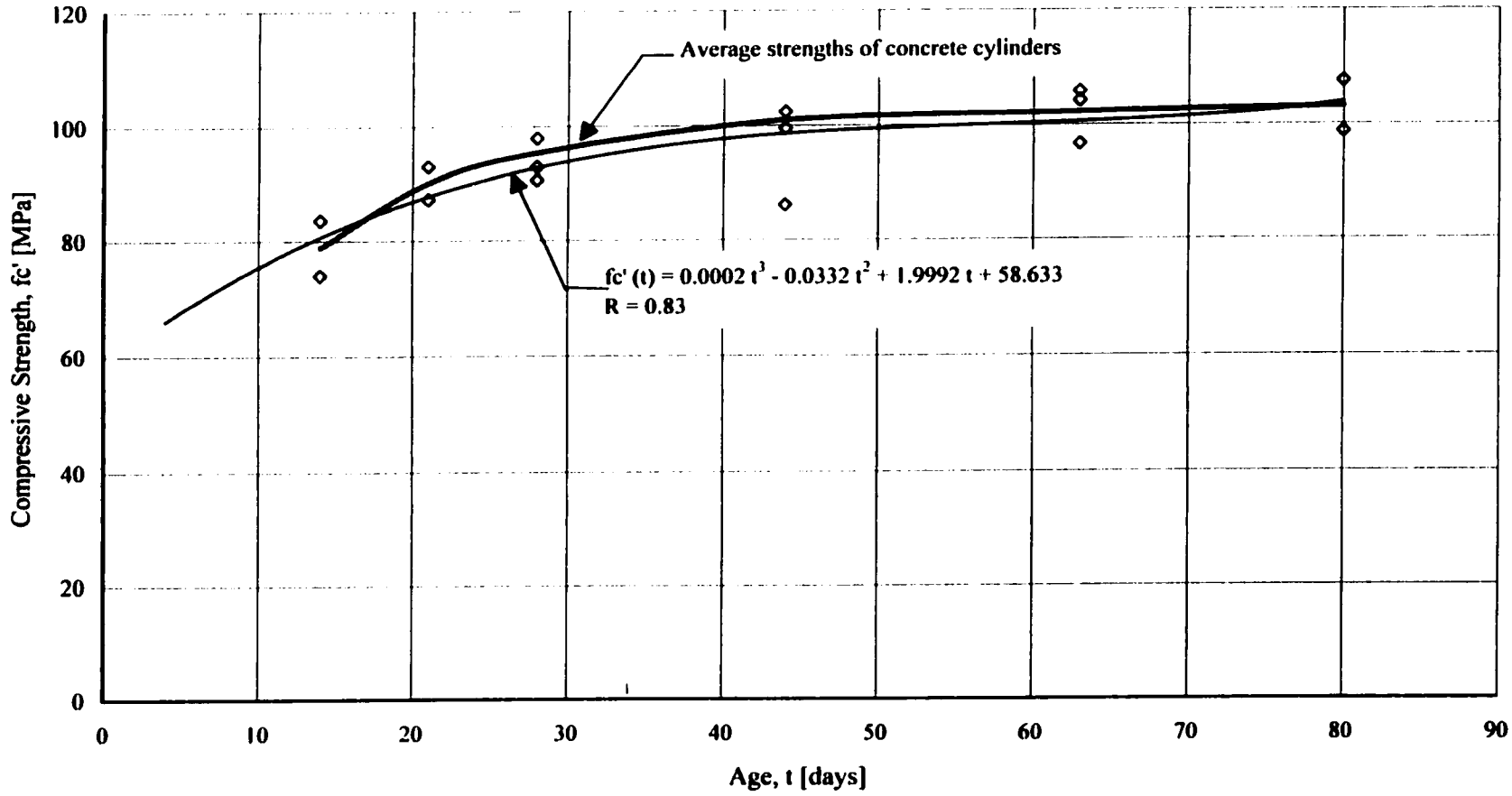

Figure 6.1 Compressive strength of high strength concrete

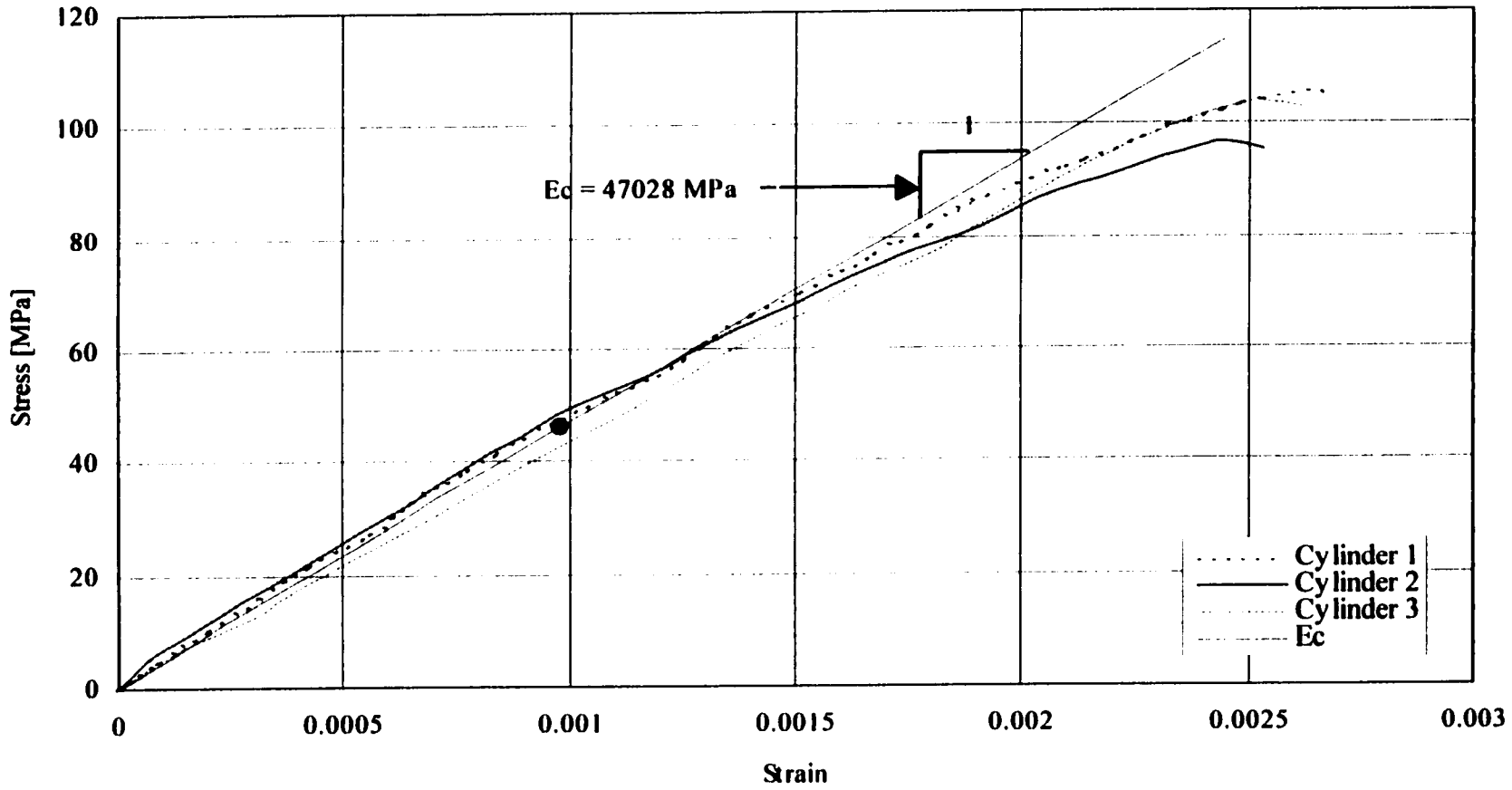

Figure 6.2 The stress-strain curve of high strength concrete tested at 44 days

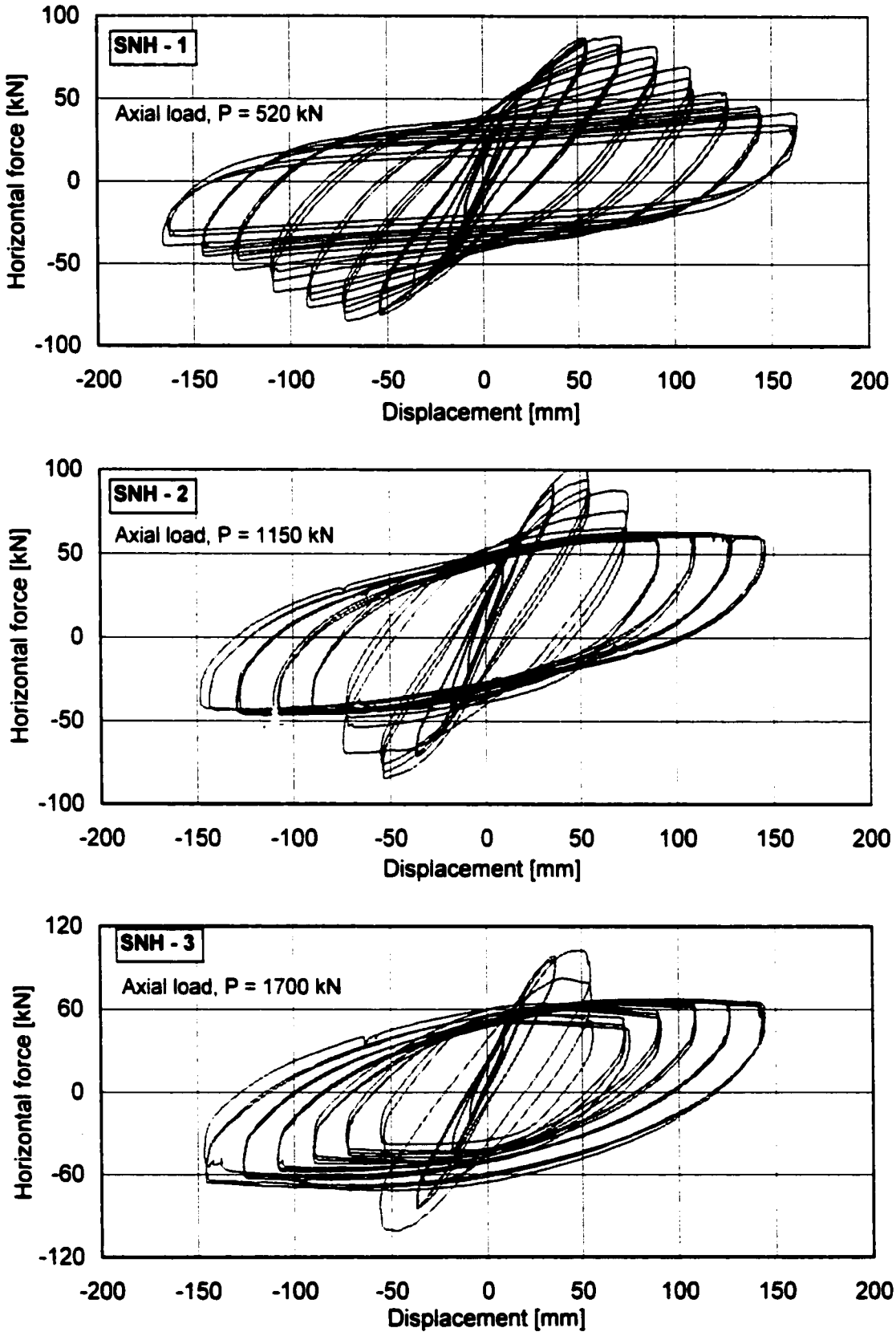

Figure 6.3 Horizontal force-displacement of horizontal actuator for SNH specimens

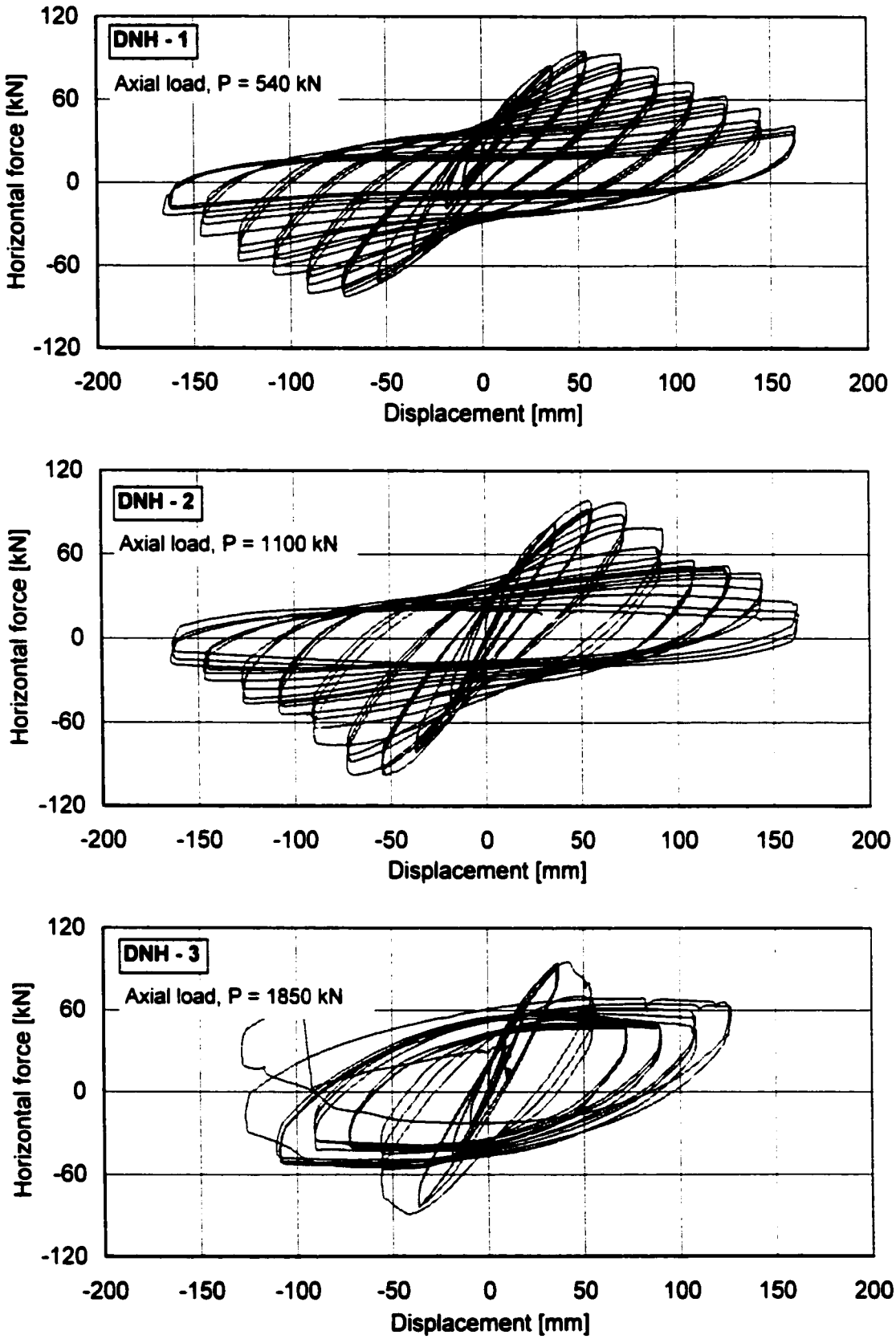

Figure 6.4 Horizontal force-displacement of horizontal actuator for DNH specimens

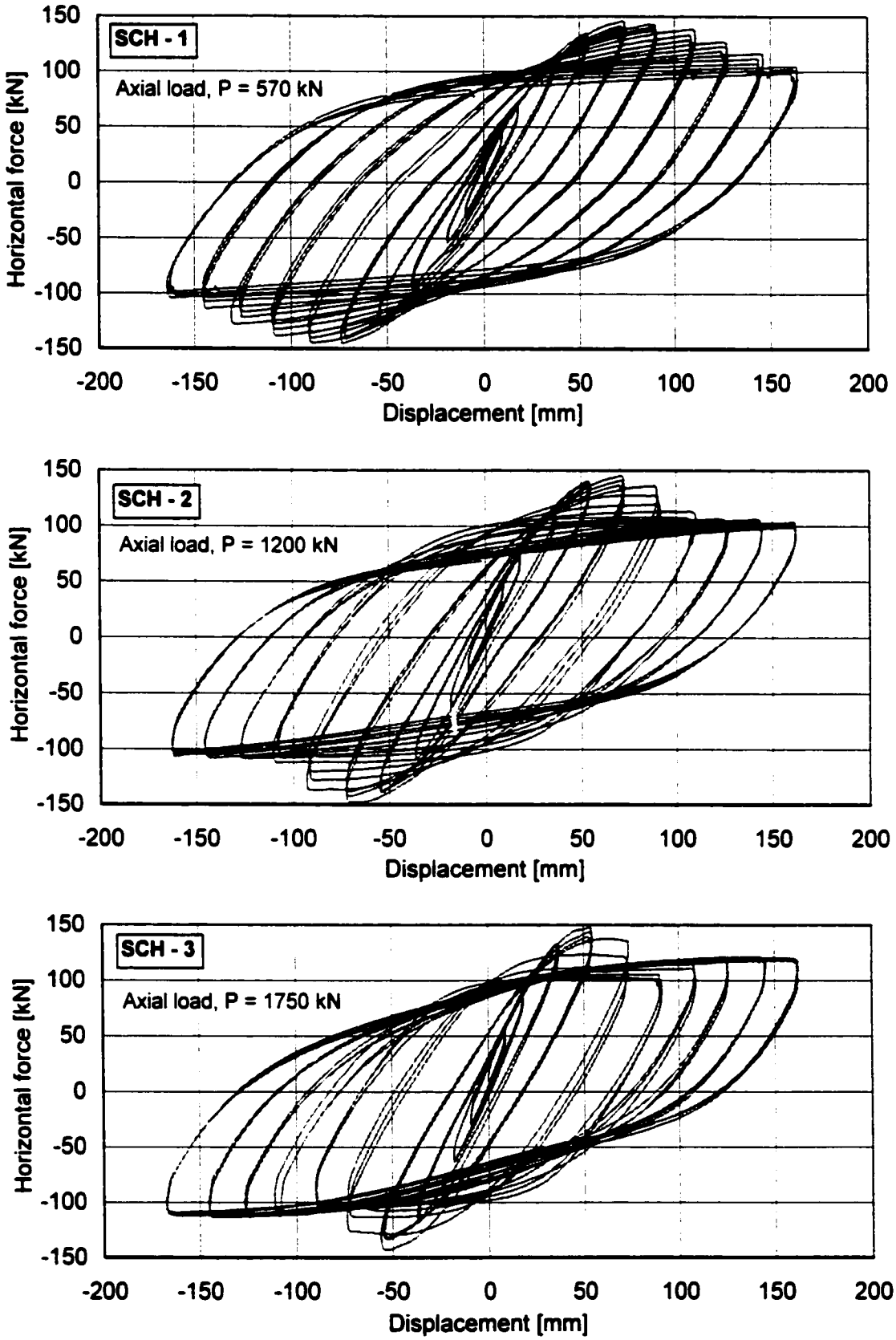

Figure 6.5 Horizontal force-displacement of horizontal actuator for SCH specimens

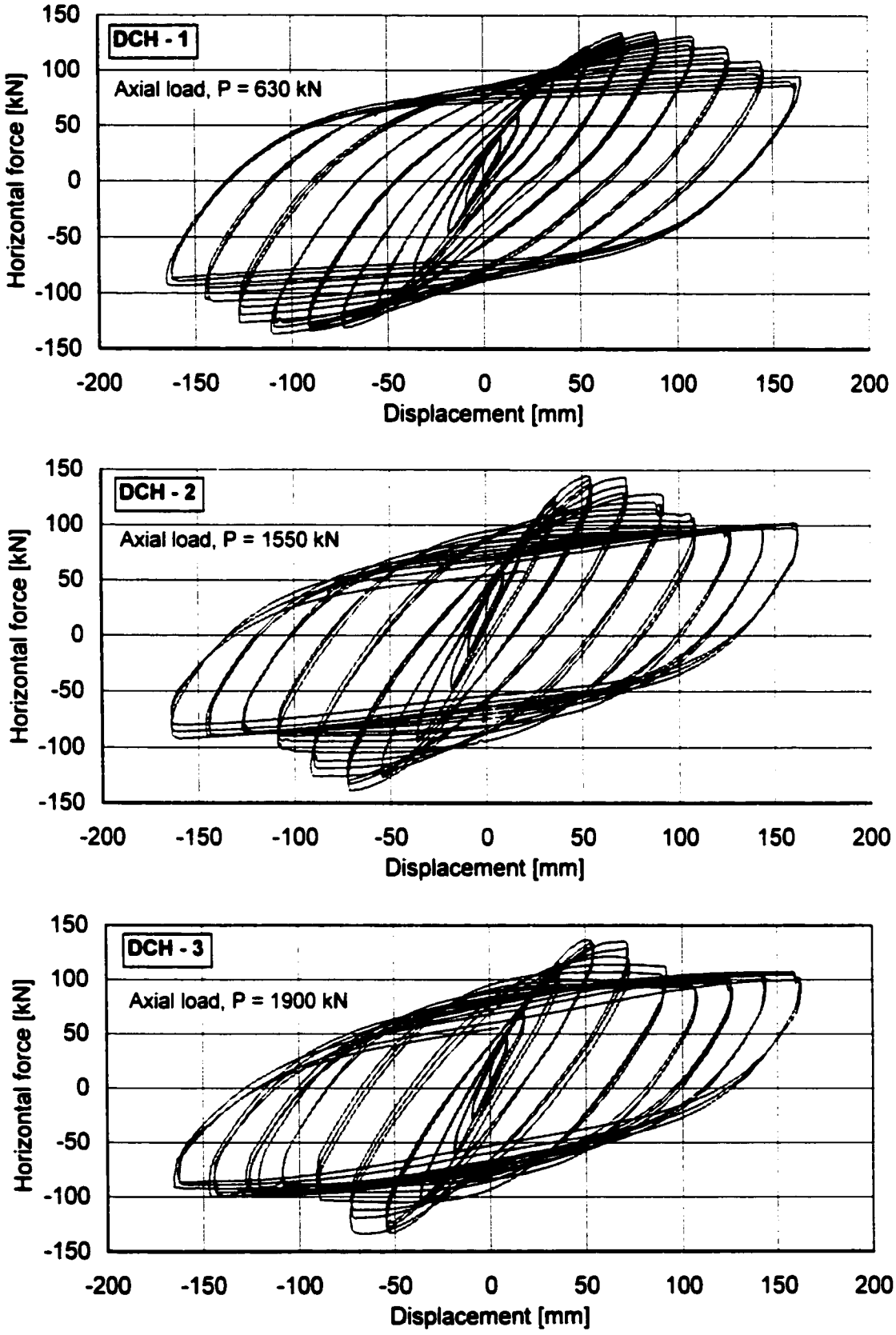

Figure 6.6 Horizontal force-displacement of horizontal actuator for DCH specimens

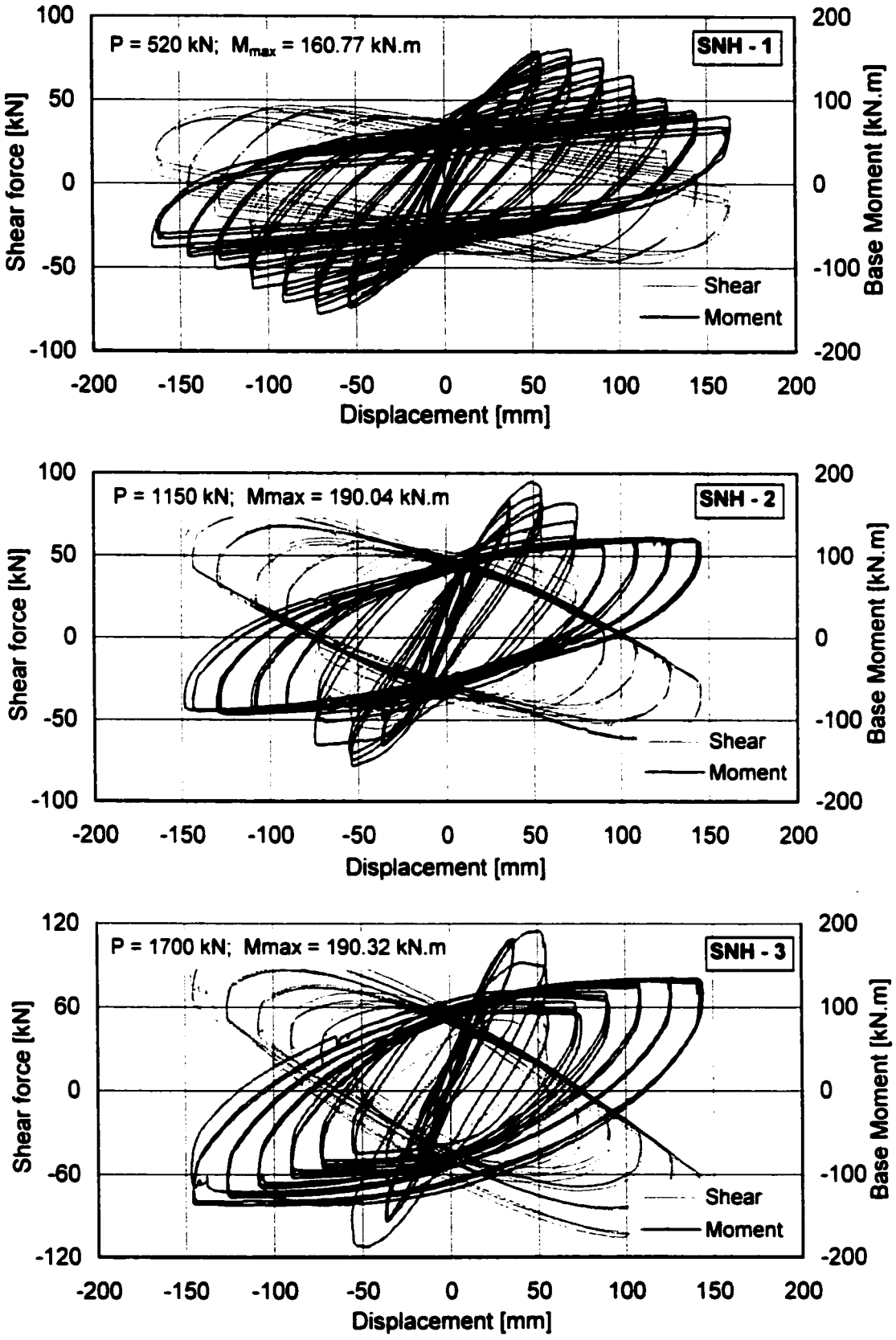

Figure 6.7 Shear Force & Moment vs Displacement of SNH specimens

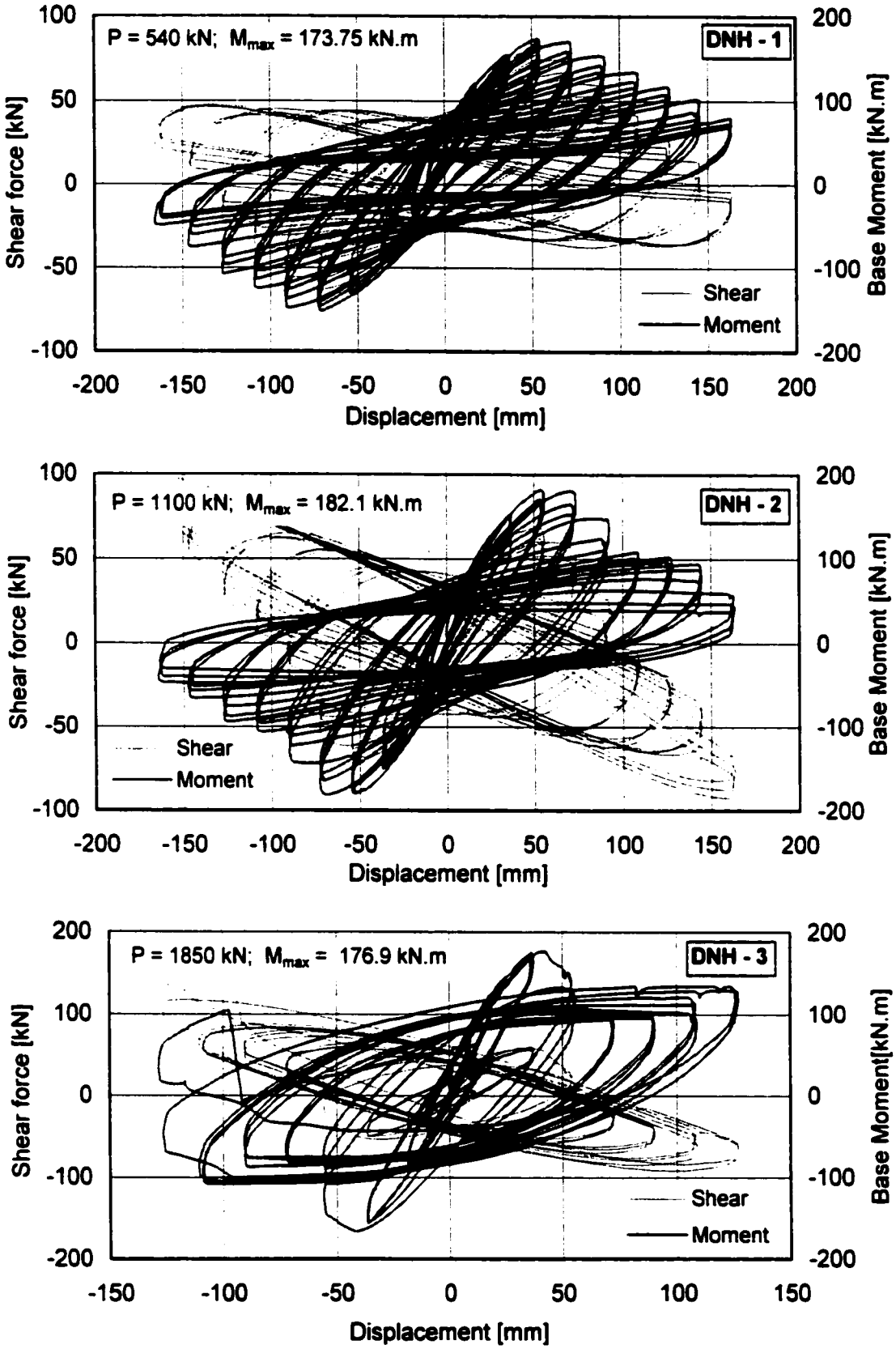

Figure 6.8 Shear Force & Moment vs Displacement of DNH specimens

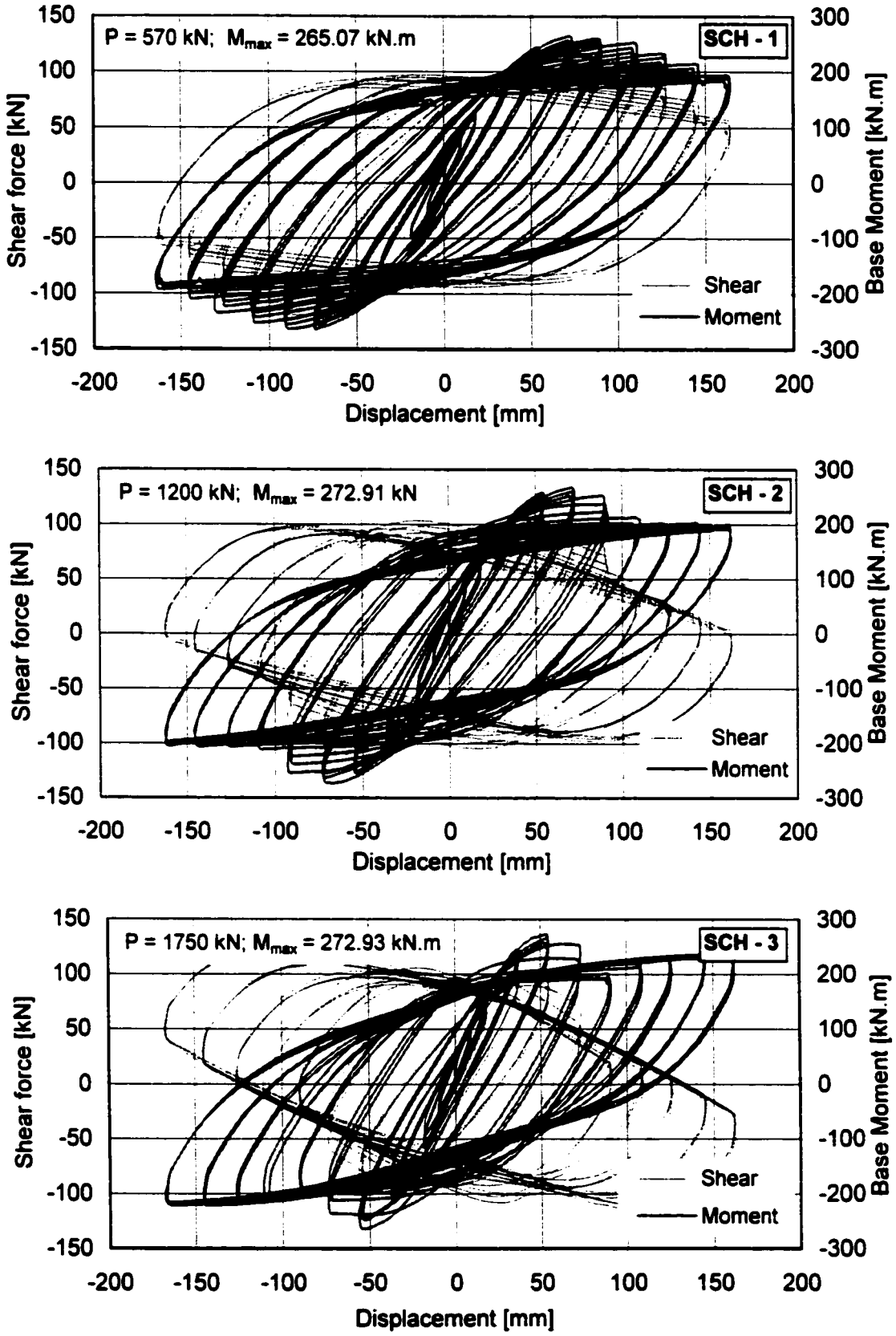

Figure 6.9 Shear Force & Moment vs Displacement of SCH specimens

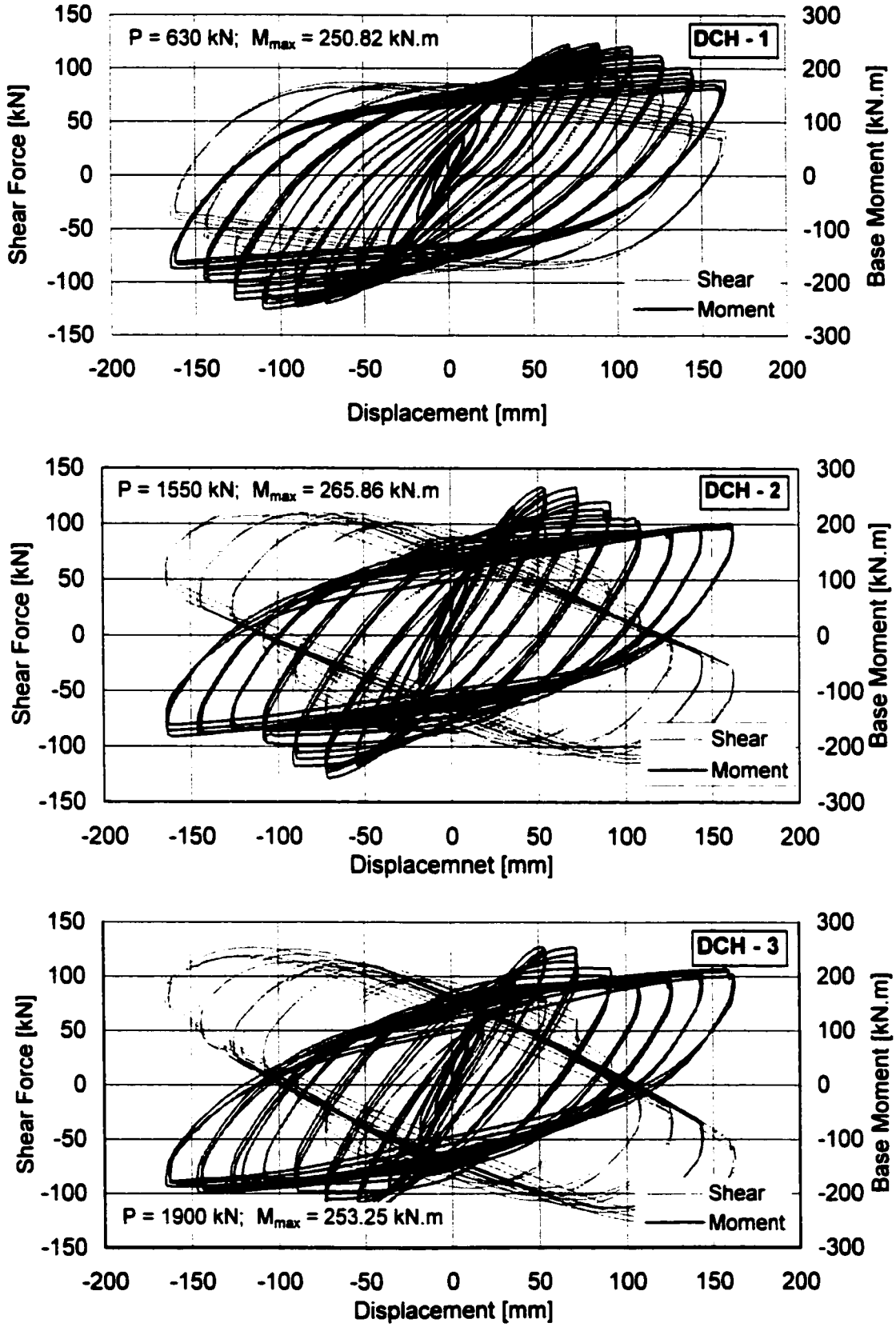

Figure 6.10 Shear Force & Moment vs Displacement of DCH specimens

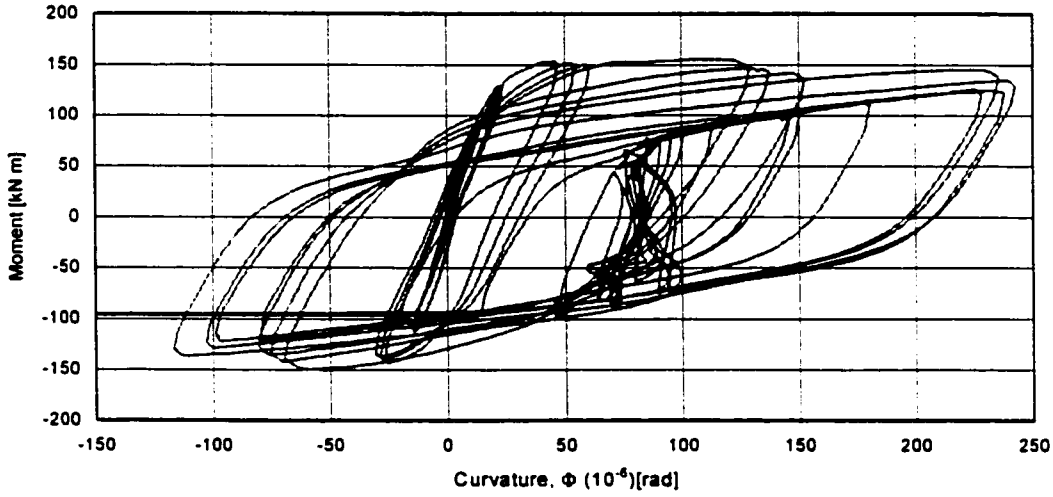

a. SNH - 1

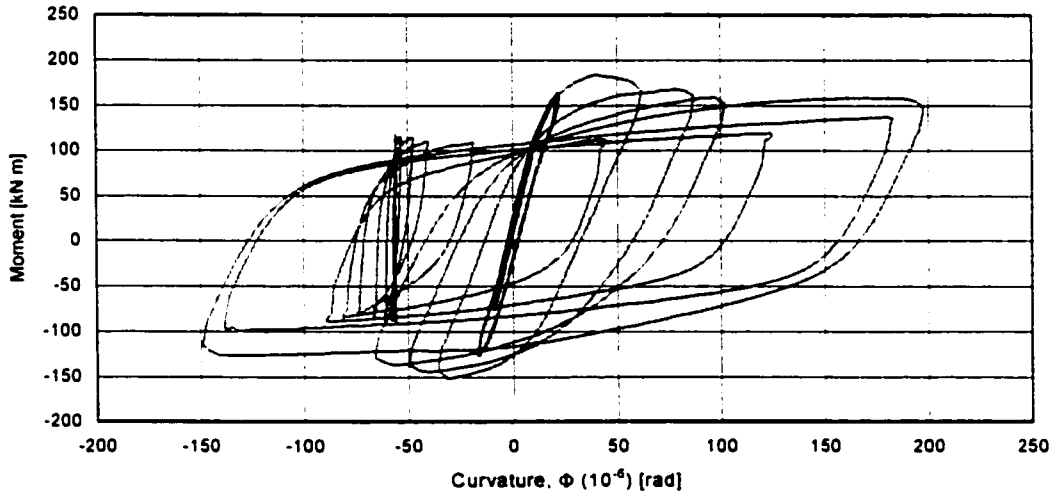

b. SNH - 2

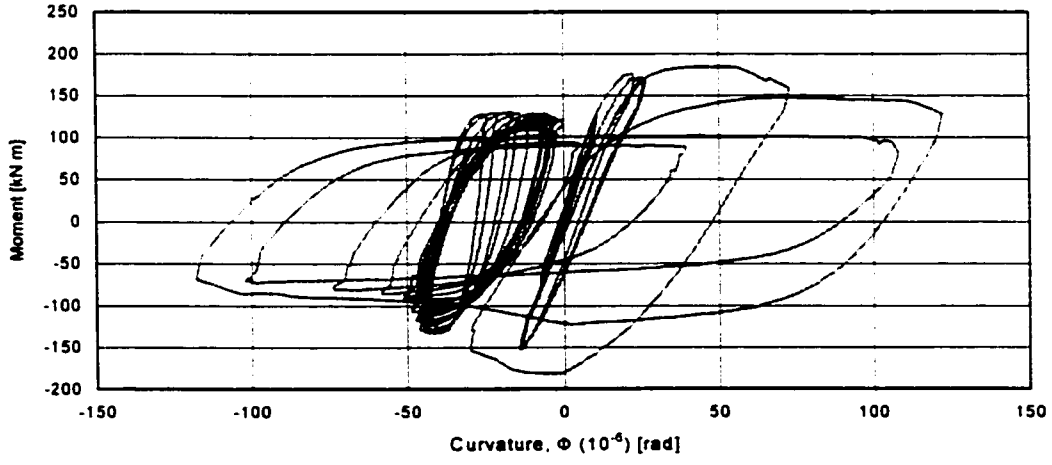

c. SNH - 3

Figure 6.11 Moment – Curvature relationship of SNH specimens

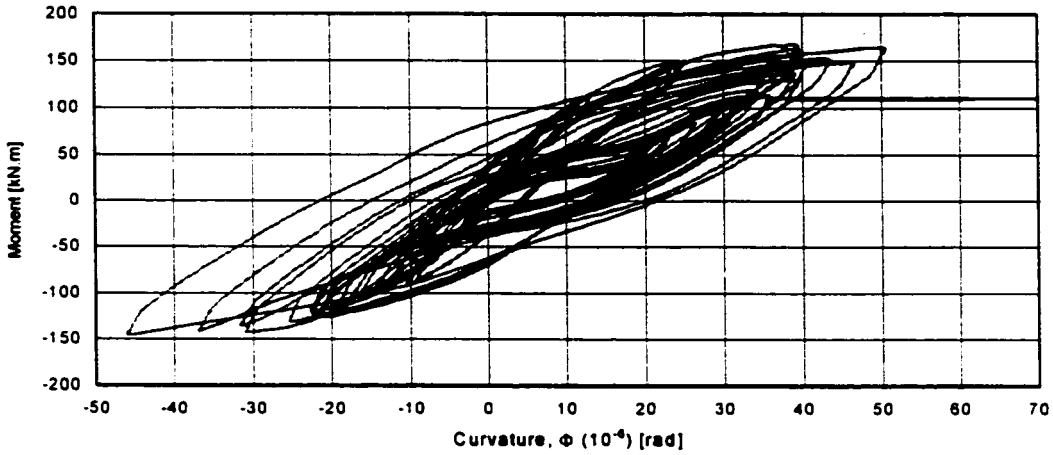

a. DNH - 1

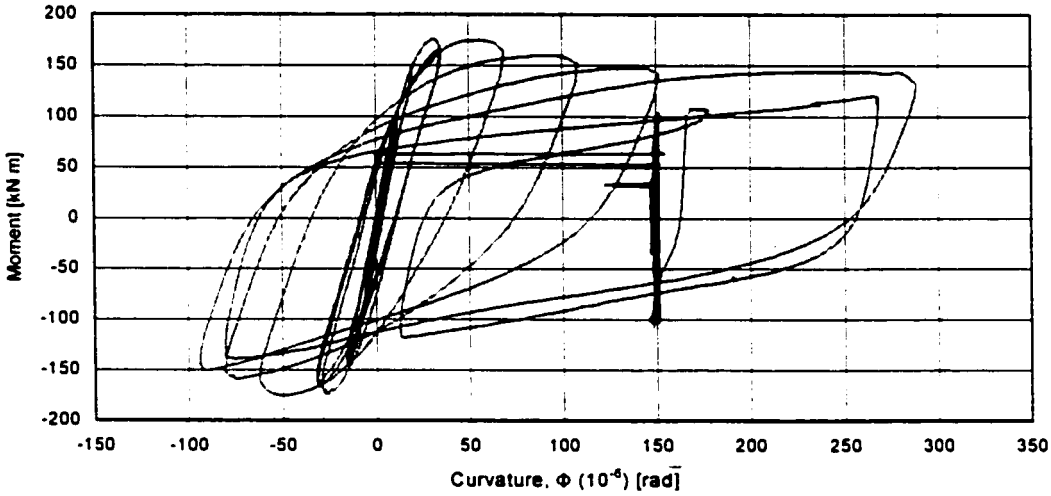

b. DNH - 2

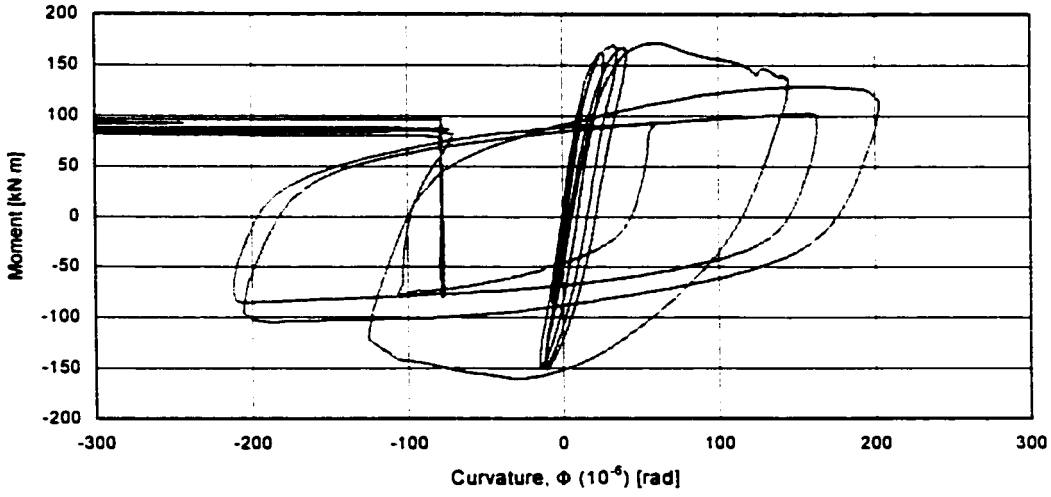

c. DNH - 3

Figure 6.12 Moment – Curvature relationship of DNH specimens

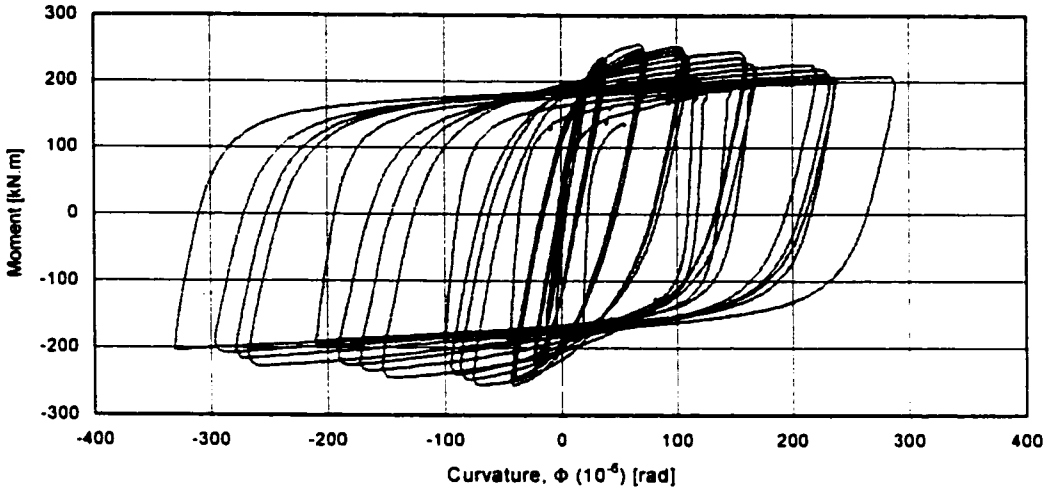

a. SCH - 1

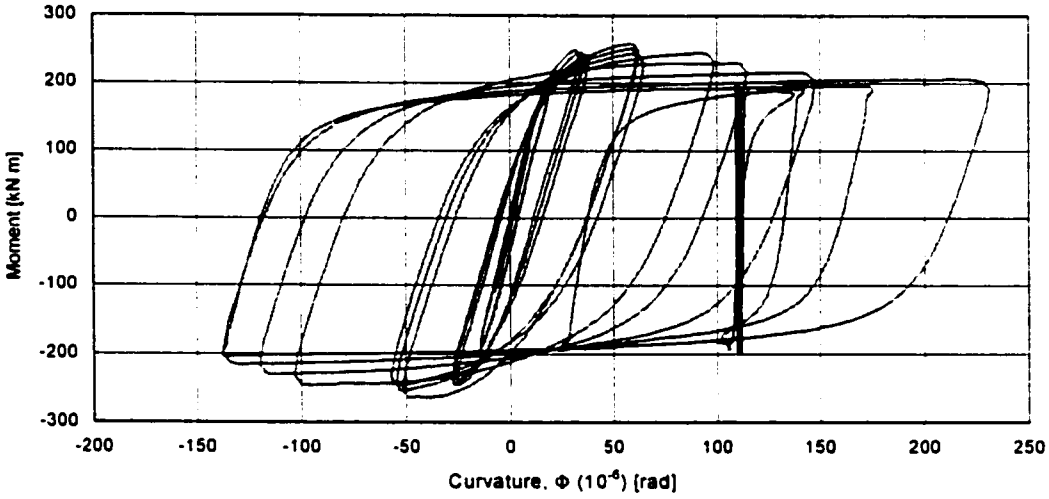

b. SCH - 2

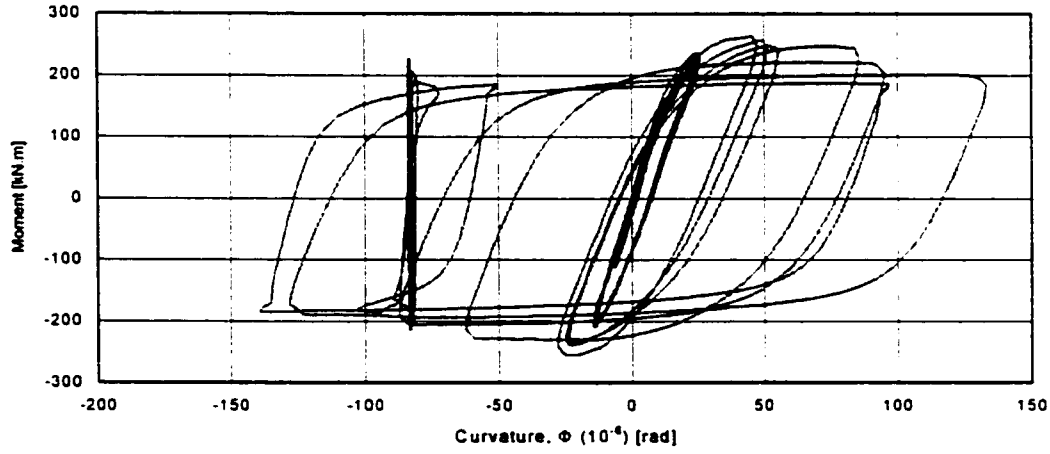

c. SCH - 3

Figure 6.13 Moment – Curvature relationship of SCH specimens

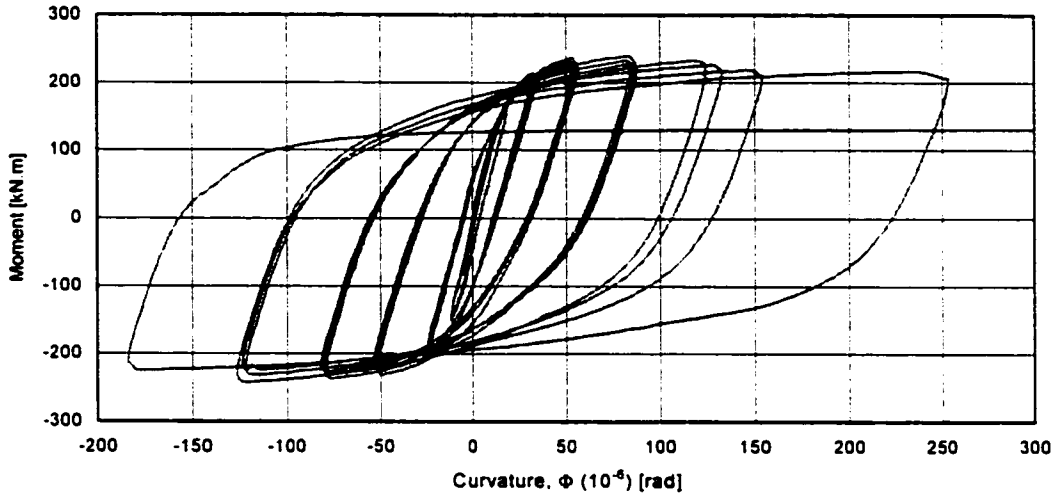

a. DCH - 1

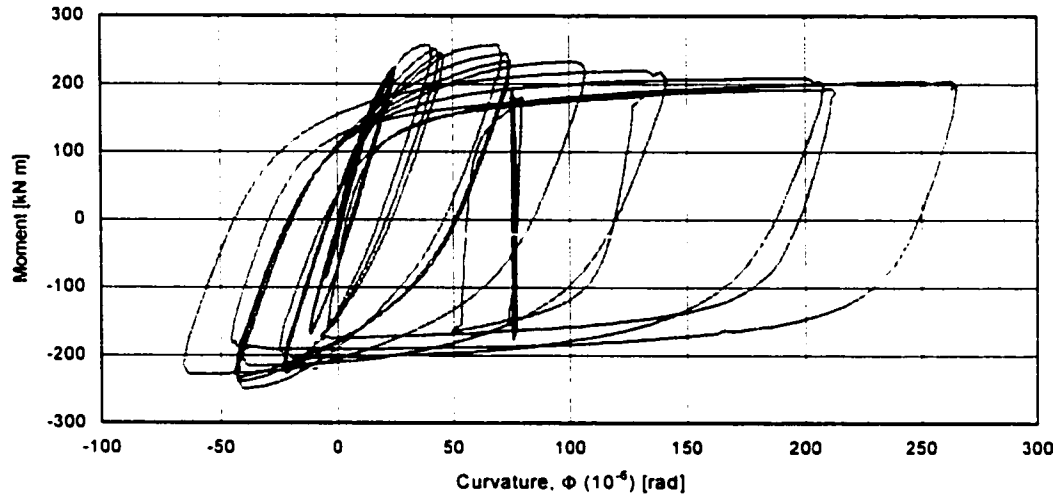

b. DCH - 2

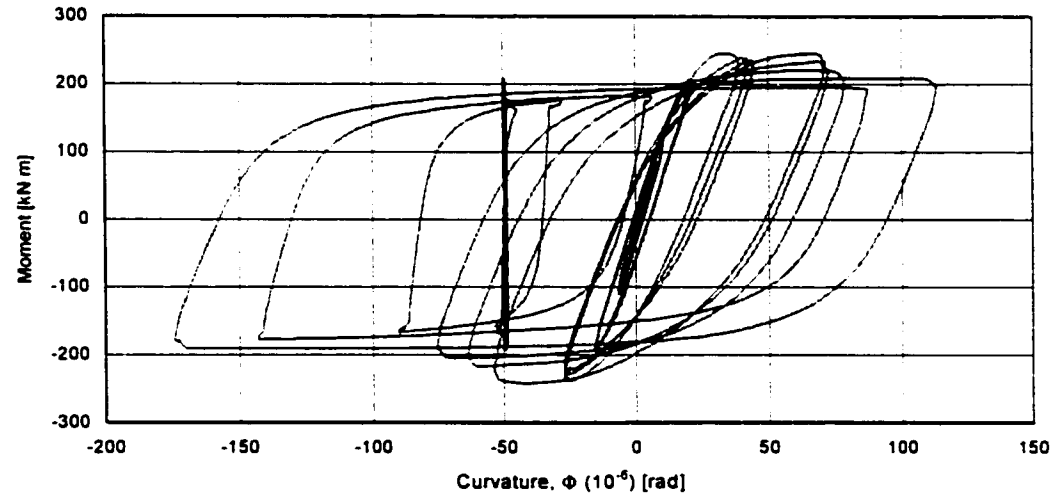

c. DCH - 3

Figure 6.14 Moment – Curvature relationship of DCH specimens

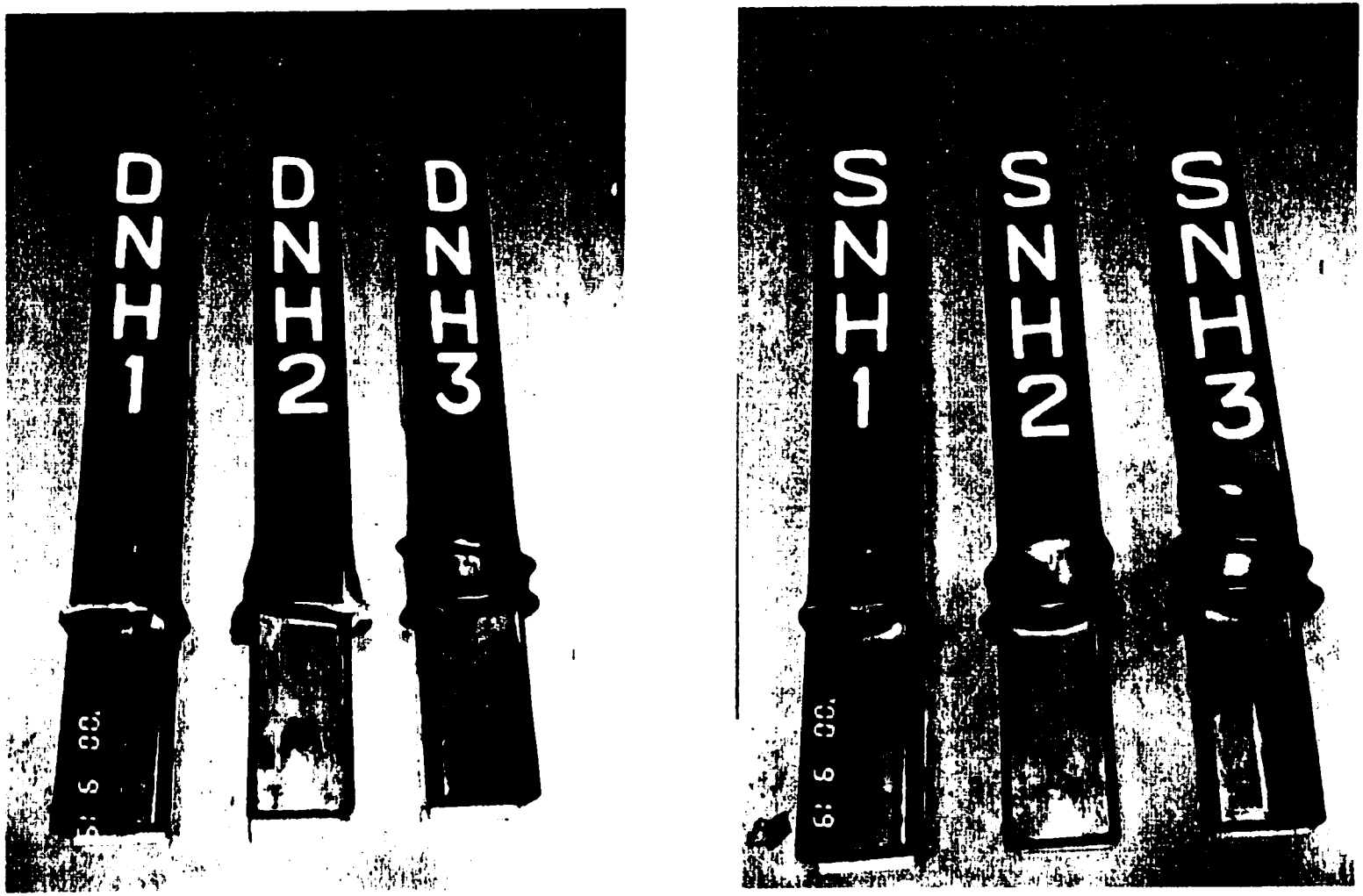

Figure 6.15 Columns DNH and SNH after tests

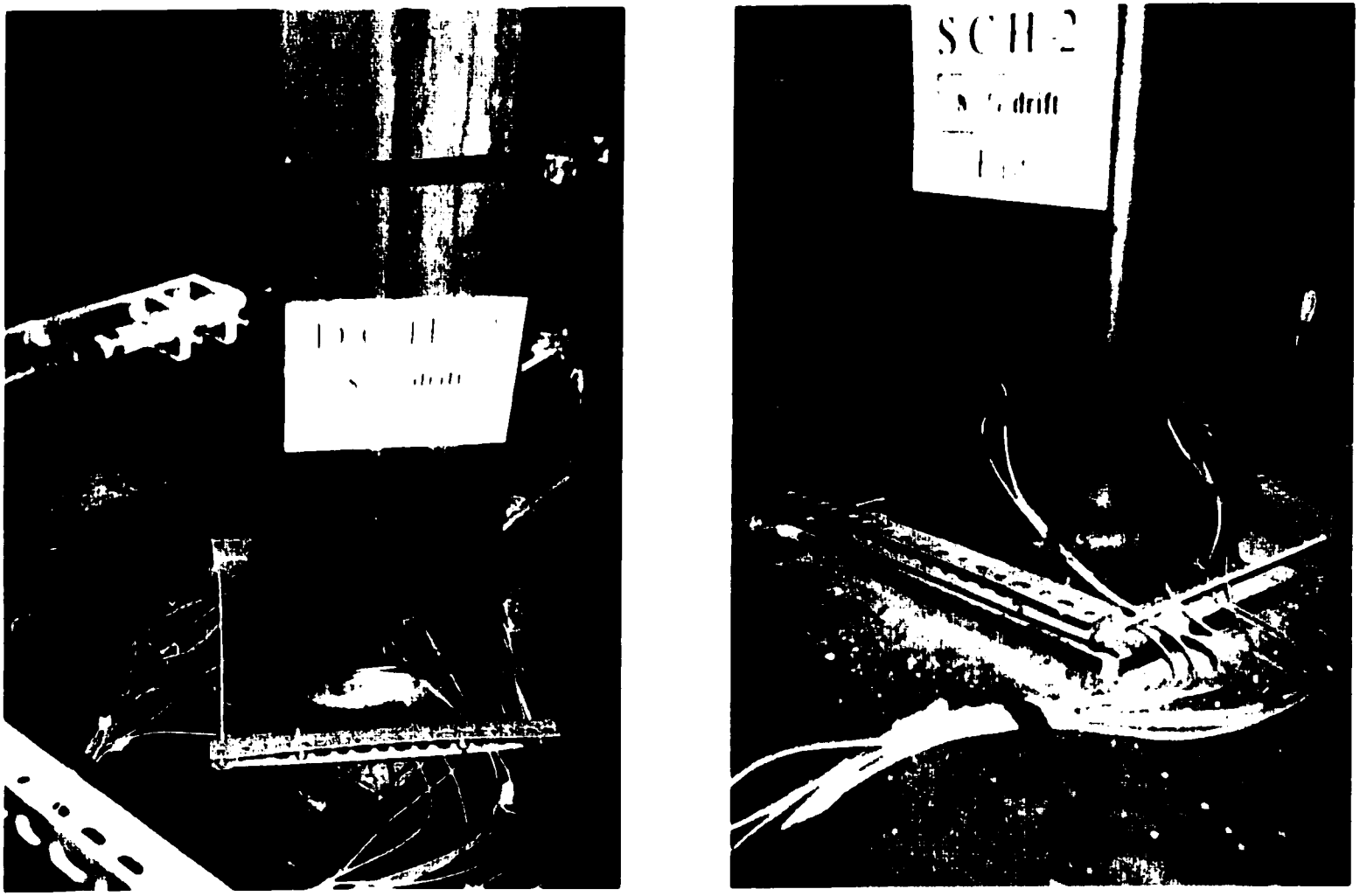

Figure 6.16 Columns DCH-2 and SCH-2 at 8 % drift

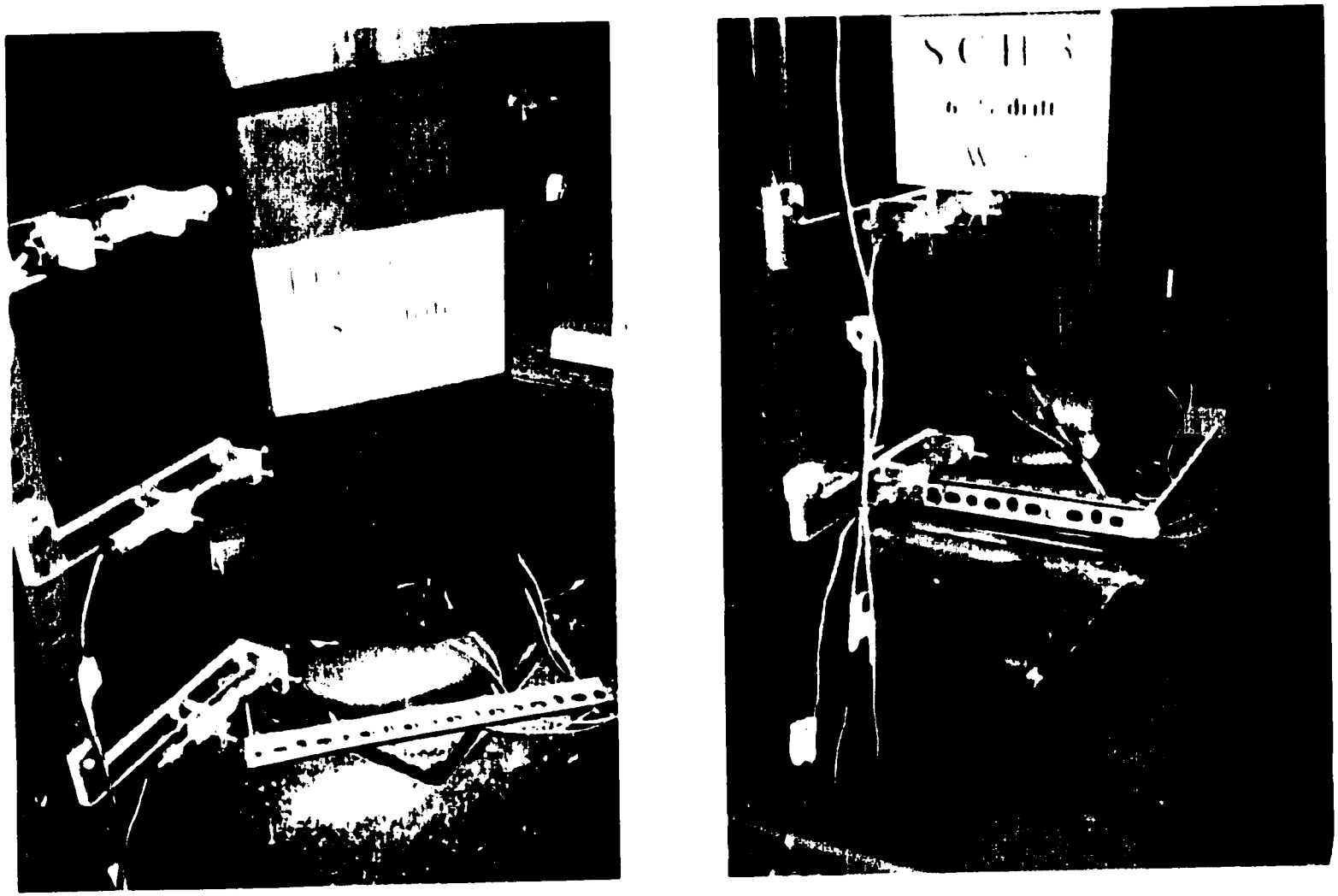

Figure 6.17 Columns DCH-3 and SCH-3 at 8 % drift

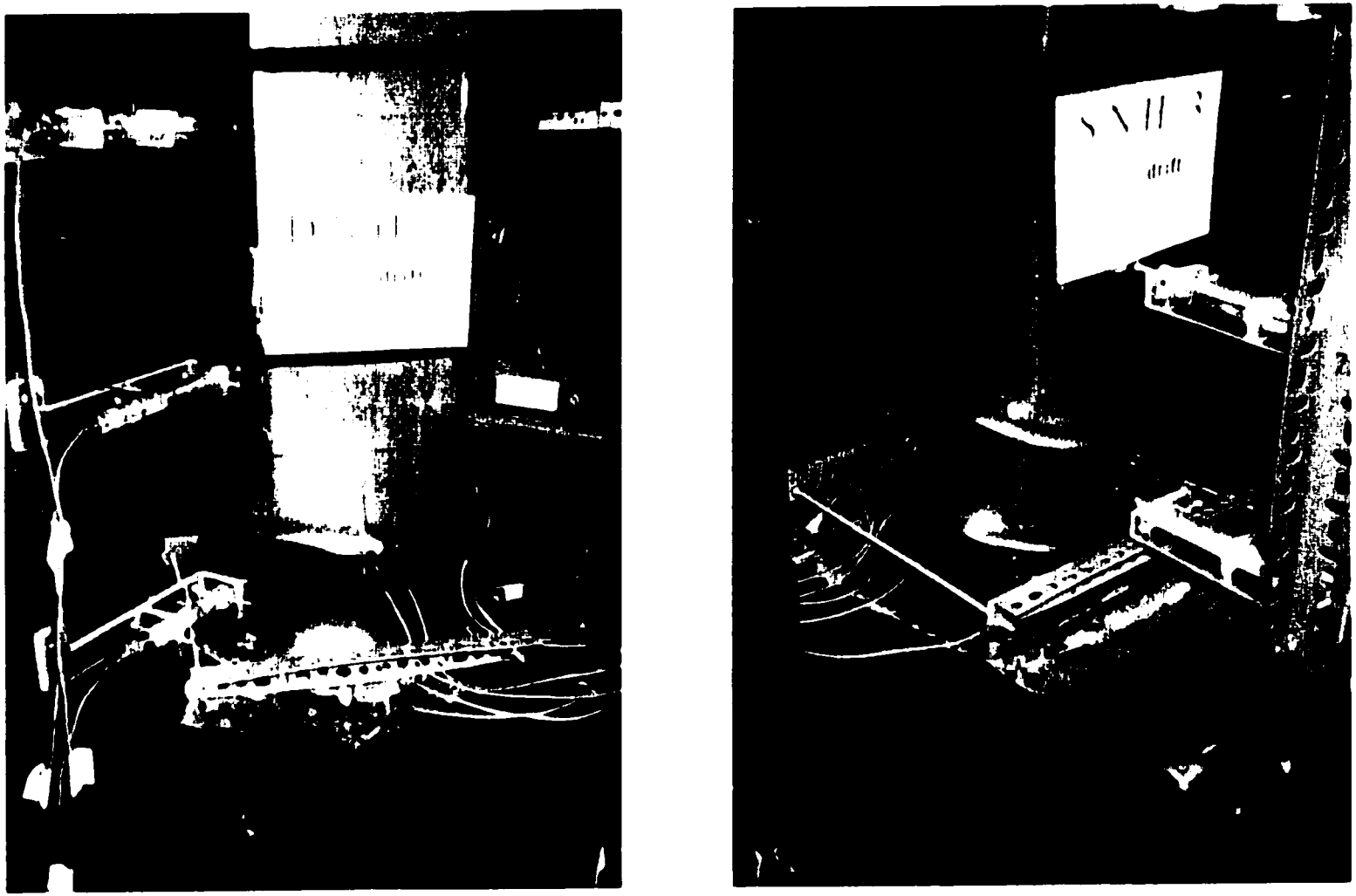

Figure 6.18 Columns DNH-3 and SNH-3 at 7 % drift

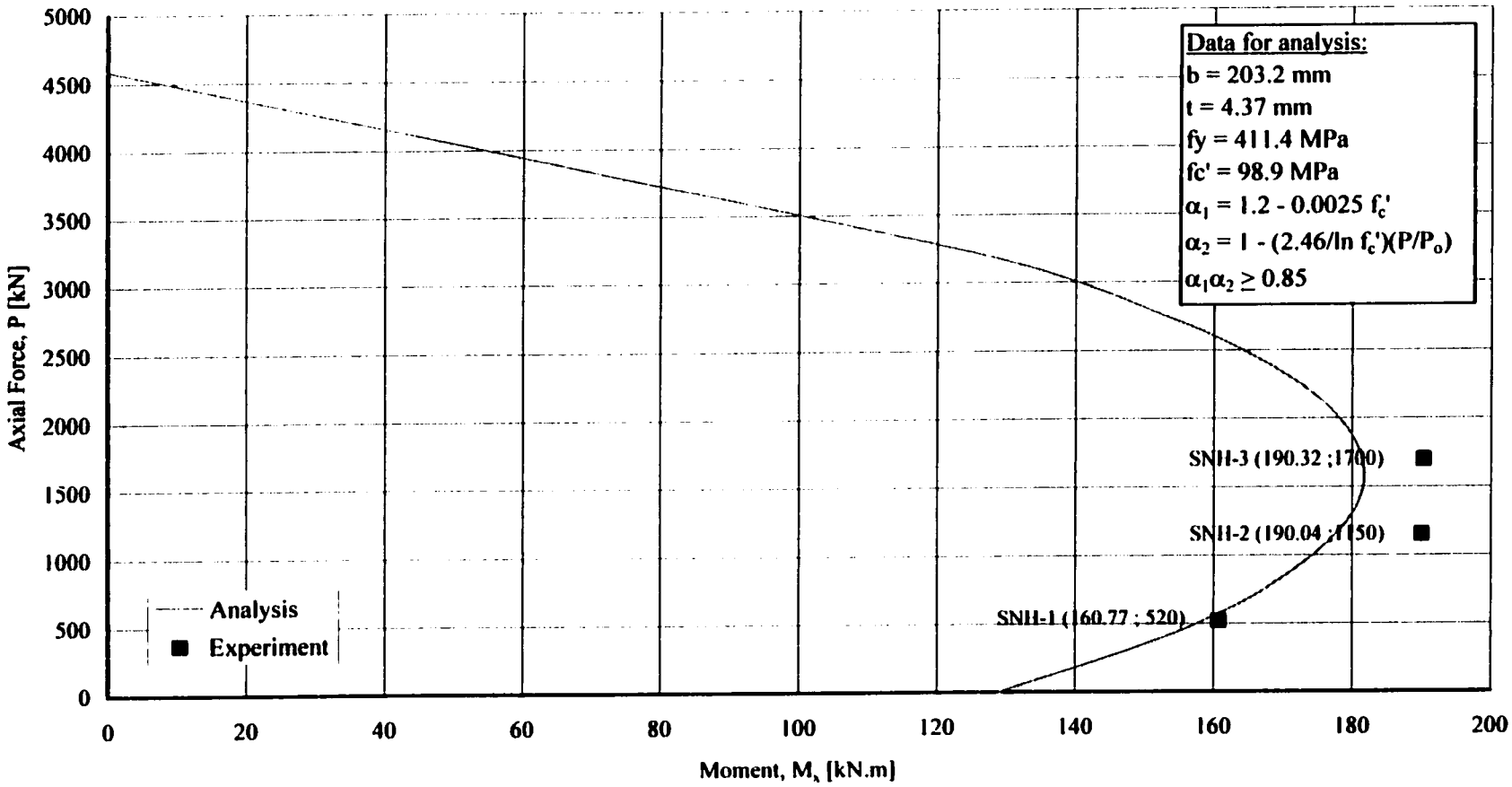

Figure 6.19 Strength Capacity of SNH Columns (without considering M_y effects)

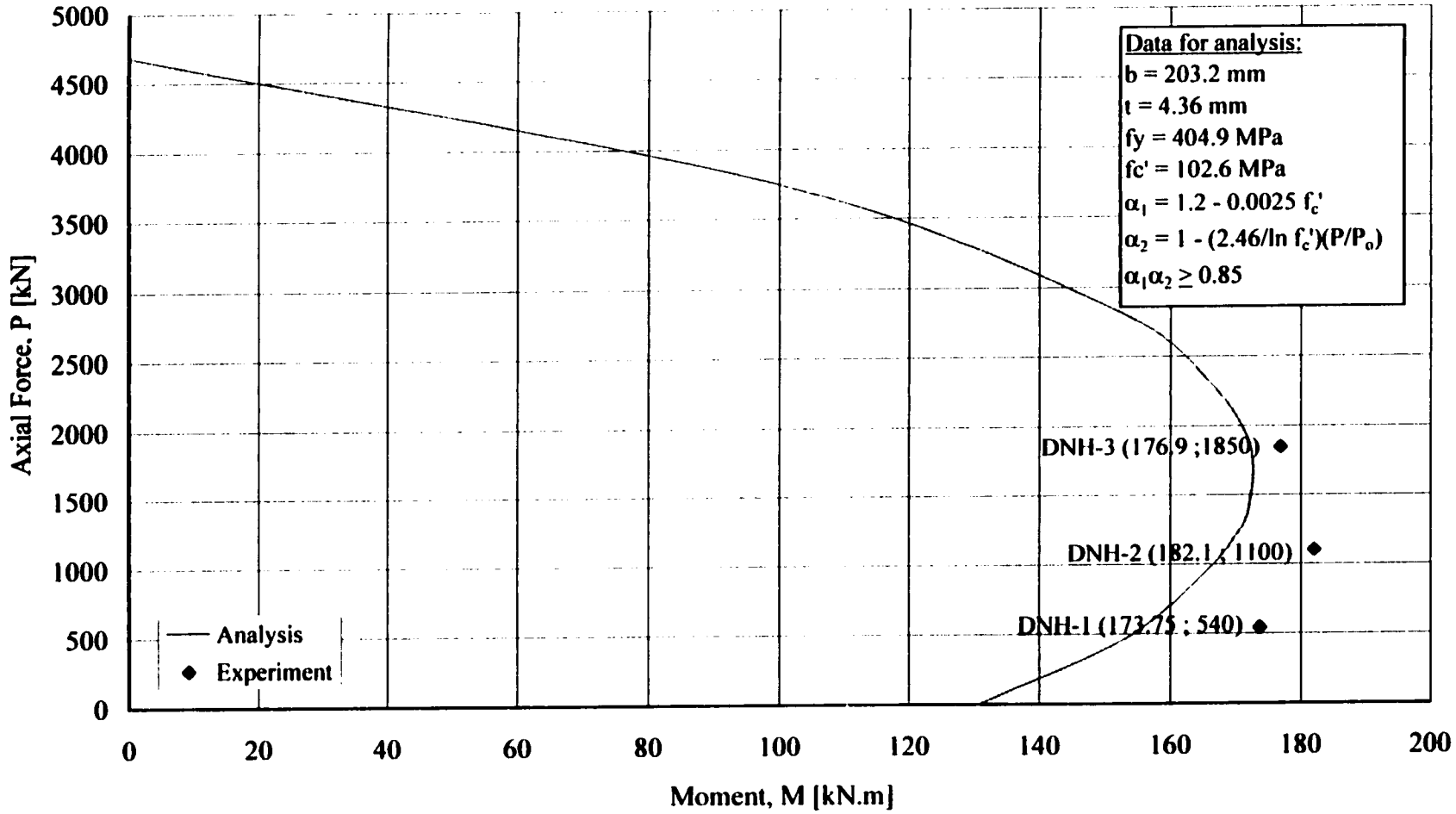

Figure 6.20 Strength Capacity of DNH Columns

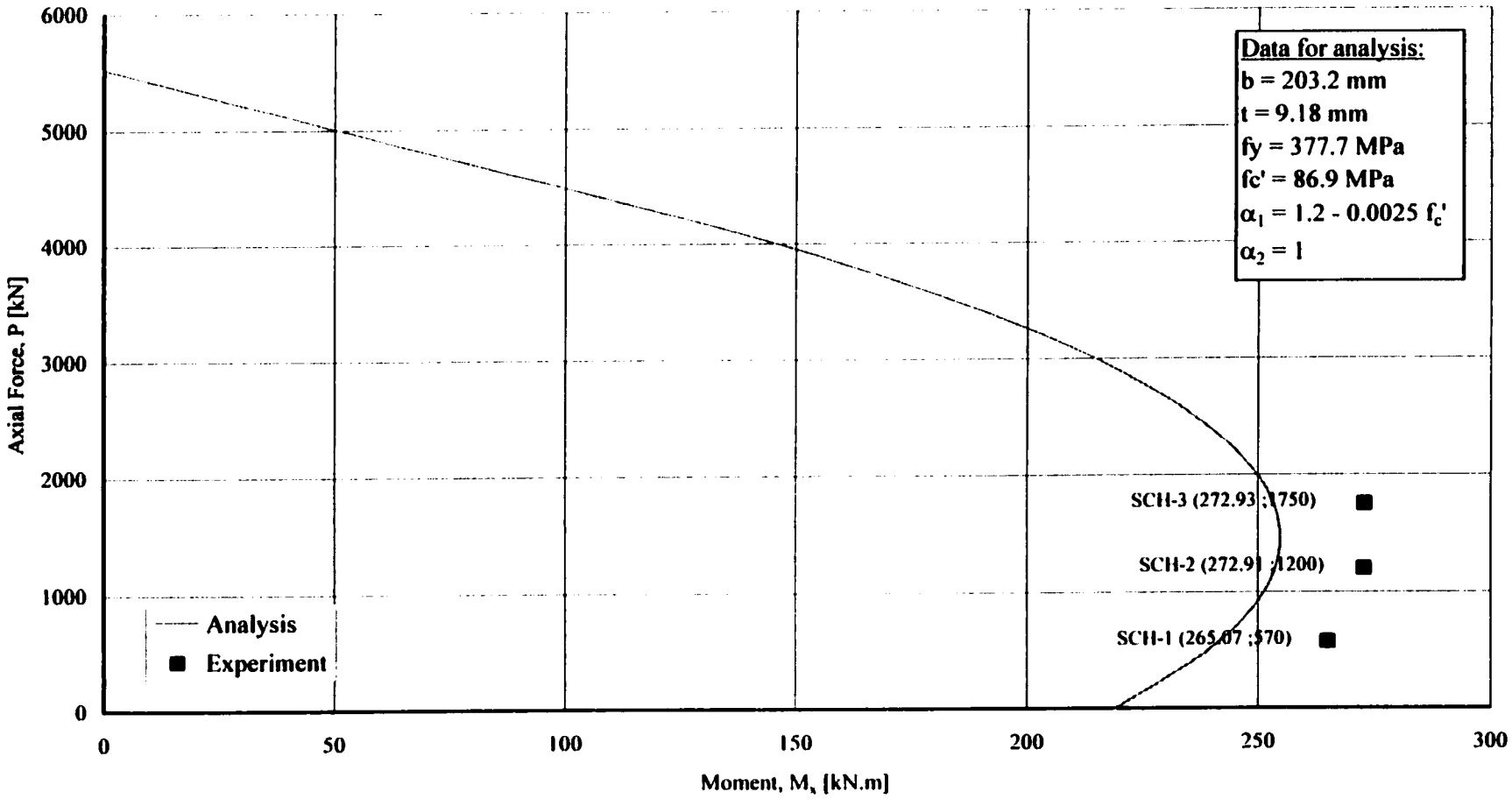

Figure 6.21 Strength Capacity of SCH Columns (without considering M_y effects)

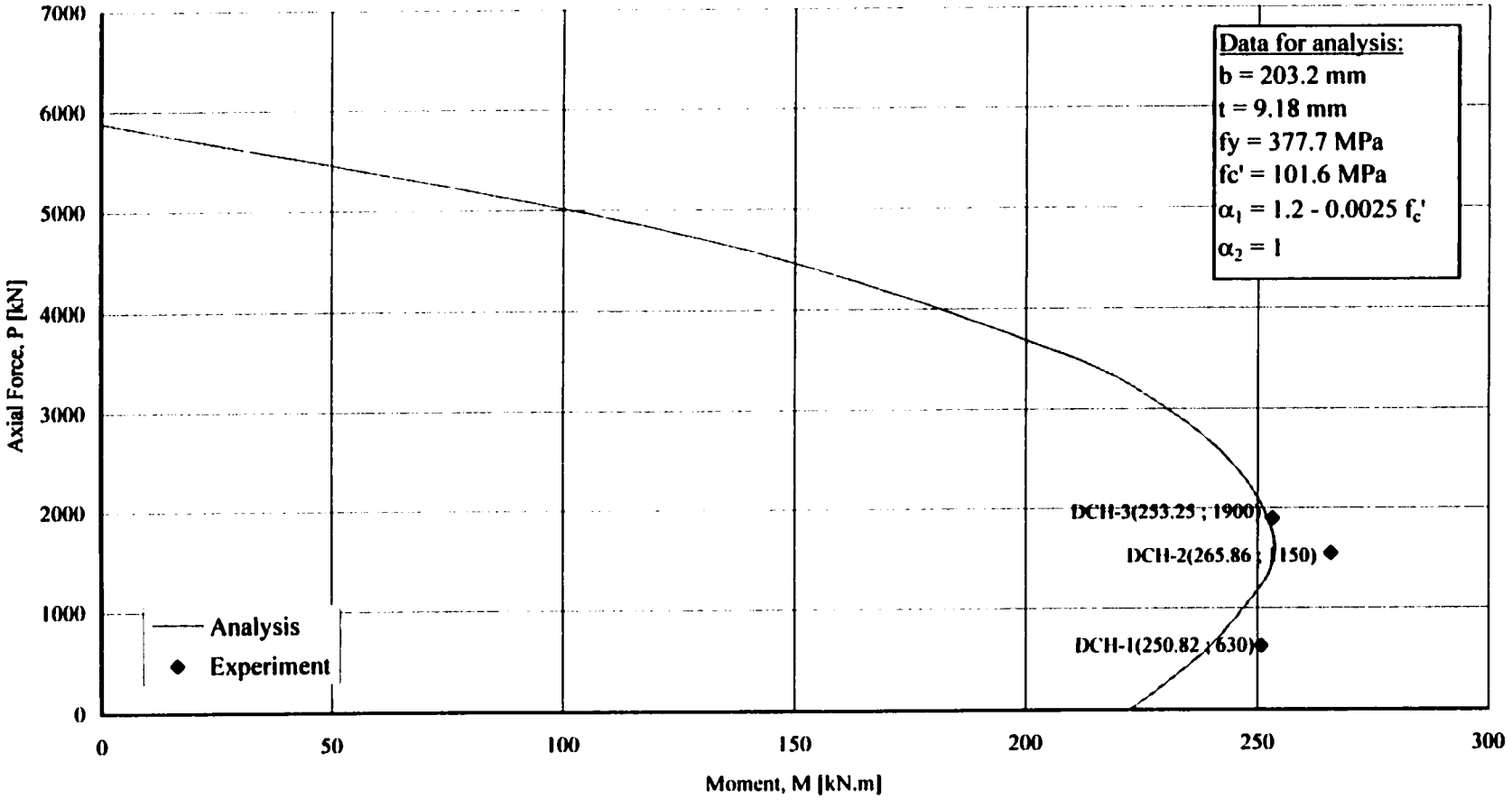

Figure 6.22 Strength Capacity of DCH Columns

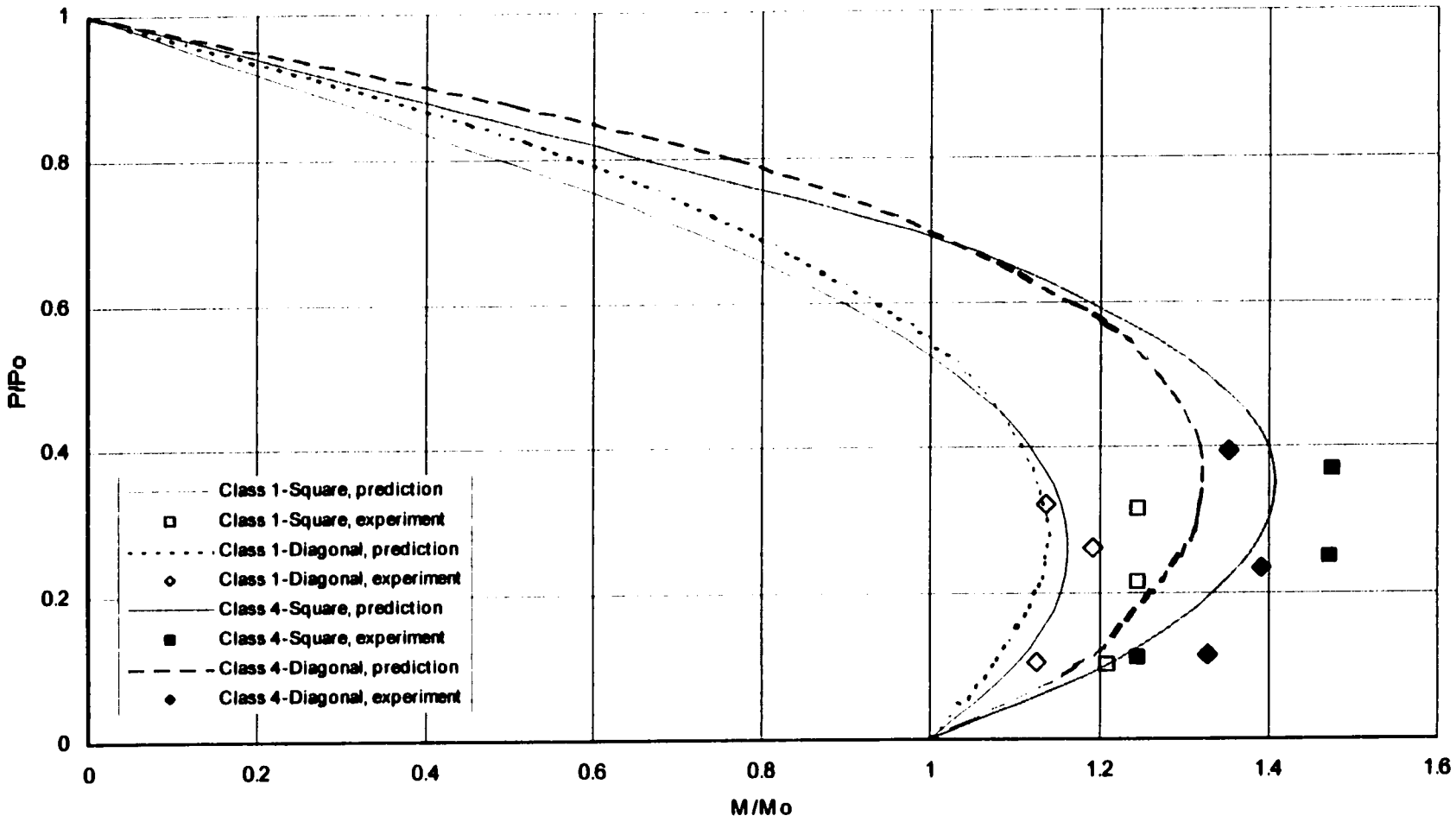

Figure 6.23 Normalized interaction diagram for high strength CFT columns

Chapter 7

SUMMARY AND CONCLUSIONS

7.1 Summary

The benefit of using steel tubes for confining normal strength concrete has been discussed/investigated for years. Experimental studies on the performance of CFT columns have confirmed that the ductility and the strength of normal concretes increase with confinement. However, most of the research does not include combined axial load and cyclic moment behaviour. A review of the literature indicates that, although research on CFT columns, especially on circular CFT columns, has increased dramatically in recent years, information related to the seismic performance of square CFT columns is still limited.

Existing design criteria for composite steel-concrete structures, presented in design standards, codes and provision specifications, are fragmented among several different sources and are incomplete for composite structures including CFT columns. This fact encourages researchers to investigate topics related to performance of these types of structures.

The research program described was designed to investigate the seismic performance of square CFT columns subjected to a combination of axial compressive load and biaxial bending moment. The square CFT columns included normal-strength and high-strength concrete-filled square steel hollow structural section columns with two ratios of tube wall thickness to tube dimension.

The studies included a comprehensive experimental program, which was done by testing twenty-four, concrete filled, square steel hollow structural section column specimens under constant axial compressive load and cyclic horizontal load with horizontal displacement control. This experimental investigation included strength capacity, ductility and flexural stiffness of CFT beam-columns for 203x203x9.5 HSS

(Class 1 compact sections) and 203x203x4.8 (Class 4 slender sections) HSS filled with either normal strength or high strength concrete.

The strength capacity of square HSS CFT columns subjected to constant axial compressive load and biaxial cyclic bending moment was treated using uniaxial approach based on column section analysis. A modified ACI procedure of reinforced concrete column section analysis is proposed for analysis of CFT column strength capacity. The section analysis is based on fully plastic behaviour for both concrete and steel. The concrete stress block is modeled as an equivalent rectangular stress block full depth from the maximum compressive stress to the neutral axis of the section and the unconfined concrete cylinder strength modified by a factor $\alpha_1\alpha_2$. Strength modification factor α_1 accommodates the confinement and seismic loading, fast concrete strain rates, effects on the CFT column sections. Coefficient α_2 is used for softening of the columns caused by large axial load.

Mean values of ratios of experimental to predicted results for normal strength concrete CFT beam columns are 1.041, 1.155, 1.105 and 1.138 for SNL, SCL, DNL and DCL specimens respectively. In addition, the coefficients of variation of these ratios vary from 0.12% to 2.12%, the values of 2.11%, 2.12%, 2.05% and 0.12% for SNL, SCL, DNL, and DCL specimens respectively. Overall, the mean value is 1.110 and the coefficient of variation is 4.39% for normal strength CFT columns. Mean values of ratios of experimental results to predicted results for high strength CFT columns are 1.044, 1.067, 1.082 and 1.031 for the SNH, DNH, SCH and DCH series respectively, and the coefficients of variation of these ratios vary from 1.62% to 4.63%, the values of 2.67%, 4.63%, 1.62% and 2.38% for SNH, DNH, SCH, and DCH specimens respectively. Overall, the mean value is 1.056 and the sample coefficient of variation is 3.25% for high strength CFT columns.

There is currently no consensus among engineers or researchers for defining column ductility. Determination of ductility is sensitive to the definition. Two kinds of ductility are considered in this investigation: displacement ductility and curvature ductility. Yield curvature, Φ_y, and yield displacement, Δ_y, are defined based from the measured first-yield curvature and measured first yield displacement respectively. The displacement ductility μ_Δ of the normal strength CFT column specimens varied from

2.920 to 9.058 and the curvature ductility μ_Φ from 3.356 to 19.814. The displacement ductility μ_Δ of the high strength CFT column specimens varied from 2.42 to 9.95 and the curvature ductility μ_Φ from 3.05 to 18.61. Because the ductility values vary widely, it is easier to use ultimate displacement drifts of columns as an indicator in illustrating the ductility of columns. It is important to recognize that the single discrete value of ductility can be misleading since the calculated ductility is very sensitive to the criterion used to establish the ductility.

Flexural stiffness of square HSS CFT columns was calculated using the ACI flexural stiffness formula with modification to the coefficient of the flexural stiffness contributed by the concrete. The proposed formula uses factors 0.3 and 0.6 for Class 1 and Class 4 HSS CFT columns respectively, instead of using factor 0.2 as used by ACI 318-99. The mean value of the ratio of measured flexural stiffness to calculated flexural stiffness is 1.0275, and the coefficient of variation is 3.23% for normal strength CFT columns and the mean ratio is 1.042, and the coefficient of variation is 5.84% for high strength CFT columns. The proposed formulas are appropriate to predict the flexural stiffness of both normal strength and high strength CFT columns subjected to combined axial compressive load and cyclic biaxial bending moment for seismic events.

7.2 Conclusions

Class 1 (compact) and Class 4 (slender) HSS CFT columns subjected to constant axial load and cyclic shear displacements exhibited excellent hysteresis behaviour using both normal strength concrete and high strength concrete. The drift ratios exceeded 7%. The moment capacities of HSS CFT columns loaded with the plane of bending across the diagonal were only slightly less than those loaded with the plane of bending parallel to the square side. This reduces the need for elaborate procedures to calculate the biaxial moment capacities at orientations between 0 and 45.

Based on the comparisons of the test results and those predicted, the following conclusions may be drawn:

1. No premature failure, local buckling before yielding, was observed for both Class 1 and Class 4 HSS CFT columns with either normal strength or high strength

concrete. This indicates that filling HSS with either normal strength or high strength concrete delays the HSS from premature local buckling.

2. Proposed capacity equations based on the superposition of the strength contribution of the steel tube and concrete core using section analysis provides predictions that agree reasonably well with measured strengths.

3. Axial load can critically affect local buckling of square HSS CFT columns. Large axial loads affect the behaviour of Class 4 HSS CFT columns. Consequently, a coefficient α_2 has been introduced to accommodate softening of the column when subjected to large axial loads. For columns made of Class 4 HSS filled with concrete, either normal strength or high strength, which are critically affected by large axial load, $\alpha_2 = 1 - (2.46/\ln f_c')(P/P_o)$. For Class 1 HSS CFT columns $\alpha_2 = 1$. The weakness of the method of strength analysis proposed by Tomii and Sakino can be treated by this coefficient appropriately.

4. To take account of the high strain rate on the concrete during the experiments the standard concrete cylinder strength should be increased by 10% in the section analyses.

5. Using first yield criteria for yield curvature and yield displacement instead of curvature and displacement at 75% of maximum bending moment is more reasonable.

6. Flexural stiffness of square HSS CFT columns can be predicted using modified ACI flexural stiffness formula, in which the coefficient of concrete flexural stiffness term was adjusted. The proposed coefficients are 0.3 and 0.6 for Class 1 and Class 4 HSS CFT columns respectively.

7. The suggestion that the limit of width-thickness ratio of CFT columns be increased by twice of that for empty tubes is confirmed to the test results.

7.3 Recommendation for Future Work

Class 1 and Class 4 HSS CFT columns have been successfully investigated. From this limited investigation, it is necessary to design further research in the following areas:

1. Investigations of the seismic resistance of Class 2 and Class 3 HSS CFT columns should be conducted to get precise design procedures for these types of CFT columns.

2. The effects of torsion and shear force on the flexural strength of CFT columns should be investigated. Some tests may be necessary.

3. Tests on square CFT columns oriented between 0 to 45 degrees could be conducted.

REFERENCES

Aboutaha, R. S., and Machado, R. I, "Seismic Resistance of Steel-Tubed High –Strength Reinforced-Concrete Columns" Journal of Structural Engineering, ASCE, Vol. 125, No. 5, 1999, pp. 485 – 494.

Aho, M. F., "A Database for Encased and Concrete-Filled Columns," M. S. Thesis, School of Civil and Environmental Engineering, Georgia Institute of Technology, Atlanta, GA, 1996.

Anonymous, "Giant Steel Columns Used in Tokyo," Civil Engineering, ASCE, November 2000, pp.13.

ACI Committee 318, "Building Code Requirements for Structural Concrete (ACI 318-95) and Commentary (ACI 318R-95)," ACI, 1996.

ACI Committee 318, "Building Code Requirements for Structural Concrete (ACI 318M-99) and Commentary (ACI 318RM-99)," ACI, 1999.

ACI Committee 318, "Building Code Requirements for Structural Concrete (ACI 318-99) and Commentary (ACI 318R-99)," ACI, 2000.

ACI Committee 363, "State-of-the-Art Report on High-Strength Concrete," ACI Journal, Proceedings V. 81, No. 4, July-August 1984, pp. 364 – 411.

AIJ, "Structural Calculations of Steel Reinforced Concrete Structures," Architectural Institute of Japan, Tokyo, 1987.

AISC, "Manual of Steel Construction. Load & Resistance Factor Design. Volume I: Structural Members, Specifications & Codes," Second Edition, American Institute of Steel Construction, Inc., USA, 1994.

Bahn, B. Y., and Hsu, C. T. T., "Stress-Strain Behavior of Concrete under Cyclic Loading," ACI Materials Journal, V. 95, No. 2, March-April 1998, pp. 178 – 193.

Basu, A. K., "Computation of Failure Loads of Composite Columns," Proc. I.C.E., 36, Oct. 1967, pp. 305 – 312.

Basu, A. K., and Sommerville, W., "Derivation of Formulae for the Design of Rectangular Composite Columns," Proc. I.C.E., Supp. vol., 1969, pp. 233 – 280.

Beedle, L. S., editor-in-chief, "Stability of Metal Structures: A World View, 2nd ed.," Structural Stability Research Council, Bethlehem, Pa, 1991.

Beutel, J. G., Perera, N., and Thambiratnam, D. P., "Monotonic and Cyclic Behaviour of Composite Beam-Column Connections," Proceedings of the Third International Conference Stessa 2000: Behaviour of Steel Structures in Seismic Areas, Montreal, Canada, 21 – 24 August 2000, Eds. Mazzolani, F. M., and Tremblay, R., A. A. Balkema, 2000, pp.119 – 124.

Bischoff, P. H., and Perry, S. H., "Compressive Behaviour of Concrete at High Strain Rates," Material and Structures, 24, 1991, pp. 425 – 450.

Boehme, J., "Strength of Thin-Walled Circular Steel Tubes Filled with High Strength Concrete," M.A. Sc. Thesis, Department of Civil Engineering, University of Toronto, Toronto, Ontario, 1989.

Bradford, M. A., "Design Strength of Slender Concrete-Filled Rectangular Steel Tubes," ACI Structural Journal, Vol. 93, No. 2, 1995, pp. 229 – 235.

Bradford, M. A., "Design Strength of Slender Concrete-Filled Rectangular Steel Tubes," ACI Structural Journal, Vol. 93, No. 2, March-April 1996, pp. 229 – 235.

Bresler, B., "Design Criteria for R. C. Columns Under Axial Load and Biaxial Bending," ACI Journal, Vol. 57, No. 5, 1960, pp. 481 – 490.

Bridge, R. Q., Ansourian, P., Rotter, J. M., Patrick, M., and Pham, L., "Australian Standard for Composite Construction," Composite Construction in Steel and Concrete, Proceedings of an Engineering Foundation Conferences, New England College, Henniker, New Hampshire, June 7 – 12, 1987, Edited by C. Dale Buckner and Ivan M. Viest, ASCE, 1987, pp. 71 – 83.

Cai, S. H., "Ultimate Strength of Concrete-Filled Tube Columns," Composite Construction in Steel and Concrete, Proceedings of an Engineering Foundation Conferences, New England College, Henniker, New Hampshire, June 7 – 12, 1987, Edited by C. Dale Buckner and Ivan M. Viest, ASCE, 1987, pp. 702 – 727.

Chabot, M., and Lie, T. T., "Experimental Studies on the Fire Resistance of Hollow Steel Columns Filled with Palin Concrete," National Research Council Canada, Internal Report No. 611, 1992.

CISC, "Handbook of Steel Construction," Fourth Edition, Universal Offset Limited, Markham, Ontario, 1985.

CISC, "Handbook of Steel Construction," Seventh Edition, Second Revised Printing, Universal Offset Limited, Alliston, Ontario, 2000.

CSA, "CAN/CSA-S16.1-94: Limit States Design of Steel Structures," CSA, Rexdale, Ontario, 1994.

CSA, "CSA Standard A23.3-94 Design of Concrete Structures," CSA, Rexdale, Ontario, 1994.

Deierlein, G. G., Sheikh, T. M., Yura, J. A., and Jirsa, J. O., "Beam-Column Moment Connections for composite frames: Part 2." Journal of Structural Engineering, ASCE, Vol. 115, No. 11, 1989

Desayi, P., and Krishnan, S., "Equation for the Stress-Strain Curve of Concrete," ACI Journal, Proceedings Vol. 61, No. 3, March 1964, pp. 345 – 350.

Dunberry, E., Leblanc, D., and Redwood, R. G., "Cross-Section Strength of Concrete-Filled HSS Columns at Simple Beam Connections," Can. J. Civ. Eng. Vol. 14, 1987, pp. 408 – 417.

ECS, "Eurocode 4: Design of Composite Steel and Concrete Structures. Part 1.1: General Rules and Rules for Buildings," European Committee for Standardization, Brussels, Belgium, 1994.

Elnashai, A. S., "European Developments in Seismic Resistance of Composite Steel/Concrete Structures," ACI SP-174: Hybrid and Composite Structures, eds. Shahrooz, B.M., and Sabnis, G. M., ACI, 1998, pp. 183 – 196.

El-Tawil, S., and Deierlein, G. G., "Strength and Ductility of Concrete Encased Composite Columns," Journal of Structural Engineering, Vol. 125, No. 9, September 1999, pp. 1009 – 1019.

Furlong, R. W., "Ultimate Strength of Square Columns Under Biaxially Eccentric Loads," Journal of American Concrete Institute, V. 32, No. 9, March 1961, pp. 1129 – 1140.

Furlong, R. W., "Strength of Steel-Encased Concrete Beam Columns," Journal of the Structural Division, Proceeding of the ASCE, Vol. 93, ST 5, October 1967, pp. 113 – 124.

Furlong, R. W., "Design of Steel Encased Concrete Beam-Columns," Proc. ASCE 94, ST1, Jan. 1968, pp. 267 – 281.

Gardner, N. J., and Jacobsen, E. R., "Structural Behaviour of Concrete Filled Steel Tubes," Proc. American Concrete Institute, Vol. 64, No. 11, July, 1967, pp. 404 – 413.

Gardner, N. J., "Use of Spiral Welded Steel Tubes in Pipe Columns," ACI Journal, Vol. 65, No. 11, November 1968, pp. 937 – 942.

Gardner, N. J., "Design of Pipe Columns," Transactions of the Engineering Institute of Canada, Vol. 13, No. 3-A, March 1970.

Gardner, N. J., and Lockman, M. J., " Design Provisions for Drying Shrinkage and Creep of Normal-Strength Concrete," ACI Material Journal, V. 98, No. 2, March-April 2001, pp. 159 – 167.

Galambos, T. V., "Guide to Stability Design Criteria for Metal Structures," Fifth Edition, John Wiley & Sons, Inc., New York, 1998.

Ghost, S. K., and Saatcioglu, M., "Ductility and Seismic Behaviour," in High Performance Concrete: Properties and Applications, Edited by S.P. Shah and S. H. Ahmad, McGraw-Hill, Inc, Great Britain, 1994, pp. 237 – 312.

Goel, S. C., "U.S. – Japan Cooperative Research Program on Composite and Hybrid Structures," ACI SP-174: Hybrid and Composite Structures, eds. Shahrooz, B.M., and Sabnis, G. M., ACI, 1998, pp. 213 – 224.

Graham, W. W., "Seismic Testing and Analysis of Full-Scale CFT to WF Beam Moment Welded and Bolted Connections," M. S. Thesis, Department of Civil and Environmental Engineering, Lehigh University, Bethlehem, PA, 1996.

Griffis, L. G., "Some Design Considerations for Composite-Frame Structures," AISC Engineering Journal, Vol. 23, No. 2, 1986, pp. 59 – 64.

Hamburger, R. O., "A Policy Guide to Steel Moment-Frame Construction," SAC Joint Venture, November 2000, 27 pp.

Hognestad, E., "A Study of Combined Bending and Axial Load in Reinforced Concrete Members," Bulletin No. 399, Engineering Experiment Station, University of Illinois, Urbana, November 1951, 128 pp.

Hsu, C. T. T., "Analysis and Design of Square and Rectangular Columns by Equation of Failure Surface," ACI Structural Journal, March-April 1988, pp. 167 – 179.

Ibrahim, H. H. H., and MacGregor, J. G., "Modification of the ACI Rectangular Stress Block for High-Strength Concrete," ACI Structural Journal, V. 94, No. 1, January-February 1997, pp. 40 – 48.

Johnson, R. P., "Composite Structures of Steel and Concrete. Vol. 1: Beams, Columns, Frames and Applications in Building," Constructional Steel Research and Development Organization, London, 1975.

Johnson, R. P., and Buckby, R. J., "Composite Structures of Steel and Concrete. Vol. 2: Bridges, with Commentary on BS 5400: Part 5," Constructional Steel Research and Development Organization, Granada Publishing Limited, London, 1979.

Johnson, R. P., and Anderson, D., "Designers' Handbook to Eurocode 4. Part 1.1: Design of Composite Steel and Concrete Structures," Thomas Telford, London, 1993.

Kanatani, H., Tabuchi, M., Kamba, T., Hsiaolien, J., and Ishikawa, M., "A Study on Concrete Filled RHS Column to H-Beam Connections Fabricated with HT Bolts in Rigid Frames," Composite Construction in Steel and Concrete – Proceedings of an Engineering Foundation Conference, New Hampshire, Eds. Buckner, C. D., and Viest, I. M., ASCE, 1987, pp. 614 – 635.

Kato, B., "Beam-to-Column Connection Research in Japan," Journal of Structural Enginnering, ASCE, Vol. 108, No. ST2, 1982.

Kato, B., "Compressive Strength and Deformation Capacity of Concrete-Filled Tubular Stub-Columns," J. Struct. Eng. AIJ, No. 468, Feb., 1995, pp. 183 – 191.

Kilpatrick, A. E., "The Behaviour of High-Strength Composite Concrete Columns," Ph.D. Thesis, School of Civil Engineering, Curtin University of Technology, September 1996, 317 pp.

Kilpatrick, A. E., and Rangan, B. V., "Tests on High-Strength Concrete-Filled Steel Tubular Columns," ACI Structural Journal, V. 96, No. 2, March-April 1999, pp. 268 – 274.

Knowles, R. B., and Park, R., "Strength Capacity of Concrete Filled Steel Tubular Columns," Journal of Structural Division, Proc. Of ASCE, Vol. 95, No. ST12, December 1969, pp. 2565 – 2587.

Knowles, R. B., and Park, R., "Axial Load Design for Concrete Filled Steel Tubes," Journal of Structural Division, Proc. Of ASCE, Vol. 96, No. ST10, OCTOBER 1970, pp. 2125 – 2153.

Lachance, L., "Ultimate Strength of Biaxially Loaded Composite Sections," Journal of the Structural Division, Proceedings of ASCE, ASCE, Vol. 108, No. ST10, October, 1982, pp. 2313 – 2329.

Lachance, L. and Hays, C. O., "Accuracy of Composite Section Nonlinear Solutions," Journal of the Structural Division, Proceedings of ASCE, ASCE, Vol. 106, No. ST11, November, 1980, pp. 2203 – 2219.

Lu, Y. Q., and Kennedy, D. J. L., "The Flexural Behaviour of Concrete-Filled Hollow Structural Sections," Structural Engineering Report 178, Department of Civil Engineering, University of Alberta, Edmonton, Alta, 1992.

Lu, Y. Q., and Kennedy, D. J. L., "The Flexural Behaviour of Concrete-Filled Hollow Structural Sections," Canadian Journal of Civil Engineering, Vol. 21, 1994, pp. 111 – 130.

Mander, J. B., Priestly, M. J. N., and Park, R., "Theoretical Stress-Strain Models for Confined Concrete," ASCE Structural Journal, V. 114, No. 8, Aug. 1988, pp. 1804 – 1825.

Martinez, S., Nilson, A. H., and Slate, F. O., "Spirally Reinforced High-Strength Concrete Columns," Research Report No. 82-10, Department of Structural Engineering, Cornell University, Ithaca, Aug. 1982.

Matsui, C., and Tsuda, K., "Strength and Behaviour of Concrete-Filled Steel Square Tubular Columns with Large Width-Thickness Ratio," Proceedings of Pacific Conference on Earthquake Engineering, Waikarei, New Zealand, 5-8 August 1987, pp. 1 – 9.

Morino, S., Uchida, Y., and Ozaki, M., "Experimental Study of SRC Beam-Columns Subjected to Biaxial Bending," Composite Construction in Steel and Concrete, Proceedings of an Engineering Foundation Conferences, New England College, Henniker, New Hampshire, June 7 – 12, 1987, Edited by C. Dale Buckner and Ivan M. Viest, ASCE, 1987, pp. 753 – 772.

Munoz, P. R., and Hsu, C. T. T, "Behavior of Biaxially Loaded Concrete-Encased Composite Columns," Journal of Structural Engineering, Vol. 123, No 9, September 1997, pp. 1163 – 1171.

NEHRP, "Composite Steel and Concrete Structure Design Requirements," in NEHRP Recommended Provisions for Seismic Regulations for New Buildings, FEMA 222/223, Federal Engineering Management Agency, Washington, DC, 1997, Chapter 7.

Neogi, P. K., Sen, H. K., and Chapman, J. C., "Concrete-Filled Tubular Steel Columns under Eccentric Loading," Structural Engineering, Vol. 47, No. 5, May 1969, pp. 187 – 195.

Nethercot, D. A., "General Report: Composite Members," International Conference on Stability of Steel Structures, September 21 – 23, 1995, Budapest, Hungary, in Further Direction in Stability Research and Design, Vol. 2, edited by M. Ivanyi, Budapest, 1995, pp. 813 – 825.

Nilson, A. H., "Structural Members," in High Performance Concrete: Properties and Applications, Edited by S.P. Shah and S. H. Ahmad, McGraw-Hill, Inc, 1994, pp. 213 – 236.

NZS, "Code of Practice for General Structural Design and Design Loadings for Buildings (NZS 4203)," New Zealand Standard, Standards Association of New Zealand, 1984.

Park, R., Priestley, M. J. N., and Gill, W. D., "Ductility of Square-Confined Concrete Columns," Journal of the Structural Division, Proceedings of ASCE, Vol. 108, No. ST4, April 1982, pp. 929 – 950.

Paulay, T. and Priestley, M. J. N., "Seismic Design of Reinforced Concrete and Masonry Buildings," John Wiley & Sons, Inc., USA, 1992.

Perenchio, W. F., and Klieger, P., "Some Physical Properties of High Strength Concrete," Research and Development Bulletin, No. RD056.01T, Portland Cement Association, Skokie, 1978, 7pp.

Pillai, U. S., "Beam Columns of Hollow Sections," J. Can. Soc. Civ. Eng., Vol. 1, 1974.

Pinkham, C., "1986 AISC LRFD – Design for Composite Buildings," Composite Construction in Steel and Concrete, Proceedings of an Engineering Foundation Conferences, New England College, Henniker, New Hampshire, June 7 – 12, 1987, Edited by C. Dale Buckner and Ivan M. Viest, ASCE, 1987, pp. 84 – 93.

Prion, H. G. L., and Boehme, J., "Beam-Column Behaviour of Steel Tubes Filled with High Strength Concrete," Can. J. Civ. Eng. Vol. 21, 1994, pp. 207 – 218.

Rangan, B. V., and Joyce, M., "Strength of Eccentrically Loaded Slender Steel Tubular Columns Filled with High-Strength Concrete," ACI Structural Journal, V. 89, N0. 6, November-December 1992, pp. 676 – 681.

Ricles, J. M., and Paboojian, S. D., "Seismic Performance of Steel-Encased Composite Columns," Journal of Structural Engineering, Vol. 120, No. 8, August, 1994, pp. 2474 – 2494.

Ricles, J. M., Lu, L. W., and Sooi, T. K., "Behaviour of CFT Column-WF Beam Moment Connections Under Seismic Loading," ACI SP-174: Hybrid and Composite Structures, eds. Shahrooz, B.M., and Sabnis, G. M., ACI, 1998, pp. 1 – 36.

Row, D. G., and Paulay, T., "Biaxial Flexure and Axial Load Interaction in Short Rectangular Reinforced Concrete Columns," Bulletin of the N. Z. Society for Earthquake Engineering, Vol. 6, No. 3, September 1973, pp. 110 – 121.

Ruoquan, H., "Behaviour of Long Concrete Filled Steel Columns," Composite Construction in Steel and Concrete, Proceedings of an Engineering Foundation Conferences, New England College, Henniker, New Hampshire, June 7 – 12, 1987, Edited by C. Dale Buckner and Ivan M. Viest, ASCE, 1987, pp. 728 – 737.

Saatcioglu, M., and Razvi, S. R., "Strength and Ductility of Confined Concrete," Journal of Structural Engineering, Vol. 118, No. 6, June, 1992, pp. 1590 – 1607.

Saatcioglu, M., and Razvi, S. R., "High-Strength Concrete Columns with Square Sections under Concentric Compression," Journal of Structural Engineering, Vol. 124, No. 12, December, 1998, pp. 1438 – 1447.

Saenz, L. P., Discussion of a paper by P. Desayi and S. Krishnan, "Equation for the Stress-Strain Curve of Concrete," ACI Journal, Proceedings Vol. 61, No. 9, September 1964, pp. 1229 - 1235.

Sargin, M., "Stress-Strain Relationship for Concrete and the Analysis of Structural Concrete Sections," Study No.4, Solid Mechanics Division, University of Waterloo, Ed. by M. Z. Cohn, University of Waterloo, 1971.

Sen, H. K., "Triaxial Effects in Concrete-Filled Tubular Steel Columns," Ph.D. Thesis, University of London, July 1969.

Shams, M., and Saadeghvaziri, M. A., "State of the Art of Concrete-Filled Steel Tubular Columns," ACI Structural Journal, V. 94, No. 5, September-October 1997, pp. 558 –571.

Sheikh, S. A., and Uzumeri, S. M., "Analytical Model for Concrete Confinement in Tied Columns," ASCE Structural Journal, V. 108, No. 12, Dec. 1982, pp. 2703 – 2722.

Sheikh, T. M., Deierlein, G. G., Yura, J. A., and Jirsa, J. O., "Beam-Column Moment Connections for composite frames: Part 1." Journal of Structural Engineering, ASCE, Vol. 115, No. 11, 1989, pp. 2858 – 2876.

Stark, J. W. B., "Eurocode 4: European Code for Composite Construction," Composite Construction in Steel and Concrete, Proceedings of an Engineering Foundation Conferences, New England College, Henniker, New Hampshire, June 7 – 12, 1987, Edited by C. Dale Buckner and Ivan M. Viest, ASCE, 1987, pp. 37 – 49.

Tebedge, N., and Chen, W. F., "Design Criteria for Steel H-Columns under Biaxial Loading," ASCE J. Struct. Div., Vol. 100, No. ST3, 1974, pp. 579 – 598.

Thoman, W. H., and Raeder, W., "Ultimate Strength and Modulus of Elasticity of High Strength Portland Cement Concrete," ACI Journal, Proceedings, V. 30, No. 3, Jan-Feb. 1934, pp. 231 – 238.

Tide, R. H. R., "A Technical Note: Derivation of the LRFD Column Design Equations," AISC Engineering Journal, Third Quarter, 2001, pp. 137 – 139.

Tomii, M., Yoshimura, K., and Morishita, Y., "Experimental Studies on Concrete-Filled Steel Tubular Stub-Columns under Concentric Loading," Proceedings of the

International Colloquium on the Stability of Structures under Static and Dynamic Loads, ASCE, Washington DC, May 1977, pp. 718 – 741.

Tomii, M., and Sakino, K., "Experimental Studies on the Ultimate Moment of Concrete Filled Square Steel Tubular Beam-Columns," Trans. of A.I.J., No. 275, Jan. 1979, pp. 55 – 68.

Tong, Z. S., and Yu, M. R., "Stress-Strain Relationship and Strength of Concrete Filled Tubes," Composite Construction in Steel and Concrete, Proceedings of an Engineering Foundation Conferences, New England College, Henniker, New Hampshire, June 7 – 12, 1987, Edited by C. Dale Buckner and Ivan M. Viest, ASCE, 1987, pp. 773 –785.

Vermaas, G. W., Ricles, J. M., and Lu, L. W., "Seismic Performance of Full-Scale Concrete Filled Steel Tube to Wide Flange Beam Moment Connections with Diaphragms," ATLSS Engineering Center Research Report, Lehigh University, Bethlehem, PA, 1996.

Virdi, K. S., and Dowling, P. J., "The Ultimate Strength of Composite Columns in Biaxial Bending," Proceedings of the Institution of Civil Engineers, Part 2, Vol. 55, March 1973, pp. 251 – 272.

Wakabayashi, M., "Japanese Standards for the Design of Composite Buildings," Composite Construction in Steel and Concrete, Proceedings of an Engineering Foundation Conferences, New England College, Henniker, New Hampshire, June 7 – 12, 1987, Edited by C. Dale Buckner and Ivan M. Viest, ASCE, 1987, pp. 53 – 69.

Wakabayashi, M., "Standards for the Design of Concrete Encased-Steel and Concrete-Filled Tubular Structures in Japan," Proceedings of the U.S.A.-Japan Seminar on Composite Structures and Mixed Structural Systems, Tokyo, Japan, 1978, pp. 69 – 84.

Yamanouchi, H., Nishiyama, I., and Kobayashi, J., "Development and Usage of Composite and Hybrid Building Structure in Japan," ACI SP-174: Hybrid and Composite Structures, eds. Shahrooz, B.M., and Sabnis, G. M., ACI, 1998, pp. 151 – 173.

Zhang, W., and Shahrooz, B. M., "Strength of Short and Long Concrete-Filled Tubular Columns," ACI Structural Journal, V. 96, No. 2, March-April 1999.

APPENDIX

1. **Transverse strain vs longitudinal strain of column specimens**
2. **Deflected shape of column specimens**

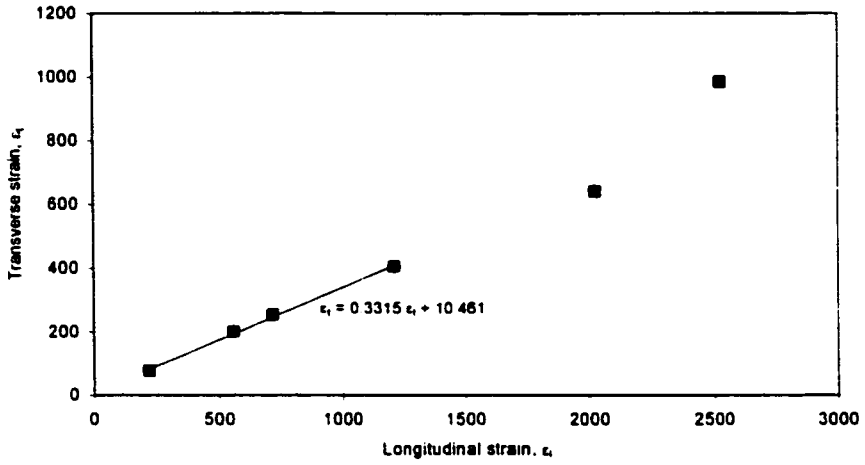

a. DNL – 1

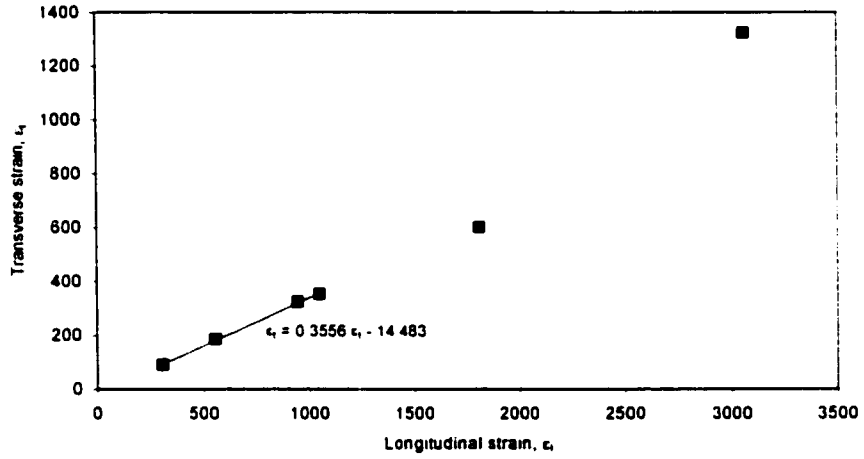

b. DNL – 2

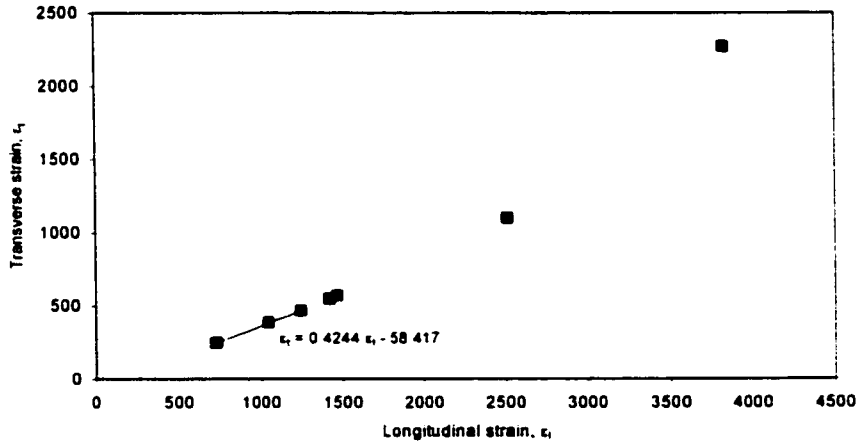

c. DNL – 3

Figure A.1 Transverse strain vs Longitudinal strain of DNL column specimens

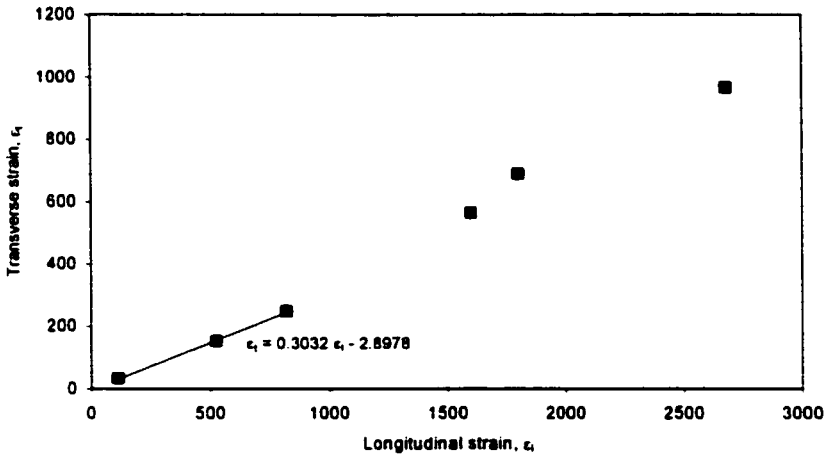

a. SNL – 1

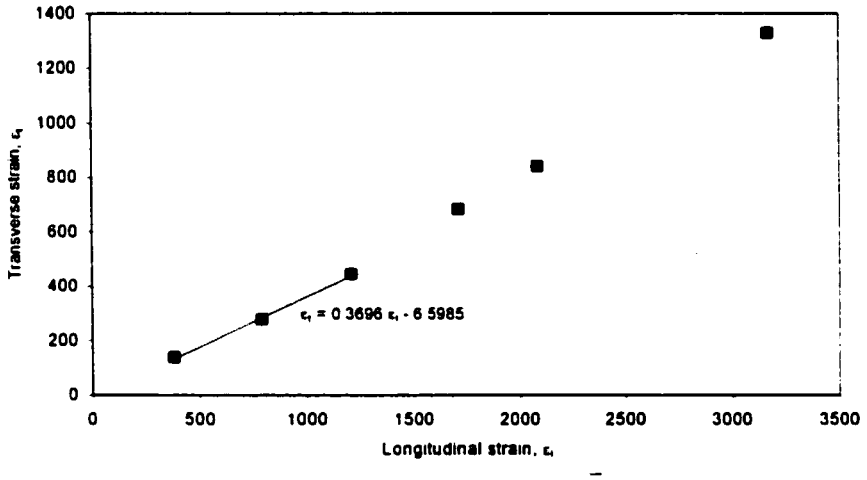

b. SNL – 2

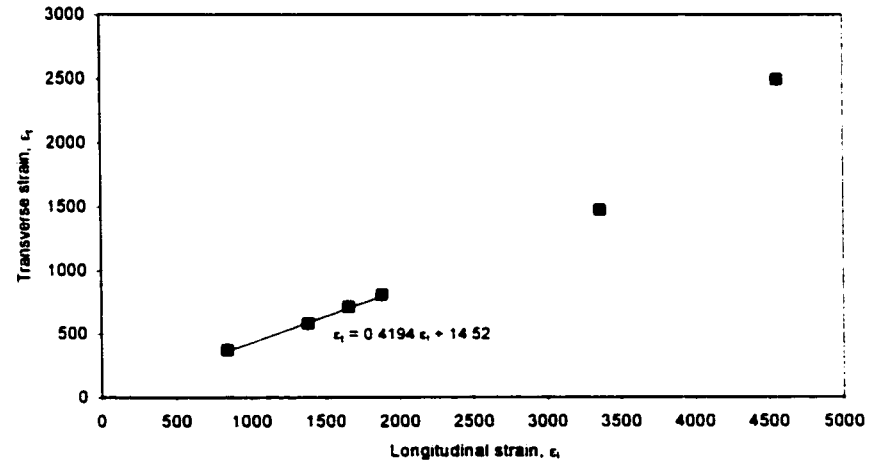

c. SNL – 3

Figure A.2 Transverse strain vs Longitudinal strain of SNL column specimens

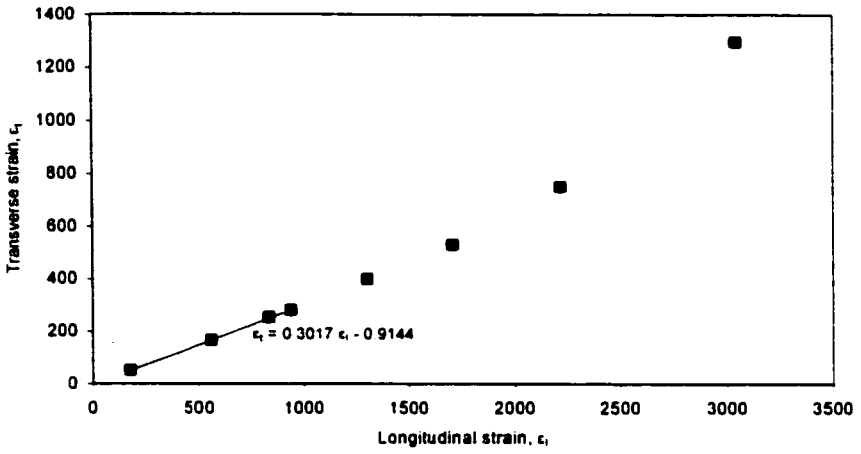

a. DCL –1

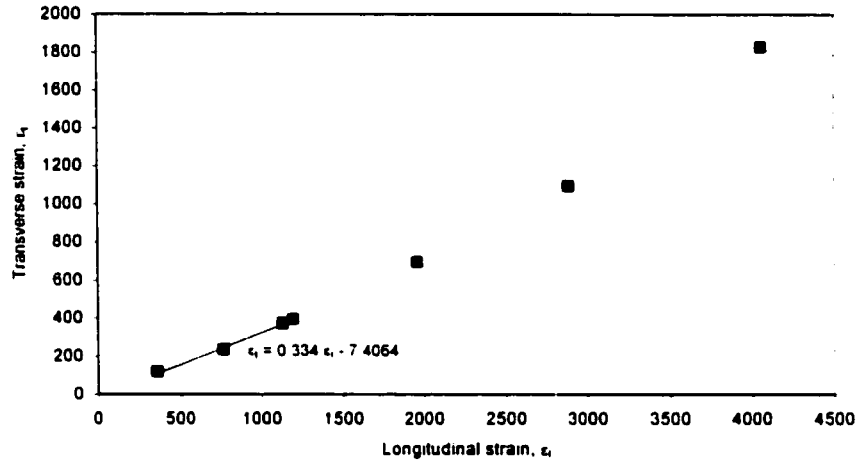

b. DCL – 2

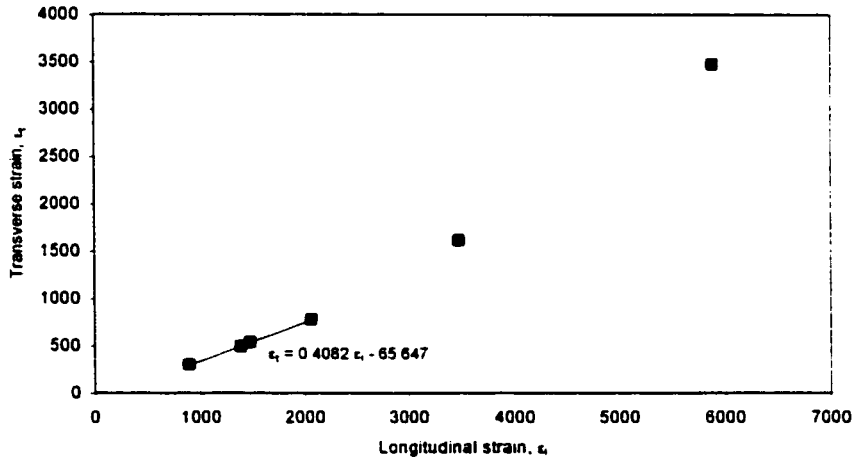

c. DCL – 3

Figure A.3 Transverse strain vs Longitudinal strain of DCL column specimens

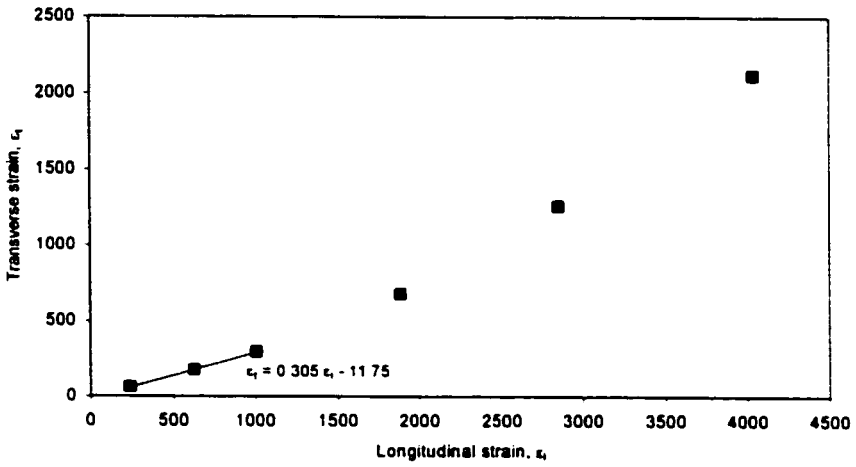

a. SCL – 1

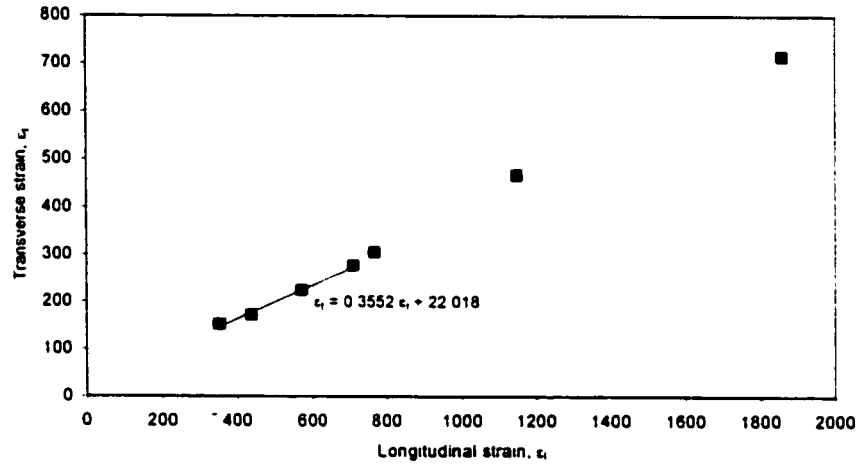

b. SCL – 2

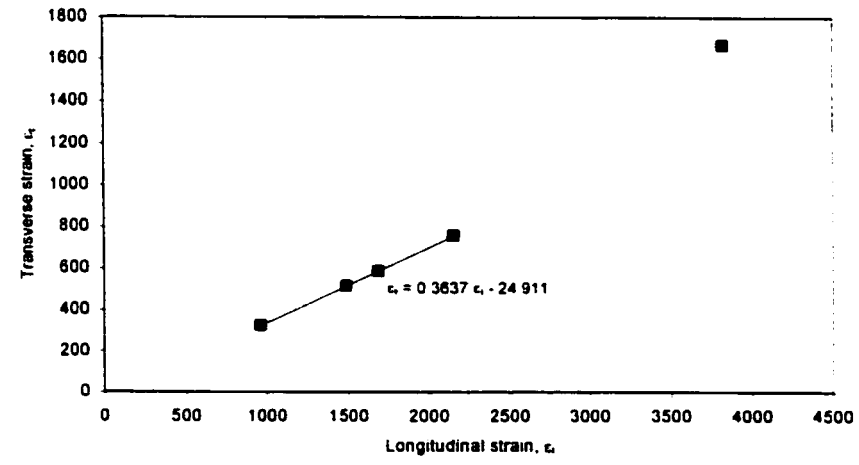

a. SCL – 3

Figure A.4 Transverse strain vs Longitudinal strain of SCL column specimens

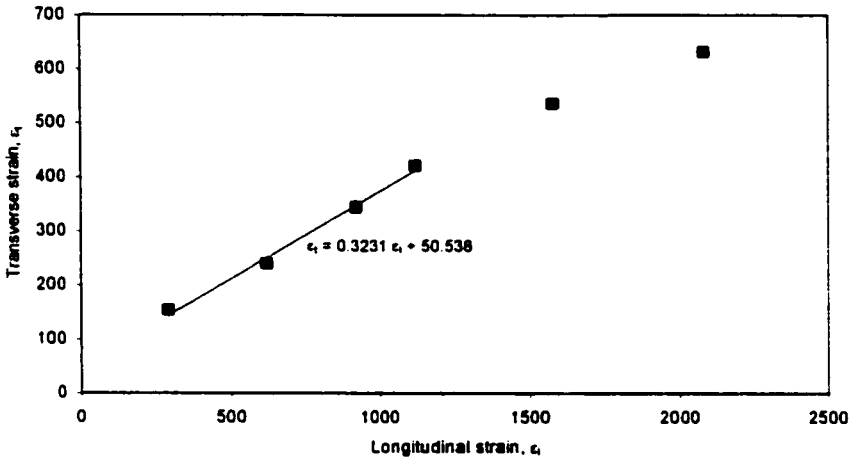

DNH – 1

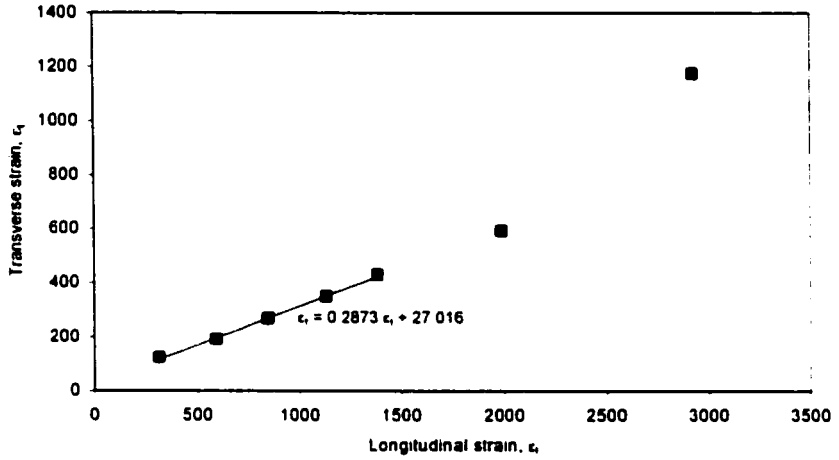

a. DNH – 2

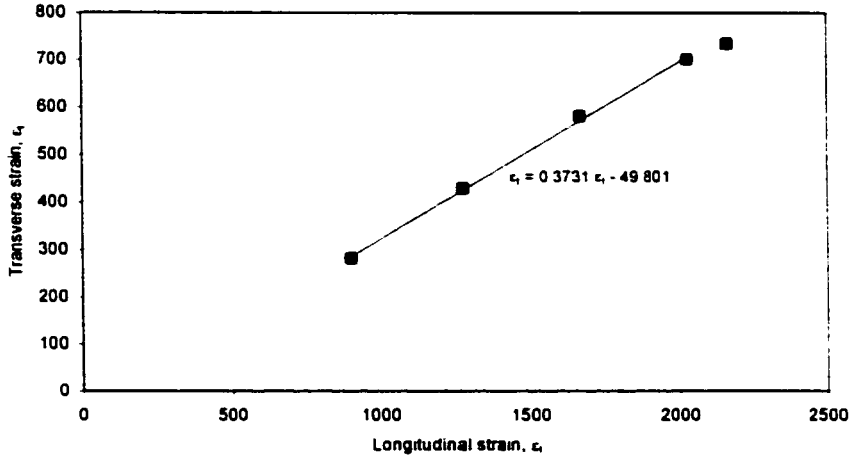

b. DNH – 3

Figure A.5 Transverse strain vs Longitudinal strain of DNH column specimens

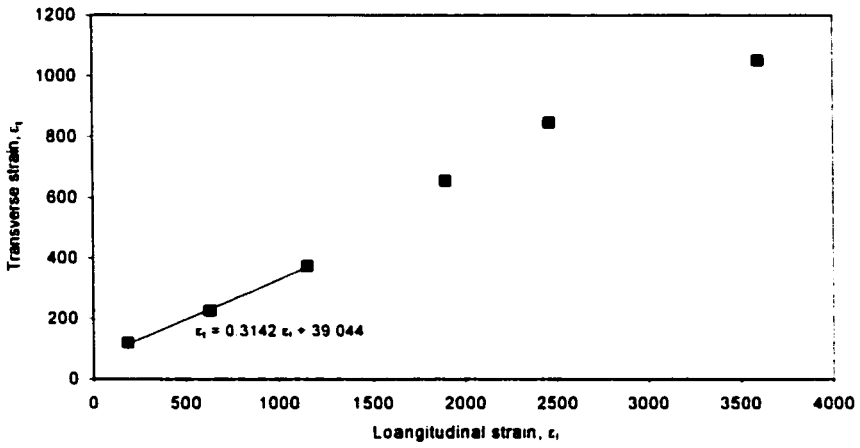

a. SNH – 1

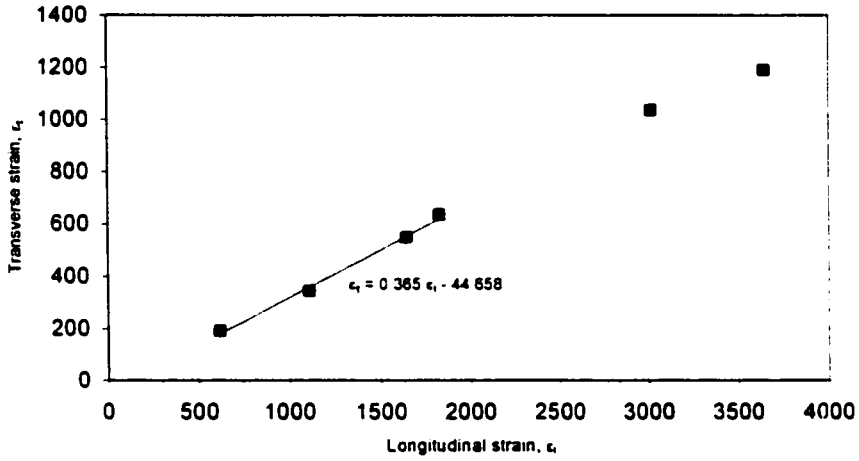

b. SNH – 2

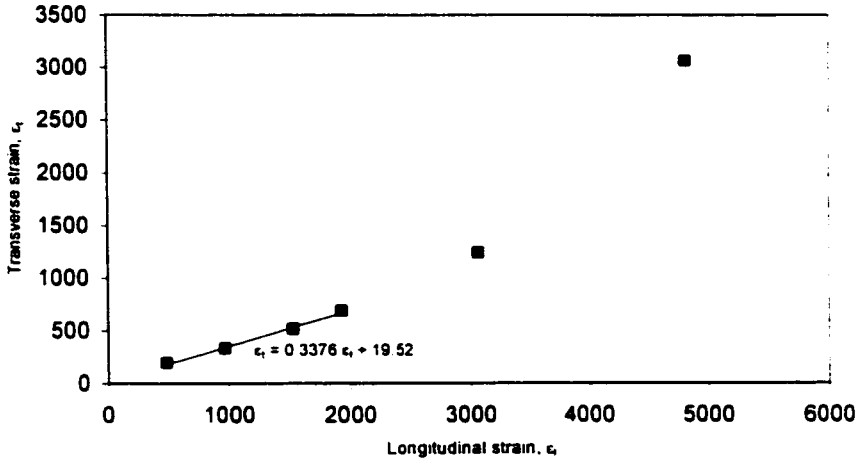

c. SNH – 3

Figure A.6 Transverse strain vs Longitudinal strain of SNH column specimens

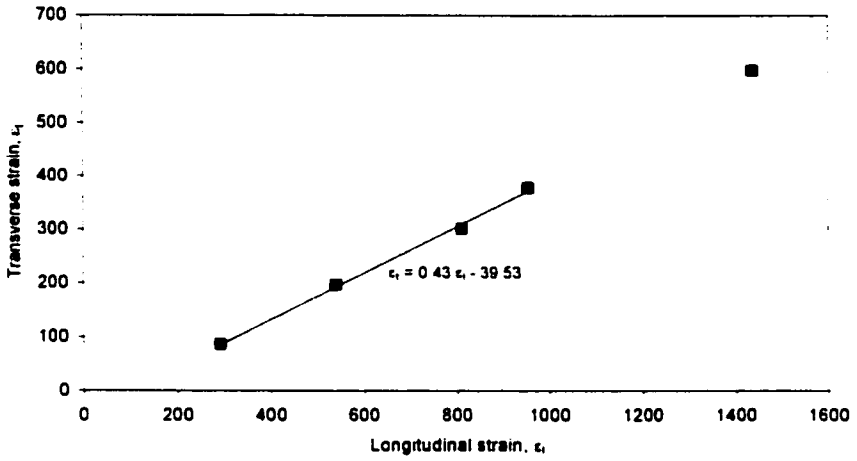

a. DCH – 1

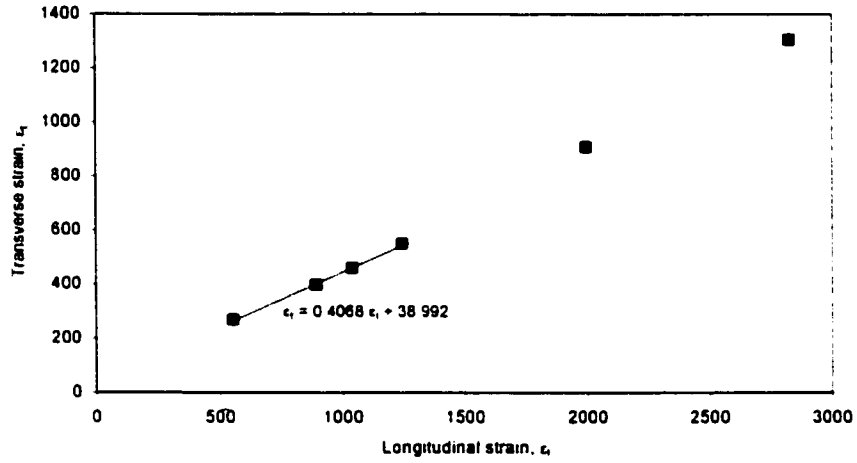

b. DCH – 2

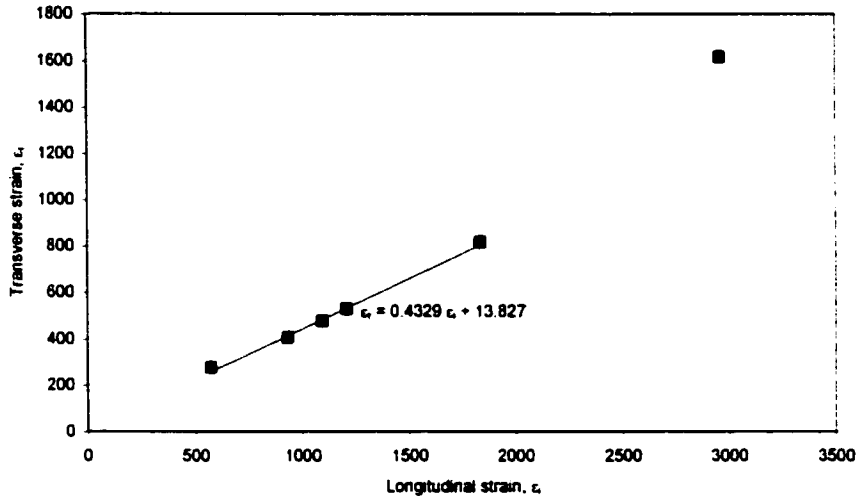

c. DCH – 3

Figure A.7 Transverse strain vs Longitudinal strain of DCH column specimens

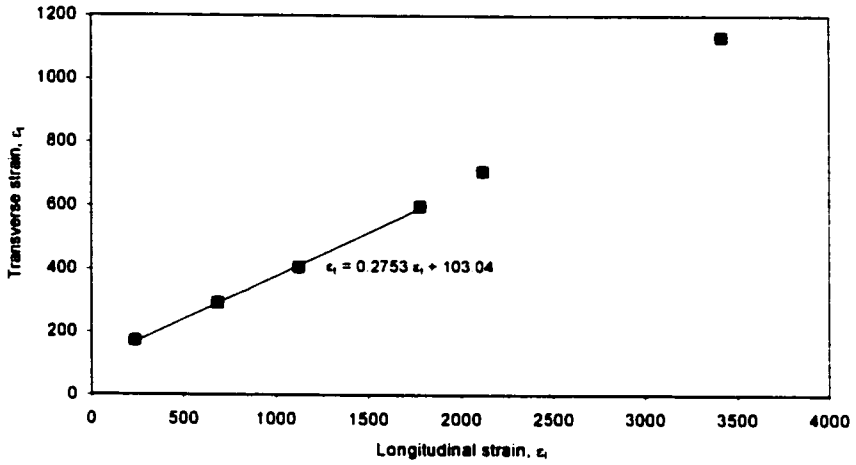

a. SCH – 1

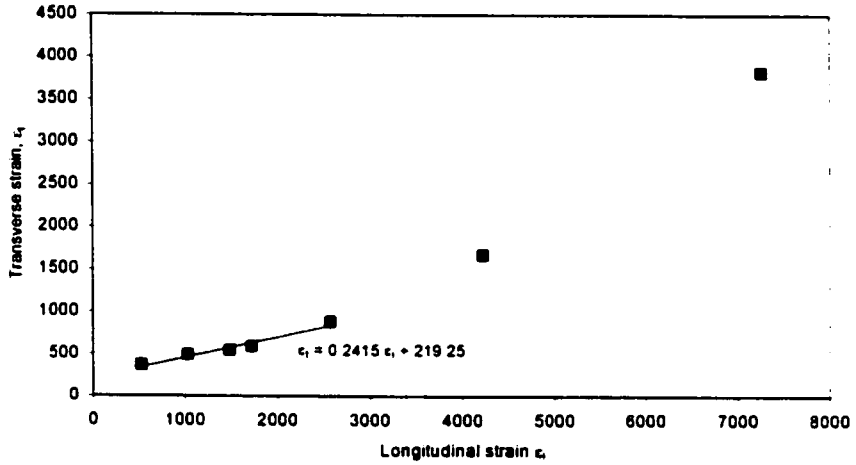

b. SCH – 2

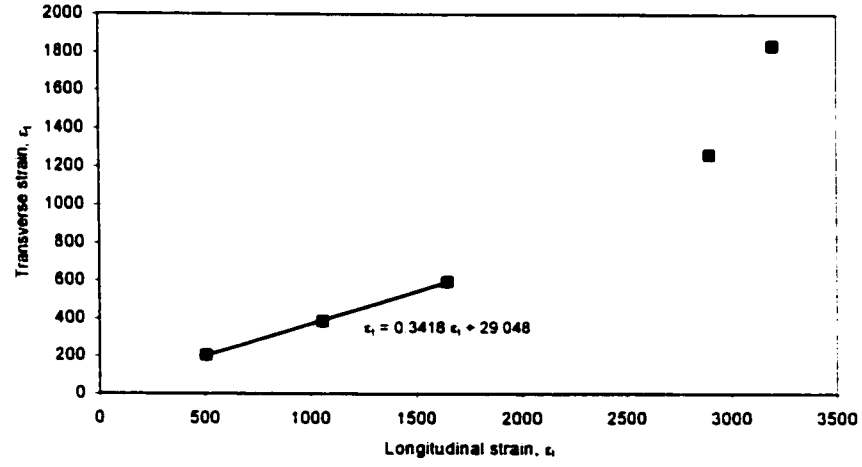

c. SCH – 3

Figure A.8 Transverse strain vs Longitudinal strain of SCH column specimens

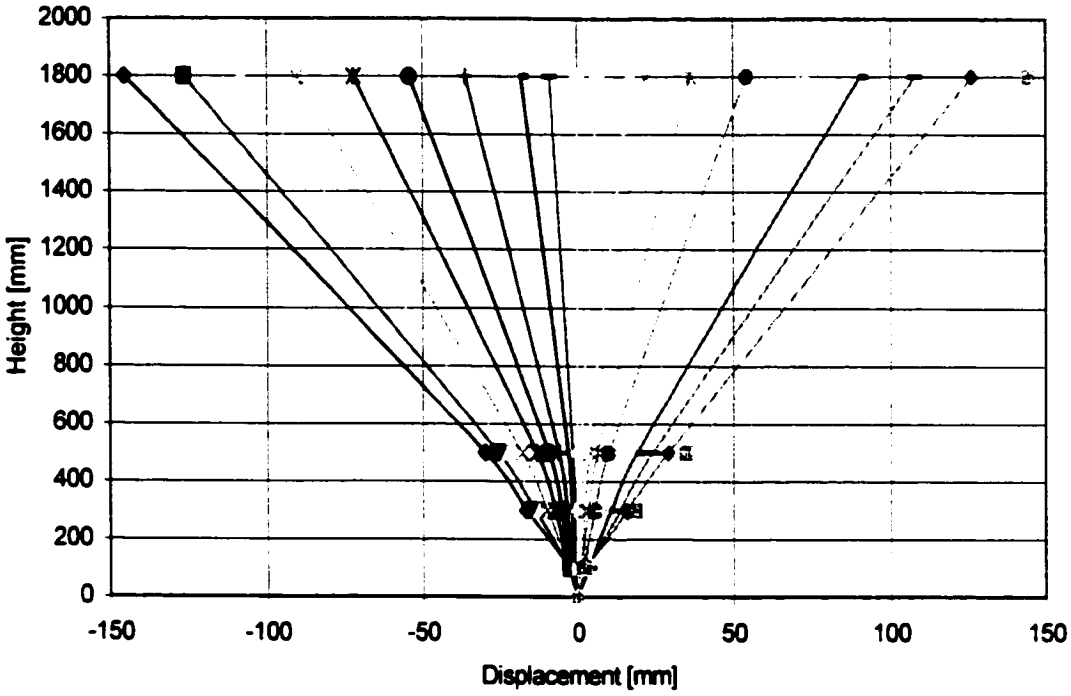

Figure A.9 Deflected shape of column DNL-1

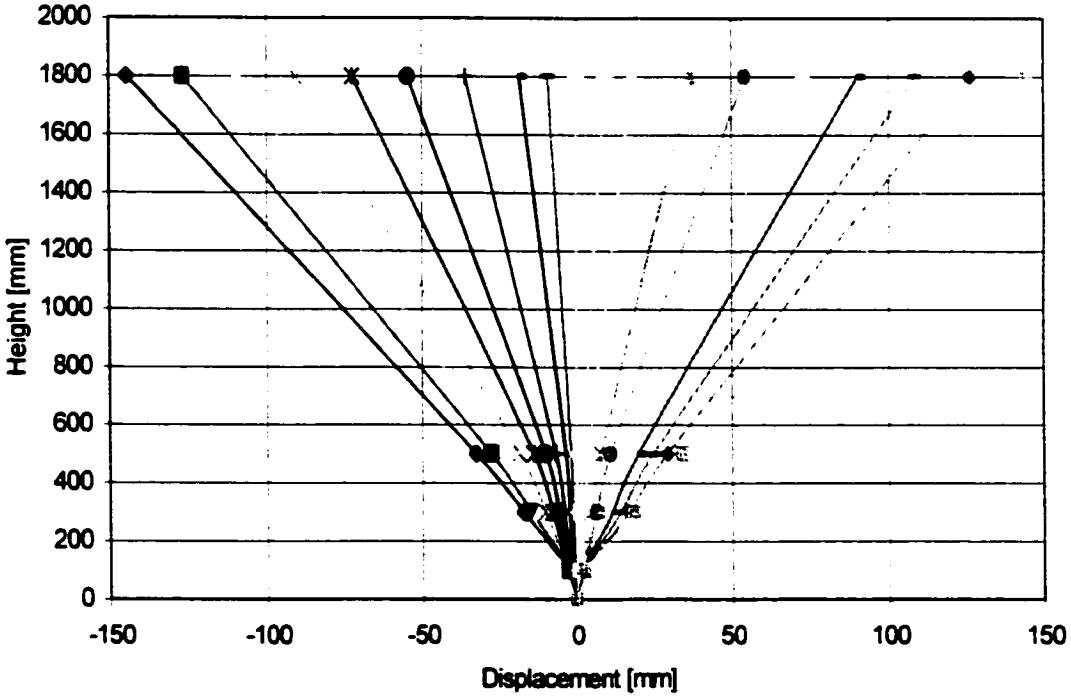

Figure A.10 Deflected shape of column SNL-1

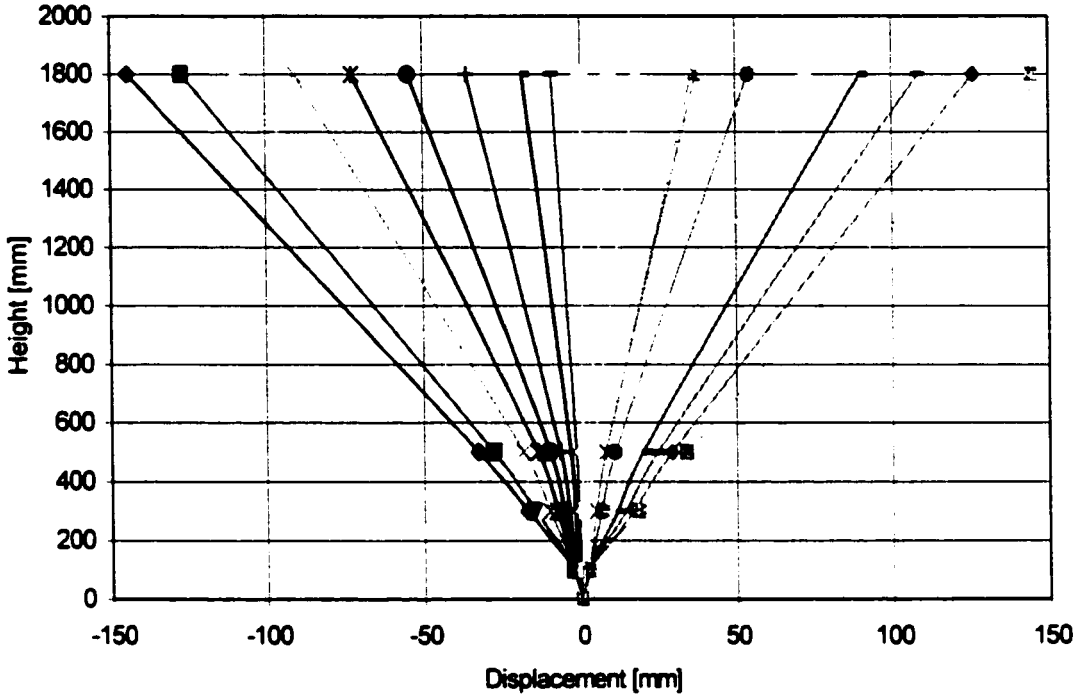

Figure A.11 Deflected shape of column DCL-2

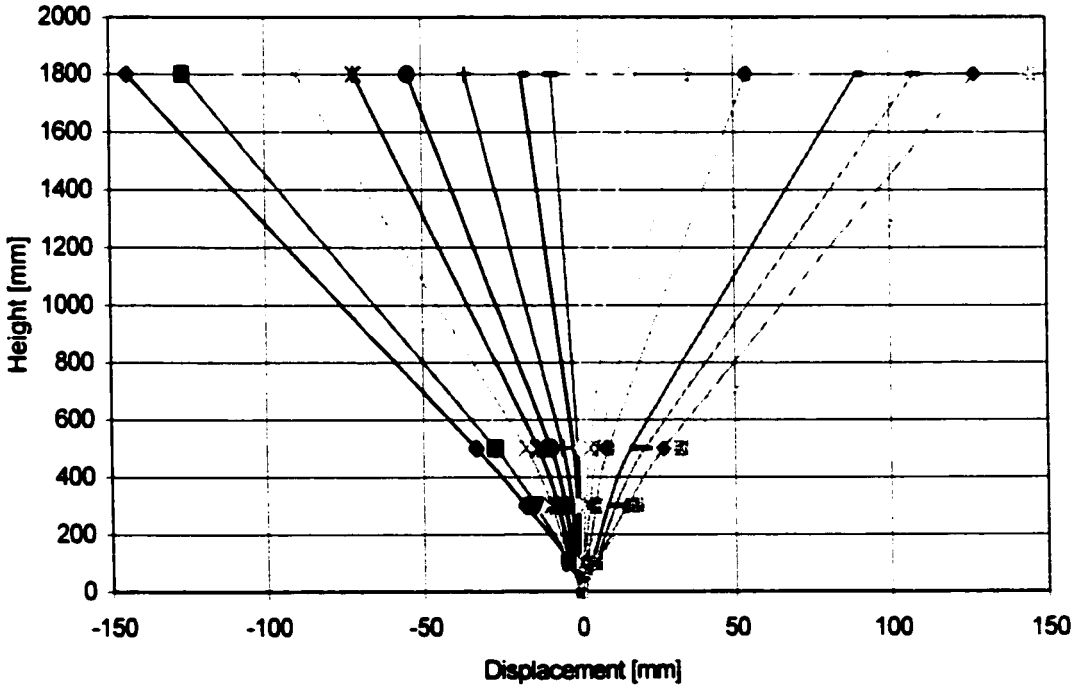

Figure A.12 Deflected shape of column SCL-2

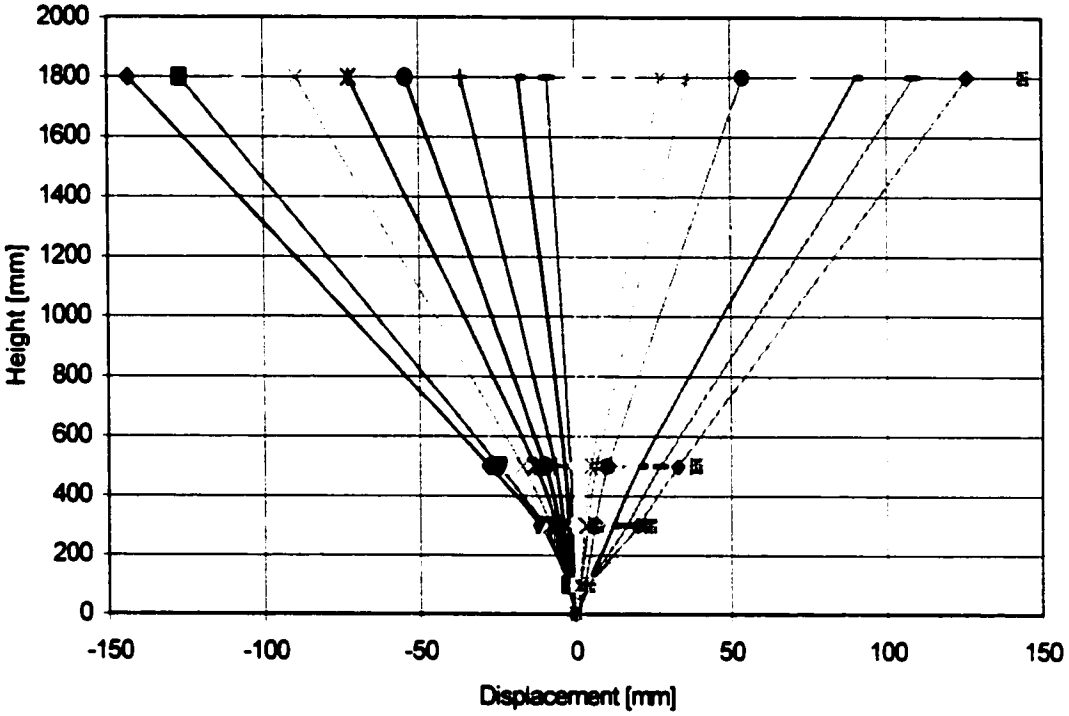

Figure A.13 Deflected shape of column DNH-2

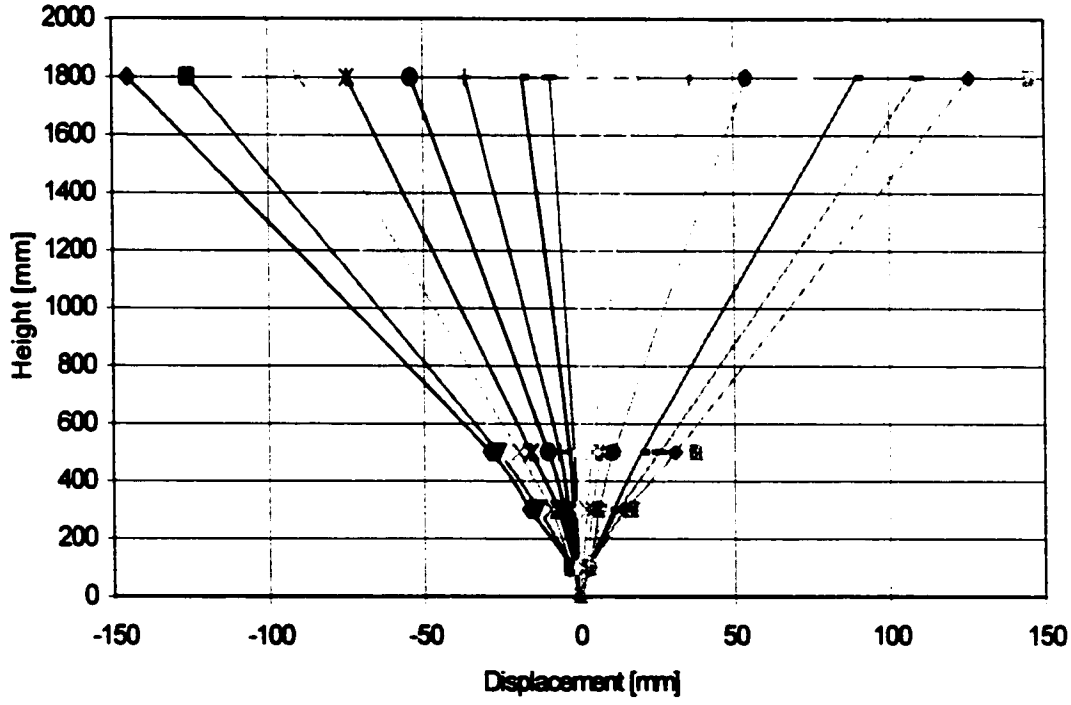

Figure A.14 Deflected shape of column SNH-2

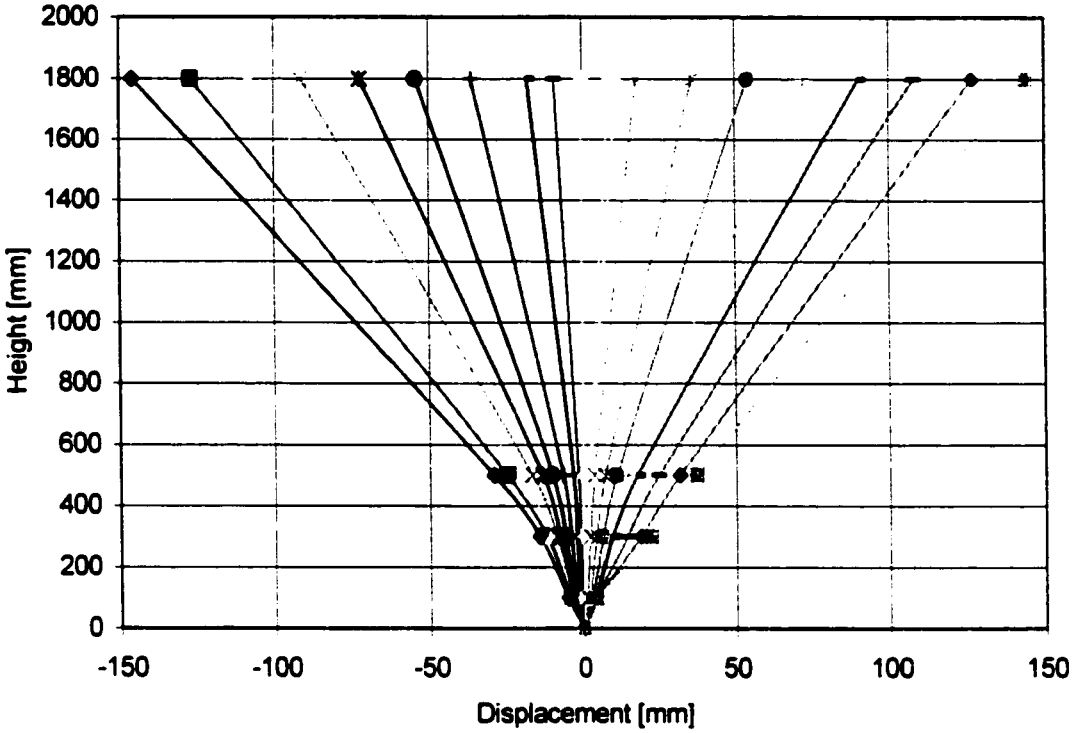

Figure A.15 Deflected shape of column DCH-2

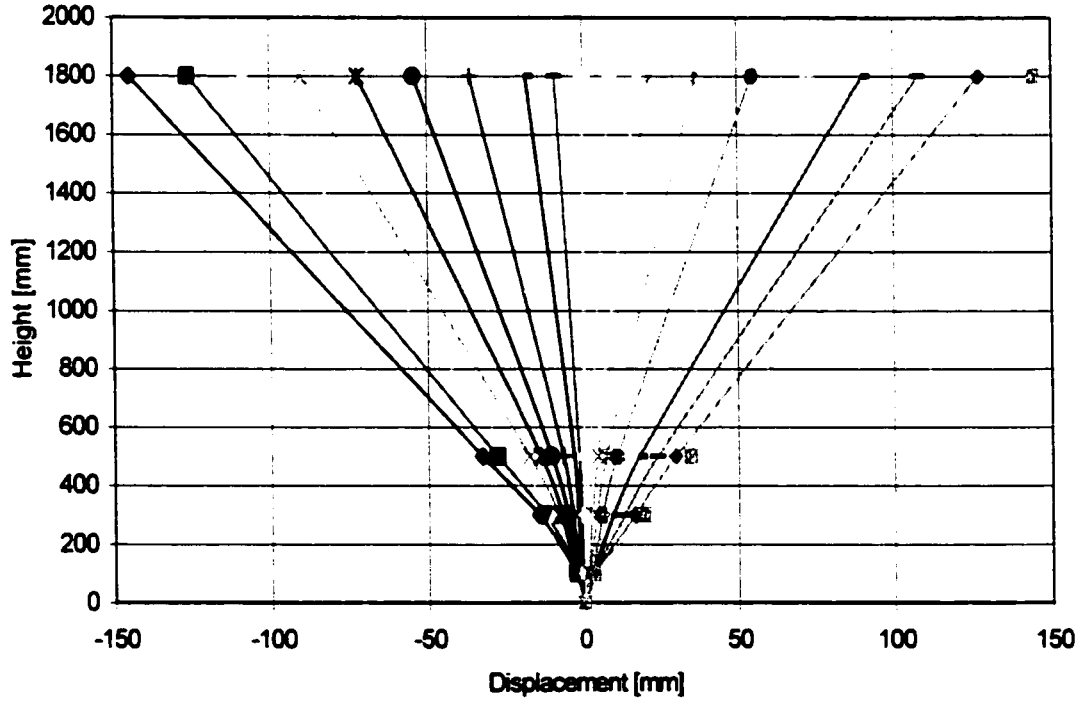

Figure A.16 Deflected shape of column SCH-2